UNIVERSITAT POLITÈCNICA DE VALÈNCIA

PROGRAMA DE DOCTORADO EN INGENIERÍA Y PRODUCCIÓN INDUSTRIAL

UNIVERSITAT
POLITÈCNICA
DE VALÈNCIA

DIAGNOSIS OF ELECTRIC INDUCTION MACHINES IN NON-STATIONARY REGIMES WORKING IN RANDOMNLY CHANGING CONDITIONS

THESIS REPORT:

FRANCISCO JOSÉ VEDREÑO SANTOS

ADVISERS:

DR. MARTÍN RIERA GUASP
DR. MANUEL PINEDA SÁNCHEZ

VALENCIA, NOVEMBER 2013

SUMMARY OF THE THESIS

Traditionally, the detection of faults in electric machines relies on the Fast Fourier Transform since most of the faults can be reliably diagnosed using it provided the machines are operating under steady state conditions for a reasonable period of time.

However, for applications in which machines work under fluctuating load and speed conditions (non-stationary conditions) such as windmills, traditional FFT has to be replaced with other techniques.

This thesis aims at developing a new methodology for the diagnosis of squirrel cage and wound rotor induction machines under non-stationary conditions, based on a new approach which relies on the slip-frequency domain analysis of the fault components of the currents .This approach is applied to the diagnosis of stator and rotor asymmetries and also for the mixed eccentricity.

The diagnosis of the electric machines in the slip-frequency domain provides the developed methodology an universal character since it is able to diagnose electrical machines irrespective of the features of the machine, the way in which the speed of the machine varies and its functioning mode (motor or generator).

The development of the methodology involves the following stages:

(i) Characterization of the evolutions of the fault components for stator and rotor asymmetry and also for the mixed eccentricity fault for both squirrel cage and wound rotor induction machines function of the speed (slip) and the frequency supply of the network from where the machine is fed.

(ii) Due to the importance of the signal processing, there is an introduction of a few basics of signal processing before going into the actual fault diagnosis processing.

(iii) The challenge of the extraction of the fault components is studied from three different filtering techniques such as the Discrete Wavelet Transform, Wavelet Packet Transform and with the proposal of a new filtering technique, the Spectral Filtering. The first two filtering techniques extract the fault components in the time domain whereas the new filtering technique works in the frequency domain.

(iv) The extraction of the fault components, in some cases, involves the shifting of the frequency signal components. The shifting of the frequency is carried out by two different techniques: the Frequency Displacement Theorem and the Hilbert Transform.

(v) Unlike other already developed techniques, the proposed methodology does not exclusively rely on in the computation of the energy of the fault component since it also involves the representation of the instantaneous frequency of the fault components, which is computed by two different techniques (Hilbert Transform and Teager-Kaiser Operator), vs. the slip. The representation of the instantaneous frequency vs. the slip prevents from false positive diagnosis improving the accuracy and quality of the diagnosis. Furthermore, the representation of the instantaneous frequency vs. the slip

enables the qualitative diagnosis that is fast and requires low computational resources.

(vi) Finally, due to the importance of the automation of the industrial processes and in order to avoid the divergence of criteria present in the qualitative diagnosis, three objective parameters are developed: Energy parameter, Similitude Coefficient and Regression parameters. The energy parameter quantifies the fault degree according to its value. It is computed in both the time and frequency domain (as a consequence of the extraction of the fault component in the frequency domain). The similitude coefficient and the regression parameters are objective parameters to discard false positive diagnosis giving a high reliability to the proposed methodology.

The diagnostic methodology is experimentally validated for the stator and rotor asymmetry faults and also for the mixed eccentricity fault in squirrel cage and wound rotor induction machines fed from the electric network and from variable frequency drives in non-stochastic stationary conditions.

RESUMEN DE LA TESIS

Tradicionalmente, la detección de faltas en máquinas eléctricas se basa en el uso de la Transformada Rápida de Fourier ya que la mayoría de las faltas pueden ser diagnosticadas con ella con seguridad si las máquinas operan en condiciones de régimen estacionario durante un intervalo de tiempo razonable.

Sin embargo, para aplicaciones en las que las máquinas operan en condiciones de carga y velocidad fluctuantes (condiciones no estacionarias) como por ejemplo los aerogeneradores, el uso de la Transformada Rápida de Fourier debe ser reemplazado por otras técnicas.

La presente tesis desarrolla una nueva metodología para el diagnóstico de máquinas de inducción de rotor de jaula y rotor bobinado operando en condiciones no estacionarias, basada en el análisis de las componentes de falta de las corrientes en el plano deslizamiento frecuencia. La técnica es aplicada al diagnóstico de asimetrías estatóricas, rotóricas y también para la falta de excentricidad mixta.

El diagnóstico de las máquinas eléctricas en el dominio deslizamiento-frecuencia confiere un carácter universal a la metodología ya que puede diagnosticar máquinas eléctricas independientemente de sus características, del modo en el que la velocidad de la máquina varía y de su modo de funcionamiento (motor o generador).

El desarrollo de la metodología conlleva las siguientes etapas:

(i) Caracterización de las evoluciones de las componentes de falta de asimetría estatórica, rotórica y excentricidad mixta para las máquinas de inducción de rotores de jaula y bobinados en función de la velocidad (deslizamiento) y la frecuencia de alimentación de la red a la que está conectada la máquina.

(ii) Debido a la importancia del procesado de la señal, se realiza una introducción a los conceptos básicos del procesado de señal antes de centrarse en las técnicas actuales de procesado de señal para el diagnóstico de máquinas eléctricas.

(iii) La extracción de las componentes de falta se lleva a cabo a través de tres técnicas de filtrado diferentes: filtros basados en la Transformada Discreta Wavelet, en la Transformada Wavelet Packet y con una nueva técnica de filtrado propuesta en esta tesis, el Filtrado Espectral. Las dos primeras técnicas de filtrado extraen las componentes de falta en el dominio del tiempo mientras que la nueva técnica de filtrado realiza la extracción en el dominio de la frecuencia.

(iv) La extracción de las componentes de falta, en algunos casos, conlleva el desplazamiento de la frecuencia de las componentes de falta. El desplazamiento de la frecuencia se realiza a través de dos técnicas: el Teorema del Desplazamiento de la Frecuencia y la Transformada Hilbert.

(v) A diferencia de otras técnicas ya desarrolladas, la metodología propuesta no se basa exclusivamente en el cálculo de la energía de la componente de falta sino que también estudia la evolución de la frecuencia instantánea de ellas, calculándola a través de dos técnicas diferentes (la

Transformada Hilbert y el operador Teager-Kaiser), frente al deslizamiento. La representación de la frecuencia instantánea frente al deslizamiento elimina la posibilidad de diagnósticos falsos positivos mejorando la precisión y la calidad del diagnóstico. Además, la representación de la frecuencia instantánea frente al deslizamiento permite realizar diagnósticos cualitativos que son rápidos y requieren bajos requisitos computacionales.

(vi) Finalmente, debido a la importancia de la automatización de los procesos industriales y para evitar la posible divergencia presente en el diagnóstico cualitativo, tres parámetros objetivos de diagnóstico son desarrollados: el parámetro de la energía, el coeficiente de similitud y los parámetros de regresión. El parámetro de la energía cuantifica la severidad de la falta según su valor y es calculado en el dominio del tiempo y en el dominio de la frecuencia (consecuencia de la extracción de las componentes de falta en el dominio de la frecuencia). El coeficiente de similitud y los parámetros de regresión son parámetros objetivos que permiten descartar diagnósticos falsos positivos aumentando la robustez de la metodología propuesta.

La metodología de diagnóstico propuesta se valida experimentalmente para las faltas de asimetría estatórica y rotórica y para el fallo de excentricidad mixta en máquinas de inducción de rotor de jaula y rotor bobinado alimentadas desde la red eléctrica y desde convertidores de frecuencia en condiciones no estacionarias estocásticas.

RESUM DE LA TESIS

Tradicionalment, la detecció de faltes en màquines elèctriques s'ha basat en l'ús de la Transformada Ràpida de Fourier ja que la majoria de les faltes poden ser diagnosticades amb ella amb seguritat si les màquines operen en condicions de règim estacionari durant un interval de temps raonable.

No obstant, per aplicacions en les que les màquines operen en condiciones de carrega y velocitat fluctuants (condicions no estacionaries) com per exemple els aerogeneradors, l'ús de la Transformada Ràpida de Fourier ha de ser substituïda per altres tècniques.

La present tesis desenvolupa una nova metodologia pel diagnòstic de màquines d'inducció de rotor de gàbia i rotor bobinat operant en condicions no estacionaries, basada en l'anàlisi de les components de falta de les corrents en el plànol lliscament freqüència. La tècnica és aplicada al diagnòstic de asimetries estatòriques, rotòriques i també per la falta d'excentricitat mixta.

El diagnòstic de les màquines elèctriques en el domini lliscament-freqüència confereix un caràcter universal a la metodologia ja que pot diagnosticar màquines elèctriques independentment de les seues característiques, de la manera en la que la velocitat de la màquina varia i de la seua manera de funcionament (motor o generador).

El desenvolupament de la metodologia comporta les següents etapes:

(i) Caracterització de les evolucions de les components de falta d'asimetria estatòrica, rotòrica i d'excentricitat mixta per les màquines d'inducció de rotors de gàbia i bobinats en funció de la velocitat (lliscament) i de la freqüència d'alimentació de la red a la que està connectada la màquina.

(ii) Com a conseqüència de l' importància del processat de la senyal, es realitza una introducció als conceptes bàsics del processat de la senyal abans de centrar-se en les tècniques actuals de processat de senyal pel diagnòstic de màquines elèctriques.

(iii) El repte de l'extracció de les components de falta s'estudia mitjançant tres tècniques de filtrat diferents: filtres basats en la Transformada Discreta Wavelet, en la Transformada Wavelet Packet i amb la proposta d'una nova tècnica de filtrat, el Filtrat Espectral. Les dos primeres tècniques de filtrat extrauen les components de falta en el domini del temps mentre que la nova tècnica de filtrat realitza l'extracció en el domini de la freqüència.

(iv) L'extracció de les components de falta, en alguns casos, comporta el desplaçament de la freqüència de les components de falta. El desplaçament de la freqüència es du a termini mitjançant dos tècniques: el Teorema del Desplaçament de la freqüència i la Transformada Hilbert.

(v) A diferència d'altres tècniques ja desenvolupades, la metodologia proposta no es basa exclusivament en el càlcul de l'energia de la component de falta sinó que també estudia l'evolució de la freqüència instantània de elles, calculant-la mitjançant dos tècniques diferents (la Transformada Hilbert i l'operador Teager-Kaiser), front al lliscament. La representació de la freqüència instantània front al lliscament elimina la possibilitat de diagnòstics fals positius millorant la precisió i la qualitat del diagnòstic. A més a més, la representació de la freqüència instantània front al lliscament permeteix dur a

termini el diagnòstic qualitatiu que són ràpids i requereixen baixos requisits computacionals.

(iv) Finalment, com a conseqüència de l' importància de l'automatització dels processos industrials i per evitar la possible divergència present al diagnòstic qualitatiu, tres paràmetres objectius de diagnòstic són desenvolupats: el paràmetre de l'energia, el coeficient de similitud i els paràmetres de regressió. El paràmetre de l'energia quantifica la severitat de la falta segons el seu valor i es calculat al domini del temps i al domini de la freqüència (conseqüència de l'extracció de les components de falta al domini de la freqüència). El coeficient de similitud i els paràmetres de regressió son paràmetres objectius que permeten descartar diagnòstics falsos positius augmentant la robustesa de la metodologia proposta.

La metodologia de diagnòstic proposta es validada experimentalment per les faltes de asimetria estatòrica i rotòrica i també per la falta d'excentricitat mixta en màquines d'inducció de rotor de gàbia i rotor bobinat alimentades des de la red elèctrica y des de convertidors de freqüència en condicions no estacionàries estocàstiques.

ACKNOWLEDGEMENTS

I would like to thank my advisors Dr. Martin Riera Guasp and Dr. Manuel Pineda Sánchez for their advices and the many hours they have spent reviewing this work.

I would also like to thank D. Eugenio Landete Marquina for his contribution that has facilitated the tests of this thesis.

I would like to thank to Ministerio de Ciencia e Inovación for the financial support to write this thesis in the framework of the "Formación de Personal Investigador" (scholarship reference BES-2009-022618).

I would like to thank the group of research on "Máquinas e Instalaciones Eléctricas" from "Instituto de Ingeniería Energética" from Universidad Politécnica de Valencia for welcoming me in the necessary researches to carry out this thesis.

I thank the unconditional support of my parents, without which this thesis would not have been finished.

INDEX

TABLE OF FIGURES

TABLE OF TABLES

TABLE OF SYMBOLS

φ	Initial phase angle of a digital signal (rad)
ρ	Spearman Correlation Coefficient
$\rho_{x,y}$	Pearson Correlation Coefficient
σ_x	Standard deviation of *x*
σ_{xy}	Covariance between *x* and *y*
τ	Wavelet Transform translation parameter Kendall Correlation Coefficient
ω	Angular frequency of a digital signal (rad/seg)
ω_{rot}^{est}	Electrical speed of the rotor in the stator reference system
ω_{rot}	Electrical speed of the rotor currents (rad/seg)
$\psi(t)$	Mother Wavelet
Φ	Initial phase angle of an analogue signal (rad)
Ω	Angular frequency of a continuous signal (rad/seg)
Ω_{rot}	Mechanical speed of the rotor
A	Amplitude of a generic signal
CF	Fault component
E_{CF_T}	Energy of the fault component in the time domain
E_{S_T}	Total energy of the signal in the time domain
E_{Nor_T}	Normalised energy in the time domain
E_{Nor_F}	Normalised energy in the frequency domain
E_f	Computed energy in the frequency domain
E_t	Computed energy in the time domain
F	Frequency of an analogue signal (Hz)
H	High pass band filters
L	Quantification level or Low pass band filter
N	Total number of samples of a discrete signal
S	Similitude coefficient
T	Period of an analogue signal (seg)
$X_{WT}(\tau, z)$	Wavelet Transform of a signal
$a[n]$	Approximation signal of Wavelet decomposition
b	Theoretical y-intercept of the lineal regression
b'	Computed y-intercept of the lineal regression
c_k	Fourier coefficients
d	Bandwidth of the Wavelet Packet Decomposition

$d[n]$	Detail signal of a Wavelet decomposition
e	Error of a signal
i	Generic acquired current signal
i_{FC}	Reduced acquired current signal associated to the studied fault component
i_f	Stator generic current fault
i_s	Stator generic current
f	Frequency of a digital signal
f_{exc}	Frequency of the eccentricity fault component (Hz)
f_{red}	Supply frequency (Hz)
f_{est}^{rot}	Frequency in the rotor currents caused by the stator currents (Hz)
f_{mag}	Frequency of the fault component of the electromagnetic harmonic of rotor asymmetry
f_{mec}	Frequency of the fault component of the electromagneticmechanical harmonic of rotor asymmetry.
f_{rot}^{est}	Frequency in the stator currents caused by the rotor currents (Hz)
f_{rot}^{k}	Frequency of the rotor currents of order *k* (Hz)
f_s	Sampling frequency of a digital signal
$f(t)$	Any signal
$g(t)$	Any signal
k	Constant of natural value 1, 2, 3,...
$k_{\inf}$	Lower order decomposition level of the Wavelet Packet that contains the minimum frequency of the range to be extracted
$k_{\sup}$	Upper order decomposition level of the Wavelet Packet that contains the maximum frequency of the range to be extracted
m	Theoretical slope of the straight line computed by the lineal regression
m'	Computed slope of the straight line computed by the lineal regression
n	Position of a sample in a discrete signal
nC	Greatest order approximation of the Wavelet Transform that contains a given frequency
nNC	Smallest order approximation of the Wavelet Transform that does not contain a given frequency

$n_{\Delta f}$	Value of the lowest order of the Wavelet Packet Transform that does not contain the given frequency
p	Number of pairs of poles
s	Slip (p.u.)
t	Time (seconds)
$x(t)$	Analogue signal
$x_d(t)$	Discrete analogue signal
$x(nT)$	No quantified discrete signal
$x_c(nT)$	Quantified discrete signal
$x[n]$	Discrete signal
z	Scale parameter of the Wavelet Transform

TABLE OF ABBREVIATIONS

CWT	Continuous Wavelet Transform
CoWT	Complex Wavelet Transform
DESA	Discrete time Energy Separation Algortihm
DFT	Discrete Fourier Transform
DiFT	Displacement Frequency Theorem
DWT	Discrete Wavelet Transform
FFT	Fast Fourier Transform
FrFT	Fractional Fourier Transform
HHT	Hilbert Huang Transform
HMC	Harmonic Main Components
HOHC	High Order Harmonic Components
HOSM	Higher Order Spectra Method
HT	Hilbert Transform
IF	Instantaneous Frequency
MCSA	Motor Current Signature Analysis
MWFA	Modified Winding Function Approach
PPT	Polinomial Phase Transform
REE	Red Eléctrica de España
SQNR	Signal to Quantification Noise Ratio
STFT	Short Time Fourier Transform
UDWT	Undecimated Discrete Wavelet Transform
VMM	Vienna Monitoring Method
WPT	Wavelet Packet Transform
WVD	Wigner-Ville Distribution
ZFFT	Zoom Fast Fourier Transform
ZMUSIC	Zoom MUltiple SIgnal Classification

CHAPTER I: INTRODUCTION

1 INTRODUCTION

Rotating electrical machines are important equipment components in the majority of industrial processes and, traditionally, they have been considered as high reliable devices requiring little attention, apart from periodical maintenance when a scheduled stop in the installation was set.

The location and importance of electrical machines in the productive processes make them to be one of the most critic elements in the industrial facilities since a sudden stop of them may produce high economical losses and compromising the security of the users. This fact together with its design with lower security margins, which increases the probabilities of failures in them, creates the need of developing incipient diagnostic fault techniques for the failures that machines may undergo.

A diagnostic technique is completely defined by its scope. The scope of a diagnostic technique contains the information related to (i) the kind of signal used for carrying out the diagnostic process, (ii) the kind of machine to be diagnosed, (iii) functioning mode, (iv) operation mode, and (v) the fault to be diagnosed.

The most used signals for the diagnosis of electrical machines are the analysis of temperature, oil, vibrations, currents, voltages, torque, flux, speed, etc.

The main types of electrical machines are asynchronous machines, synchronous machines -wound poles and permanents magnets-, direct current machines and reluctance machines.

Because of the reversibility of electrical machines, they have two possible functioning modes: motor and generator.

In the current thesis, the operation mode of the electrical machines is classified in three categories that are coherent with the technical literature in the field of diagnosis: operation in stationary conditions, operation in transient conditions, and operation in non-stationary conditions. The belonging to one of those three operation modes is function of the evolution of the fundamental magnitudes (load torque, speed, current, voltage, frequency, etc) of the machine.

The operation in stationary conditions, or steady state regime, is defined as those where the fundamental magnitudes of the machine (voltage, frequency, load torque, etc) do not change for the chosen diagnostic interval (Fig. 1). Examples of this type of operation mode may be lifts, which are loaded with steady weight, fans, or pumps working under constant head and flow. The technical literature mainly focuses on this operation mode.

The operation in transient state -transient regime- becomes when the machine changes its operation mode from a stationary state to another different stationary state, where the values of the fundamental magnitudes are known for both stationary states. The variation of the functioning conditions

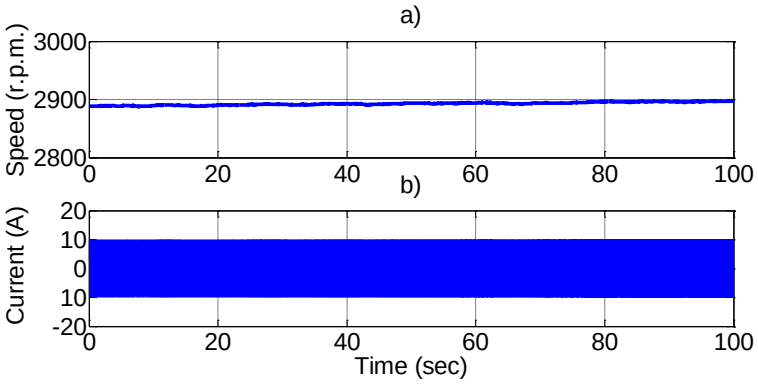

Fig. 1 Steady state regime. a) Evolution of the speed b) Evolution of the current.

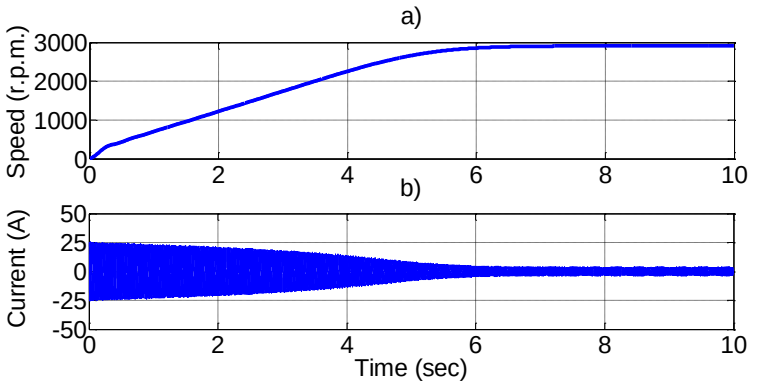

Fig. 2 Transient regime. a) Evolution of the speed b) Evolution of the current.

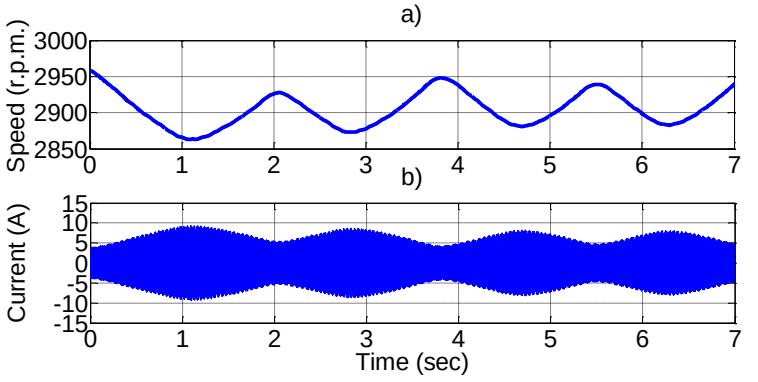

Fig. 3 Non-stationary stochastic regime. a) Evolution of the speed b) Evolution of the current..

between both stationary states causes a change in the fundamental magnitudes of the machine since they evolve from the values of the initial stationary state to reaching the values of the new stationary state during a limited time and with a predetermined and known evolution. In the practise, the diagnosis in transient state focuses on the start up transient. (Fig. 2). In this regime, the electrical machine goes from sleep mode to a stationary state determined by the load state. The speed of the machine evolves increasing its value from zero to the rated state speed, the slip decreases from one to a value close to zero, the root mean square current value goes from 5 or 8 times the value of the rated current to a smaller value of the rated current and the voltage and the frequency do not change their values during the start up. Diagnostic techniques for transient states have experienced an important development in the last decade.

Finally, the non-stationary operation -non-stationary regime- concerns all the applications where the electrical and mechanical magnitudes that characterise the functioning of the machine change in a continuous and random way, imposed by the process powered by the electrical machine (Fig. 3). Examples of applications where that functioning mode may occur are windmill generators, electrical vehicles in urban cycles, ball mills, presses, etc. The technical literature that is focused on the diagnosis in non-stationary conditions is very scarce, although lately it has been detected a growing interest in this field.

The current thesis focuses on the development of diagnostic techniques in failures on induction machines in non-stationary regime. The non-stationary operating mode will be named in the current document as "non-stationary stochastic regime" or for short, "stochastic regime", in order to emphasise the random nature of the evolution of the characteristic magnitudes.

This report develops a new methodology for diagnosis in induction machines, squirrel cage and wound rotor, through the analysis of their current, irrespective of the operating mode, motor or generator, when they operate under non-stationary stochastic regimes before the failures of rotor and stator asymmetry and mixed eccentricity.

The type of machine to diagnose, squirrel cage and wound rotor induction machine, responds to the great use in industry as a motor of the first, whereas the second is increasingly used by the wind industry in the generation of electricity.

The selection of the current as measured physical magnitude to perform the proposed diagnostic methodology is consequence of the many advantages that its analysis has as for instance its low invasive nature.

Regarding the chosen operation mode, it must be highlighted how difficult is to find, in certain industrial processes, stationary state conditions for enough time to allow the use of conventional diagnostic techniques based on the spectral analysis in the frequency domain with a satisfactory accuracy.

On the other hand, the use of techniques for transient regimes (start up) requires stopping the machine to analyze for being diagnosed. This means that its use is unfeasible in many applications if the machines do not

frequently start. On machines fed through variable speed drives (VSD) these techniques are not applicable since the start up transient itself does not exist.

As a consequence of the inconveniences present in the techniques of diagnosis of machines in stationary and transient states in growing importance applications, is justified the interest in developing new diagnostic techniques for non-stationary stochastic regimes, that is, techniques that can perform the diagnosis on machines when they continuously undergo small changes into its load conditions around its rated functioning point.

The bases of the proposed methodology to diagnose electrical machines in the current thesis are mainly based on three concepts: (i) extraction of the fault component, (ii) computation of the energy of the fault component and, (iii) characterization of the origin of the computed energy.

The extraction of the fault components in the current document is performed by means of three different filtering techniques based on (a) Discrete Wavelet Transform, (b) Wavelet Packet Transform, and (c) Discrete Fourier Transform.

The extraction of the fault components through the Discrete Wavelet Transform is adopted due to its wide use and acceptation in the diagnosis of electric machines in transient regimes.

The Wavelet Packet Transform is chosen as a consequence of, a priori, its greater versatility for the extraction of the different fault components, although its use is far less widespread in the field of diagnosis of electrical machines.

The main drawbacks of the filters based on the Wavelet Transform is, on one side, its rigidity in the selection of the frequency bandwidth required for the extraction of the fault components due to its dependence on the sampling frequency of the signal to be filtered and, on the other, the overlapping of the different filtering bands, due to its non-ideality.

In order to solve the well-known inconveniences of the Wavelet Transform filters, in this thesis a new filtering method is proposed, named spectral filter, based on the properties of the Discrete Fourier Transform.

Once the fault component has been extracted, the computation of its energy allows the assessment of the state of the machine.

The computation of the energy in this document is performed in both time domain (conventional method) and, as a novelty and direct consequence of the use of the proposed spectral filter, in the frequency domain due to the Plancherel's Theorem.

The already developed diagnostic methodologies for the diagnosis of electrical machines in non-stationary stochastic regimes compare the value of energy of fault component with the preset threshold, establishing that the machine is in faulty state when the fault component exceeds that value.

However, due to the practical process of the extraction of the fault component, there is always the uncertainty that the increase of the energy of the fault component is due to a cause not related to the state of the machine such as load or supply voltage fluctuations. That may lead to misdiagnosis.

In order to avoid the problem of the uncertain origin of the increase of the energy of the fault component, in this thesis is proposed the computation of

the instantaneous frequency of the fault component, by means of the Hilbert Transform (conventional method) and the operator Teager-Kaiser.

The representation of the evolution of the instantaneous frequency is performed in the frequency-slip domain and not in the slip frequency-time domain, since the evolution of the instantaneous frequency of the fault components in the slip domain, unlike its evolution in the time domain, allow in first place an independent diagnosis of the machine versus the variations of its speed, and, consequently, of the load variations that the machine is subjected; secondly, the evolution of the instantaneous frequency in the frequency slip domain defines lineal characteristic evolutions for each type of faults that a machine may undergo.

The comparison of the theoretical evolutions of characteristic instantaneous frequencies of each type of fault with the evolution of the extracted component determines whether the detected energy increase is a result of a failure or other cause, thus eliminating the uncertainty of the origin of the computed energy during the diagnostic process.

The proposed methodology is validated through several tests, analysing the current of squirrel cage rotor, and wound rotor machines, in a wide range of powers with rotor and stator asymmetries and mixed eccentricity, functioning as motor and generator in non-stationary stochastic operating regimes.

Finally and although the proposed methodology is mainly conceived for the diagnosis of electrical machines directly connected to electric network, the methodology is also applied to the diagnosis of machines fed from variable speed drives, showing the great versatility of the developed methodology for the diagnosis of electric induction machines.

2 OBJECTIVES

The overall goal of this thesis is to develop a new diagnostic technique capable of detecting the rotor and stator asymmetry faults and mixed eccentricity in electrical induction machines operating in non-stationary stochastic regimes through analysis of its currents.

The developed technique will diagnose machines with squirrel cage rotors or wound rotors, without affecting their normal functioning, irrespective of whether they generate (generator mode) or consume (motor mode) electrical energy.

Achieving the proposed overall goal is based on the attainment of the following partial objectives:

1.- Evaluation of the existing techniques for the diagnosis of electric induction machines, both in stationary and transient and non-stationary regimes.
2.- Study of the fault components of stator and rotor asymmetry components and mixed eccentricity in squirrel cage and wound rotor induction machines irrespective of whether they work as motor or generator.

3.- Proposition of a new diagnostic technique that allows the detection of the different studied faults in non-stationary stochastic regimes, justifying the technique in a theoretically way.
4.- Definition and establishment of scope and comparison with the existing developed techniques.
5.- Proposition of a scheme that allows the automation of the diagnostic process and its implementation in electronic devices.
6.- Proposition of indicators to assess the degree of damage to the machine.
7.- Validation of the proposed methodology through laboratory tests.

3 STRUCTURE OF THE THESIS

To achieve the objectives of this thesis, it is developed as follows:

In Chapter II, the literature review of the diagnostic techniques in electrical machines is performed from its beginnings to the present time. The literature review focuses on the techniques based on the MCSA (Motor Current Signature Analysis) methodology for stationary regimes, transient regimes and finally in an exhaustively way for the non-stationary stochastic regimes.

Chapter III discusses the various physical phenomena when each of the considered faults (rotor and stator asymmetries and mixed eccentricity) in this thesis, in both squirrel cage rotor and wound rotor induction machines, occur.

Chapter IV introduces the proposed methodology in this thesis and introduces its practical application schema, step by step, for its general application for the diagnosis of faults in induction machines.

Chapters V, VI, VII, VIII develop the different scope of applications (signal acquisition, signal filtering, frequency shifting of the signal, computation of the instantaneous frequency, computation of the energy of the signal, linear regression parameters and, similarity coefficient) necessary for the development and application of the proposed methodology in Chapter IV.

Chapter V is focused on the problem of the acquisition of the signals from the machine to be analyzed. Chapter V shows the differences between the analysis of analogue signals (signals that occur in the machine) and digital signals (those that result of the process of signal acquisition). Finally, the problem of selecting the sampling frequency is also discussed in this chapter.

Chapter VI is structured into two parts: (i) extraction of fault components through different filtering techniques and (ii) frequency shifting of the harmonic components of the signal.

The first part of Chapter VI develops the theoretical and practical application for the extraction of the fault components by filters based on the Discrete Wavelet Transform, Wavelet Packet Transform and a new spectral filter based on the properties of the Discrete Fourier Transform that is a contribution of this work.

The second part of Chapter VI introduces two techniques, the Displacement Frequency Theorem and the Hilbert Transform, to shift in the

frequency domain the different harmonic components of the to be analysed current signals. The application of the frequency shifting is performed when there are significant frequency components whose frequencies are similar to the fault components that are intended to be extracted.

Chapter VII introduces the computation of the instantaneous frequency through the Hilbert Transform (conventional method) and Teager-Kaiser Operator.

The last chapter that develops the theoretical concepts of the proposed methodology is Chapter VIII, which introduces the computation procedure of the objective parameters used by the proposed diagnostic methodology: (i) the computation of the energy, (ii) the linear regression parameters, and (iii) the new coefficient of similarity proposed.

Chapters IX, X and XI focus on the validation of the proposed methodology through the analysis of the results of the many performed tests for the faults of rotor and stator asymmetry and mixed eccentricity, respectively. The validation of the methodology is performed on squirrel cage and wound rotor induction machines either working as motor or generator in non-stationary stochastic regimes.

Chapter XII is carries out the assessment of the feasibility of using the proposed methodology, already validated in the previous chapters, for the diagnosis of electrical machines fed from VSD, at constant and variable frequency. This chapter exposes the practical scheme of the application of the methodology for machines fed from VSDs, validating the results with laboratory tests.

Finally, Chapter XIII summarizes the conclusions of this thesis, whereas chapter XIV exposes the future research.

CHAPTER II: STATE OF ART

1 INTRODUCTION

The main objective of this chapter is the review of the most used techniques and methodologies for the diagnosis of electrical machines at the present.

The chapter is structured in three clearly differentiated parts: (i) review of the stationary regime techniques, (ii) review of the techniques in transient regimes -start up- and (iii) review of the techniques in non-stationary stochastic regimes.

A machine operates at steady state when its power conditions (voltage and frequency) and load (resistive torque) are held constant, by determining its speed -slip- and the root mean square value of the absorbed current by the machine not suffer variations over time (Chapter I, Fig. 1).

A transient regime comes when the machine is subjected to preset variations in speed -slip- and current on a specific time interval (Chapter I, Fig. 2). The transient regimes for the diagnosis of electric machines usually entail large variations in speed (slip).

A machine is subjected to a non-stationary stochastic regime when there are completely random continuous variations of its speed -slip- near its rated operation point due to load variations (Chapter I, Fig. 3) or changes in feeding conditions (voltage or frequency).

Most, by far, of the published papers in the technical literature are framed within the steady state analysis. However, the diagnosis of non-stationary stochastic regimes has increasingly grown in importance in the last decade.

This thesis focuses on the development of diagnostic techniques for machines operating in non-stationary stochastic regimes. The diagnosis in these conditions has seldom been addressed in the literature.

The review of the state of art begins with the analysis of the techniques related to the fault diagnosis in steady state for the stator asymmetry faults, mixed eccentricity and rotor asymmetry.

After that, the literature review focuses on the study of methodologies adopted for the detection of faults in machines operating in transient regimes.

The literature review concludes with a review of the techniques used for the diagnosis of machines subjected to non-stationary stochastic regimes. The critical review of the methodologies that comprise this last group is of paramount importance, since this thesis frames this specific field.

In the industrial scope, electric machines are the major generating elements of driving force, where they are widely used and considered very sturdy and reliable elements with a very low failure rate, especially in the case of squirrel cage rotor induction machines, being also devices with very low maintenance requirements.

However, the current trend to reduce its cost and use them in new applications in more demanding conditions causes materials to work closer to their mechanical and electrical limits, increasing the likelihood of failure.

Electric machines are usually subjected to many disturbances, -electrical, mechanical, environmental, thermal, chemical, etc.- that favour the emergence of several failures in the different parts that compose the machine [1], [2].

The emergence of faults in the electrical machines prevents them from its right functioning, which may cause malfunction in the manufacturing process, such as unplanned shutdown, resulting in an increase of the production costs and in some cases, it even leads to lack of safety conditions.

That is why there is a need for the development of new diagnostic methods that allow the detection of different faults in an incipient state in electrical machines to prevent, thus, the sudden stop of production processes as a result of the failure of any of the integrated machines in them.

Electric machines are complex systems that can undergo both electrical -stator and rotor asymmetries- and mechanical failures -bearings and eccentricities- or a combination of both of them. Any of these failures can be due to excessive thermal stress to which the machines are subjected or due to the tough working environment conditions that they endure.

Often failures in electrical machines appear in transient processes, especially in the start up or on reconnecting to the feeding network because in those moments the currents flowing through the windings of the machine and the mechanical stresses to which are subjected are very high, therefore on one side the thermal stress to which the machine is subjected increases, and on the other, the deterioration of the insulation is favoured. Furthermore, abrupt changes in the speed increase the mechanical stress of the different elements of the machine, causing fatigue in the components and leading to its deterioration.

It must be noted that electric machines are usually in critical points in complex systems, and therefore, an unscheduled stop has serious consequences for the functioning of the production process. This fact makes more and more necessary monitoring systems on them to allow the detection of possible incipient faults.

Despite its sturdiness, faults such as broken bars and short circuit rings on large machines, bearing breakages, short circuits due to insulation failures, eccentricities, etc., occur in induction machines.

That is why more and more in the industry more maintenance plans based on the monitoring of the status of the machine (condition monitoring) allowing the detection of faults that occur in the machines in the earliest stages are followed.

The condition monitoring consists of a continuous analysis of certain acquired signals, such as currents, voltages, temperature, speed, etc., through several sensors that reflect the condition of different parameters of the machine in its regular operating regime.

A great number of techniques based on condition monitoring have been developed in recent years in order to know the status of the machines practically in real time.

One of the main advantages of diagnostic systems based on the condition monitoring is its efficiency that is mainly characterized by two parameters: (i)

high accuracy in the diagnosis and (ii) the ability to quantify the degree of failure.

One of the most common drawbacks of these systems is the need for a specialised operator, with the enough degree of expertise to distinguish between normal and abnormal operation of the machine for a correct interpretation of the obtained results to result in a reliable enough diagnosis.

Great efforts to reduce or limit this problem have recently been conducted, favouring the development of practical methods and with an enough high degree of reliability in order to be applied to the detection of the most common faults at industrial level with the minimum possible specialisation.

Another drawback of the condition monitoring techniques is its installation cost, despite being relatively low, compared with the required investment for the installation of large motors or generators.

Finally, recall that induction machines are mainly composed of two parts: stator and rotor. The stator is the fixed part of the electrical machine, consisting of a stack of sheets of ferromagnetic material, where the stator windings are hosted, through which the currents, which induce the rotating magnetic field, circulate. The rotor is the part of the electrical machine that rotates due to the induction of currents, produced by the rotating magnetic field caused by the circulating currents in the stator, in the rotor coils, if the rotor is wound, or in the bars, in the case of a squirrel cage rotor. In [3] it can be found a detailed description of the advantages and disadvantages of each of the two configurations that can take the rotor in an induction machine.

The stators and rotors of the electrical induction machines are subjected to lot of disturbances that can cause different faults in them. Disturbances and causes that produce the different faults are studied in [2], [4].

2 LITERATURE REVIEW

The review of the state of the art has been structured in three blocks, dedicated to the three modes of operation established in the previous section: stationary state, transient regime and non-stationary stochastic regime.

Within each of the operating regimes, a new subdivision, function of the studied fault, can be performed, mainly classifying them in three groups: (i) stator asymmetry, (ii) broken bars or unbalances in the rotor windings and (iii) eccentricity [5].

The vast majority of diagnostic methods or techniques published in the literature focus on the study of electrical machines operating in stationary regimes [6]-[59]. The diagnostics of machines operating in transient regimes has been studied to a lesser extent [60]-[84] whereas there is a scarcity of publications focused on the study of non-stationary stochastic regimes [87]-[95], despite its great interest. This scarcity of publications is mainly due the difficulty involved in the development of methodologies for the right diagnosis in such conditions.

2.1 STATIONARY REGIME

The analysis of stationary regime techniques for the diagnosis of electric machines is organised according to the following three subdivisions: (i) stator asymmetry [6]-[18], (ii) eccentricity [19]-[31] and (iii) rotor asymmetry [34]-[59].

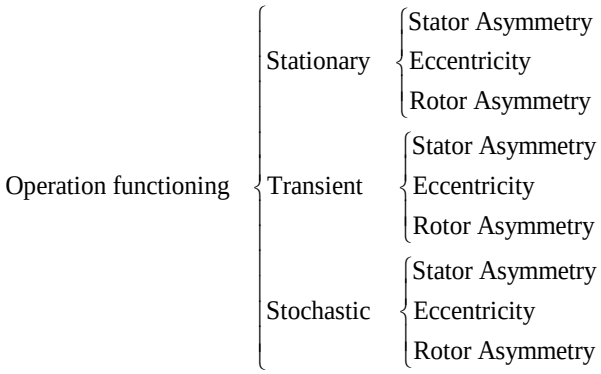

Fig. 4 Classification of faults diagnosed with the MCSA methodology according to the operating regime of the machine and the type of fault.

2.1.1 STATOR ASYMMETRY

First investigations on stator asymmetry failures are carried out by Williamson [6] in 1985, in which it is introduced one of the first studies on the mechanisms of generation of faults in the stator windings of the machines.

The difficulty of the diagnosis of the stator asymmetry is noted in the fact that there is no significant advancement in the diagnosis of this failure until 1996 when Kliman *et al.* [7] introduce a new technique for the automatic detection of inter-turn short circuit through the analysis of the negative sequence of current that occurs when there is an asymmetry in the stator windings, as a result of a short circuit between turns.

It is not until five years later, in 2001, when Cruz *et al.* [8] introduce a study of the detection of faults in the windings of asynchronous machines using the Park vector, extending the theory used in [9] for the diagnosis of eccentricities.

One year later of the publication of the work of Cruz *et al.*, Nandi *et al.* [10] introduce one of the first works on the detection of short circuits between windings by the measure the voltages induced in the stator windings after the shutdown. Furthermore, Lee in [11] introduces a method of diagnosing short circuits between coils based on the measure of its impedance.

Back in 2006, Mirafzal *et al.* [12] propose a method for the diagnosis of short-circuited turns based on the oscillation of the space vector of the

magnetic field, which is also applied to the detection of rotor asymmetries in squirrel cage rotor induction machines.

More recently, Stefani *et al.* [13] introduced one of the first diagnostic work on doubly fed induction machines through the analysis of the rotor currents, which allows the easily diagnosis of the state of the stator windings. The importance of this work is, in addition to the contribution to the diagnosis of the stator asymmetry, the study of the doubly fed generators, whose importance is currently booming due to its high degree of penetration into the field of wind power generation.

In [14] da Silva *et al.* propose a method for the diagnosis of the stator asymmetry by the use of the envelope of the stator current, applying the mixed model methodology and the reconstruction of the Gaussian spatial phases, which is also applied to the detection of the rotor asymmetry.

In [15] Yazidi *et al.* compare three methods for the diagnosis of the stator asymmetry: the analysis of the rotor currents, the measurement of the leakage flux and the analysis of the currents through the stator current space vector, concluding that the measurement of the leakage flux is the best technique of all three for the diagnosis of this type of faults.

Yazidi *et al*. continue their work on the development of techniques for the diagnosis of short circuits between turns, introducing in [16] a method for the diagnosis of short-circuited turns in rotors of wound rotor induction machines based on the use of the technique of the bispectrum, by using the stator currents.

One of the latest studies submitted for the diagnosis of the stator asymmetry is [17], where it is proposed the detection of the stator asymmetry through the analysis of the negative sequence of the impedance and the use of the Park's vector, but the interest of this work is the use of a finite element model for the simulation of short circuits between turns.

Finally, Pusca *et al.* [18] propose a new method for the detection of short circuits between turns through the study of transversal leakage of the magnetic flux when the machine is in operation.

2.1.2 ECCENTRICITY

One of the first publications that refers to the diagnosis of the eccentricity dates at 1986 [19], when Cameron *et al*. introduced one of the first works dealing with the detection of eccentricities in electrical induction machines through the vibration analysis and the monitoring of the currents.

It is not until 1993 when Cardoso *et al.* [9] introduce a significant advance in the diagnosis of eccentricities submitting a method for detection of eccentricities in electric induction machines operating in steady state with the Park's vector. The Park's vector allows the decomposition of the currents in the axes p-q. When the machine is completely symmetrical the use of the Park's vector decompose the currents in the p-q axes, obtaining the pattern of a circle in the p-q plane representation. However, when an eccentricity is present, the currents plotted on the p-q axes distort, drawing an ellipse. The more elliptical pattern, the higher the degree of eccentricity the machine is subjected.

In 1997, Dorrell *et al* [20] conducted a study on the static and dynamic eccentricity from the point of view of the current and vibration analysis, subjecting the studied machines to different load states in steady state.

Furthermore, in 1999 Milimonfared *et al*. [21] introduced one of the first methods of the detection of eccentricities and rotor asymmetries based on the measurement of the induced voltages in the shutdown. This methodology is based on the observation of the induced voltage in the stator windings after the disconnection. Once the machine is shutdown, the stator currents quickly take null values and thus, the residual voltages measured in the stator windings are induced by the rotor currents that have not been extinguished yet, thereby allowing the detection of eccentricities and rotor asymmetries.

Nandi *et al.* introduced in [22] one of the pioneering works for the detection of eccentricities in steady state by the use of the Modified Winding Function Analysis (MWFA), in addition to make considerations of great value for the detection of eccentricity, such as the harmonic current in machines affected by the eccentricity depend on the number of pairs of poles and slots on the machine causing that the eccentricity harmonics are not observable in all types of induction machines.

In [23] Liu *et al.* introduced a method based on the computation of the instantaneous power for the detection of eccentricities and broken bars in steady state when both faults occur simultaneously. The drawback of the techniques based on the measure of power is the need to acquire more signals for diagnosis than those based only on the analysis of one stator current, increasing the investment for the implementation of the method. The second drawback of this technique is that the spectral analysis of the instantaneous power provides the same result as the spectral analysis of a single current with a much higher installation cost, due to the need of more sensors.

Despite the complexity of the diagnosis of eccentricity some methods for the diagnosis of the eccentricity in off-line have also been developed [24]. In [24] the surge test technique is introduced. The surge test technique involves the application of an overvoltage at the terminals of the stator windings while the rotor is externally turned. Since the stator windings and the rotor are coupled only through the air gap, then any abnormality in it -an eccentricity- can be detected.

In [25] is introduced a method for the diagnosis of the eccentricity through the measure of the current and voltage harmonics determined by the negative sequence of the spectral components in order to determine whether it is possible to separate the effects caused by an eccentricity to the effects caused by a pulsating load. In this publication is determined that the harmonic pulsating loads have a higher amplitude than the eccentricity harmonics. Though this result is generally true, it should be noted that the conclusion comes from an incorrect hypothesis, since if the amplitude of the pulsating load is sufficiently reduced the harmonics caused by the pulsating load and the eccentricity would have similar amplitude values, preventing their separation by the value of its amplitude.

In [28] the techniques used in [26] and [27] for the detection of eccentricities with the use of the apparent power are extended, reaching diagnostic results similar to those reached with the use of a single stator

current. The similarity of the results of this technique with those that only use one stator current is a major disadvantage for this type of methods as discussed above.

In [29] is studied the detection of the eccentricity fault when the machine is fed from VSD through the vibration and currents analysis and the measurement of the electromotive force by an explorer turn. In [29] is concluded that the detection of the eccentricity is satisfactory by the measure of the electromotive force whereas the use of the vibration and currents does not determine clearly the existence of the fault. Vibration analysis does not allow satisfactory the diagnosis due to its dependence on the speed of the machine, whereas the current analysis is not possible because of the increase of the noise since the machine is fed from a VSD.

In [30] Faiz *et al.* conducted a dynamic study of the effect of the mixed eccentricity on a machine performing several tests at steady state with different loads, determining the great influence of the load effect on the diagnosis of the mixed eccentricity.

In [31] is introduced the analysis of eccentricity through the measure of the induced voltages in the stator windings after the shutdown of the machine stating that such methods are valid only for certain number of pole pairs-number of slots, preventing its universally implementation and agreeing with the fact already mentioned in [22]. Another drawback of this technique is that it forces the shutdown -stop- of the device, condition that is usually inadmissible in the production processes.

Finally, in [32] is proposed a diagnostic method based on the study of the magnetic field outside of the machine for the detection of eccentricities and bar breakage in squirrel cage induction machines. However, the authors do not present experimental results that validate the proposed methodology for the diagnosis of eccentricities. Furthermore, the use of techniques based on the measure of the magnetic field outside the machine is strongly dependent on the location of the sensor used for the measurement of the magnetic field, preventing its implementation at industrial level.

2.1.3 ROTOR ASYMMETRY

This section discusses some of the most relevant references related to the diagnosis of rotor asymmetries in steady state.

The first research conducted for the diagnosis of rotor asymmetries dates at 1982 with the works of Deleroi [34] and Williamson [35]. These two studies focus on the research on failures in the rotors of induction machines in stationary state performing the analysis of the mechanisms that cause the generation of the fault as well as the development of the first detection methods.

Years later, in 1988, Kliman [36] introduces a method for the diagnosis of broken bars in induction machines operating in steady state that paved the way for the development of many techniques for the detection of faults in electrical machines through the signal analysis, laying the foundations for the condition monitoring.

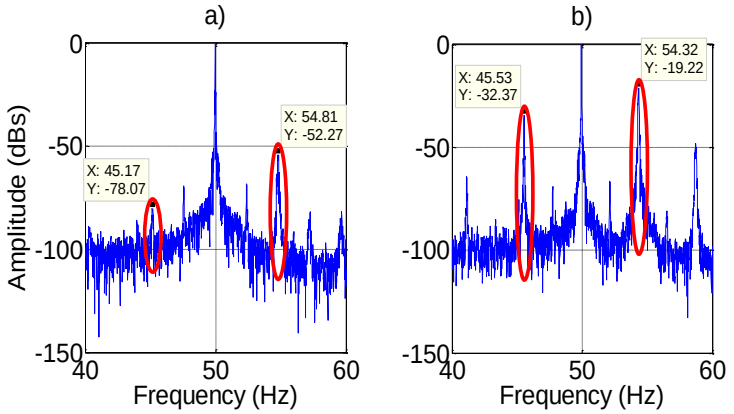

Fig. 5 Diagnosis of a rotor asymmetry through the FFT in steady state. a) Healthy Machine b) Faulty machine.

Fig. 5.a shows the spectrum of the current of a squirrel cage rotor induction machine in steady state in healthy state, whereas Fig. 5.b shows the spectrum when the machine has a rotor asymmetry, showing the increase in amplitude of the characteristic harmonics of failure.

In 1995, Schoen [37] introduces a new diagnostic method that improves the diagnosis of broken bars introduced seven years earlier in [36].

Furthermore, in 1999 Bangura *et al.* [38] introduce an interesting study that characterises the evolution of the rotor asymmetry in induction machines, based on models computed by finite elements. Contemporaneous to Bangura *et al.* and in 1999, Milimonfared *et al.* [21] proposed one of the first detection methods for rotor asymmetries based on the measure of the induced voltages in the stator windings after shutdown.

It is not until 2000, when three works [39]-[41] to improve the diagnosis of rotor asymmetries in steady state using new diagnostic techniques are introduced.

In [39] Arthur *et al.* use the High Order Spectrum Method (HOSM) to detect broken bars in steady state. This technique reduces the problem of the noise when the FFT is used for the diagnosis of broken bars, but requires a very high computational cost. In [40] Kostic-Perovic *et al.* propose the use of the fluctuations in the phase of the flux vector for the diagnosis of broken bars, whereas [41] Kral *et al.* propose the use of spatial phasors for the diagnosis of machines in steady and transient regimes by the Vienna Monitoring Method (VMM), although they do not achieve good enough results for the transient analysis diagnosis but they do in steady state.

Already in 2001 Bellini *et al.* [42] performed a comparative study of the techniques of FFT, current vector module, instantaneous power and torque, showing that the FFT-based methods improve the results of the other techniques studied. The major contribution of this publication is the demonstration that the sum of the two lateral fault components is a more stable indicator that the use of one of the side components, since they are less affected by the inertia and load variations. Another major contribution of this

publication is the justification of the relationship between the higher side harmonic and the oscillations of the speed caused by the lower side harmonic. Finally, the third contribution of this work is to obtain that the relation between the amplitude of fault side harmonics depends on the inertia of the system and load (torque) that the machine is subjected.

In [43] Kral *et al.* improved the technique of the Vienna monitoring method, although it remains valid only for the steady state analysis. In [44] Zhang *et al.* introduce a technique of detection of broken bars in steady state through the analysis of the oscillations of the filtered signals by the Wavelet Transform.

In [45] Benbouzid discusses different diagnostic techniques up to date, in order to determine which the best of them all is. Benbouzid concludes that the diagnostic techniques in steady state may be enough for the diagnosis of electric machines, whereas pointing out that the use of the Wavelet Transform and time-frequency transforms as emerging techniques for the development of new methods of diagnosis.

In [23] Liu introduces a method based on the computation of the instantaneous power for the detection of broken bars and eccentricities in steady state, when they occur simultaneously. In [46] Cupertino *et al.* introduced a methodology for the diagnosis of broken bars by the induced voltages in the stator winding in the shutdown, analysing the induced space voltage phasor in the stator windings. In [47] it is proposed the diagnosis of broken bars by the excitation of the fault components, injecting electrical signals to the machine and measuring the magnetic field that they produce, besides the application of classical analysis using FFT.

Another of the great contributions in the diagnosis of rotor asymmetries is [48], where Henao *et al.* develop an equivalent circuit of the machine that facilitates the understanding of the mechanisms of the rotor asymmetry fault in them. Henao *et al.* determine that the rotor asymmetry produces a reverse rotating magnetic field in the rotor, causing one of the side fault harmonics of the rotor asymmetry.

One of the main disadvantages of the Fourier Transform is its low frequency resolution, since often the acquisition times cannot be long to avoid the violation of the steady condition that requires the FFT. To solve this problem Bellini *et al.* proposed in [49] the maximum covariance method, improving the frequency resolution of the FFT-based methods.

Back in 2006, Mirafzal *et al.* [12] propose a method for the diagnosis of short circuited turns and broken bars based on the oscillations of the space vector of the magnetic field.

In the last five years, the development of diagnostic techniques for the steady state has continued yielding many new techniques.

Among them are off-line methods for the detection of broken bars introduced in [50]-[53]. In [50] and [51] is developed a technique based on the measurement of the magnetic flux outside of the machine. In [52] is proposed a technique with similar physical principles to those shown in [51] for the diagnosis of broken bars, through the measurement of the magnetic field at a stator tooth through an explorer turn. The authors of [52] shown in

[53] the development of a portable diagnostic equipment based on the technique developed in [52].

Moreover, the development of techniques for the steady state for the detection of rotor asymmetries has not stopped, since in [54] is shown the improvement in the frequency resolution by the technique ZMUSIC versus the FFT, where the reached resolution values are similar to the ZFFT with much lower computational costs.

In [13] is introduced one of the first papers for the diagnosis of doubly fed machines through the analysis of the rotor currents, which allow the easy diagnosis of the state of the stator and rotor windings. The importance of this work lies in the study of a type of machine whose importance is continuously increasing, since they are the most installed in the wind generators at the present.

In [55] is introduced a method for the detection of broken bars using low sampling frequencies values, eliminating the fundamental component of the current through a notch filter. Whereas in [14] is performed the diagnosis of broken bars and short circuited coils by the use of the envelope of the stator currents.

In [56] is proposed the use of the coefficients of the Complex Wavelet Transform (CoWT) for the diagnosis of rotor asymmetries. This paper compares the influence of the use of six different windows in the application of the Fourier Transform.

The development of diagnostic techniques continues with [27] that proposes the use of reactive power for the diagnosis of induction machines with broken bars by applying the FFT and Welch Transform, which provides better spectral resolution in the reactive power frequency spectrum. In [28] is introduced a technique based on the measurement of active and reactive power for detection of broken bars and eccentricity improving the technique introduced in [27].

In [57] a new on-line and off-line method for the diagnostics of rotor asymmetries when machines operating in no load conditions or at low slip is introduced. The proposed method is based on the properties of the Hilbert Transform to avoid the problem of spectral dispersion, enabling the detection of the rotor asymmetry fault through FFT in conditions of complete lack of load.

In [58] is introduced a study on the bar breakage in double cage rotors, that explains the variation of the amplitude of the lower sideband harmonic function of the relative position of the broken bars. The value of this publication is that in case of a double failure the methodology can distinguish it from simple one, and even detect the breakage, since depending on the position of the double breakage, it may not always be detected by the use of conventional side harmonics.

In [59] a comparison of the analysis of the broken bars and the loss of one phase while the machine is working at its rated point is performed, comparing the results obtained through the DWT, the Wavelet Packet (WPT) and FFT.

In [32] is introduced a method based on the measurement of the magnetic field outside of the machine that allows the detection of both eccentricities

and bar breakage. One of the main contributions of this paper is the use of an inverted machine (the stator works as a secondary) allowing the measurement of currents for each one of the "bars" of the machine, thus making easier the study of the external magnetic field of the machine. Although the results are compelling, the application of such techniques in an industrial environment is difficult to be performed since the position of sensor for the measurement of the external magnetic field has a large influence on the results.

Finally, in [33] is proposed the use of the Wavelet Transform for the diagnosis of permanent magnet machines in steady state for local failures and the demagnetization of the magnets that comprise them.

2.2 TRANSIENT REGIME

Since the operation of the machines in strictly stationary regime is a difficult condition to meet in the industry, due to the difficulty of guaranteeing that the machine does not change its operation mode for long enough times, the need of the diagnosis of machines in transient regimes, where the methods related to the start-up were firstly developed [60]-[84].

The diagnosis of machines in the start up processes have the advantage of greater current amplitude at the start in front of the current amplitude at its rated operating regime and, therefore, the amplitude of harmonics is also increased, facilitating the processes of diagnosis.

2.2.1 STATOR ASYMMETRY

The only reference found that studies the diagnosis of short circuited turns in the start up transient regime dates at 1995, where Toliyat [60] makes an interesting contribution to the field of the diagnosis, modelling the behaviour of the fault of stator asymmetry in transient regime from a theoretically point of view. The proposed model is validated through the analysis of the current in a start up.

2.2.2 ECCENTRICITY

Among the techniques for the diagnosis in transients regimes for eccentricities is highlighted the work [63] that extends the methodology introduced in [61], [62] for the diagnosis of broken bars to a method that allows the detection of the eccentricity at the start up through the extraction of the fault components with the Discrete Wavelet Transform.

Furthermore, in [64] is extended the method of the detection of rotor asymmetries for start up transients [65], [66] and eccentricities [63] for the detection of double faults -rotor asymmetry and eccentricity.

The use of finite elements as a tool for the development of techniques in transient regimes is introduced in [67] where the authors compared the spectrum obtained from the extracted current from a motor in its rated conditions with the current computed in a finite element model, allowing the comparison between the two of them and making easier to reach a reference that simplifies the process of diagnosis. The main drawback of this technique is the long computation time that requires the use of finite elements.

The technique introduced in [68] for the diagnosis of broken bars through the analysis of the lower side harmonic through instantaneous frequency is extended in [69] for the diagnosis of eccentricities.

In [70] is conducted a very good theoretical analysis of the influence of pulsating loads on the current spectrum, showing that the eccentricities generate the same spectral components that pulsating torque.

In [72] is introduced a method that extends the one already proposed in [71] for the detection of eccentricities in induction machines fed from VSD with variable feed conditions, although the variation of the conditions employed is restricted since it is considered only an acceleration and/or deceleration ramp to apply the technique of start up developed in the previous papers [63], [64] and [69].

2.2.3 ROTOR ASYMMETRY

Finally, the diagnosis of rotor asymmetries in transient regimes also starts with the work of Toliyat [60] that introduces a theoretical model of the evolution of the rotor asymmetry in transient regime similar to the one introduced for the stator asymmetry in the same publication.

In 2004 [73] Douglas *et al*. introduce a new algorithm for the detection of broken bars through the analysis of the start up currents of the machine through the Wavelet Transform. Douglas *et al*. improve the method proposed in [73] in [74] but they do not fully develop it. These two works of Douglas *et al*. are of inestimable value in the transient diagnosis of electric machines since they are the pioneers in the development of a diagnostic technique in transient regime, with frankly acceptable results.

One of the principles on which Douglas *et al*. are based on is in the greater amplitude of the start up currents versus the amplitude of the currents in the rated operation favouring thus, the observation of the fault sideband components. Furthermore, the large slip that is subjected to the machine in the start up allows the extraction of the components related to the fault component since in the rated operating state both components are very close, preventing its observation due to the small order of magnitude of the fault components, and due to phenomena such as a leakage.

In 2006 Antonino *et al.* [61], [62] improved the diagnostic techniques in broken bars for the start up transient regimes proposed by Douglas *et al*. in [73] and [74] through the use of the Discrete Wavelet Transform, achieving more than satisfactory results and providing a physical interpretation thereof.

The technique proposed by Antonino *et al.* is based on the monitoring of the evolution of the fault harmonic component through the different frequency bands (Fig. 6), after the application of the Discrete Wavelet Transform.

Supangat *et al.* [75] propose a method similar to those developed in [61], [62] through the use of the Continuous Wavelet Transform (CWT) although the computation time that is required is much greater than that necessary in [61], [62], not improving the already achieved results.

In [76] Blodt *et al.* study the different effects of different types of pulsating loads that cause in the spectra of the currents of electrical machines

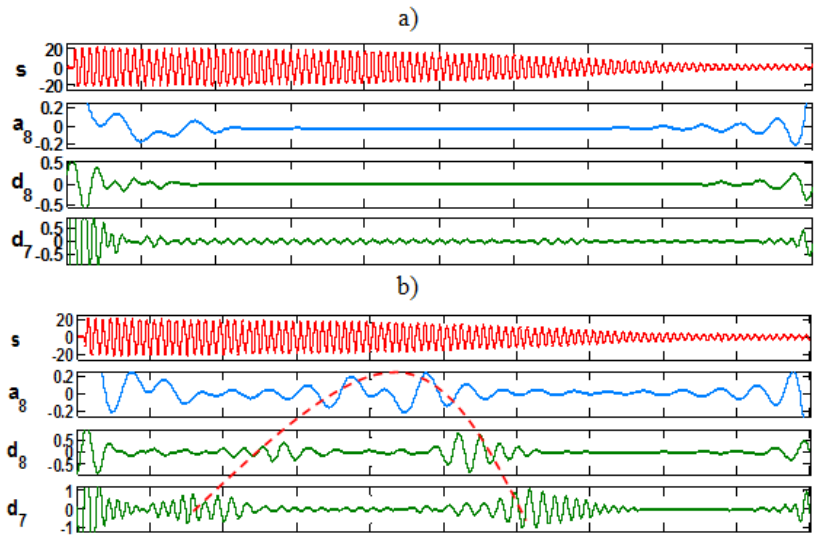

Fig. 6 Diagnosis of a rotor asymmetry in transient regime [61]. a) Healthy machine b) Faulty machine

with the time-frequency transform Wigner-Ville, showing the already emerging interest that would occur in the coming years for the transient analysis of the currents of electrical machines in non-stationary stochastic regimes.

Papers [77] and [78] are quite similar. In [77] a rotor asymmetry is diagnosed through the application of the Wavelet Transform to the current, extracting the fault harmonic component, but previously applying the Hilbert Transform to it. This action has two effects on the stator current (i) it displaces the fundamental component of the current, confining it in the low frequency values of the spectrum and (ii) the overlap of the two side harmonics, thereby reducing the uncertainty in its quantification as it is pointed out in [42]. These two studies together with [57] provide the necessary tools for the extraction of frequency components that are very close to each other, fact that is extremely important for the future development of techniques. Continuing the line proposed in [77], in [78] is shown the results after the application of the technique introduced in [77] to a wound rotor machine, achieving similar results to those obtained for squirrel cage rotor induction machines.

Furthermore, the work introduced by Riera *et al.* in [65], [66] are quite similar, one being the continuation of the other. In [65] is performed a thorough study of the temporal evolution of the lateral side fault component on the start up, being a pattern justified physically, including the evolution in amplitude and frequency that ends with the proposition of a method for its simulation. The technique proposed in [65] is structured in the extraction of the side fault component and its comparison with the simulated pattern computed in the previously developed study. It also introduces a method for the quantification of the fault, dividing the energy of the fault component by the total energy of the start up signal. In [66] the methodology introduced in

the previous papers is systematised and extended theoretically to any type of induction machine in which its fault components are a function of the slip, providing a practical guide for the application of the methodology.

Contemporary with the work of Riera *et al*., Briz *et al*. introduced in [79] a method for the detection of rotor asymmetries through the use of the Complex Wavelet Transform on the start up, but it requires the measurement of the three currents to perform the same diagnosis that is performed in previous works [63], [65] and [66] with the acquisition of one current.

Furthermore, in [64] is extended the already introduced methodology for the detection of rotor asymmetries in [65], [66] and eccentricities [63] for the detection of double faults -rotor asymmetry and eccentricity.

Pineda *et al*. introduce the measure of the instantaneous frequency for the diagnosis of electric machines with rotor asymmetries in [68]. The technique of the instantaneous frequency is based on the extraction of fault components associated with the frequency band and the computation of the instantaneous frequency must correspond, in case of failure, with the V pattern described in [61], [62]. This work is one of the cornerstones on which is based the new diagnosis method proposed in this thesis.

In [80] Pineda *et al*. propose the use of the Fractional Fourier Transform (FrFT) for the diagnosis of rotor asymmetries. The Fractional Fourier Transform is based on the rotation of the time-frequency plane. This publication shows that when performing the proper rotation in the time-frequency plane, the drawback of the fault harmonics vary its frequency is eliminated, and it can be plotted in a rotated frequency spectrum with the FrFT, as a peak analogue to when the FFT is performed when the speed of the machine is constant. The value of the necessary rotation to show a peak in the rotated frequency spectrum determines the slope of the evolution of the fault component, allowing the diagnosis of rotor asymmetry, because of its characteristic value.

The application of new diagnostic techniques for the diagnosis of start up -transient regimes- continues with the technique introduced in [81] that utilizes Polynomial Phase Transform (PPT) to diagnose the machine with the stator current in a similar way than in [80]. The difference between the two publications is that in [81] the slope of the evolution of the frequency of the fault component is extracted in an approximated way as a mean value of the current phase and not as the value of the rotation performed through the FrFT.

In [82] Antonino *et al*. raise the automation of the method shown in [63], [64] through pattern recognition, using 2-D transforms that contain the characteristic V fault patterns already analyzed. The proposed transforms standardise the results in a way that they are independent of features of the machine and may be compared among themselves although they are not exactly the same. Antonino *et al*. expand its work with the publication of [83] where they apply the methodology developed in the previous works to double cage machines allowing the detection of faults in the outer bars of the cage during the start up, since in the rated operation, the circulating current through the outer bars is very low, increasing the difficulty of the diagnosis with the use of the conventional diagnostic techniques in steady state.

In [72] is extended the diagnostic techniques for the start up through the development of the diagnosis through the Analytic Wavelet Transform, which allows the observation of high order harmonics, facilitating the diagnosis of machines. Finally, in [84] the Gabor Transform is applied to the analysis of the rotor asymmetries and eccentricities in the start up, improving the frequency resolution achieved in [72], [80]-[82].

On the other hand, [85] is focused on the diagnosis of the outer cage induction machine with double cage in transient conditions. This publication presents several contradictions by their authors from the instant that they say the current circulating through the outer cage is very low for low slips and thus the use of the FFT is not feasible for diagnosis, whereas they use the same waves for the diagnosis in transient regimes. Following with the contradictions present in this publication, the authors state that the diagnosis is not possible in steady state but with the results presented it is clear that detection is possible. Another contradiction occurs when the authors of [85] propose the shifting of the higher side harmonic, action that cannot be performed as it will be mathematically demonstrated in this thesis.

Back in 2013 in [86] is introduced a technique where induction machines are diagnosed through the Principal Slot Harmonic (PSH) from the vibration to which the machine is subjected when there is a broken bar in transient regimes through the Wigner-Ville Transform.

2.3 NON-STATIONARY STOCHASTIC REGIME

Although it is true that all the techniques discussed and analyzed so far are of undeniable value, it is no less important to consider that its implementation is difficult in many industrial scopes due to their intrinsic characteristics.

In the case of techniques based on the steady state, it is obvious that guaranteeing a stationary load regime in the actual working conditions for a period long enough for the application of techniques based on the Fourier transform, is not always possible.

The diagnosis through the transient techniques reduces the problem that those techniques deal with in steady state and they even are, in some applications, perfectly adapted for the intermittent operation of machines, as for instance lifts.

However, the application of transient techniques in transient regimes generates another inconvenience, with the exception of machines working in intermittent mode: the application of these techniques require the shutdown of the machine to perform the start up, action that usually is inadmissible in the industrial environment since it requires stopping the production process, being the major drawback of this type of techniques.

These considerations have led several authors to develop techniques that allow the diagnosis of the machines, while operating in non-stationary stochastic regimes as stated in [87]-[95].

One of the pioneering works dealing with the diagnosis in non-stationary stochastic conditions is introduced by Blödt *et al.* in [87], where there is conducted a theoretical analysis of the different effects in the currents caused

by pulsating loads due to mechanical failures that the machines undergo, which usually worsen the quality of the diagnosis. The analysis introduced in [87] is based on the time-frequency transform Wigner-Ville and the results achieved are compared with results achieved after the application of the conventional methods.

In [88] is introduced a method for non-stationary pseudo-stochastic regimes for the detection of broken bars and short circuits between turns by the analysis of the spectrogram computed by applying on one side the STFT and on the other the spectrogram computed after application of the DWT and the power spectral analysis. The use of this methodology for non-stationary stochastic regime is of doubtful application, since in the tests shown the changes of the test conditions are so slow that it can be considered that the signal is analysed by a succession of steady states that is the basis of STFT analysis.

The methodology used in [89] for the diagnosis of rotor asymmetries acquires current signal of the machine and its speed, then it splits the signals into small time intervals to which they apply the required frequency shifting each moment, demodulating the signal and causing that the harmonics are always in the same frequency. This action allows the computation of the Fourier Transform to compute the frequency spectrum, then this technique goes from a non-stationary stochastic analysis technique to a technique that analyses small stationary regimes.

The diagnosis of machines in actual stochastic regimes is not actually performed until 2011 when Gritli *et al.* introduce the first work that diagnoses an electrical machine in non-stationary stochastic operation [90]. In this paper Gritli *et al.* use the frequency shifting of the signal developed in [89] and the filtering DWT techniques from [63]-[66] combining them so to allow the diagnosis of the machine in completely non-stationary stochastic conditions.

In [90] is diagnosed a rotor and stator asymmetry of a doubly fed induction machine in a non-stationary stochastic regime, using the methodology proposed by Gritli *et al*., based on the frequency shifting of the signal and the filtering of it by using Discrete Wavelet Transform. The first action taken in [90] is to shift the harmonic fault components to the low frequency region of the spectrum using the technique called frequency sliding, technique that is nothing more than the application of Displacement Frequency Theorem. The frequency shifting of the signal is mandatory, since the dyadic filtering of the Wavelet Transform does not allow the setting of the band pass filter for the particular needs of the transient current waveforms of the electrical machines since the filtering bands set by the DWT filter are too large. However, it is possible adjust finely the lower frequency band, since it will be simply necessary to increase the level of decomposition of the Wavelet Transform to reduce the filtering band width to the desired width and, with the aid of the frequency shifting the harmonic is located in the band previously computed. After the frequency shifting, the extraction of the fault component is performed by a filter based on the Discrete Wavelet Transform.

Although it is true that the contribution of [90] is highly important in the development of diagnostic techniques in the stochastic regime, some drawbacks remain unresolved.

One of the major drawbacks unresolved in the method proposed in [90] is the difficulty in extracting the harmonics that are close to the fundamental harmonic current in the case of a rotor asymmetry.

It might be thought that since the Displacement Frequency Theorem allows the displacement of the frequency harmonic components in the spectrum to the position that is wanted and, since increasing the order of approximation of the Wavelet, the extracted filtering bandwidth is halved for each order increased, then the extraction of the components very close to each other may be performed.

That fact that from a theoretical point of view is true, in the practice has drawbacks. The reason that the frequency components close to each other cannot be extracted using the technique proposed in [90] is due to the non-ideality of the Wavelet filters, that is, although that may be obtained band pass filters narrow enough, there is always an overlap between the approximation a_n and a_{n+1} that prevents the extraction of the two signal components close to each other [66].

Furthermore, it is noteworthy that the aforementioned drawback is not present in the diagnosis of the stator asymmetry since the fault component is away enough from the fundamental component of the current to be extracted without undergoing the overlapping bands effect of filters used for it.

The second major drawback of [90] is that its bases of diagnosis are based on the computation of the energy of the extracted signal. Although it is true that the theoretical rationale applied in [90] is correct, on a practical level has unresolved inconveniences. Among them there is the fact that the proposed methodology with an increase in the energy extracted filtering band filter, may determine that the machine is in faulty state, despite the increase of the energy may have been be caused by any cause beyond the machine as for instance a change in the load applied to the machine. Another drawback to be highlighted, especially for the diagnosis of stator asymmetry, is the width of the selected filtering bands since they tend to be too large, favouring the inclusion of other frequency components than the fault component that can eventually cause false positive diagnosis.

In [91] and [92] continues the work begun in [90], diagnosing a machine with a rotor asymmetry in non-stationary stochastic regime, providing a new method for the quantification of the fault, subdividing the signal into small intervals where the signal energy is computed, thus enhancing the quantification criterion proposed in [90]. These two studies provide no solution to the problems already discussed in the criticism made to [90], since there is no change in the proposed methodology, since they focus on the improvement of the quantification of the method.

Kia *et al*. in [93] introduces a methodology similar to that developed by Gritli *et al.* in [90] since its diagnostic method is also based on the computation of the energy in a predetermined frequency band where it should be found the fault component.

The methodology proposed by Kia *et al*. raises the problem of the diagnosis of induction machines in non-stationary stochastic regimes, analysing the rotor and stator asymmetry on wound rotor induction machines [93].

The basis of the methodology proposed in [93] is the same than the already exposed by Gritli *et al.* in [90], that is, it is computed the energy of the band where the fault there is supposedly only the fault component.

The difference between [90] and [93] is in the pre-signal processing performed for the extraction of the fault component. In [93] the pre-processing of the signal is based on the Hilbert Transform, which introduces a shifting in the spectrum by subtracting to the frequency of each component a frequency equal to the fundamental frequency component, so that the fundamental component becomes a continuous component and the component next to it are in the low frequency region of the spectrum, similar to what is stated in [57] and [77] allowing more accurate diagnostics than those in [90] in the case of a rotor asymmetry.

For the extraction of the fault components of stator asymmetry in the rotor currents, the methodology introduced in [93] has the same drawbacks as [90].

Although the methodology introduced in [93] allows a better extraction of the fault components for the rotor asymmetry its application is conditioned by the same drawbacks than in [90]. Recall that this method is also based on the computation of energy in a specific frequency band and therefore it cannot ensure that an increase of energy in that frequency band is due exclusively to the fault to be diagnosed. Furthermore, another major drawback of this work is the complexity of extracting the spectral components due to the variations in amplitude of the fundamental component, to solve this problem is proposed a complex method based on the construction of the envelopes of the wave computed by the Hilbert transform.

Fig. 7 shows the rotor currents analyzed in [93] for the diagnosis of a stator asymmetry in a wound rotor induction machine. Fig. 8 shows the result after the extraction of the fault components with the application of a filter based on the Discrete Wavelet Transform in [93].

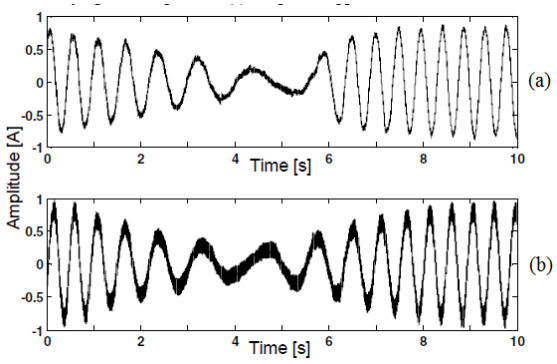

Fig. 7 Rotor current of rotor wound induction machine in non-stationary stochastic conditions. (a) Healthy (b) Stator asymmetry [93]

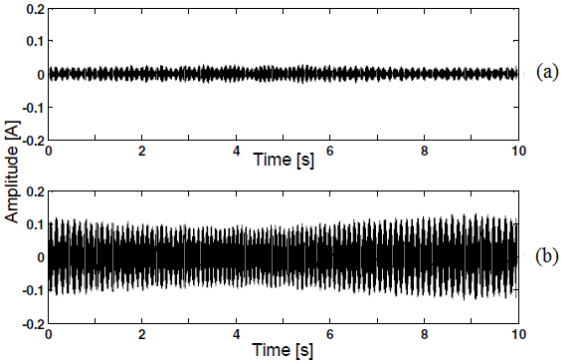

Fig. 8 D4 detail coefficient normalized by the rated rotor current. (a) Healthy. (b) Stator Asymmetry [93]

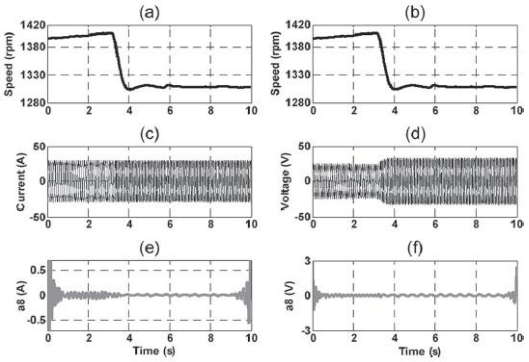

Fig. 9 Experimental results of the methodology introduced in [95] for healthy machine. First column results from the analysis of the currents; Second column results from the analysis of the voltages.

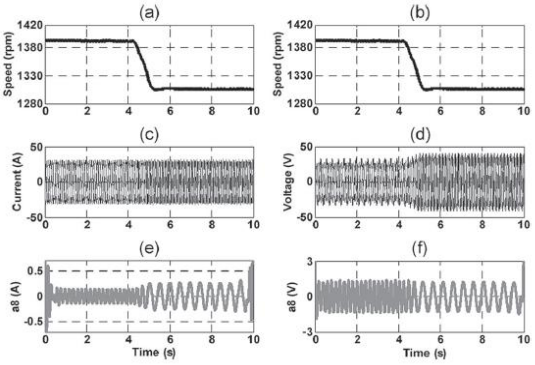

Fig. 10 Experimental results of the methodology introduced in [95] for rotor asymmetry. First column results from the analysis of the currents; Second column results from the analysis of the voltages.

In 2012 is introduced [94] where the diagnosis of induction machines by the measure of the angle between the active and reactive power, fact that can distinguish between the oscillations due to the load with those caused by a broken bar. Despite the advantages of this method, it still possesses the disadvantage of measuring the three currents and three voltages in order to determine the values of the active and reactive power of the machine, making its implementation to industrial level more expensive.

Finally, the last work published for the diagnosis of induction machines in non-stationary stochastic regimes is from the current year, 2013, whose authors are Gritli *et al*. [95].

This last paper published in the diagnostic field in non-stationary stochastic regimes has the following new features of interest:

Firstly the diagnosis of wound rotor induction machines is performed under conditions more realistic supply power conditions at industrial level, since the rotor of the analyzed electric machine is fed from a VSD.

Secondly in this publication is introduced the analysis of the rotor voltages to carry out the diagnosis of the machine for the faults of stator and rotor asymmetry.

Conceptually, [95] does not introduce any new significant enough contribution respect to [90] since it is shifting the frequencies of the analysed signal (current or voltage) to the low frequency range of the spectrum by the Displacement Frequency Theorem and once the harmonic fault components to be extracted are located in the desired place, a filter based on the Discrete Wavelet Transform for its extraction is applied. Furthermore, the method is still based only on the quantification of the energy of the extracted fault component and, therefore the same drawbacks of uncertainty remain for the discrimination of the fault against another type of phenomena already discussed for [90].

3 SUMMARY AND CONCLUSIONS OF THE CHAPTER

After an exhaustive analysis of the literature in the field of the diagnosis of electrical induction machines is reached the first partial objective of this thesis, concluding that there is a need to develop techniques that enable the diagnosis of electrical machines in non-stationary stochastic regimes in a more effective way than the existing ones, since there are currently very few techniques developed for the diagnosis of electric machines in non-stationary stochastic regimes ([90] and [93] basically).

These techniques have the disadvantage that their basis of diagnosis is exclusively based on the computation of the increase of energy in a frequency band where the fault harmonic evolves and therefore it can lead to false positive diagnosis, as it has already been discussed in the literature review.

Moreover, the diagnostic techniques for induction machines in generator mode are scarcely treated in the technical literature. It should be noted that the last recent years there has been a large increase in the installation of wind induction generators [96].

This fact, according to the author's point of view, will result in the need for the development of techniques focused on the diagnosis of failures in these machines when operating in generator mode.

Although it is true that many of the techniques designed for the diagnosis of motors can quickly be adapted for the diagnosis of asynchronous generators, it remains to solve the problem of the diagnosis of electrical machines in non-stationary stochastic load regimes, as it is the specific case of the wind generators.

The non-stationary stochastic regime operating conditions, due to its specifics, cause that all the techniques already developed, either for stationary or transitory regimes, are not useful since they cannot perform a reliable enough diagnosis for these conditions.

In this thesis, it is proposed a new diagnostic method for electric induction machines in non-stationary stochastic regime around the rated operating point of the machine. The proposed method is valid for the diagnosis of motors and generators. The basis of the method are based on the inputs of [57], [63]-[66], [68], [69], [77], [90], [93] and [95], allowing the diagnosis of rotor asymmetries in both squirrel cage rotor and wound rotor induction machines, mixed eccentricity and stator asymmetries in the wound rotor machines which are currently used on wind turbines.

The proposed methodology in this thesis is based on the extraction of the fault component to be diagnosed using several techniques of pre-processing of the signal, similar to [90] and [93] but avoiding the problem of the uncertainty that have those methods based on the computation of the energy in a specific frequency band, by determining the origin of the energy extracted by the evolution of the instantaneous frequency of the fault component. That defines a unique and unambiguous characteristic for each type of studied fault, eliminating the ambiguity present in the methods based only on the analysis of the increase of energy in a predetermined frequency band, reducing the uncertainty in the diagnosis and improving the contributions already published in the technical literature.

This thesis also introduces a new method of extracting the fault components, based on the application of the filtering in the frequency domain due to the Plancherel's Theorem.

The first advantage of the filtering in the frequency domain is that it allows a greater accuracy in the extraction the fault components than the filters used so far (based on the extraction of the fault components in the time domain) and as direct consequence, it introduces improvements in the sensitivity of the diagnosis.

Finally, another significant development that is introduced because of the filtering in the frequency domain is the evaluation of the energy of the fault components in the frequency domain, instead of being carried out in the time domain. That reduces the computation time as well as the computational requirements, facilitating the implementation of the proposed methodology in low cost electronic devices.

CHAPTER III: FAULTS TO BE DIAGNOSED

1 INTRODUCTION

The equations for the low order fault components of the stator asymmetry [6]-[18], rotor [34]-[59] and eccentricity [19]-[31] for squirrel cage induction machines have been widely studied in the literature.

However, the analysis of the state of the art conducted shows a lack of study of the equations that model the high order fault harmonic either in squirrel cage rotor and wound rotor induction machines for the rotor asymmetry failure. Furthermore, there are also deficiencies in the study of the fault components for rotor wound induction machines in any operating mode.

Another noteworthy aspect is the fact that the development of the different fault equations, in the technical literature, is performed under the hypothesis of motor operation.

This chapter aims to develop the equations that characterise the fault components for the diagnosis of the different faults studied in this thesis.

The achievement of the proposed goal provides three developments in the field of the diagnosis of electrical machines: (i) the generalization of the fault equations from the motor to generator operation, (ii) the theoretical development of the high order fault equations for the rotor asymmetry and (iii) the theoretical development of the equations for wound rotor machines, either for motor and generator operation.

The importance of electric induction machines is undeniable since approximately 60% of world production of electricity is consumed by them, since they represent about 90% of electrical machines used in the industry [100].

Regarding power generation, according to REE 18% of the energy generated in Spain in 2012 was produced by induction generators, due to its high degree of implantation in the wind turbines, representing 22% of the total installed capacity in the Spanish electricity system [101]. At global level, it is estimated that the implantation of wind power will continue with a high growth rate and consequently the implantation of induction generators will increase, at a rate of 20% of the installed power from 2015 to 2020, reaching 3817 MW of installed capacity worldwide [102].

Due to the large installation of induction machines in the industry and in the service sector, is mandatory for the functioning of the economy and effective maintenance and diagnosis of them.

The majority of faults in electrical machines can be classified according to the following scheme [4]:

- Faults in the stator due to the loss or short circuit between turns of one or more phases of the stator winding.
- Abnormal connection of the stator windings.
- Broken bars or short circuit rings breakage.
- Static and/or dynamic irregularities at the air gap.

– Bending of the shaft causing friction between the rotor and the stator causing catastrophic damage to the stator armature and windings.
– Short circuit in the rotor windings.
– Bearings and gearboxes.

Out of the described fault types, the most common are bearing, stator and rotor (broken bars) failures as shown in Table 1.

TABLE 1. DISTRIBUTION OF FAULTS IN ELECTRIC MACHINES

Fault	A	B	C	D	E	F
Bearings	75%	95%	41%	41%	42%	21%
Stator	9%	2%	37%	36%	13%	35%
Rotor	6%	1%	10%	9%	8%	44%
Other	10%	2%	12%	14%	38%	-

A) OEM predictions using FMEA techniques (1995-1997) [103]
B) MOD survey, 1999 [104]
C) Large motor survey IEEE, 1985, [105]
D) Motors in accessory applications, 1986 [106]
E) Motors in offshore and petrochemical industry, 1995 [107]
F) Ratio in 80 of published papers in IEEE and IEE in the period 1981-2007 [103]

Table 1 shows that about 40% of faults that occur in electric induction machines are due to bearing failures, while 50% is due to stator or rotor faults. Finally, 10% is due to other causes.

One of the key goals of this thesis is to develop a technique capable of diagnosing an asynchronous machine, through the analysis of its currents, in non-stationary stochastic operation regimes.

However, electric induction machines may also work, and it is becoming more common, fed from VSD or doubly fed. Nevertheless, this thesis focuses on the study of machines connected directly to the electric network, although it should be emphasised that the developed equations in this thesis are valid either for machines fed from the electric network or from VSD.

In the following subsections is developed the equations that correspond to the rotor and stator asymmetry faults and mixed eccentricity necessary to characterise the faults and performing the diagnosis.

The derivation of the different fault equations for the low order components for squirrel cage rotor induction machines is largely resolved in the technical literature for the rotor asymmetry fault [34], [36], [109], stator asymmetry [13], [110] and eccentricity [19], [20]. However, there is a lack of studies related to the fault expressions for wound rotor induction machines, as well as for the high order fault components for the rotor asymmetry for either squirrel cage rotor and wound rotor machines.

Thus, previously of the introduction of the proposed method is carried out the study of the fault components for each one of the faults to be diagnosed, for the two configurations of the rotors of induction machines.

The developed equations allow the knowledge of the value of the frequency for each harmonic fault component in the stator or rotor current, depending on the slip and the supply frequency, for the studied fault.

The evolution of the frequency of the fault components depends on the speed (slip) and allows the determination of the origin of the energy of the extracted fault component from the current of the studied machine, and eventually it enables the determination of the state -healthy or faulty- in which the machine is operating.

This chapter is structured as follows: section 2 examines the equations of rotor asymmetry for squirrel cage and wound rotor induction machines for the main fault components first, and then, for higher order fault components.

Section 3 develops the equations of stator asymmetry for wound rotor induction machines since the diagnosis of squirrel cage induction machines is impossible due to the need of acquiring the rotor current.

Section 4 studies the mixed eccentricity fault. The mixed eccentricity fault is independent of the topology of the machine due to its mechanical nature.

2 ROTOR ASYMMETRY

The rotor asymmetry is one of the most studied faults in the literature [34]-[60] and [73]-[95].

In the case of squirrel cage rotor induction machines, a rotor asymmetry initially does not causes serious consequences, and the machine can practically continue operating without loss in its performance. However, if a broken bar is not detected in its initial state, the fault spreads to adjacent bars and can cause a catastrophic failure, since once the asymmetry begins -broken bar- the adjacent bars to the broken bar deteriorate more quickly due to the increase of stress they must endure.

In the case of the wound rotor induction machines, as there is an asymmetry in one of the three rotor phases, a similar effect occurs, since the two healthy windings are overloaded and consequently its lifetime is reduced.

To avoid this chain effect, the detection of the rotor asymmetry in its incipient state -long before that appears directly observable symptoms- is necessary.

The rotor asymmetry causes an imbalance in the rotor currents and pulsating torques that eventually lead to a reduction in the average torque of the machine [97].

Once the rotor asymmetry has begun, a series of side effects, which cause the development of new defects, appear. For example, after the bar breakage in a squirrel cage rotor induction machine the current of adjacent bars to it can increase up to 20% from its rated value [98]. The increase of the current that those bars suffer causes overheating in the rotor that worsens the condition of the machine [97], and can even cause the bending of rotor, causing an eccentricity [99]. In addition, a rotor asymmetry also causes vibrations in the rotor, favouring the appearance of bearing faults.

2.1 SQUIRREL CAGE MACHINE

The rotor of a squirrel cage rotor induction machine is composed of a set of bars joined at both ends by two rings, called short circuit rings. The magnetic core of the rotor is composed of laminations, stacked and insulated from each other, filling the space between the bars, therefore, the only way that current flows in the rotor is through the bars themselves.

The bar breakages, -if the phenomena of interlaminar currents is neglected- are mainly caused for the following reasons [4], mainly occurring in the transient regimes of the machine (mostly in the start up):

- Thermal stresses due to starting currents and thermal overloads and imbalances that cause dilatation and mechanical stress.
- Magnetic stress due to electromagnetic forces, electromagnetic noise, vibration, unbalanced magnetic forces.
- Residual stresses.
- Environmental stress caused, for example, by pollution and abrasion of the rotor material due to moisture and corrosive chemicals.
- Mechanical stress due to laminations, fatigue, bearing failure.

The stated problems can start even during the construction of the machines as a result, for example, of a defective injection of aluminium for aluminium cast rotors, or a defective joints in the case of short circuit rings, welded or assembled together thus appearing high electrical resistance joints or porosities, resulting in hot spots on the rotor cage.

The bars breakage usually begins in the vicinity of the junction with the short circuit ring or even in the same ring, since in that area is where the mechanical stress of the structure mainly concentrate.

2.1.1 SQUIRREL CAGE ROTOR INDUCTION MACHINE: HARMONIC COMPONENT IN THE STATOR OF A HEALTHY MACHINE

In practice, despite the fact that the electric machines are fed with a purely sinusoidal voltage, the flow of fundamental current through the stator windings generates a current sheet that is not purely sinusoidal, since its configuration is not ideal since it possesses a limited number of coils distributed in the stator slots.

As a consequence of this fact, in addition to the fundamental current sheet of p pole pairs and speed $\frac{f_{red}}{p}$ revolutions per second (r.p.s.) generated by the stator, there are also harmonic current sheets of $(6\cdot k\text{-}1)\cdot p$ and $(6\cdot k\text{+}1)\cdot p$ pairs of poles, whose speeds are $\frac{-f_{red}}{(6\cdot k-1)\cdot p}$ and $\frac{f_{red}}{(6\cdot k+1)\cdot p}$ respectively.

In the squirrel cage rotor induction machines, each of the harmonic stator fields induce in the cage a field with the same number of pair of poles -since the cage has not a predefined number of pair of poles and reflects the harmonic stator fields- that turn at the same absolute speed that the main field and therefore inducing electromotive forces of fundamental frequency.

On the other hand, the currents induced in the rotor conductors -cage bars- by the fundamental stator field are a polyphase system of currents with frequency $s\cdot f_{red}$, that creates a current sheet, as in the case of the stator, has a

fundamental spatial component of p pairs of poles and also contains the harmonic components.

Thus, the fundamental component of the rotor field turns at a relative speed $\frac{s \cdot f_{red}}{p}$ r.p.s. relative to the rotor and an absolute speed $\frac{f_{red}}{p}$ r.p.s. to the stator, generating e.m.f.'s of frequency f_{red}.

Notice that the rotor winding has a very high number of phases, so as bars. The result of this high number of phases is that the orders of the harmonic components are not given by the equations $(6 \cdot k \pm 1)$ as in three-phase systems, but by equations that depend on the number of bars that lead to values much higher than the orders 5 and 7 ($k = 1$) used for the diagnosis and characteristic of the three-phase systems.

In [108] is performed a detailed analysis of the structure of the current sheet generated by a winding in a cage where it is shown that a machine with four poles with 28 bar rotors –configuration that coincides with one of the machines tested in this thesis- the frequency of the lowest frequency of harmonic component of the stator current due to the non-ideality of the winding is $(13\text{-}14 \cdot s) \cdot f_{red}$, which value is above 600 Hz for conventional slip values.

In any case, the harmonic rotor current sheets induce in the stator frequency components higher than electromagnetic harmonic components, deduced in the preceding paragraphs, and not interfering, in any case, in the diagnostic process.

The conclusion of the above considerations is that the theoretical spectrum of a healthy squirrel cage rotor induction machine is free of harmonics in the frequency band typically used for the diagnosis.

Nevertheless in practice there are always detected harmonics of small amplitudes at the characteristic frequencies of the rotor asymmetry, since due to the unavoidable tolerances of the manufacturing process is nearly impossible to build a perfectly symmetrical cage.

On the machines tested in this thesis, the amplitudes of these intrinsic harmonics were always below -55 dB for healthy machines.

2.1.2 SQUIRREL CAGE ROTOR INDUCTION MACHINES: HARMONIC COMPONENTS INDUCED IN THE STATOR BY THE EXISTENCE OF A BAR BREAKAGE

When there is a broken bar the current cannot flow through it, resulting in an imbalance of currents in the cage. Therefore, some harmonic fields, which do not exist in healthy state, raise, inducing the specific harmonic frequencies in the stator current of the machine.

2.1.2.1 ELECTROMAGNETIC HARMONIC COMPONENTS

The generation of these harmonics can be explained through the theory of the current fault introduced by Deleroi [34] in 1982. The theory of the current fault allows the analysis of the effect of a broken bar superimposing two current distributions in the rotor cage;

- A distribution that corresponds to the healthy machine state (polyphase system of currents whose frequency is $s \cdot f_{red}$).

- Other distribution caused by the fault current flowing through the broken bar that is distributed throughout the rest of bars and across the short circuit rings.

The fault current is at all times equal to the current that corresponds to the bar in a healthy state but with the opposite sign, thus, when both currents are superimposed, the total current flowing through the broken bar is zero.

The first current distribution in Fig. 11 corresponds to a squirrel cage rotor induction machine in healthy state, which causes a current sheet whose fundamental component of p pairs of poles turns at the speed $\frac{s \cdot f_{red}}{p}$ r.p.s. relative to the rotor. This current sheet also contains harmonic components of order $(6 \cdot k - 1)$ that turn in negative sequence, at the speed $\frac{-s \cdot f_{red}}{(6 \cdot k - 1) \cdot p}$ r.p.s. and harmonic components of order $(6 \cdot k + 1)$ that turn in positive sequence at the speed $\frac{s \cdot f_{red}}{(6 \cdot k + 1) \cdot p}$ r.p.s.

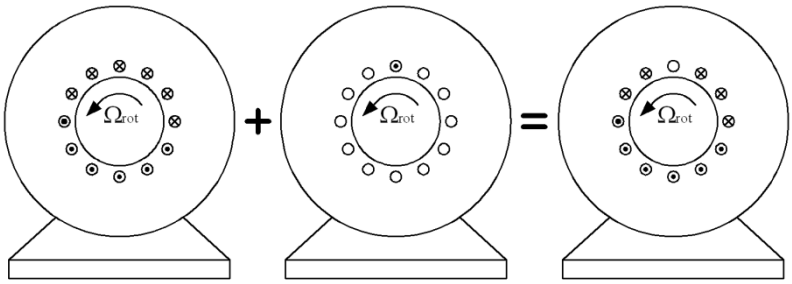

Fig. 11 Decomposition of the rotor currents according to the theory of the current fault.

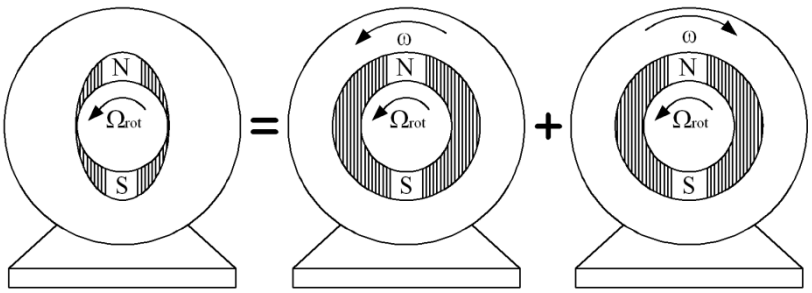

Fig. 12 Decomposition of the induction wave fixed in space by Leblanc's Theorem for the fundamental current sheet.

The second current distribution creates an induction wave with fixed position in the rotor and pulsating amplitude in time. This current sheet waveform has no symmetry of semi-wave and therefore contains harmonic components of all orders, though only the odd order components and multiple of p induce e.m.f.'s in the stator windings.

By Leblanc's Theorem (Fig. 12), each component of that oscillating wave can be decomposed into a sum of two spatial waves of current sheet with constant amplitude and equal to half of the amplitude of the original component and with electrical rotation speed constant and opposite, equal to $s \cdot f$ electrical revolutions per second (e.r.s.) and $-s \cdot f$ e.r.s.

The positive sequence components of the fault field whose order is 1 and $6 \cdot k+1$, behave exactly like the components of order p and $6 \cdot k+1$ of the current sheet caused by the current distribution of the healthy machine, not inducing new harmonic components in the stator. Applying the same reasoning, this fact may be extended to the negative sequence field fault components of order $6 \cdot k-1$.

Consequently, only the negative sequence current sheet components of order 1 and $6 \cdot k+1$ and the positive sequence current sheet components of order $6 \cdot k-1$, caused by the fault current cause new harmonics at the specific frequencies in the stator currents.

The inverse component of order 1 turns relative to the rotor at the speed $\frac{-s \cdot f_{red}}{p}$ e.r.s. and relative to the stator at $f_{rot} - \frac{s \cdot f_{red}}{p}$, so it induces in the wires of the stator e.m.f.'s of frequency equal to its absolute electrical speed

$$f_{mag}^{1} = p \cdot \left(f_{rot} - \frac{s \cdot f_{red}}{p} \right) = p \left[(1-s) \frac{f_{red}}{p} - \frac{s \cdot f_{red}}{p} \right] = (1-2 \cdot s) \cdot f_{red} \quad (1)$$

Equation (1) shows the frequency of the lower side harmonic (main electromagnetic harmonic).

The components of order $6 \cdot k-1$ that turns relative to the rotor at speeds $\frac{\pm s \cdot f_{red}}{(6 \cdot k-1) \cdot p}$ r.p.s. and relative to the stator at $f_{rot} \pm \frac{s \cdot f_{red}}{(6 \cdot k-1) \cdot p}$, so they induce in the wires of the stator e.m.f.'s of frequency equal to its absolute electrical speed

$$f_{mag}^{6 \cdot k-1} = p \cdot (6 \cdot k-1) \cdot \left(f_{rot} \pm \frac{s \cdot f_{red}}{p \cdot (6 \cdot k-1)} \right) = p \cdot (6 \cdot k-1) \cdot (1-s) \cdot \frac{f_{red}}{p} \pm s \cdot f_{red} \quad (2)$$

finally resulting in two frequency components

$$\begin{aligned} f_{mag\_+}^{6 \cdot k-1} &= \left[(6 \cdot k-1) - 6 \cdot k \cdot s \right] \cdot f_{red} \\ f_{mag\_-}^{6 \cdot k-1} &= \left[(6 \cdot k-1) - (6 \cdot k-2) \cdot s \right] \cdot f_{red} \end{aligned} \quad (3)$$

The components of order $6 \cdot k+1$ that turns relative to the rotor at speeds $\frac{\pm s \cdot f_{red}}{(6 \cdot k+1) \cdot p}$ r.p.s. and relative to the stator at $f_{rot} \pm \frac{s \cdot f_{red}}{(6 \cdot k+1) \cdot p}$, so they induce in

TABLE 2. FREQUENCY OF THE MAIN FAULT HARMONICS WITH ELECTROMAGNETIC ORIGIN CAUSED BY THE BREAKAGE OF A BAR IN SQUIRREL CAGE ROTOR INDUCTION MACHINES

Order	**Positive sequence fault field**	**Negative sequence fault field**
Order 1 (k = 0)	f_{red}	(1 - 2·s) f_{red}
Order 6·k-1, (k = 1), Order 5	(5 - 6·s)·f_{red}	(5 - 4·s)·f_{red}
Order 6·k+1, (k = 1), Order 7	(7 - 6·s)·f_{red}	(7 - 8·s)·f_{red}

the wires of the stator e.m.f.'s of frequency equal to its absolute electrical speed:

$$f_{mag}^{6\cdot k+1} = p\cdot(6\cdot k+1)\cdot\left(f_{rot} \pm \frac{s\cdot f_{red}}{p\cdot(6\cdot k+1)}\right) = p\cdot(6\cdot k+1)\cdot(1-s)\cdot\frac{f_{red}}{p} \pm s\cdot f_{red} \quad (4)$$

finally resulting in two frequency components

$$\boxed{\begin{aligned} f_{mag\_+}^{6\cdot k+1} &= \left[(6\cdot k+1)-6\cdot k\cdot s\right]\cdot f_{red} \\ f_{mag\_-}^{6\cdot k+1} &= \left[(6\cdot k+1)-(6\cdot k+2)\cdot s\right]\cdot f_{red} \end{aligned}} \quad (5)$$

Table 2 summarizes the main frequency fault harmonics, with electromagnetic origin, for values of k = 0 and k = 1.

2.1.2.2 ELECTROMAGNETIC-MECHANICAL HARMONIC COMPONENTS

The rotor asymmetry, besides the electromagnetic components, introduces another family of components whose frequency corresponds to the equation [109]

$$f_{mec}^{k} = (1-2\cdot k\cdot s)\cdot f_{red} \text{ con } k = 1,2,3,... \quad (6)$$

The origin of these harmonics are the speed and torque oscillations caused by the electromagnetic harmonic components, derived in the previous section, whose justification is found in [109]: the harmonic fault component of frequency (1-2·s)·f_{red} (lower side harmonic) generates a rotating field in the stator of speed $(1-2\cdot s)\cdot\frac{f_{red}}{p}$ that reacts with the main rotor rotating field whose speed is $\frac{f_{red}}{p}$. That results in a pulsating torque of frequency 2·s·f_{red} that produces an speed oscillation and current modulation that modules the amplitude of the fundamental current sheet with a frequency 2·s·f_{red} generating a new series of harmonic whose origin is electromagnetic-mechanical.

The mathematical proof of the generation of the electromagnetic-mechanical harmonic components, consequence of the oscillation of the machine speed caused by the torque oscillations, is shown below.

When there is a bar breakage in one of the bars of the cage of the machine, there is a modulation in the current of the machine, leading to the fault current:

$$i_f(t) = A'(t) \cdot \cos(\omega \cdot t + \varphi) \tag{7}$$

with $A'(t) = A \cdot (1 + \cos(2 \cdot \pi \cdot 2 \cdot s \cdot f_{red} \cdot t + \varphi'))$ y $\omega = 2 \cdot \pi \cdot f_{red}$.

Then, equation (7) changes to:

$$i_f(t) = A \cdot (1 + \cos(2 \cdot \pi \cdot 2 \cdot s \cdot f_{red} \cdot t + \varphi')) \cdot \cos(2 \cdot \pi \cdot f_{red} \cdot t + \varphi) \tag{8}$$

applying trigonometric relations lead to:

$$i_f(t) = A \cdot (\cos(2 \cdot \pi \cdot f_{red} + \varphi) + \cos(2 \cdot \pi \cdot (1 \pm 2 \cdot s) \cdot f_{red} \cdot t + (\varphi \pm \varphi'))) \cdot \tag{9}$$

that is, there are two fault harmonics, with electromagnetic-mechanical origin at a distance of $2 \cdot s \cdot f_{red}$ of the fundamental harmonic, caused by the torque oscillation due to the bar breakage, eventually causing the speed oscillation. These components will be referred to as electromechanical components hereafter.

The above reasoning can be applied to fault components of frequency $(1-2 \cdot s) \cdot f_{red}$ and $(1+2 \cdot s) \cdot f_{red}$. The amplitude of these components is also modulated with the frequency $2 \cdot s \cdot f_{red}$ imposed by the speed oscillation and therefore each of them will originate two harmonic components whose frequencies differ $\pm 2 \cdot s \cdot f_{red}$ from the frequency of the fault harmonics that originate them, appearing two new harmonic whose origin is electromechanical at the frequencies $(1 \pm 4 \cdot s) \cdot f_{red}$. Repeating this reasoning for the new harmonics, it is justified the onset of the series of harmonics $(1 \pm 2 \cdot k \cdot s) \cdot f_{red}$.

Notice that the frequency expression of one of the electromechanical main fault components coincides with the frequency equation of the electromagnetic component, being impossible their split in the frequency spectrum. The amplitude of the electromechanical components is strongly reduced when k increases.

Table 3 summarizes the components associated with the rotor asymmetry whose origin is electromechanical.

TABLE 3. FREQUENCIES OF THE MAIN FAULT HARMONIC WITH ELECTROMECHANICAL ORIGIN, CAUSED BY THE BAR BREAKAGE IN A SQUIRREL CAGE ROTOR INDUCTION MACHINE

Order	**Fault component**	
Order 1 (k = 1)	$(1 - 2 \cdot s)\, f_{red}$	$(1 + 2 \cdot s)\, f_{red}$
Order 2, (k = 2)	$(1 - 4 \cdot s) \cdot f_{red}$	$(1 + 4 \cdot s) \cdot f_{red}$
Order 3, (k = 3)	$(1 - 6 \cdot s) \cdot f_{red}$	$(1 + 6 \cdot s) \cdot f_{red}$

2.1.3 SUMMARY AND CONCLUSIONS OF THE HEALTHY AND FAULTY FREQUENCIES FOR SQUIRREL CAGE ROTOR INDUCTION MACHINES

The summary of the harmonic components in the stator current that can be seen for any squirrel cage rotor induction machine is shown in Table 4, classified according to their origin, electromagnetic or electromechanical the status of the machine, healthy or faulty and the order of the component.

The conclusions drawn from the study of fault expressions for a squirrel cage rotor induction machine when there is broken bar are the following:

Firstly, harmonic components should not theoretically exist in the zone of the spectrum commonly used for diagnosis ($f \leq 500$ Hz) when the machine is healthy, although in practice small amplitude components are detected at the specific frequencies of the rotor asymmetry, due to the unavoidable constructive asymmetries.

When a bar breakage occurs, due to the negative sequence magnetic field that appears in the machine, the amplitudes of the harmonic components of electromagnetic origin increase.

Simultaneously to this process, there is the emergence of a new harmonic components, whose origin is electromechanical, that are only present when the machine is undergoing a rotor asymmetry.

The conclusions drawn are validated by the observation of different stator currents spectrums, comparing the spectrum of a healthy machine with the spectrum resulting from the analysis of the current of a machine with a broken bar.

Fig. 13 shows the Fourier spectrum of the stator current in the area near the fundamental harmonic of the current for a squirrel cage rotor induction machine with a broken bar (red colour) and the Fourier spectrum of the stator current for a squirrel cage rotor induction machine in healthy state (green colour) functioning as a motor.

TABLE 4. OBSERVABLE HARMONIC COMPONENTS IN THE STATOR CURRENT FOR A SQUIRREL CAGE ROTOR INDUCTION MACHINE IN HEALTHY AND FAULTY STATE (ROTOR ASYMMETRY)

	Origin	**Main**	**1st High order harmonic**	**2nd High order harmonic**
Healthy	Magnetic	f_{red}	Do not exist	Do not exist
	Mechanical	Do not exist	Do not exist	Do not exist
Faulty	Magnetic	f_{red}	$(5 - 6\cdot s)\cdot f_{red}$	$(7 - 6\cdot s)\cdot f_{red}$
	Magnetic	$f_{red}\cdot(1-2\cdot s)$	$(5 - 4\cdot s)\cdot f_{red}$	$(7 - 8\cdot s)\cdot f_{red}$
	Mechanical	$f_{red}\cdot(1\pm 2\cdot s)$	$(1 \pm 4\cdot s)\cdot f_{red}$	$(1 \pm 6\cdot s)\cdot f_{red}$

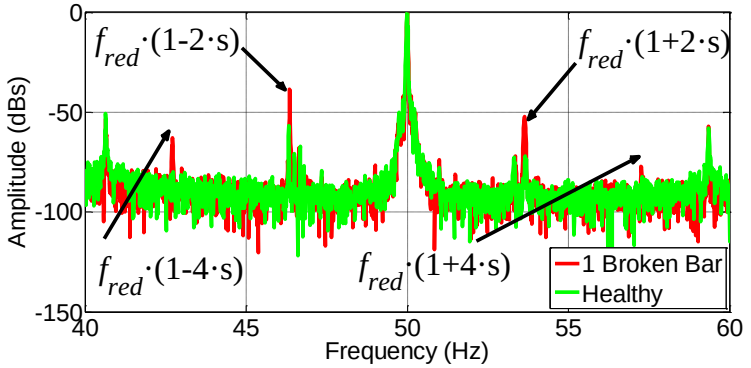

Fig. 13 Fourier spectrum of a squirrel cage rotor induction machine working as motor with a broken (red) and healthy state (green) for the main fault components.

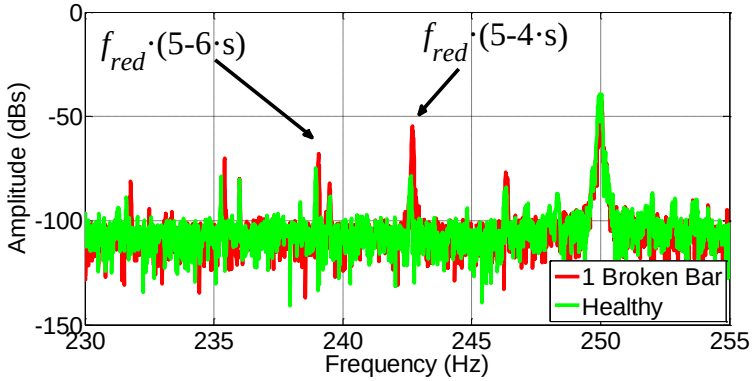

Fig. 14 Fourier spectrum of a squirrel cage rotor induction machine working as motor with a broken (red) and healthy state (green) for the fault components of order 5 (1st high order harmonic)

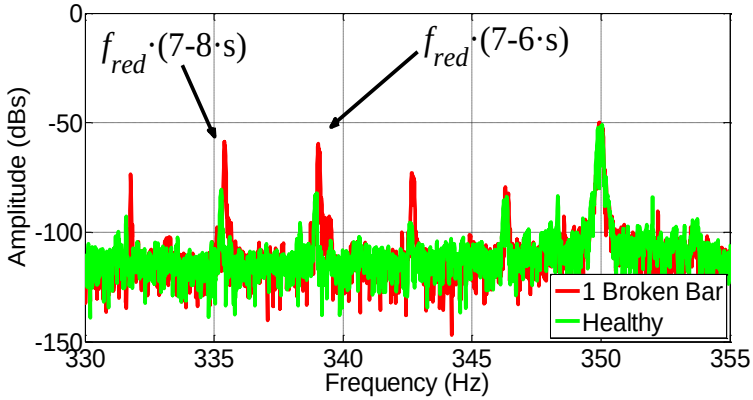

Fig. 15 Fourier spectrum of a squirrel cage rotor induction machine working as motor with a broken (red) and healthy state (green) for the fault components of order 7 (2nd high order harmonic)

Fig. 13 shows the existence of both electromagnetic $f_{red}\cdot(1-2\cdot s)$ and electromechanical $f_{red}\cdot(1+2\cdot s)$ harmonics. Moreover, there is also the fundamental current harmonic located at the 50 Hz and the electromechanical harmonics electromechanical $(1-4\cdot s)\cdot f_{red}$, $(1+4\cdot s)\cdot f_{red}$.

Fig. 14 and Fig. 15 show the high order harmonics for squirrel cage rotor induction machines, frequency components $(5-4\cdot s)\cdot f_{red}$, $(5-6\cdot s)\cdot f_{red}$ (first high order harmonic) are shown in Fig. 14 and $(7-6\cdot s)\cdot f_{red}$, $(7-8\cdot s)\cdot f_{red}$ (second high order harmonic) are shown in Fig. 15, respectively.

The first conclusion to be drawn from the analysis of Fig. 13 is that the main characteristic harmonics of rotor asymmetry are detectable when the machine is healthy since they are present either when the machine is healthy and with a broken bar. This fact is consequence of the manufacturing tolerances that the electrical machines are subjected.

The second conclusion from the analysis of Fig. 13 is the increase that occurs in the amplitude of both the electromagnetic and electromechanical harmonics, as it was previously demonstrated, when the machine is subjected to a broken bar.

Notice that, usually, the electromagnetic harmonic is known in the literature as the LSH (Lower Slot Harmonic) since the conducted studies are on machines working as motors. However, the position of the electromagnetic harmonic is a function of the operating mode of the machine and it can be located above or below the fundamental frequency.

2.2 WOUND ROTOR INDUCTION MACHINE

The main feature of the wound rotor induction machines is that their rotors have a three-phase winding as any asynchronous induction machine has in its stator.

The phases of the rotor windings are usually connected in star, connecting the free ends of the windings through slip rings housed on the rotor shaft.

The rotor windings are short-circuited through brushes located on the slip rings and, therefore, the rotor currents are accessible. In addition, it is possible to change the resistance of the rotor windings in order to change the torque-speed feature of the machine by connecting additional resistors.

Wound rotor machines are more expensive than squirrel cage rotor induction machines and also require more maintenance due to the use of brushes and slip rings. Because of its higher cost of maintenance, wound rotor machines are less used in the industry.

However, in the field of wind energy, the rotor wound induction machines are growing [112] due to the advantages of the access to the rotor currents, fact that allows a better control of the machine.

A rotor asymmetry in a wound rotor induction machine rotor becomes when one or more of one of the coils of the rotor winding, due to a failure, are short-circuited or, due to failures at the connections between the windings or in the contact brush-ring an imbalance in the induced rotor voltages of the electric machine occurs.

That rotor imbalance rotor causes an unbalanced system of currents in the rotor that results in the appearance of a negative sequence current that creates

new rotating magnetic fields that rise new harmonic components of specific frequency in the current of the stator.

Since the use in industry of the wound rotor induction machines is low, the theoretical analysis of the fault components for this type of machine is little studied in the literature. In fact, given the nature of the machine, it is usually adopted the fault expressions developed for squirrel cage rotor induction machines as valid expressions to model the behaviour of the harmonic components in the rotor of the wound rotor induction machines.

In the following subsections, it is carried out the theoretical analysis of the harmonic components in the stator current for wound rotor induction machines, when they are in healthy and faulty state, similar to the analysis carried out for the squirrel cage rotor induction machines.

2.2.1 WOUND ROTOR INDUCTION MACHINE: HARMONIC COMPONENTS IN THE STATOR CURRENT FOR HEALTHY MACHINE

In the same way than for the squirrel cage rotor induction machines, the flow of fundamental component of the stator current generates a current sheet of p pairs of poles that turns at $\frac{f_{red}}{p}$ r.p.s. and also current sheets of $(6\cdot k\text{-}1)\cdot p$ pairs of poles that turns at $\frac{-f_{red}}{(6\cdot k-1)\cdot p}$ r.p.s. and current sheets of $(6\cdot k\text{+}1)\cdot p$ pairs of poles that turns at $\frac{f_{red}}{(6\cdot k+1)\cdot p}$ since the stator windings are not ideal due to their finite distribution (housed in a finite number of slots in the stator).

The fundamental stator current sheet and current sheets of $(6\cdot k\pm 1)\cdot p$ pairs of poles generate a series of harmonics in the stator current. The study of the harmonics caused by the stator current sheets is discussed in the following points.

2.2.1.1 HARMONICS CAUSED BY THE FUNDAMENTAL STATOR CURRENT SHEET

The fundamental stator current sheet turns relative to the rotor rotates at a relative speed of $\frac{f_{red}}{p} - f_{rot}$ r.p.s. and induces currents of frequency $\left(\frac{f_{red}}{p} - f_{rot}\right)\cdot p$ in the rotor wires.

These currents generate in the rotor a fundamental current sheet of p pairs of poles that turns relative to the rotor at $p\cdot\frac{\frac{f_{red}}{p}-f_{rot}}{p} = \frac{f_{red}}{p} - f_{rot}$ r.p.s. and relative to the stator at $f_{rot} + \frac{f_{red}}{p} - f_{rot} = \frac{f_{red}}{p}$,, inducing currents in the stator whose frequency is $p\cdot\frac{f_{red}}{p} = f_{red}$ Hz.

In addition, the rotor currents generate two families of harmonic current sheets:

– With $(6\cdot k\text{-}1)\cdot p$ pairs of poles, that turns in negative sequence at speed $-p\cdot\frac{\frac{f_{red}}{p}-f_{rot}}{(6\cdot k-1)\cdot p}$ r.p.s. relative to the rotor and at $f_{rot} - p\cdot\frac{\frac{f_{red}}{p}-f_{rot}}{(6\cdot k-1)\cdot p}$ relative

to the stator, inducing e.m.f.'s in the stator wires whose frequencies are equal to

$$f'_{mag} = (6\cdot k-1)\cdot p\cdot\left[f_{rot} - p\cdot\frac{\frac{f_{red}}{p} - f_{rot}}{(6\cdot k-1)\cdot p}\right] = \left[(6\cdot k-1) - 6\cdot k\cdot s\right]\cdot f_{red} \quad (10)$$

– With $(6\cdot k+1)\cdot p$ pairs of poles, that turns in positive sequence at speed $p\cdot\frac{\frac{f_{red}}{p}-f_{rot}}{(6\cdot k+1)\cdot p}$ r.p.s. relative to the rotor and at $f_{rot} + p\cdot\frac{\frac{f_{red}}{p}-f_{rot}}{(6\cdot k+1)\cdot p}$ relative to the stator, inducing e.m.f.'s in the stator wires whose frequencies are equal to

$$f''_{mag} = (6\cdot k+1)\cdot p\cdot\left[f_{rot} + p\cdot\frac{\frac{f_{red}}{p} - f_{rot}}{(6\cdot k+1)\cdot p}\right] = \left[(6\cdot k+1) - 6\cdot k\cdot s\right]\cdot f_{red} \quad (11)$$

Table 5 summarizes the frequencies of the main harmonic of electromagnetic origin in healthy wound rotor induction machines.

2.2.1.2 HARMONIC GENERATED BY THE HARMONIC STATOR CURRENT SHEETS

In addition to the fundamental current sheet of p pairs of poles, when the fundamental current flows through the stator windings generates in the air gap harmonic current sheets of $(6\cdot k\text{-}1)\cdot p$ and $(6\cdot k\text{+}1)\cdot p$ pairs of poles.

The current sheets of $(6\cdot k\text{-}1)\cdot p$ pairs of poles turns in negative sequence to the field caused by the fundamental current at speed $\frac{-f}{(6\cdot k-1)\cdot p}$ r.p.s. relative to the stator and at $-f_{rot} - \frac{f_{red}}{(6\cdot k-1)\cdot p}$ r.p.s. relative to the rotor. That current sheet induces in the rotor wires currents whose frequency is $(6\cdot k-1)\cdot p\cdot\left(-f_{rot} - \frac{f_{red}}{(6\cdot k-1)\cdot p}\right) = -(6\cdot k-1)\cdot p\cdot f_{rot} - f_{red}$ Hz.

These currents generate a fundamental current sheet of p pairs of poles in the rotor, that turns in positive sequence relative to the rotor (negative sequence to the inductive field $(6\cdot k\text{-}1)\cdot f_{red}$), at speed $\frac{-(6\cdot k-1)\cdot p\cdot f_{rot} + f_{red}}{p}$ and relative to the stator at a speed equal to $f_{rot} - \frac{(6\cdot k-1)\cdot p\cdot f_{rot} + f_{red}}{p}$.

TABLE 5. FREQUENCIES OF THE MAIN ELECTROMAGNETIC HARMONICS CAUSED BY THE FUNDAMENTAL ROTOR CURRENT SHEET IN HEALTHY WOUND ROTOR INDUCTION MACHINES

Order	**Healthy machine**
Order 1	f_{red}
Order $6\cdot k$-1, (k = 1), Order 5	$(5 - 6\cdot s)\cdot f_{red}$
Order $6\cdot k$+1, (k = 1), Order 7	$(7 - 6\cdot s)\cdot f_{red}$

Finally, the rotor current sheet of p pairs of poles induces e.m.f.'s in the stator wires whose frequencies are

$$f'^{(6\cdot k-1)\cdot p}_{mag} = p\cdot\left[f_{rot} - \frac{(6\cdot k-1)\cdot p\cdot f_{rot} + f_{red}}{p}\right] = \left[(6\cdot k.-2)\cdot s - (6\cdot k-1)\right]\cdot f_{red} \quad (12)$$

Current sheets of $(6\cdot k+1)\cdot p$ pairs of poles turn in negative sequence to the field caused by the fundamental current at a speed rotate in opposite directions to the field produced by the current speed $\frac{f}{(6\cdot k+1)\cdot p}$ r.p.s. relative to the stator and at $f_{rot} + \frac{f_{red}}{(6\cdot k+1)\cdot p}$ r.p.s. relatively to the rotor. That current sheet induces current in the rotor wires currents whose frequencies are $(6\cdot k+1)\cdot p\cdot\left(f_{rot} + \frac{f_{red}}{(6\cdot k+1)\cdot p}\right) = -(6\cdot k+1)\cdot p\cdot f_{rot} + f_{red}$ Hz.

These currents generate a fundamental current sheet of p pairs of poles in the rotor, that turns in positive sequence relatively the rotor (negative sequence to the inductive field $(6\cdot k\text{-}1)\cdot f_{red}$), at a speed $\frac{(6\cdot k+1)\cdot p\cdot f_{rot} - f_{red}}{p}$ relative to the stator at a speed equal to $f_{rot} + \frac{(6\cdot k+1)\cdot p\cdot f_{rot} - f_{red}}{p}$.

Finally, the rotor current sheet of p pairs of poles induces e.m.f.'s, in the stator wires, whose frequencies are

$$f'^{(6\cdot k+1)\cdot p}_{mag} = p\cdot\left[f_{rot} + \frac{(6\cdot k+1)\cdot p\cdot f_{rot} - f_{red}}{p}\right] = \left[(6\cdot k.+1) - (6\cdot k+2)\cdot s\right]\cdot f_{red} \quad (13)$$

Table 6 summarizes the frequencies of the main electromagnetic harmonic in healthy wound rotor induction machines caused by the harmonic rotor current sheets.

TABLE 6. FREQUENCIES OF THE MAIN ELECTROMAGNETIC HARMONICS CAUSED BY THE ROTOR CURRENT SHEETS IN HEALTHY WOUND ROTOR INDUCTION MACHINES

Order	**Healthy machine**
Order $6\cdot k$-1, (k = 1), Order 5	$(4\cdot s$ - 5$)\cdot f_{red}$
Order $6\cdot k$+1, (k = 1), Order 7	$(7$ - $8\cdot s)\cdot f_{red}$

2.2.2 WOUND ROTOR INDUCTION MACHINES: HARMONIC STATOR CURRENT COMPONENTS FOR ROTOR ASYMMETRY

When there is an asymmetry in the windings of a wound rotor induction machine an unbalanced system of currents in the rotor of the electric machine is induced, that unbalance is reflected by the appearance of some harmonic components in the stator current.

The mechanism of generation of these harmonics is similar to the one already discussed for squirrel cage rotor induction machines, since the Fortescue's Theorem states that any n-phase unbalanced system can be written as the sum of *n* balanced systems according to the superposition principle.

In a three phase system, the result of the application of the Fortescue's Theorem leads to that any unbalanced three-phase system can be decomposed as the sum of three balanced three-phase system with one of them rotating in positive sequence, the other in negative sequence, and a last system of zero sequence that oscillates but not turns (see Fig. 16)

In order to determine the harmonic components in the stator current caused by the imbalance in the rotor currents, it will be enough to study each one of the three balanced systems because of the application of Fortescue's Theorem to the unbalanced three-phase system of the rotor currents.

The study is individually performed for each sequence, determining the observable harmonic components due to the stator current magnetic field caused by the positive, negative and zero sequence, in which the unbalanced three-phase currents system of the rotor can be decomposed.

The fundamental positive sequence of the rotor current system (whose frequency is $s \cdot f_{red}$) generates a current sheet whose structure is identical to that generated by the fundamental current system of the healthy machine, then it induces in the stator currents the same components that appear for healthy machine whose frequencies are f_{red}, $[(6 \cdot k\text{-}1)\text{-}6 \cdot k \cdot s] \cdot f_{red}$ and $[(6 \cdot k\text{+}1)\text{-}6 \cdot k \cdot s] \cdot f_{red.}$

The fundamental negative sequence of the rotor current system (whose frequency is $s \cdot f_{red}$) generates a current sheet with the same harmonic rotating components that the negative sequence fault field of a squirrel cage rotor induction machine with a broken bar. Hence it induces in the stator currents the same components than the fault of the negative sequence field of the squirrel cage rotor induction machine whose frequencies are $(1\text{-}2 \cdot s) \cdot f_{red}$, $[(6 \cdot k\text{+}1)\text{-}(6 \cdot k\text{+}2) \cdot s] \cdot f_{red}$ and $[(6 \cdot k\text{-}1)\text{-}(6 \cdot k \cdot \text{-}2) \cdot s] \cdot f_{red.}$

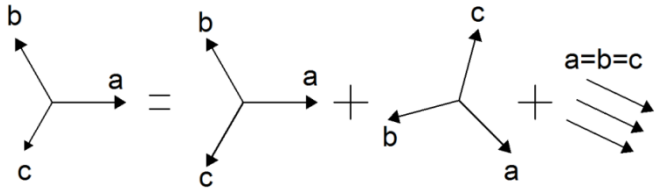

Fig. 16 Decomposition of an unbalanced three-phase system by Fortescue's Theorem, in a balanced system of a positive sequence system, another of negative sequence current and a third one oscillating of zero sequence.

Since the fundamental fault component is modulated in amplitude at a frequency of $2 \cdot s \cdot f_{red}$, as it was discussed in section 2.1.2, there will be induced new pairs of harmonics of electromechanical origin, as it was the case of the main fault components, at a distance $\pm 2 \cdot s \cdot f_{red}$ of the position of the electromagnetic harmonics, generating new pairs of harmonics of electromechanical origin whose frequencies in the stator current spectrum is shown in equations (14) and (15), for the case of the current sheet of order $6 \cdot k$-1, whereas equations (16) and (17) show the frequencies of the components caused by the fault current sheet of order 6 k+1.

$$f_{rot\_mec-}^{est\_6k-1} = f_{red} \cdot \left[(6 \cdot k - 1) - (6 \cdot k - 2) \cdot s \right] \quad (14)$$

$$f_{rot\_mec+}^{est\_6k-1} = f_{red} \cdot \left[(6 \cdot k - 1) - (6 \cdot k + 2) \cdot s \right] \quad (15)$$

$$f_{rot\_mec-}^{est\_6k+1} = f_{red} \cdot \left[(6 \cdot k + 1) - (6 \cdot k - 2) \cdot s \right] \quad (16)$$

$$f_{rot\_mec+}^{est\_6k+1} = f_{red} \cdot \left[(6 \cdot k + 1) - (6 \cdot k + 2) \cdot s \right] \quad (17)$$

Notice that the value of the harmonic components governed by (14) and (17), whose origin is electromechanical, coincide with the harmonics components of electromagnetic origin, as it was the case for the main harmonic fault components, being impossible to split them.

Finally, the study of the zero sequence component determines that it does not cause any harmonics in the stator current spectrum since the rotors of the wound rotor induction machines are usually connected in star, preventing the zero sequence component from being established in the rotor windings.

2.2.3 SUMMARY AND CONCLUSIONS OF THE FREQUENCIES FOR HEALTHY AND FAULTY MACHINE FOR WOUND ROTOR INDUCTION MACHINES

The summary of the equations that govern the different fault components in the stator current of a wound rotor induction machine in a healthy state and with a rotor asymmetry are shown in Table 7.

If the fault equations for a squirrel cage rotor induction machine (Chapter III, section 2.1.3 Table 4) are compared with the fault equations for the wound rotor induction machine (Table 7) for the fundamental fault components is concluded that, although the generating and propagating mechanism of the failure is different for both machines due to their different topology, the frequency equations of the harmonic components of the stator current coincide.

This fact allows the extrapolation of all conclusions stated and discussed in section 2.1.3 for the case in which the machine has a wound rotor.

The particularization of the equations shown in Table 7 for $k = 1$ is shown in Table 8.

Finally, as in the case of the squirrel cage rotor induction machine, the theoretical results from the analysis of the magnetic fields created when the machine is in a healthy and faulty state are validated by several experimental results, showing the Fourier spectrum of the stator currents of a wound rotor induction machine working as a generator.

TABLE 7. SUMMARY OF THE STATOR CURRENT HARMONICS INDUCED BY THE ROTOR CURRENT IN HEALTHY AND FAULTY STATE (ROTOR ASYMMETRY) FOR A WOUND ROTOR INDUCTION MACHINE

	Origin	**Order 1**	**Order**	**Order 6·k-1**	**Order 6·k+1**
Healthy	Magnetic	f_{red}	Do not	$f_{red}\cdot\left[(6\cdot k-1)-6\cdot k\cdot s\right]$	$f_{red}\cdot\left[(6\cdot k+1)-6\cdot k\cdot s\right]$
	Mechanical	Do not exist	Do not	Do not exist	Do not exist
Faulty	Magnetic	f_{red}	Do not	$f_{red}\cdot\left[(6\cdot k-1)-6\cdot k\cdot s\right]$	$f_{red}\cdot\left[(6\cdot k+1)-6\cdot k\cdot s\right]$
	Magnetic	$f_{red}\cdot(1-2\cdot s)$	Do not	$f_{red}\cdot\left[(6\cdot k-1)-(6\cdot k-2)\cdot s\right]$	$f_{red}\cdot\left[(6\cdot k+1)-(6\cdot k+2)\cdot s\right]$
	Mechanical	$f_{red}\cdot(1\pm 2\cdot k\cdot s)$	Do not	$f_{red}\cdot\left[(6\cdot k-1)-(6\cdot k\pm 2)\cdot s\right]$	$f_{red}\cdot\left[(6\cdot k+1)-(6\cdot k\pm 2)\cdot s\right]$

TABLE 8. PARTICULARIZATION OF THE STATOR FAULT HARMONICS ($K = 1$) IN HEALTHY AND FAULTY STATE (ROTOR ASYMMETRY) FOR WOUND ROTOR INDUCTION MACHINES

	Origin	**Order 1**	**Order 3·k**	**Order 6·k-1**	**Order 6·k+1**
Healthy	Magnetic	f_{red}	Do not exist	$f_{red}\cdot(5-6\cdot s)$	$f_{red}\cdot(7-6\cdot s)$
	Mechanical	Do not exist	Do not exist	Do not exist	Do not exist
Faulty	Magnetic	f_{red}	Do not exist	$f_{red}\cdot(5-6\cdot s)$	$f_{red}\cdot(7-6\cdot s)$
	Magnetic	$f_{red}\cdot(1-2\cdot s)$	Do not exist	$f_{red}\cdot(5-4\cdot s)$	$f_{red}\cdot(7-8\cdot s)$
	Mechanical	$f_{red}\cdot(1\pm 2\cdot s)$	Do not exists	$f_{red}\cdot(5-4\cdot s)$ $f_{red}\cdot(5-8\cdot s)$	$f_{red}\cdot(7-4\cdot s)$ $f_{red}\cdot(7-8\cdot s)$

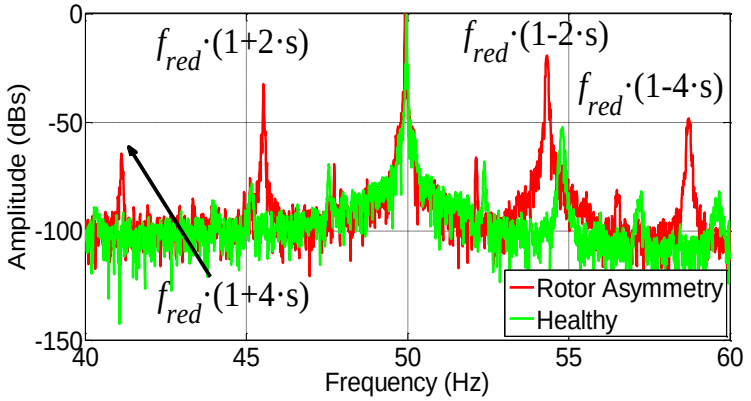

Fig. 17 Fourier spectrum of a wound rotor induction machine working as generator with a rotor asymmetry (red) and healthy state (green) for the main fault components.

Fig. 17 shows the Fourier spectrum of the stator current in the zone near the fundamental current harmonic, for a wound rotor induction machine with a rotor asymmetry (red colour) and the Fourier spectrum of the stator current for a healthy wound rotor asynchronous machine (green colour) working as a generator.

Fig. 17shows the existence of electromagnetic harmonic $f_{red}\cdot(1-2\cdot s)$, such as the electromechanical harmonics, $f_{red}\cdot(1+2\cdot s)$, $f_{red}\cdot(1+4\cdot s)$ y $f_{red}\cdot(1-4\cdot s)$ as it has previously been justified in the theoretical analysis. At the frequency of 50 Hz is seen the fundamental current stator harmonic.

The conclusions drawn from the analysis of Fig. 17 are the same as those discussed in the analysis Fig. 13. This fact is not surprising since the expressions of the harmonic components, for both squirrel cage rotor induction machine and wound rotor induction machine are identical.

However, the most outstanding fact is shown in Fig. 17, when it is compared with Fig. 13, is that the amplitude of the harmonic on the right of the fundamental current component of current is greater than the amplitude of the harmonic set to the left of the fundamental current component, which does not occur with the harmonics shown in Fig. 13. That is due to the negative slip to which the machine is subjected when is working as generator, causing that the electromagnetic and electromechanical fault harmonic swap their positions in the current spectrum.

This fact opens a possible new discussion on the nomenclature of these harmonics, since in the technical literature are known as side fault harmonics of rotor asymmetry rotor, and there is no distinction among them, what from the point of view of the author is little rigorous and may mislead in some specific cases.

Fig. 18 shows the harmonics located near the area of influence of the 5th order harmonic or first harmonic of order $6\cdot k$-1. Fig. 18 depicts the slight increase in amplitude of the electromagnetic harmonic due to healthy current sheet $f_{red}\cdot(5-6\cdot s)$, whereas the electromagnetic fault harmonic $f_{red}\cdot(5-4\cdot s)$, and the electromechanical fault harmonic electromechanical $f_{red}\cdot(5-8\cdot s)$,

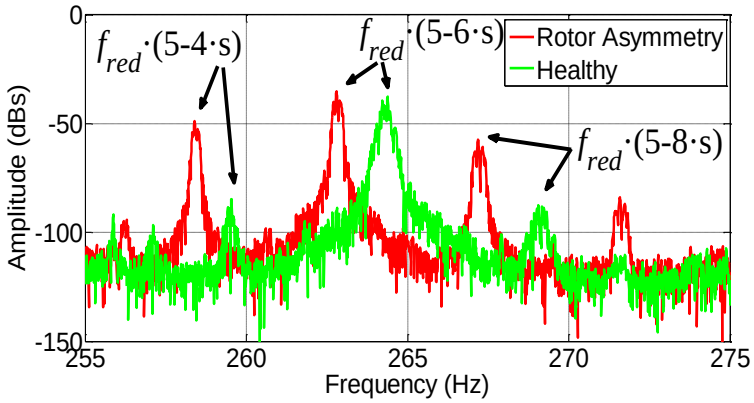

Fig. 18 Fourier spectrum of a wound rotor induction machine working as generator with a rotor asymmetry (red) and healthy state (green) for the first high order harmonic of order $6\cdot k$-1.

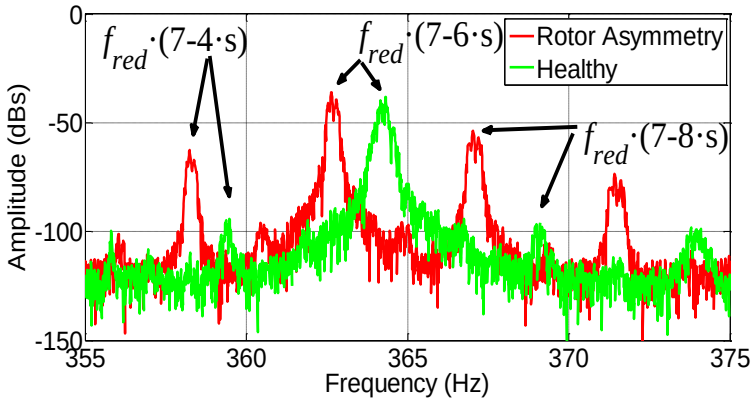

Fig. 19 Fourier spectrum of a wound rotor induction machine working as generator with a rotor asymmetry (red) and healthy state (green) for the first high order harmonic of order $6 \cdot k+1$.

increase their amplitudes noticeably, being the amplitude of the electromagnetic harmonic greater than the amplitude of the electromechanical harmonic allowing the diagnosis of the electrical machine through the study of these components.

Finally, in Fig. 19 are shown the harmonics located near the area of influence of the 7th order harmonic or first harmonic of order $6 \cdot k+1$. The considerations for the harmonics of order $6 \cdot k-1$ are valid for the harmonics of order $6 \cdot k+1$, where the electromagnetic harmonic is detected in both healthy and faulty state and it is governed by the expression $f_{red} \cdot (7-6 \cdot s)$, whereas the electromagnetic fault harmonic is governed by $f_{red} \cdot (7-8 \cdot s)$, and the electromechanical harmonic by $f_{red} \cdot (7-4 \cdot s)$.

3 STATOR ASYMMETRY

The stator asymmetry is considered one of the most difficult faults to be successfully diagnosed before the complete destruction of the stator winding [7].

The difficulty of the detection of the stator asymmetry fault has prompted the development of several diagnostic techniques using the stator current [7], [8], [12], [14], [16], [17], with off-line techniques [10], [11], through the rotor current [13] and other techniques such as stray flux [15], [18].

Most of the developed techniques for the diagnosis of the stator asymmetry include the use of one stator current. This is due to the reduced use of wound rotor induction machines and the impossibility of acquiring the current circulating through the cage of a squirrel cage rotor induction machine.

However, with the massive installation of wind turbines with doubly fed induction machines, the access to the rotor current is possible, encouraging to the development of new diagnostic techniques through its use. An example of this is the technique introduced in [13].

One goal of this thesis is to develop a diagnostic technique for electrical machines operating in non-stationary stochastic regimes, measuring the rotor current for the diagnosis of the stator asymmetry.

Clearly and given the constructive restrictions of squirrel cage rotor induction machines, the technique to be developed is only feasible for wound rotor induction machines.

The drawback of the development of a diagnostic technique for an unique specific group of machines is greatly overcome by the added value of the development of a technique that detects stator asymmetries in a type of machine that, given their power features and operating requirements (wind generators) has an increasingly importance from the industrial and economic point of view.

Thus, the study of the stator asymmetry fault will be focused on the diagnosis of the wound rotor induction machines.

A stator asymmetry in a wound rotor induction machine occurs when one or more of one of the turns of one of the stator windings of the machine cannot let the current flow through them. That causes an imbalance in the stator currents, inducing specific harmonics in the rotor windings.

An imbalance in any three phase system can be decomposed into three-phase balanced systems, one of positive sequence, another of negative sequence and one of zero sequence by the Fortescue's Theorem as it was already discussed in the previous section.

Each one of the different three-phase systems computed by Fortescue's Theorem induces a series of harmonics that appear in the spectrum of the rotor currents.

Therefore, in order to know the state of the electrical machine at any instant through the analysis of the rotor current, it must be known the value of the fault harmonics in healthy and faulty state in order to determine, by comparison, which harmonics are significant enough to perform the diagnose of the machine.

In the following sections this analysis is carried out, firstly studying the harmonics induced in the rotor current due to the magnetic field in the air gap caused by the fundamental current component in stator windings in healthy state.

Once this study has been carried out, there will be analysed the performance of the machine in front of the imbalance in the stator windings. The imbalance in them will induce new harmonics in the rotor currents, allowing the diagnosis of the electric machine diagnosed through the monitoring of such components.

3.1 INDUCED FREQUENCIES IN THE ROTOR DUE TO THE STATOR CURRENT IN HEALTHY STATE

It has already been stated that in practice, the current sheet or magnetic voltage wave in the air gap of electric machines is not merely sinusoidal which entails that it possesses an intrinsic content in harmonics. Therefore, it is expected that the induced currents in the rotor windings contain at least the same amount of harmonics than in the original stator current sheet.

If it is considered that a random electric machine in healthy state, the currents flowing through its stator windings will produce a three-phase balanced currents system that will cause a fundamental current sheet of p pairs of pole and turning at f_{red}/p and a series of harmonic current sheets, consequence of the non-ideal configuration of the stator windings. The frequencies that these rotating fields induce in the rotor wires were deduced in 2.2.1 resulting $s \cdot f_{red}$, $[(6 \cdot k\text{-}1) \cdot s\text{-}6 \cdot k] \cdot f_{red}$ and $[(6 \cdot k\text{+}1) \cdot s\text{-}6 \cdot k] \cdot f_{red}$ Hz respectively induced by the fundamental current sheet, and by the harmonic sheets of order $6 \cdot k$- 1 y $6 \cdot k$+1.

3.2 INDUCED FREQUENCIES IN THE ROTOR WINDING DUE TO THE STATOR CURRENT IN FAULTY STATE

When a fault occurs in one of the stator windings of an electrical machine, its symmetry is lost and thus the balanced three-phase current system in the stator becomes an unbalanced three-phase system.

This unbalanced current system can be decomposed by the Fortescue's Theorem in three balanced fields, one with positive sequence, another with negative sequence and a third one of zero sequence.

The magnetic field corresponding to the current positive sequence of the decomposition of the symmetrical components produces the same harmonics that would be produced in healthy state, since this field is equivalent to the fundamental field in the stator of a healthy machine. The frequencies of the harmonic components of the rotor current induced by this field have already been derived in section 2.2.1 of this chapter, and may be summarized in the equation

$$f_{rot}^{k,sana} = \left[(6 \cdot k \pm 1) \cdot s - 6 \cdot k \right] \cdot f_{red} \tag{18}$$

Moreover, the negative sequence current system of the decomposition of the symmetrical components will produce a fundamental stator current sheet of p pairs of poles that rotate at speed $\frac{-f_{red}}{p}$ r.p.s. relative to the stator (negative sequence) and harmonic current sheets of order $(6 \cdot k\text{-}1)$ y $(6 \cdot k\text{+}1)$.

The fundamental wave of current sheet generated by the negative sequence stator current system turns in reverse relative to the rotor at speed $\frac{-f_{red}}{p} - f_{rot}$ r.p.s. and it induces currents in the rotor wires whose frequencies are $p \cdot \left(\frac{-f_{red}}{p} - f_{rot} \right) = (s-2) \cdot f_{red}$.

Current sheets of $(6 \cdot k\text{-}1) \cdot p$ pairs of poles turn in positive sequence relative to the rotor (since it rotates in negative sequence relative to the reverse fundamental field) at a speed $\frac{f_{red}}{(6 \cdot k-1) \cdot p}$ r.p.s. speed relative to the stator and at $-f_{rot} + \frac{f_{red}}{(6 \cdot k-1) \cdot p}$ r.p.s. relative to the rotor. This current sheet induces currents in the rotor wires whose frequencies are

$$f_{rot}^{6k-1} = (6 \cdot k-1) \cdot p \cdot \left[-f_{rot} + \frac{f_{red}}{(6 \cdot k-1) \cdot p} \right] = \left[6 \cdot k(s-1) + (2-s) \right] \cdot f_{red} \tag{19}$$

Current sheets of $(6\cdot k+1)\cdot p$ pairs of poles turn in negative sequence (in the same direction as the fundamental field caused by the negative sequence current system) at a speed $\frac{-f_{red}}{(6\cdot k+1)\cdot p}$ relative to the stator and at $-f_{rot}+\frac{f_{red}}{(6\cdot k+1)\cdot p}$ r.p.s. relative to the rotor. This current sheet induces currents in the rotor wires whose frequencies are

$$f_{rot}^{6k+1}=(6\cdot k-1)\cdot p\cdot\left[-f_{rot}+\frac{f_{red}}{(6\cdot k-1)\cdot p}\right]=\left[6\cdot k(s-1)-(2-s)\right]\cdot f_{red} \qquad (20)$$

In summary, the frequencies of the harmonic components of the currents of the rotor caused by a stator asymmetry are given by the equation:

$$f_{k,rot}^{As\_Est}=\left[6\cdot k\cdot(s-1)\pm(2-s)\right]\cdot f_{red} \qquad (21)$$

Hence the fundamental fault components are in two sidebands spaced $\pm s\cdot f_{red}$ from the frequency $2\cdot f_{red}$.

Reference [48] addresses the same problem, proposing the equation (22) for the computation of the frequencies of the fault components in the rotor currents caused by the stator asymmetry:

$$f_{rot}^{k}=\left(\frac{k}{p}\cdot(1-s)\pm 1\right)\cdot f_{red} \qquad (22)$$

this expression is equivalent to that derived in this section for the computation of the fundamental fault components $\left(\frac{k}{p}=1\right)$.

The zero sequence component case is developed in the following paragraphs, considering that the stators of electrical machines can be connected in two different ways: star and delta.

When the stator is connected in star there is no possibility for the circulation of zero sequence currents through the stator windings and, therefore, there will not be induced any current in the rotor windings, preventing the zero sequence from generating new harmonics.

When the stator windings is delta connected, the zero sequence currents can be established through the stator winding generating a magnetic field of fixed position in space, but pulsating, which by the Leblanc's Theorem can be decomposed into two fields with fixed amplitude but opposite turn directions, one in the positive sequence of the fundamental field and another in the negative sequence of it.

The positive sequence field resulting from the decomposition of zero sequence field when the machine is delta connected generates the same harmonics that the stator fundamental field since both rotate in the same direction at the same speed, whereas the reverse field resulting from the decomposition of the zero sequence field when the machine is delta connected generates the same harmonic components than the reverse field computed by the decomposition of the symmetrical components of the unbalanced stator current system.

TABLE 9. SUMMARY OF THE ROTOR CURRENT HARMONICS INDUCED BY THE STATOR CURRENT FOR A HEALTHY MACHINE AND A MACHINE WITH A STATOR ASYMMETRY FOR A WOUND ROTOR INDUCTION MACHINE

	Healthy	**Fault**	
Frequency	$s \cdot f_{red}$	$s \cdot f_{red}$	$((1-s)\pm 1)\cdot f_{red}$

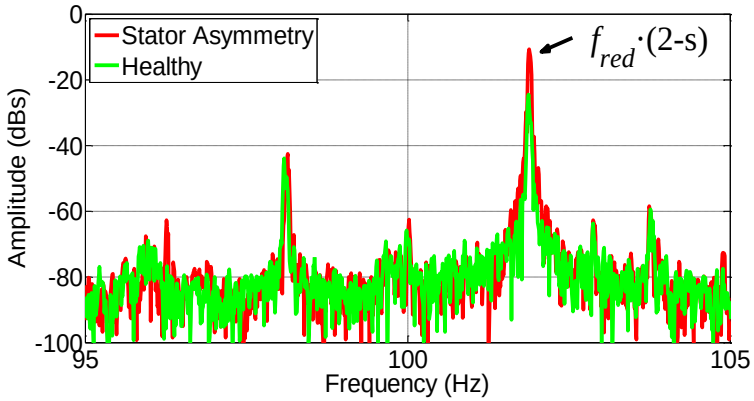

Fig. 20 Fourier spectrum for a wound rotor induction machine ,in generator mode, with stator asymmetry (red) and healthy state (green).).

3.3 SUMMARY OF THE FREQUENCIES IN HEALTHY AND FAULTY STATE FOR WOUND ROTOR INDUCTION MACHINES

Finally a summary of the equations that govern the harmonic fault components in the rotor current of a wound rotor induction machine rotor, for both when the machine is in healthy state and with a stator asymmetry. The equations derived in the previous sections are shown in Table 9.

This section ends showing a spectrum of the rotor current where it is compared the spectrum of a machine with stator asymmetry (red colour) with a healthy machine (green) in Fig. 20.

Fig. 20 depicts the harmonic that discriminates the state of the machine since the machine is in faulty state, the harmonic governed by the equation f_{red} ·(2-s) raises the value of its amplitude.

4 ECCENTRICITY

Eccentricity is one of the most common faults in induction machines.

The failure of eccentricity can be classified as a fault of mechanical origin (non-uniform air gap), therefore the derivation of all the fault equations are independent of the type of rotor of the studied induction machine. Therefore, the study conducted in the following subsections is valid for both squirrel cage rotor and wound rotor induction machines.

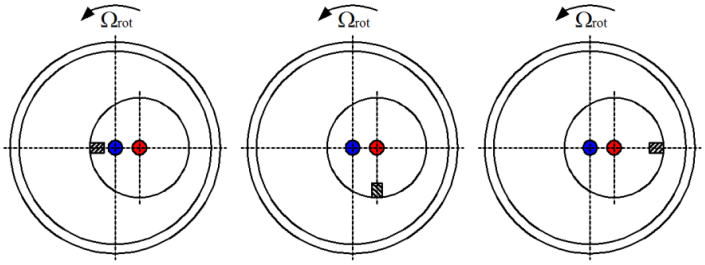

Fig. 21 Evolution of the air gap where there is a static eccentricity.

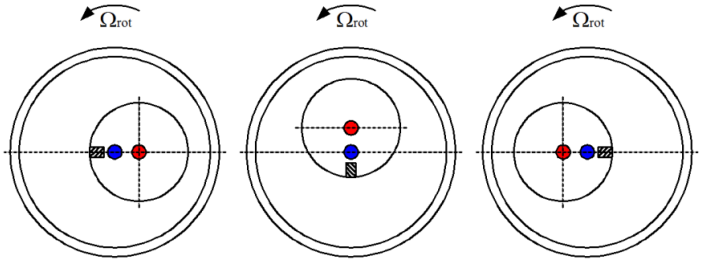

Fig. 22 Evolution of the air gap where there is a dynamic eccentricity.

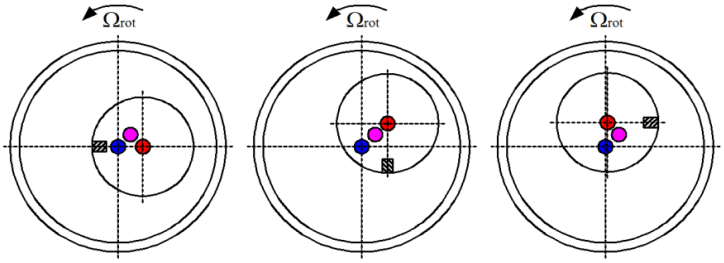

Fig. 23 Evolution of the air gap where there is a mixed eccentricity.

The eccentricity causes a non-uniform air gap and as a result that the radial thickness, which should be constant throughout its development, it is larger in some parts of the machine whereas in other is smaller.

Eccentricity induces flux harmonics that are reflected in the stator currents [19]. When there is no eccentricity in an electric machine, the geometric centre of the rotor, the geometric centre of the stator and the centre of rotation of the rotor coincide. When there is an eccentricity, one of these axes does not coincide with the other two or there is no coincidence among any of them.

When the geometrical centre of the stator does not coincide with the geometrical centre of the rotor appears the static eccentricity (Fig. 21) since in this case, the position and the minimum and maximum air gap value remain constant.

When the geometrical centre of the rotor does not coincide with the geometrical centre of the stator and the rotation centre position of the rotor

the maximum and minimum values of air gap rotate with it, which value is constant, appears the dynamic eccentricity (Fig. 22).

Finally, if none of the centres is located at the same spatial position what is known as mixed eccentricity appears, then the position of minimum and maximum air gap varies with time as well as varying its value (Fig. 23). The mixed eccentricity is always present in the electrical machines due to manufacturing tolerances [20]. The unbalance of magnetic forces caused by the mixed eccentricity can cause the bending of the shaft, bearing failures and finally the rotor can scrape the stator what has catastrophic consequences for the machine [4].

In [111] is discussed that when there is only static eccentricity or dynamic eccentricity, specific eccentricity harmonics do not appear in the low frequency spectrum of stator current. Observable harmonics in the low frequency spectrum of stator current are only generated for the existence of the mixed eccentricity.

Mixed eccentricity is a failure that is always present in any electrical machine, even in new machines, due to construction tolerances [20].

When there is mixed eccentricity in the air gap of an induction machine magnetic flux harmonics appear, producing current harmonics at certain frequencies in the stator currents. The fundamental fault harmonic of mixed eccentricity is, in the stator currents, at the frequency [20] given by

$$f_{exc} = f_{red} \pm \frac{f_{red}}{p} \cdot (1-s) \tag{23}$$

where f_{exc} is the frequency of the fundamental harmonic of mixed eccentricity in the stator current, f_{red} is the supply frequency for the stator winding, p is the number of pairs of poles and s is the slip.

The demonstration of the equation (23) is justified in a similar way than for the electromechanical rotor asymmetry harmonics, since when there is an asymmetry in the electric machine, the air gap is not constant and thus the amplitude of the current sheet in the air gap is modulated with a frequency equal to the mechanical rotation of the rotor.

$$i_{f_{exc}} = A(t) \cdot \cos(\omega \cdot t + \varphi) \tag{24}$$

with $A(t) = A \cdot \left(1 + B \cdot \cos\left(2 \cdot \pi \cdot \frac{f_{red}}{p} \cdot (1-s) \cdot t + \varphi'\right)\right)$ y $\omega = 2 \cdot \pi \cdot f_{red}$,

when substituted in (24), leads to:

$$i_{f_{exc}} = A \cdot \cos(2 \cdot \pi \cdot f_{red} \cdot t + \varphi) + A \cdot B \cdot \cos\left(2 \cdot \pi \cdot \frac{f_{red}}{p} \cdot (1-s) \cdot t + \varphi'\right) \cdot \cos(2 \cdot \pi \cdot f_{red} \cdot t + \varphi) \tag{25}$$

and applying trigonometric relations in (25) yields

$$i_{f_{exc}} = A \cdot \cos(2 \cdot \pi \cdot f_{red} \cdot t + \varphi) + A \cdot B \cdot \cos\left(2 \cdot \pi \left(f_{red} \pm \frac{f_{red}}{p}(1-s)\right) \cdot t + \varphi \pm \varphi'\right) \tag{26}$$

therefore it is noticed that when there is a mixed eccentricity in an electric machine two harmonics at a distance $f_{red}/p\cdot(1\text{-}s)$ from the fundamental current harmonic appear as it is shown in Fig. 24.

The conducted analysis for the fundamental component of the current sheet can be extended to the rest of harmonics thereof and, therefore, it will be noticed that for each existing harmonic in the current sheet there will appear two harmonics at a distance $f_{red}/p\cdot(1\text{-}s)$ regardless of the order of the harmonic of the studies current sheet.

Fig. 25 shows the Fourier spectrum centred at the frequency of 5th order current sheet harmonic of the stator current and the two corresponding side harmonics at a distance $f_{red}/p\cdot(1\text{-}s)$.

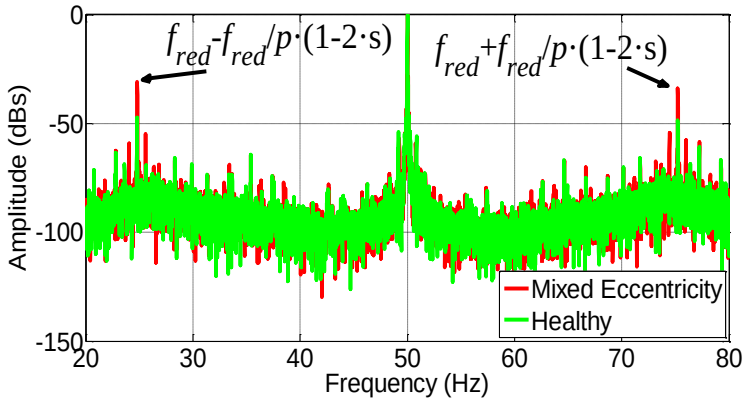

Fig. 24 Fourier spectrum of a squirrel cage induction machine, in generator mode, with mixed eccentricity (red) and healthy state (green) for the fundamental harmonic.

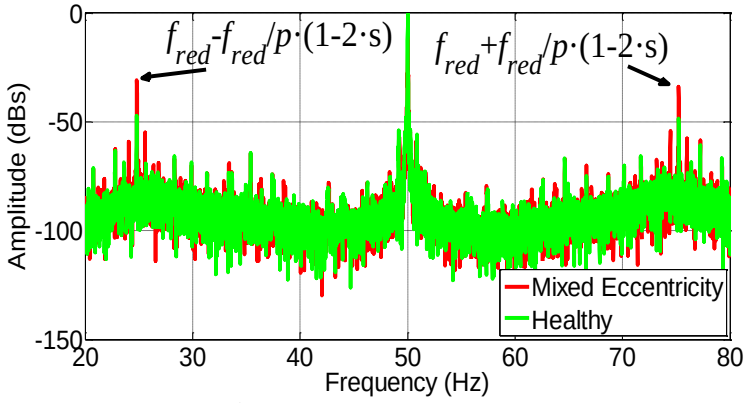

Fig. 25 Fourier spectrum of a squirrel cage induction machine, in generator mode, with mixed eccentricity (red) and healthy state (green) for the 5th order harmonic.

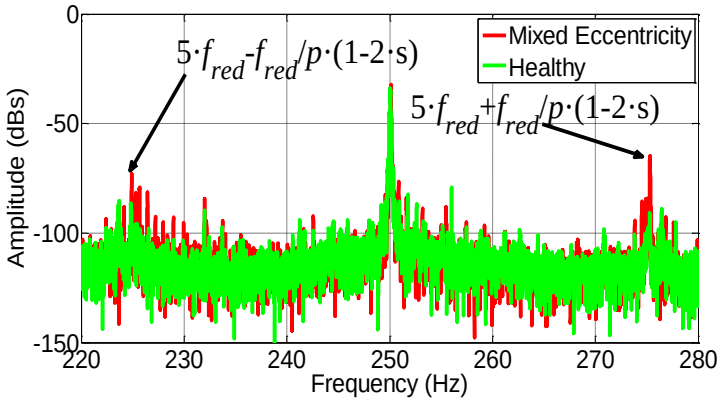

Fig. 26 Fourier spectrum of a squirrel cage induction machine, in generator mode, with mixed eccentricity (red) and healthy state (green) for the 7th order harmonic.

TABLE 10. SUMMARY OF THE CURRENT STATOR HARMONICS FOR HEALTHY MACHINE AND WITH MIXED ECCENTRICITY FOR INDUCTION MACHINES

	Healthy	**Fault**	
Frequency	f_{red}	f_{red}	$k \cdot f_{red} \pm \frac{f_{red}}{p} \cdot (1-s)$

with k=1,5,7,11,13,...

Fig. 26 shows the Fourier spectrum centred at the frequency of the 7th order harmonic and it can be seen the existence of the mixed eccentricity harmonics at distance $f_{red}/p \cdot (1\text{-}s)$ from the 7th order harmonic.

Finally, Table 10 shows the value of the frequencies where the harmonics for healthy and with mixed eccentricity for induction machines appear.

5 SUMMARY AND CONCLUSIONS OF THE CHAPTER

The theoretical derivation of the equations that characterise the frequencies of the fault components function of the slip required for the diagnosis of rotor and stator asymmetry and mixed eccentricity has been carried out in this chapter thus reaching the second partial goal of this thesis.

The developed equations are valid for the motor and generator mode for asynchronous machines regardless of its type of rotor.

Firstly the fault equations have been derived for the fundamental fault components and for the high order components for the rotor asymmetry for both squirrel cage rotor and wound rotor induction machine through the analysis of a stator current.

In the case of the stator asymmetry has been noticed the need of the acquisition of a rotor current for a more reliable diagnosis than the already developed in the technical literature. However, this technique cannot be applied to squirrel cage rotor induction machines since the current flowing through the bars of the cage is inaccessible.

TABLE 11. FREQUENCIES IN THE FOURIER SPECTRUM FUNCTION OF THE STATE OF THE INDUCTION MACHINE, THE ORDER OF THE HARMONIC AND THE FAULT TO BE DIAGNOSED

	Order	Healthy	Fault
Rotor asymmetry	1	f_{red}	Electromagnetic: $f_{red}\cdot(1-2\cdot s)$ Electromechanical: $f_{red}\cdot(1\pm 2\cdot s)$
	3·k	Do not exist	
	6k-1	Squirrel cage rotor Do not exist Wound rotor $f_{red}\cdot\left[(6\cdot k-1)-6\cdot k\cdot s\right]$	Electromagnetic: $f_{red}\cdot\left[(6\cdot k-1)-(6\cdot k-2)\cdot s\right]$ Electromechanical: $f_{red}\cdot\left[(6\cdot k-1)-(6\cdot k\pm 2)\cdot s\right]$
	6k+1	Squirrel cage rotor Do not exist Wound rotor $f_{red}\cdot\left[(6\cdot k+1)-6\cdot k\cdot s\right]$	Electromagnetic: $f_{red}\cdot\left[(6\cdot k+1)-(6\cdot k+2)\cdot s\right]$ Electromechanical: $f_{red}\cdot\left[(6\cdot k+1)-(6\cdot k\pm 2)\cdot s\right]$
Stator asymmetry	1	$s\cdot f_{red}$	$s\cdot f_{red}$ $\left((1-s)\pm 1\right)\cdot f_{red}$
Mixed eccentricity	$k\cdot f_{red}$	f_{red}	f_{red} $k\cdot f_{red}\pm\frac{f_{red}}{p}\cdot(1-s)$

Finally, it has been derived the equations for the mixed eccentricity. The main feature of this type of failure is its mechanical character, making it independent of the rotor of the induction machine. As a result, the derived equations for the diagnosis of this type of fault are valid for both types of rotors.

The main conclusions of this chapter are:

– The existence of an asymmetry in the rotor or stator windings of an induction machine regardless of its rotor can be studied as a linear combination of three current sheet of positive, negative and zero sequence, respectively.

– The fundamental component of the positive fault current sheet creates harmonics in the same positions where there are located the current harmonics produced by the fundamental current sheet of the stator current when the machine is in healthy state, thus being impossible separate from each other.

– The fundamental component of the negative fault current sheet creates harmonics in different positions where there are located the current harmonics produced by the fundamental current sheet of the stator

current when the machine is in healthy state in the case of a squirrel cage rotor induction machine, and increases the amplitude of the pre-existing harmonic components in wound rotor induction machines. They are function of the slip that the machine is subjected.

– The zero sequence component, if it can be established, may be decomposed into a current sheet of positive and negative sequence (by Leblanc's Theorem) and their results are analogue to those of the current sheet of positive and negative sequence already discussed in the two preceding paragraphs.

Table 11 summarizes all the fault equations derived in this chapter for the diagnosis of electric induction machines for the different faults to be diagnosed in this thesis.

All the derived equations are linear function of the slip.

The representation of the fault equations versus the slip shows a linear evolution that determines a specific slope and y-intercept function of the diagnosed fault and independent of the evolution of the speed transient that the analysed machine is subjected.

CHAPTER IV: PROPOSED METHODOLOGY

1 INTRODUCTION

The conventional diagnosis of electric induction machines in non-stationary stochastic regimes is based on the computation of the energy in the band or frequency bands in which are contained the fault components when there is a failure in the machine [90]-[93], [95] comparing the value of the energy computed in the same band, or bands when the machine is in healthy state.

However, the use of this methodology has high uncertainty in its practical application.

The uncertainty is mainly due to three factors:

The first source of uncertainty is result of the use of non-ideal filters for the extraction of the fault component. These filters have transition zones (non-ideal filters) that favour the inclusion of unwanted harmonic components in the filtering band which should only contain the fault component as a consequence of the failure.

The second source of uncertainty is the great width of the filtering bands used for the extraction of fault components, when the DWT filter is the filtering tool for its extraction that as in the first source of uncertainty, favours the inclusion of unwanted harmonic components in the extracted frequency band.

Finally, the third cause of uncertainty is that, although it could be carried out a filtering process without transition zones and the width of the frequency band for the extraction of the fault was minimized, the increase of the energy in the extracted frequency band cannot be associated, for sure, with the diagnosed fault since there is always the uncertainty that the increase of the energy can be caused by other external causes not considered and as a result they might cause false positive diagnosis.

The methodology proposed in this thesis aims to solve these problems.

The first two are solved by the use of a new filtering method, spectral filter or filter in the frequency domain, that allows an accurate extraction of the fault component, since it lets adjust exactly the filter band to the interval of frequency where the fault component evolves.

To solve the third drawback, it is proposed the analysis of the instantaneous frequency of the fault components in the slip frequency domain.

The three mentioned drawbacks have been solved for the diagnosis of electrical machines in non-stochastic transient regimes [61]-[75] through the study of the evolution in the time-frequency domain of the fault harmonic components.

The disadvantages can be overcome in these transient regimes since they are processes clearly defined in the time domain and allow the establishment of specific pattern evolutions in the time-frequency domain, allowing the discrimination whether the increase of energy is due to the faulty state of the machine (the fault component follows the previously established pattern in

the time-frequency domain) or other cause (the fault component does not follow any pre-established pattern in the time-frequency domain).

However, the solution for the diagnosis of transient regimes in electrical machines cannot be extended to the non-stationary stochastic regimes since they are completely unpredictable in the time-frequency domain, thereby preventing the establishment of specific pattern evolutions.

To extend the idea of following the evolution of the fault harmonics that has very good results for the diagnosis of machines in transient regimes, it will be necessary to find a new variable that substitutes the variable time and, at the same time, allows the establishment of evolutions of the instantaneous frequency of the fault component independent of the load conditions of the machine.

From the fault expressions derived in Chapter III can be concluded that the evolution of the frequencies of the fault components are function of supply frequency at which the machine is fed and the slip to which the machine is subjected.

If it is taken into account that most of the electric machines are directly fed from the electric power network, at a constant supply frequency, and when the load conditions (higher or lower resistive torque) or voltage (greater or lesser internal torque of the machine) of a machine vary, the value of the slip changes as a consequence of the change of the speed of the machine, therefore it can be concluded that the depiction of the frequency of the fault component in slip-frequency domain can allow the establishment of fault patterns independent of the features, voltage and load to which the machines are subjected.

The evolution of the instantaneous frequencies of the fault components (summarized in Chapter III, Table 11) are characterised by straight lines of constant, known and independent of the changes in the load, voltage and features of the machine values of slope and y-intercept. The two requirements necessary to characterise the theoretical fault evolution patterns that induction machines can be subjected are to know the stator supply frequency and the slip. Additionally, for the faults considered as mechanical -eccentricity- is also needed to know the number of pairs of poles.

The hypotheses in the preceding paragraphs are corroborated by plotting the frequency of the different fault components that an induction machine can undergo versus the slip (Fig. 27).

A drawback of the use of the slip as independent variable lies in the need of knowing -measuring- the speed of the machine at all times and it may cause a small increase in the installation cost of the diagnostic system if the speed is not already monitored in the process where the machine to be diagnosed is installed.

It must be taken into account that many machines in the industry, especially large wind generators, currently include in its monitoring system the acquisition of the speed. Therefore, the proposed diagnostic system does not imply any extra cost if such systems were installed.

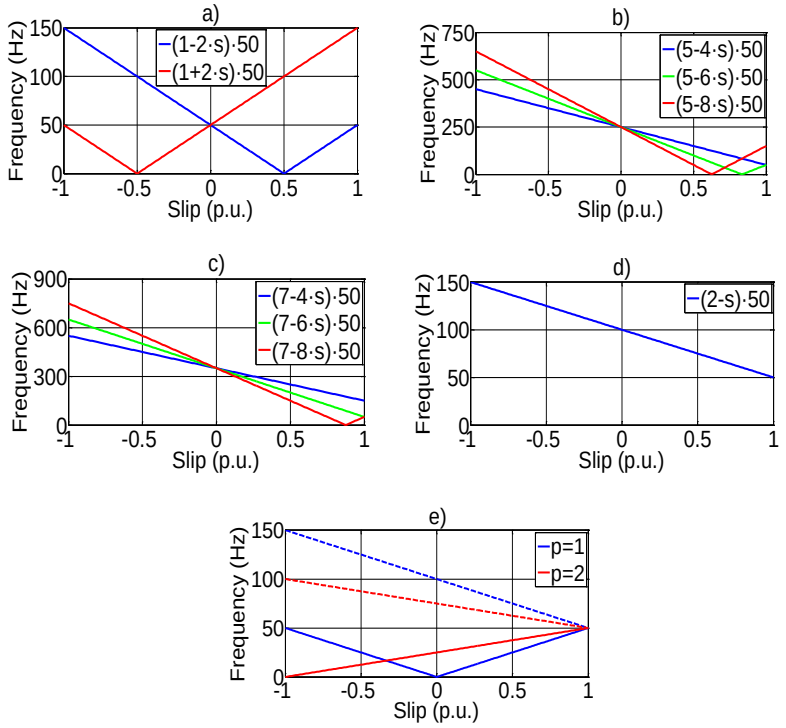

Fig. 27 Evolution of the fault components in the frequency-slip plane for f_{red} = 50 Hz. a) Rotor asymmetry : Components of order 1. b) Rotor Asymmetry: Components of order $6 \cdot k$-1, with k=1. c) Rotor Asymmetry: Components of order $6 \cdot k$+1, con k=1. d) Stator asymmetry. e) Mixed Eccentricity

The scheme of the methodology used for the diagnosis of electric induction machines in non-stationary stochastic regimes in this thesis is summarized in Fig. 28.

The proposed methodology consists of five steps: (i) signal acquisition (phase or line current and speed), (ii) pre-treatment of the acquired signals (extraction of the fault components), (iii) computation of the energy of the fault component, (iv) computation of the instantaneous frequency of the fault component and (v) diagnostic decision by the evaluation of the patterns (qualitative criterion) and fault parameters (quantitative criterion).

Table 12 summarizes the equations of the frequencies of the fault components function of the slip for the different types of faults shown in Fig. 27 function of the supply frequency and the slip of the machine, showing the specific values -theoretical- slope and y-intercept that define each one of the different evolutions for the different fault components.

The generalization of the fault equations, shown in Table 12, allows the directly application of the proposed methodology for machines fed from VSD and/or variable supply frequencies.

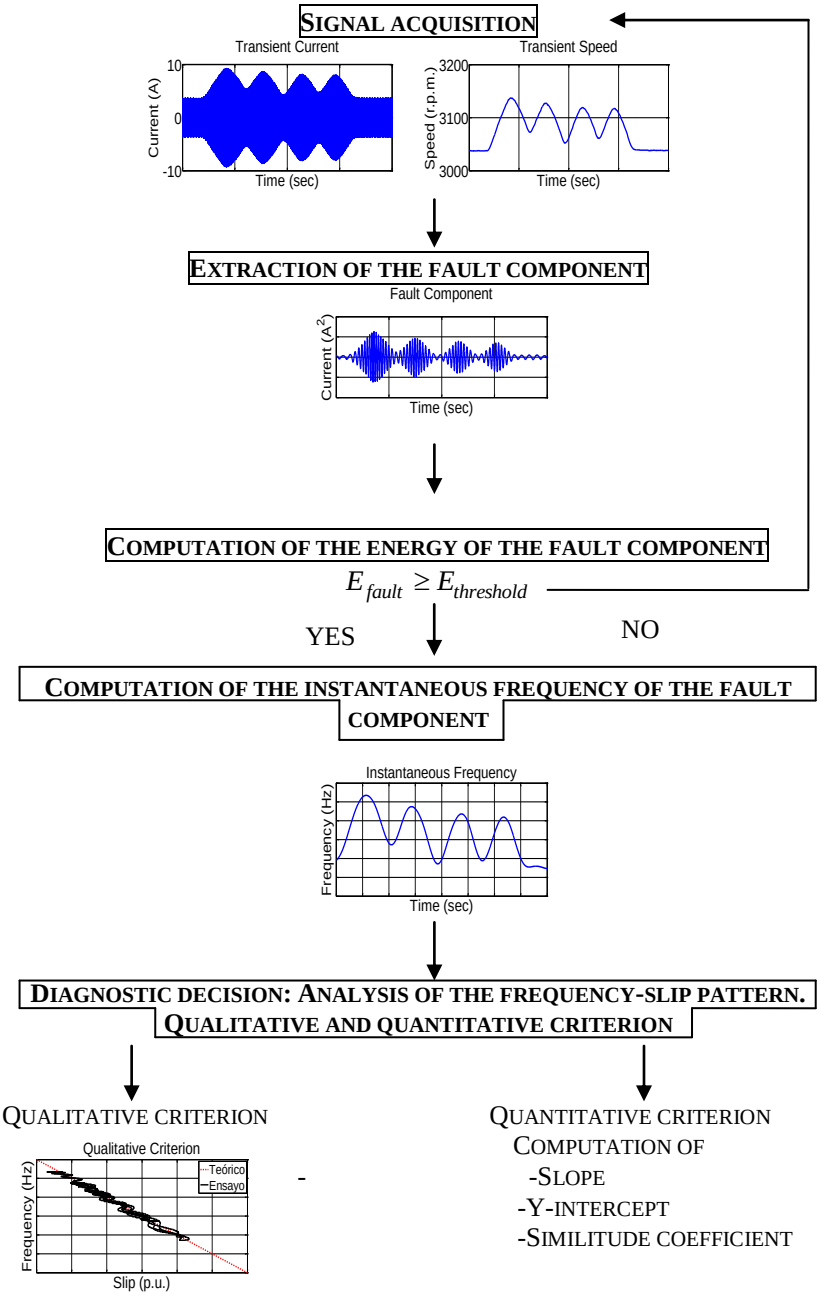

Fig. 28 Proposed methodology for the diagnosis of electrical induction machines.

TABLE 12. THEORETICAL VALUES OF SLOPE AND Y-INTERCEPT FUNCTION OF THE FAULT FOR INDUCTION MACHINES FED AT CONSTANT FREQUENCY

	Fault Frequency Evolution	Slope	Y-intercept
Rotor Asymmetry	$f_{red} \cdot (1-2 \cdot s)$	$-2 \cdot f_{red}$	f_{red}
	$f_{red} \cdot (1+2 \cdot s)$	$2 \cdot f_{red}$	f_{red}
	$f_{red} \cdot (5-4 \cdot s)$	$-4 \cdot f_{red}$	$5 \cdot f_{red}$
	$f_{red} \cdot (5-6 \cdot s)$	$-6 \cdot f_{red}$	$5 \cdot f_{red}$
	$f_{red} \cdot (5-8 \cdot s)$	$-8 \cdot f_{red}$	$5 \cdot f_{red}$
	$f_{red} \cdot (7-4 \cdot s)$	$-4 \cdot f_{red}$	$7 \cdot f_{red}$
	$f_{red} \cdot (7-6 \cdot s)$	$-6 \cdot f_{red}$	$7 \cdot f_{red}$
	$f_{red} \cdot (7-8 \cdot s)$	$-8 \cdot f_{red}$	$7 \cdot f_{red}$
Stator Asymmetry	$(2-s) \cdot f_{red}$	$-f_{red}$	$2 \cdot f_{red}$
Mixed Eccentricity	$f_{red} \pm \frac{f_{red}}{p} \cdot (1-s)$	$\mp \frac{f_{red}}{p}$	$f_{red} \pm \frac{f_{red}}{p}$

2 SIGNAL ACQUISITION

The proposed methodology begins with the acquisition of a current signal, regardless of phase or line, and the speed at which the machine is turning in the stochastic regime (Fig. 29).

In the case of rotor asymmetry and mixed eccentricity failures, it will be necessary the acquisition of the stator current of, at least, a current of one of the phases of the machine, whereas for the diagnosis of the stator asymmetry for wound rotor induction machines will be necessary the acquisition of a rotor current.

The fundamental features that define the acquired current signal are its instantaneous value, the sampling frequency, and the total acquisition time of the signal.

The right acquisition of the instantaneous value of the current signal is of great importance since in them there is all the necessary information to carry out the diagnosis of the machine. Amplitude values wrongly acquired lead to misdiagnosis.

The value of the sampling frequency (f_s) with the waveform is captured is the parameter that determines the maximum frequency that can be observed and extracted (f_{ext_max}) of the acquired current waveform according to the Nyquist-Shannon criterion [121]-[123].

$$f_{ext\_\max} = \frac{f_s}{2} \tag{27}$$

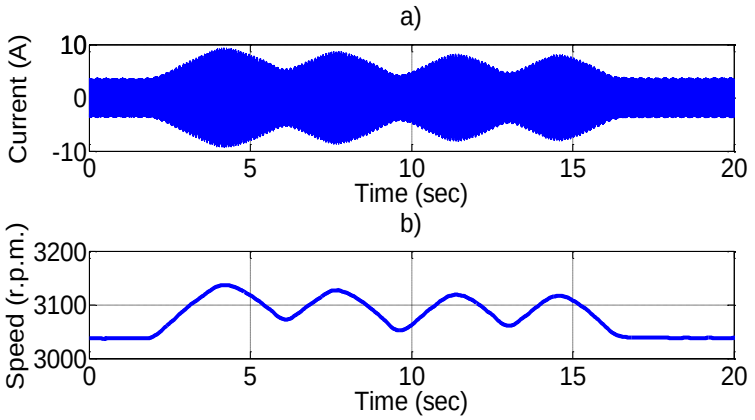

Fig. 29 Signals to be acquired for the application of the methodology a) Current signal b) Speed signal

The right selection of the sampling frequency with the application of a low pass filter prevents the phenomenon known as aliasing that may occur in the acquisition of analogue waveforms when they are digitalized.

The correct signal acquisition is detailed in Chapter V. In it is discussed and analyzed the main concepts of digital signal processing to avoid errors in the signal acquisition.

3 EXTRACTION OF THE FAULT COMPONENT

After the acquisition of the necessary signals to carry out the process of diagnosis and before the computation of the energy and the instantaneous frequency of the fault components, it must be performed a series of pretreatments to the acquired current signal that allow the extraction of the fault components of it.

More precisely, the goal of these pretreatments is the extraction of a reduced signal, $i_{FC}(t)$, of the acquired current $i(t)$. The reduced signal $i_{FC}(t)$ shall consist of the components that belong to a limited frequency band according to the following two conditions:

1.- The frequency band $[f_{inf}, f_{sup}]$ where the reduced signal $i_{FC}(t)$ is limited includes the frequency band $[f_{min}, f_{max}]$ that contains the fault components for the stochastic regime (see Fig. 30).

2.- The fault component is the predominant component in the extracted frequency band, that is, it is the predominant component of the extracted signal ($i_{FC}(t)$).

If both conditions are simultaneously met, the reduced signal $i_{FC}(t)$ can be considered, in the time interval in which the signal is acquired, as an approximation of the fault component.

The pretreatment for the extraction of the fault components is not universal being different for each type of studied fault. This is due to the different nature of the studied faults in this thesis, since the fault components are located in different regions of the spectrum and, consequently, its relative

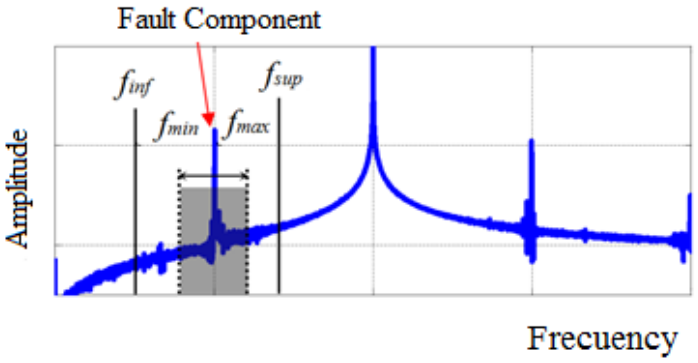

Fig. 30 Extraction of the fault component through a filtering process.

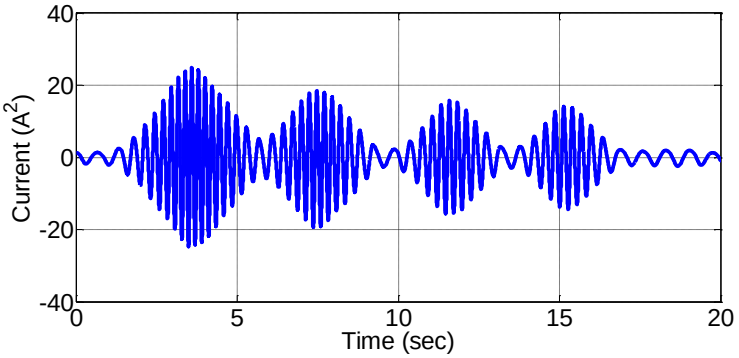

Fig. 31 Extracted fault component, $i_{FC}(t)$, of the non-stationary current from Fig. 29.a through a DWT filter.

amplitude and position to other frequency components, which may interfere with the process of diagnosis, compels the performance of a specific pretreatment for each type of fault.

In this thesis, the pretreatments are basically carried out in two steps: frequency shifting and filtering of the fault components. The need of the pretreatments depends on the studied fault as it is detailed in Chapter IX, X, XI and XII where it can be used both or just one of them.

For the filtering of the fault components there are several techniques in the technical literature such as the Discrete Wavelet Transform (DWT) [61], [64], [66], [74], [77], [124]-[126], the Wavelet Packet Transform [128], the Undecimated Discrete Wavelet Transform (UDWT) [129], Continuous Wavelet Transform (CWT) [79], [88], [129], Hilbert Transform (HT) [130], Hilbert -Huang Transform (HHT) [131], [132], Wigner-Ville Distribution (WVD) [87], [133] and any of them may be used for this purpose.

Of all the possible mentioned filtering techniques, the extraction of the fault components will be performed in three different ways using filters based on the Discrete Wavelet Transform, the Wavelet Packet Transform and through a new filtering method based on the properties of the Discrete Fourier Transform, designated as Spectral Filter or filter in the frequency domain.

Moreover, the frequency shifting is performed using the Hilbert transform [57] or the frequency sliding method [91], [92] and [95].

The theoretical bases of the filtering techniques in this thesis, as well as the theoretical details of the frequency sliding are detailed in Chapter VI.

4 COMPUTATION OF THE ENERGY

Once the fault component has been extracted from the acquired current signal is necessary to compute its energy.

The computation of the energy of the fault component is twofold. First, the comparison of the value of its energy with the value of the energy of the same component when the machine is in healthy state (or with a preset threshold value) will allow an initial discrimination to determine whether the machine is in faulty state or not. The second goal is to determine the severity of the damage to which the machine is subject, since the greater damage is, the more energy the extracted fault component contains.

It is noteworthy that, unlike the techniques already proposed in the literature [90], [93], based exclusively on the computation of the increase of the energy of the fault component, in this thesis the increase of the energy is a necessary condition but not enough to determine whether the machine is in faulty state, since it has been already discussed in previous chapters, an increase of energy in a given frequency band of the current spectrum may be due to the machine has a failure or to other cause (noise, load or voltage oscillations, etc..) and it can cause false positive diagnosis. Therefore, it is necessary to develop a reliable indicator that determines with absolute certainty that the increase in energy is only due to the fault that the machine is undergoing.

The computation of the energy of the fault component is performed in this thesis into two different domains: (i) time domain and (ii) frequency domain.

The computation of the energy of the fault component in the time domain is performed similar to [90], [93]:

$$E_t = \frac{\sum_{t=1}^{N} i_{FCi}^2(t)}{\sum_{t=1}^{N} i_i^2(t)} \tag{28}$$

For the computation of the energy in the frequency domain, in this thesis, is proposed the use of a new equation based on the Plancherel's Theorem [135]. This method is introduced in Chapter VIII.

$$E_e = \frac{\sum_{f=f'_{\min}}^{f=f'_{\max}} \left| FFT\left(i_i(f)\right)\right|^2}{\sum_{f=0}^{f=f_{\max}} \left| FFT\left(i_i(f)\right)\right|^2} \tag{29}$$

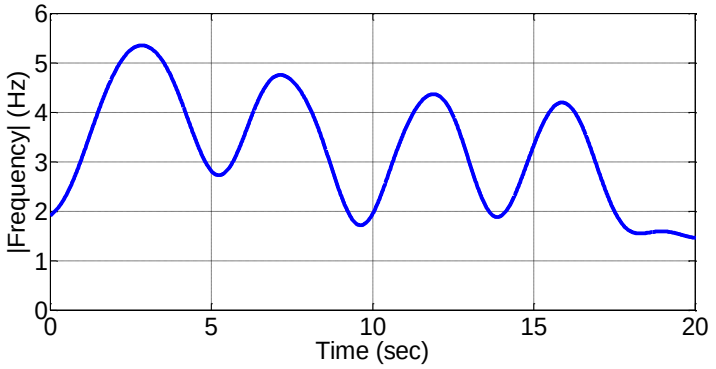

Fig. 32 Computed instantaneous frequency for the extracted fault component from Fig. 31.

5 COMPUTATION OF THE INSTANTANEOUS FREQUENCY

Once the fault component has been extracted and its energy computed, if energy exceeds the threshold, it is performed the computation of the instantaneous frequency of the fault component to determine its origin.

The goal of the computation of the instantaneous frequency is to establish with absolute certainty that the origin of the increase of the computed energy in the preceding section is exclusively due to one of the faults in the analysed electric machine, or due to another cause, being these two facts exclusive of each other.

The computed instantaneous frequency in this section, along with the computed energy value in the previous section, allows a highly reliable diagnosis to determine the state of the machine.

In this thesis, the computation of the instantaneous frequency is performed by two methods: (i) the conventional method based on the Hilbert Transform [68], [69] and (ii) a method based on the Teager-Kaiser operator [144].

The theoretical development of the several equations that allow the computation of the instantaneous frequency is discussed in Chapter VII, whereas the practical application of the two techniques is carried out in Chapters IX, X, XI and XII, discussing its advantages and disadvantages in its application for the detection of faults in electrical induction machines.

6 DIAGNOSTIC DECISION

Finally, the culmination of the application of the proposed methodology is carried out making the decision of the state in which the analyzed machine is.

The diagnostic decision is made based on the computed results from the two preceding sections, energy and instantaneous frequency, and the use of three new indicators that are introduced in this section: slope and y-intercept of the instantaneous frequency of the alleged fault component plotted versus the slip and the similitude coefficient.

The process for the diagnostic decision comprises the following steps: (i) Analysis of the energy of the extracted fault component extracted in the

pretreatment process, (ii) analysis of the slope and y-intercept in the plot of the instantaneous frequency versus the slip and (iii) analysis of the similitude coefficient.

The analysis of the energy of the fault component is the first indicator analysed to determine whether the machine is in healthy or faulty state. During the regular operation of the machine in healthy state, the value of the energy of the fault component takes a certain value, thus establishing the reference energy value. When the machine is subjected to an irregularity in its regular operation, the value of the energy of the extracted fault component increases and if it exceeds a certain reference value, the machine can be in faulty state. Otherwise, the machine is in healthy state.

The increase of the energy of the extracted fault component is the indicator used in [90]-[93] and [95] to determine the healthy or faulty state of the machine. However, from the author's point of view, the increase of energy of the extracted fault component is necessary but not enough to determine the state of the machine, since the origin of that increase is unknown.

Therefore, once it is detected an increase in the energy of the extracted fault component that exceeds the threshold, it is proceeded to analise of the plot of the instantaneous frequency in the frequency-slip plane. The depiction of the instantaneous frequency versus the slip is mandatory since, as it is shown in Fig. 32, its evolution follows no pattern in the time domain. However, if it is depicted versus the slip, it is noted that the evolution of the instantaneous frequency, in case that there is a failure, tends to concentrate, following the evolution of a specific straight line (Fig. 34 and Fig. 35).

The instantaneous frequency analysis in the frequency-slip plane involves the comparison of the theoretical evolutions of the instantaneous frequencies of the different faults in the slip plane (Fig. 27), versus the evolution of the computed instantaneous frequency from the acquired currents for the diagnosis.

After the depiction of instantaneous frequency of the extracted fault component versus the slip, there are two cases: (i) the evolution of the instantaneous frequency does not coincide with the theoretical evolution, (ii) the evolution of the instantaneous frequency coincides with the theoretical evolution.

When the depiction of the instantaneous frequency does not coincide with the theoretical evolution of the studied fault Fig. 33, it indicates that the increase of the computed energy in the third step of the method is not as result of a failure, and therefore it can be concluded that the machine is not subjected to the analysed fault.

Moreover, the fact that the evolution of the instantaneous frequency matches the theoretical evolution Fig. 34 indicates that the increase of the energy in the third section of the methodology is, with high probability, consequence of the analysed fault.

The depiction of the evolution of the instantaneous frequency in the frequency-slip plane is the qualitative diagnostic criterion of the proposed methodology, since the diagnostic decision is made by observing a graph and along with the value previously computed of energy.

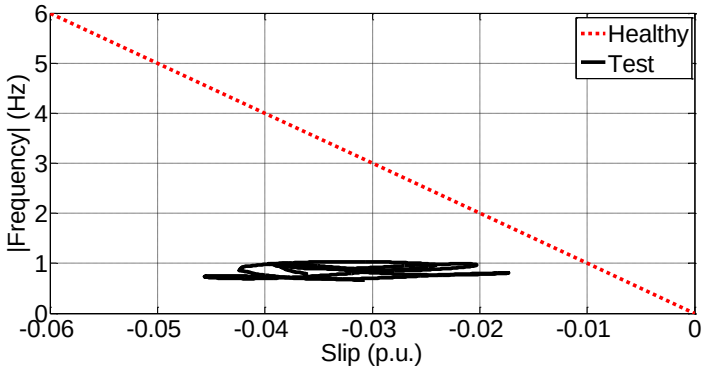

Fig. 33 Instantaneous frequency vs. slip for a wound rotor induction machine, working as generator in healthy state for the rotor asymmetry failure.

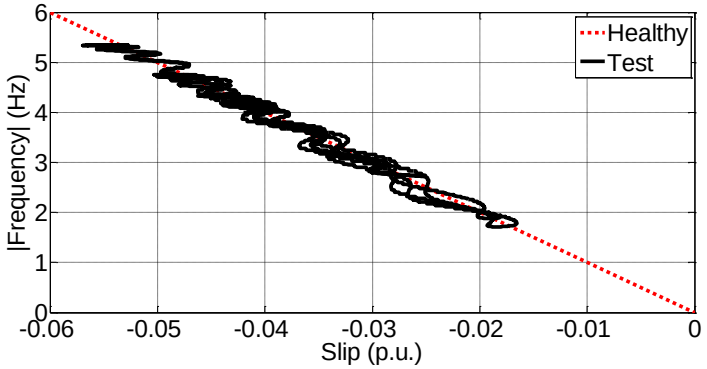

Fig. 34 Instantaneous frequency vs. slip for a wound rotor induction machine, working as generator in faulty state for the rotor asymmetry failure.

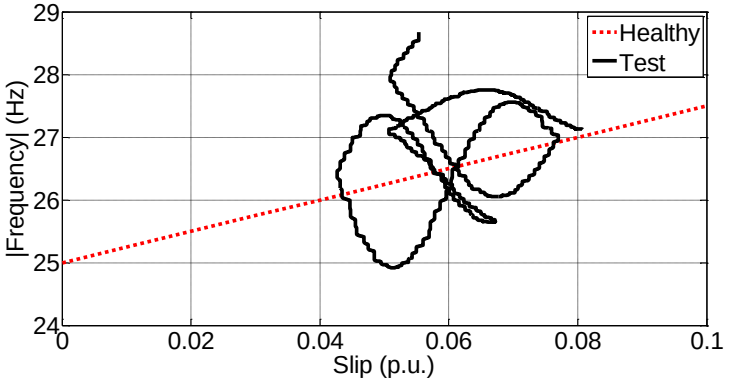

Fig. 35 Instantaneous frequency vs. slip for a squirrel cage rotor induction machine, working as motor in healthy state for the mixed eccentricity failure.

The advantages of the qualitative criterion are undeniable due to its simplicity, reliability, and easy understanding (Fig. 33 and Fig. 34). However, its use always raises uncertainty since there is not a clear definition to determine when the depiction of the computed frequency-slip points are located close enough to the theoretical straight line of the theoretical frequency evolution in the slip plane (Fig. 35).

Furthermore, the use of the graphical method is difficult to be applied in automated equipment, therefore it requires the analysis by a specialized operator or with a certain degree of expertise in the analysis of the frequency-slip graphs.

These drawbacks recommend the development of a quantitative method to determine objectively how close the computed frequency points are to the theoretical points.

The quantitative method is based on the computation of three objective parameters: (i) the slope of the line of fault analysed, (ii) the y-intercept of the analysed fault and (iii) the value of the similitude coefficient proposed by the author of this thesis.

The value of the slope and y-intercept are theoretical and known values, therefore, they can be compared with the computed values of the set of computed points by the linear regression analysis through the use of the least squares regression interpolation (see chapter VIII). If the theoretical values of slope and the y-intercept and the computed ones match or are close enough, it is determined that the machine is in faulty state, otherwise the machine is in healthy state.

For the application of the objective criterion in a more simple way, the author proposes a similitude coefficient (see Chapter VIII) that determines the degree of approximation of the computed points to theoretical points per unit.

To establish a diagnostic criterion by the application of the similitude coefficient is enough to set a maximum value of similarity to determine the status of the machine. In case that the similitude coefficient value is higher than the selected threshold of similitude coefficient, the machine will be diagnosed as faulty, whereas if the similitude coefficient value is below the threshold value the machine will be diagnosed as healthy machine in its regular operation.

7 SUMMARY AND CONCLUSIONS OF THE CHAPTER

This chapter has introduced the proposed diagnostic methodology proposed in this thesis and it has been reached the partial goals 3, 4, 5 and 6 of this work.

The proposed methodology is structured into five actions that are sequentially performed.

Firstly it is necessary the acquisition of a current and speed. For the diagnosis of a rotor asymmetry and a mixed eccentricity, the acquired current must be a stator current. For the diagnosis of a stator asymmetry in wound rotor induction machines, the rotor current must be acquired.

After the acquisition of the current is performed its pretreatment whose main goal is the extraction of the fault component associated with the studied fault. The pretreatment for the extraction of the fault component depends on the studied fault.

After extraction of the fault component, its energy is computed and there are two possible scenarios: (i) the computed energy of the extracted fault component does not exceed a preset threshold value leading to the completion of the diagnostic process since the machine is in healthy state, (ii) the computed energy exceeds the preset threshold, what forces the computation of the instantaneous frequency to determine the origin of the computed energy.

The preset energy value of the threshold must be set by the user according to the features of his application and/or machine to be diagnosed and according to the desired degree of sensitivity for the alarm.

After the computation of the instantaneous frequency, it is depicted in the slip domain, since in the non-stationary stochastic regimes in the time domain, the instantaneous frequency does not follow any pattern. This action is possible due to the acquisition of the speed at the first step.

After the depiction of instantaneous frequency in the frequency-slip plane, the parameters that allow the objective diagnosis of the machine are computed.

The proposed methodology in this thesis is valid for the diagnosis of electrical induction machines fed at constant frequency, for both squirrel cage and wound rotor, on any operating mode, motor or generator, under any stochastic regime even in regimes characterised by small random fluctuations around an operating point, as for instance wind turbines, conditions under steady state or transient diagnostic methods provide not satisfactory diagnosis. The method is applicable to the detection of faults of rotor asymmetry, stator asymmetry -only for wound rotor induction machines- and mixed eccentricity.

CHAPTER V: SIGNAL ACQUISITION

1 INTRODUCTION

This chapter summarises the basic concepts in the field of signal processing theory, used in the following chapters of the thesis. The main sources of this chapter have been [117]-[120].

The acquisition and treatment of the signals -signal processing- is an area little studied from the point of view of electrical engineering, despite its high importance, since the acquired signals to carry out the diagnostic process contain all information of state of the machine.

An incorrect signal acquisition may lead, with no doubt, to an incorrect diagnosis. Moreover, a treatment that does not fit the nature of the processed signal also limits the ability of diagnosis.

The aim of this chapter is to show the differences between the analogue and digital signals from the point of view of its acquisition as well as from the point of view of its treatment, collecting the most relevant information published in different references [113]-[123].

To achieve this goal, there is a brief historical introduction to the signal processing, followed by the basics of the digital signal processing.

Then it is shown the difference between the continuous -analogue- and discrete signals, and it is introduced the basis of the analogue-digital conversion.

Finally, there is a summary and the conclusions of this chapter.

1.1 HISTORICAL INTRODUCTION TO SIGNAL PROCESSING

The term signal processing refers to the science that analyses the variation in time of the physical processes through the acquired signals of a process.

Signal processing is structured into two areas: (i) analogue signal processing and (ii) digital signal processing.

The analogue signal term refers to signals that are continuous in time and can take any value in a wide range of values.

Furthermore, the discrete signal term describes those signals in which its independent variable, usually time, is quantified, and it is only known the values of the signal for the previously quantified values of the independent variable.

Therefore, a discrete time signal is not represented by a continuous waveform in time but by a sequence of values in which in addition to the quantification of the time variable, it is quantified the value of the acquired signal in those time instants, as it is shown in Fig. 36 which depicts an analogue cosine signal (Fig. 36.a) and the discrete signal after analogue to digital conversion (Fig. 36.b).

The digital signal processing is a field much larger than the depiction of continuous signals through discrete signals, as it also involves the processing and transforming of discretized signals.

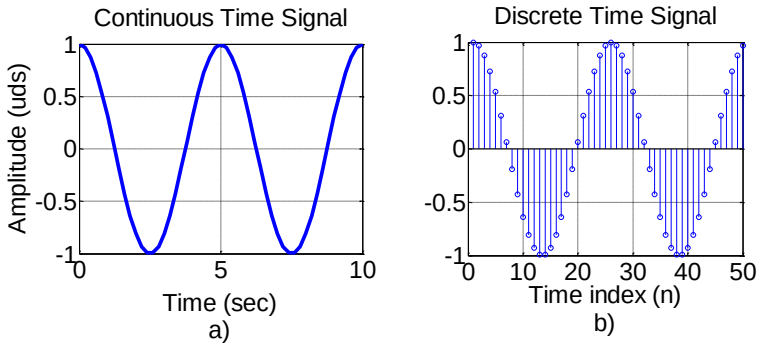

Fig. 36 Cosine signal in time domain: a) Continuous signal b) Discrete signal.

Back in the eighteenth century Euler, Bernoulli and Lagrange developed different methods of numerical integration and function interpolation, but it was not until the early nineteenth century, when Gauss discovered the fundamental principle of the Fast Fourier Transform, allowing the development of several applications in subsequent years [113] such as the telephone in 1877 or the radar in 1934.

In the late 1940s, there is the possibility of the implementation of filters using digital circuits, although the lack of appropriate hardware, as their cost, size and reliability were not adequate, ended in the processing of analogue signals by electronic, or even mechanical, circuits, although the existence of computers. The use of electronic circuits had as major drawbacks, in the 1940s, a very limited capacity and processing time, preventing the processing of signals in real time.

In 1950 the use of computers to simulate and evaluate signal processing electronic circuits before its manufacturing starts to spread, but it was not until the middle of the decade when the effect of the sampling frequency was completely studied.

One of the first uses of computers in the digital signal processing was for the oil exploration where seismic data was recorded on magnetic tapes for its subsequent processing, due to the low computational power of computers at the time that prevented real time signal processing.

In mid-1960, the integration of silicon circuits favours the advance of digital systems, even despite its high cost allows the development of a formal theory of digital signal processing, and it may be even implemented digital FIR filters that could compete with the analogue IIR filters.

Cooley and Tukey in 1965 [115] introduce an efficient algorithm to compute the Fourier Transform that reduces by several orders of magnitude the required computation time as well as the hardware requirements for its computation, facilitating the use of the many applications developed for it, encouraging the reformulation of many analogue techniques in discrete

terms. The work of Cooley and Tukey is a revolution in the discrete signal analysis since it allows the implementation of the FFT algorithm in specific hardware for it.

At the same time, the development of the microelectronics causes a significant lowering production costs and increases the performance of electronic equipment concerned to signal analysis.

As the processor capacity was increased, the complexity of the developed digital processing algorithms increased with them, facilitating the implementation of time-vary and adaptive filters in 1970 [116] and non-linear and Kalman filters that cannot be built with analogue circuits.

In mid-1980, there are already architectures that allow the implementation of floating point algebra allowing time signal processing in real time as it is known today.

2 BASIC CONCEPTS OF DIGITAL SIGNAL PROCESSING

The concept of signal appears in a wide variety of fields, therefore the ideas and techniques associated with this concept play important roles in such diverse areas as communications, aeronautical, etc. Although the nature of the signals in each of these areas can be completely different, they all have in common the need of the acquisition of signals to monitor the system to be controlled.

A signal is defined as a physical quantity that varies with time, space, or any other independent variable or independent variables. [117]. Mathematically, a signal is described as a function of one or more independent variables. For example, the functions

$$\begin{aligned} \rho(T) &= \rho_1(0)\cdot\left(1+\alpha\cdot\left(T-T_1(0)\right)\right) \\ x(t) &= x_0 + v_0\cdot t + \frac{1}{2}a\cdot t^2 \end{aligned} \tag{30}$$

wherein the first function corresponds to the linear variation of resistivity of a material as function of temperature, whereas the second corresponds to the final position of a mobile in a uniformly accelerated linear motion that is quadratically dependent on time. Another example would be,

$$T(x,y) = 500 - 0.6\cdot x^2 - 1.5\cdot y + 8\cdot x\cdot y \tag{31}$$

This function describes a signal with two independent variables x and y that may represent the spatial coordinates of a plane.

The signals shown in (30) and (31) belong to the class of signals that are perfectly defined by specifying the functional dependence with independent variable. However, there are cases in which this functional relationship is unknown or too complex to have practical utility.

For example, the electric current flowing through the windings of an electrical machine cannot functionally be described as an equation like (30). In general, an electric current can be described with a high degree of accuracy as the sum of a series of sine and cosine functions of different amplitudes, frequencies, and phases as

$$i(t) = \sum_{i=1}^{N} A_i(t) \cdot \cos\left(2 \cdot \pi \cdot f_i(t) \cdot t + \varphi_i(t)\right) \tag{32}$$

Where $A_i(t)$, $f_i(t)$ and $\varphi_i(t)$ are the values of the amplitudes, frequencies and phases, variable with time, of the cosine signals that compose the current. In fact, one way to interpret the information that an electrical signal contains is computing the amplitudes, frequencies, and phases of the studied signal.

The currents in electric machines, electrocardiograms, acoustic signals, etc., are examples of signals that vary as functions of a single independent variable, time.

Signals associated with the signals, there are the systems that generate them. For example, when a voltage is set on the terminals of the stator of an electric machine is generated an electric current that produces a rotating magnetic field that induces a current in the rotor of the machine inducing a rotating magnetic field that causes the movement of the rotor. Another example is the human voice that is generated by forcing the air to pass through the vocal cords. Therefore, the manner in which signals are generated is associated with a system that responds to a stimulus or force.

A system can be defined as a physical device that performs an operation on a signal [117]. For example, a filter that reduces noise and interferences that distort the signal that contains the desired information. In this case, the filter performs some operations on the signal, with the aim of reducing, filtering, the noise and interferences in the signal.

When a signal passes through a system, as in the case of a filter, it is said that the signal has been processed. In this case, the signal processing means extracting the desired signal from the noise and interferences.

In the scope of this work, it is appropriate to extend the system definition to include not only physical devices but also the changes made by the application of software operations on a signal.

In digital signal processing, operations that are performed on a signal, consists of a set of basic mathematical operations specified in a program. In this case, the program is an implementation of a system using software. Furthermore, the digital signal processing can also be performed by the implementation of operations specified by hardware, action that takes place through a physical device. In a wider sense, a digital system can be implemented as a combination of hardware and software, each performing a particular set of functions.

The majority of signals of interest for diagnosis are analogue. This fact forces to consider the problem of the analogue to digital signal conversion to enable its processing in a computer.

The set of finite prewritten instructions or rules that allow the performance of the required mathematical operations by the system is called algorithm [117]. The amount of algorithms that can be generated to the implementation of system can be very high, therefore, in practice the focus

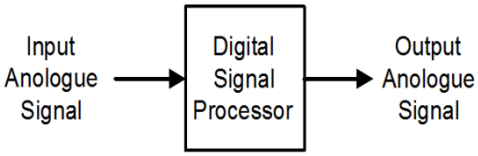

Fig. 37 Digital processing of analogue signals.

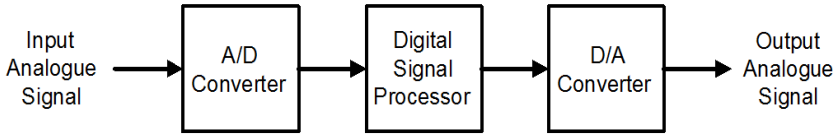

Fig. 38 Analogue-digital digital-analogue conversor for the processing of analogue signals.

will be set on the design algorithms that are computationally efficient and fast. Thus, one of the fundamental topics in digital signal processing will be the development of efficient algorithms to perform the operations required by the system.

Most of the signals that appear in engineering are of analogue nature, that is, those signals are functions of a continuous variable, such as time or space, and usually continuously vary within a range. Such signals can directly be processed by analogue systems, such as filters, in order to extract or remove certain information of the signal. In this case, it is said that the signal has been processed in an analogue way as illustrated in Fig. 37 where both the input signal and the output signal of the system are analogue.

The digital signal processing provides an alternative method for the processing of analogue signals as shown in Fig. 38. To perform the digital processing it is required an interface between the analogue and digital signal processor. This interface is called the analogue-digital converter. The output of the analogue-digital converter is a discretised signal suitable as input to the digital processor. In applications where the output of the digital processor is to be analogue, another interface is required to convert the digital signal to an analogue one, and it is named digital to analogue converter.

There are several advantages why the digital signal processing is preferred over the analogue signal processing.

The first of them is the flexibility offered by a digital system for the reconfiguration, as it occurs with the automation in the industry by PLC's compared with the automation with wired logic since the reconfiguration of an analogue system usually requires the redesign of the hardware associated with it.

The second advantage is the greater ease in controlling the accuracy of the designed system since in an analogue system the tolerances of the several components make the control of the accuracy extremely difficult, whereas in a digital system it would be enough to select the accuracy of the analogue-digital converter to know the accuracy of the system.

Another major advantage of digital signals is that they can be stored with no loss of its fidelity whereas that is not possible for the analogue signals. In addition, the digital signal processing allows the implementation of more

sophisticated methods than those that can be implemented using analogue components.

Finally, digital signal processing systems are cheaper than the equivalent analogue systems [118].

Because of these advantages, it follows that the digital signal processing is set in a large amount of disciplines.

However, digital signal processing systems have as a drawback a practical limitation for the acquisition of high frequency analogue signals due to the limited speed of the analogue-to-digital converters and digital signal preprocessors [118].

3 CONTINUOUS SIGNALS VERSUS DISCRETE SIGNALS

Signals can be classified into two different categories depending on the features of the independent variable, usually time, and the values that can take the signal magnitude.

The classification of the independent variable and the signal magnitude are performed according to the nature, continuous or discrete of the variable. Analogue signals, or continuously in time, are defined at any point in time and can take any value in the continuous interval (a, b) with $a < b$, $a \geq -\infty$, $b \leq \infty$, whereas signals on discrete time are defined only for certain values of time. Those time instants do not have to be equidistant, but in practice they are for reasons of simplicity. The value of the magnitude of a discrete time signal is found by taking the values of an analogue signal at certain instants of time.

Furthermore, the magnitude of a time signal -continuous or discrete- can be continuous or discrete as well. If a signal takes all possible values in an interval, it is said that the signal is continuous. On the contrary if it only takes a finite set of values in an interval is said that it is a discrete signal.

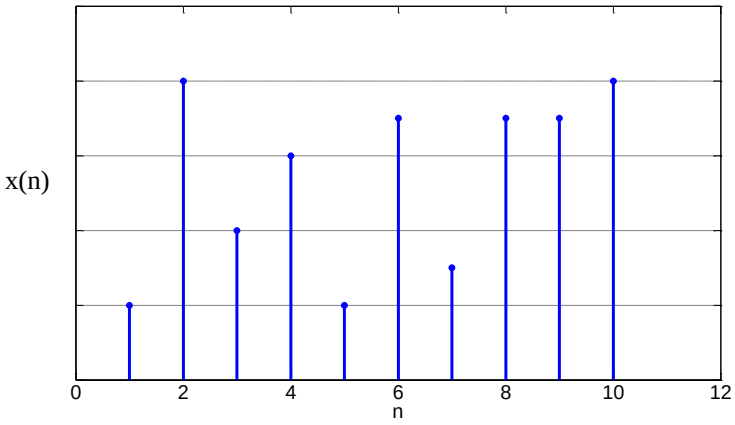

Fig. 39 Discrete signal.

A digital signal is characterised by taking discrete values in discrete time as shown in Fig. 39.

To process a signal digitally it must be a digital signal, that is, it must have discrete time values and discrete magnitude values.

If the signal to be processed is analogue, the time or magnitude must be converted to a digital signal sampling it in time, thereby acquiring a discrete signal in both time and magnitude.

The process of the conversion from an analogue signal into a digital signal is known by the name of quantification, process that is done by truncating or rounding the captured values of the original signal.

3.1 THE CONCEPT OF FREQUENCY IN CONTINUOUS AND DISCRETE TIME SIGNALS

The concept of frequency in a signal is directly related to the concept of time. In fact, the magnitude of the frequency is the inverse of the magnitude of time, which is why it should be expected that the features of the variable time -continuous or discrete- affect the properties of the frequency.

3.1.1 CONTINUOUS TIME SINUSOIDAL SIGNALS

A harmonic oscillator is mathematically written by the following equation in time:

$$x(t) = A \cdot \cos(\Omega \cdot t + \Phi), \quad -\infty < t < \infty \tag{33}$$

Harmonic oscillators are characterised by three parameters: the amplitude of the sine curve *A*,, the pulsation of the oscillator, Ω in rad/sec, and phase Φ in radians. In Fig. 40 is shown an example of a continuous harmonic oscillator in time.

Usually it is common to replace the oscillator pulse Ω in rad/sec for the frequency in Hertz, *F*, since:

$$\Omega = 2 \cdot \pi \cdot F \tag{34}$$

Then, equation (33) can be rewritten as:

$$x(t) = A \cdot \cos(2 \cdot \pi \cdot F \cdot t + \Phi), \quad -\infty < t < \infty \tag{35}$$

An analogue sine signal is characterised by [119]:

- Be periodical for all fixed frequency value *F*. This fact is easily demonstrated since any harmonic oscillator holds:

$$x(t+T) = x(t) \tag{36}$$

Where $T = \frac{1}{F}$ is the fundamental period of the sine signal.

- The continuous time signals with different frequencies are different.
- The increase in frequency *F* results in an increase in the rate of oscillation of the signal, that is, the number of periods of the signal at a given interval is increased.

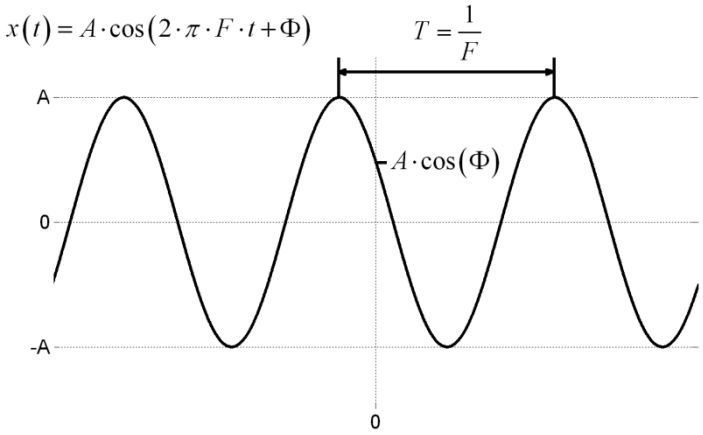

Fig. 40 Depiction of the magnitudes that define an analogue signal. Amplitude and frequency.

By definition, frequency is a positive physical quantity. This is obvious if the frequency is interpreted as the number of cycles per unit time of a signal in an interval.

However, in many cases for mathematical convenience it is required the introduction of negative frequencies. It is known that a sinusoidal signal can be defined as the sum of two complex exponential signals of equal amplitude and frequency in absolute value, since one of them spins counter clockwise, positive frequency values, and the other rotates clockwise, negative values of frequency.

In order to facilitate mathematical developments, in this thesis both positive and negative frequencies in this thesis are used although it must be noticed that there is a folding of the frequency at 0 Hz, that is, the frequency range for an analogue signal is bounded to $0 \leq F < \infty$, since it is indistinguishable the rotation of them in a frequency spectrum and thus F^+ and F^- will be located at the same position in the frequency spectrum.

3.1.2 DISCRETE TIME SINUSOIDAL SIGNALS

A discrete time harmonic oscillator can be expressed as:

$$x(n) = A \cdot \cos(\omega \cdot n + \varphi), \quad -\infty < n < \infty \tag{37}$$

Where n is an integer variable, known as the sample number, A is the amplitude of the signal, ω is the pulse in radians per sample, and φ is the phase in radians.

If instead of ω, in radians per sample, it is use the frequency f in hertz per sample defined by

$$\omega = 2 \cdot \pi \cdot f \tag{38}$$

Equation (37) becomes

$$x(n) = A \cdot \cos(2 \cdot \pi \cdot f \cdot n + \varphi), \quad -\infty < n < \infty \tag{39}$$

The features of the discrete time harmonic oscillators are [119]:

– A discrete time harmonic oscillator is periodic only if its frequency *f* is a rational number.

By definition a discrete signal $x(n)$ is periodic with period N, $N>0$, if and only if

$$x(n+N)=x(n) \quad \forall\, n \tag{40}$$

The smallest value of N for which (40) is fulfilled is called the fundamental period.

– Discrete harmonic oscillators whose frequencies are spaced apart by an integer multiple of $2\cdot\pi$ are identical.

To prove this fact is taken $\cos(\omega n + \varphi)$ and it is easily verified that

$$\cos\left((\omega+2\cdot\pi)\cdot n+\varphi\right)=\cos\left(\omega\cdot n+2\cdot\pi\cdot n+\varphi\right)=\cos\left(\omega\cdot n+\varphi\right) \tag{41}$$

Therefore, all harmonic oscillators governed by

$$x_i(n)=A\cdot\cos\left(\omega_i\cdot n+\varphi\right) \quad i=0,1,2,... \tag{42}$$

Where

$$\omega_i=\omega+2\cdot i\cdot\pi \quad -\pi\le\omega\le\pi \tag{43}$$

are identical and indistinguishable from each other.

From (41) comes two results: (i) two harmonic oscillators of frequencies in the range $-\pi\le\omega\le\pi$ of $-\frac{1}{2}\le f\le\frac{1}{2}$ are different. (ii) Any sequence that results from a harmonic oscillator whose frequency is $\omega>|\pi|$ o $f>\left|\frac{1}{2}\right|$ is identical to a sequence from a harmonic oscillator of frequency $-\pi\le\omega\le\pi$ o $-\frac{1}{2}\le f\le\frac{1}{2}$.

Because of this similarity, the harmonic oscillator whose frequency is $\omega>\pi$ is named alias of harmonic oscillator whose frequency is $0\le\omega\le\pi$ [119].

This fact supports that harmonic oscillators with frequencies in the range $-\pi\le\omega\le\pi$ or $-\frac{1}{2}\le f\le\frac{1}{2}$ are unique whereas all those who have frequencies $\omega>|\pi|$ or $f>\left|\frac{1}{2}\right|$ are alias of the unique harmonic oscillators. This is one of the main differences between harmonic oscillators in continuous and discrete time, since it must be reminded that the unique frequencies in a continuous time harmonic oscillator are within the range $-\infty\le F<\infty$.

The second result is that the highest rate of oscillation of a discrete harmonic oscillator is reached when $\omega=\pi$.

4 ANALOGUE-DIGITAL CONVERSION

The majority of signals of interest in the scientific world are analogue. To process these analogue signals, they must be converted in a first step into digital signals, that is, the analogue signal must be transformed into a sequence of numbers of finite precision. This process is called analogue-digital conversion or A/D, a scheme of it is shown in Fig. 41 that consists of three stages:

- Sampling: Process by which it is acquired the value of the analogue signal into a series of specific instants.
- Quantification: The quantification is the conversion of values from the sampling process of an analogue signal into discrete values with finite precision. The magnitude of each acquired sample from the signal is achieved by choosing it from a finite set of possible values. The difference between the sample without being quantified $x(nT)$ and quantified sample $x_c(nT)$ is called quantification error.
- Codification: The codification process is the one that is the last performed action that provides each discrete value of the sampled and quantified signal, $x_c(nT)$, a binary sequence of b bits.

Despite the fact that in Fig. 41 the analogue-digital converter has been modelled with a sampler followed by a quantifier and an codificator, in practice the process of analogue-digital conversion is performed in a single device from which the an analogue signal input $x(t)$ generates a sequence of binary numbers.

In the following sections, it is shown that the sampling operation of an analogue signal does not introduce any distortion to the information contained in the original analogue signal if it has a finite bandwidth since an analogue signal can be reconstructed from its samples provided the sampling rate of the digitalised signal is high enough to avoid the aliasing.

On the other hand, it should be noticed that the quantification process is an irreversible process that always results in signal distortion. Relative to the quantification, it will be demonstrated that the accuracy of the measurement of an analogue signal is a function of the number of bits of the analogue-digital acquisition system.

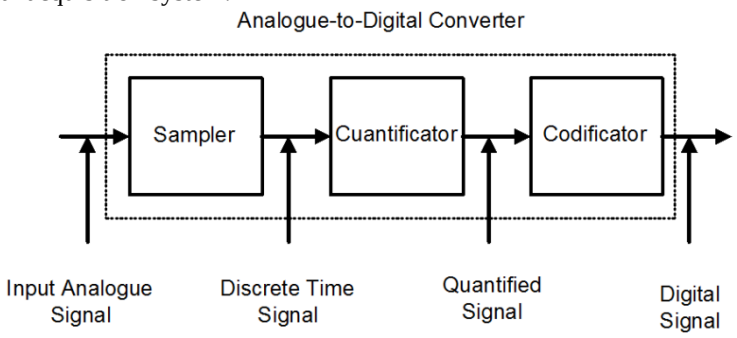

Fig. 41 Analogue-digital conversor scheme.

4.1 SAMPLING OF ANALOGUE SIGNALS

The possibilities for sampling a signal are almost infinite, however, this thesis will be restricted to the study of uniform sampling since that is the most commonly sampled methodology used in practice. The periodic sampling can be modelled as

$$x_d(n) = x(nT) \tag{44}$$

Where $x_d(t)$ is the discrete signal of sampling of the analogue signal $x(t)$ every T seconds. The time interval T between two successive samples of the analogue signal is called sampling period and its reciprocal, $\frac{1}{T} = f_s$ is known as the rate or sampling frequency whose dimension are hertz.

The periodic sampling establishes a relationship between the time variable, t, of the analogue signal and the variable sample, n, of the digital signal. The relationship between these two variables are linearly related through the sampling period T or F_s, as

$$t = nT = \frac{n}{F_s} \tag{45}$$

From equation (45) can be drawn that there is a relationship between the frequency of the analogue signals, F, and the frequency of digital signals f.

Consider an analogue signal whose form is

$$x(t) = A \cdot \cos(2 \cdot \pi \cdot F \cdot t + \Phi) \tag{46}$$

after taking periodic samples with a sampling frequency $F_s = \frac{1}{T}$ it becomes

$$x(nT) = A \cdot \cos(2 \cdot \pi \cdot F \cdot n \cdot T + \varphi) = A \cdot \cos\left(\frac{2 \cdot \pi \cdot F \cdot n}{F_s} + \varphi\right) \tag{47}$$

The comparison between (47) with (37) reveals that the variables F and f are linearly related according to

$$f = \frac{F}{F_s} \tag{48}$$

Recall that the range of F for continuous time harmonic oscillators in is

$$0 \le F \le \infty \tag{49}$$

However, for discrete time harmonic oscillators, it is

$$-\frac{1}{2} \le f \le \frac{1}{2} \tag{50}$$

The substitution of (48) into (50) gives that the frequency of a continuous time harmonic oscillator when it is sampled at a sampling frequency $F_s = \frac{1}{T}$ must be in the range

$$-\frac{F_s}{2} \le F \le \frac{F_s}{2} \tag{51}$$

and since by definition frequencies are only positive, then

$$0 \le F \le \frac{F_s}{2} \tag{52}$$

From these relationships, it is concluded that the fundamental difference between continuous and discrete signals is the range of values that their respective frequencies can take. The periodic sampling of an analogue signal is a correspondence between a range of frequencies corresponding to an infinite value of *F* and a finite range of frequencies corresponding to the value of *f*. Therefore, the maximum frequency of a discrete signal is $f = \frac{1}{2}$ and the maximum value of the frequency of a continuous signal *F*, for a sampling frequency F_s is

$$F_{\max} = \frac{F_s}{2} \tag{53}$$

Thus due to sampling of an analogue signal, an ambiguity is introduced as the maximum frequency that can be determined from an analogue signal sampled at a sampling frequency F_s is $F_{\max} = \frac{F_s}{2}$.

Let us see what occurs with frequencies higher than $\frac{F_s}{2}$

Generally, the sampling of continuous time harmonic oscillator time

$$x(t) = A \cdot \cos\left(2 \cdot \pi \cdot F \cdot t + \Phi\right) \tag{54}$$

with a sampling rate of $F_s = \frac{1}{T}$ produces a discrete signal

$$x(n) = A \cdot \cos\left(2 \cdot \pi \cdot f \cdot n + \varphi\right) \tag{55}$$

where $f = \frac{F}{F_s}$. Assuming that $0 \le F \le \frac{F_s}{2}$, the frequency *f* of *x*(*n*) is in the range $0 \le f \le \frac{1}{2}$ which is the range of frequencies for discrete signals. In this case, the relationship between *F* and *f* is univocal and therefore, it is possible to reconstruct the analogue signal *x*(*t*) from the samples of *x*(*n*).

Moreover, if the harmonic oscillator is

$$x(t) = A \cdot \cos\left(2 \cdot \pi \cdot F_i \cdot t + \Phi\right) \tag{56}$$

where

$$F_i = F + i \cdot F_s, \quad i = 1, 2, 3, \ldots \tag{57}$$

and it is sampled with a sampling frequency F_s it is clear that the frequency F_i is outside the range of (52), then the sampled signal is:

$$\begin{aligned} x(n) &= A \cdot \cos\left(\frac{2 \cdot \pi \cdot \left(F + i \cdot F_s\right) \cdot n}{F_s} + \varphi\right) = \\ &= A \cdot \cos\left(\frac{2 \cdot \pi \cdot F \cdot n}{F_s} + 2 \cdot \pi \cdot i \cdot n + \varphi\right) = \\ &= A \cdot \cos\left(2 \cdot \pi \cdot f \cdot n + \varphi\right) \end{aligned} \tag{58}$$

signal that is identical to the discrete signal (55) that has been acquired from the sampling process of the analogue signal (54). Thus it can be said that an infinite amount of analogue signals can be expressed by the same set of samples. Therefore, from the samples of $x(n)$ is not possible to know which analogue signal they represent. Similarly it can be said that the frequencies $F_i = F + i \cdot F_s$ with $-\infty < i < \infty \quad i \in \mathbb{Z}$ are indistinguishable from the frequency.

Fig. 42 shows an example of aliasing. It shows two harmonic oscillators whose frequencies are $F_1 = \frac{10}{11}$ Hz, $F_2 = \frac{1}{11}$ Hz, sampled with a sampling frequency $F_s = 1$ Hz capturing the same samples regardless of which signal is sampled. This fact follows directly from the application (57), since for $i = -1$, $F_1 = \frac{10}{11} - 1 \cdot \frac{11}{11} = -\frac{1}{11}$ and due the folding of the frequencies whose values are negative, then $F_1 = \frac{1}{11} = F_2$ [120].

Since $\frac{F_s}{2}$ corresponds to $\omega = \pi$, what is the highest frequency that can unambiguously be reconstructed given sampling frequency F_s. Furthermore, it is easy to determine the correspondence between any frequency above $\frac{F_s}{2}$ and its equivalent frequency below $\frac{F_s}{2}$, since the maximum frequency $\frac{F_s}{2}$ is a folding point, as it is the frequency whose value is 0, and therefore the alias frequencies are reflected.

Given a random analogue signal, to select the sampling frequency is needed some background information of the features of the signal to be sampled. In particular, it is needed to know some general information about the frequency content of the signal to be acquired.

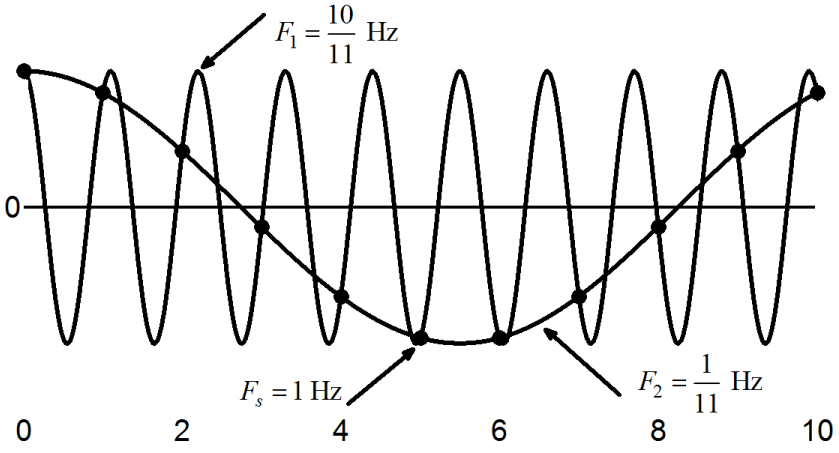

Fig. 42 Aliasing effect

Despite this consideration may seem difficult to be achieved, in general, this information is always available since, for example, in a current signal in an electrical machine is known that the values of frequency of the more important components are below 1 kHz .

It can be said that the information contained in the analogue signals are in the amplitudes, frequencies and phases of the several frequency components that the analogue signal contains, which are unknown components.

In fact, signal processing is the extraction of those characteristics then it is mandatory to establish a sampling frequency value to start the whole signal processing. To do this, it will be enough to know or set the maximum frequency of the signal to be studied for the conversion of an analogue to digital signal in an unambiguous way, allowing an accurate diagnosis.

Any analogue signal can be denoted as a sum of sines and cosines of different amplitudes, frequencies and phases, according to the Fourier Transform, that is, any signal can be denoted as:

$$x(t) = \sum_{i=1}^{N} A_i \cdot \cos\left(2 \cdot \pi \cdot F_i \cdot t + \Phi_i\right) \tag{59}$$

where N denotes the number of frequency components that composes the analogue signal. If it is needed to ensure that the analogue signal to be studied, whose frequency components are unknown, does not exceed F_{max} it will be enough to perform a low pass filter to strongly attenuate the components above F_{max}.

Therefore, it will be absolutely sure that there are no frequency components above the value of interest preventing the phenomenon of aliasing.

In practice, the low-pass filtering to remove high frequency components must be performed before the sampling of the analogue signal.

Knowing the maximum frequency component of the sampled analogue waveform allows the correct selection of the sampling frequency, accepting the limitation that the highest frequency that can unambiguously be reconstructed when the signal is sampled with a sampling frequency F_s is $\frac{F_s}{2}$. Any frequency above $\frac{F_s}{2}$ will produce identical samples than the components within the range $0 \le F \le \frac{F_s}{2}$. To avoid the aliasing a sampling frequency high enough must be chosen, that is, the chosen F_s must meet

$$F_s > 2 \cdot F_{\max} \tag{60}$$

where F_{max} is the highest frequency to be captured that the analogue signal contains.

Since $f = \frac{1}{2}$ is the highest and unique frequency in a discrete signal, the choice of the sampling frequency according to (60) avoids the problem of aliasing, that is, the condition $F_s > 2 \cdot F_{max}$ ensures that all the harmonic components of the analogue signal will correspond to the frequency

components of the discrete signal, then all the frequency components of the analogue signal will unambiguously be part of the sampled signal.

Thus, the analogue signal can be reconstructed without distortion from the discrete signal samples using a suitable interpolation method. The appropriate interpolation is specified by the sampling theorem.

The sampling theorem states that if the highest frequency contained in an analogue signal $x(t)$ is $F_{max} = B$ and the signal is sampled with a sampling frequency $F_s > 2 \cdot F_{max}$, then $x(t)$ can completely be reconstructed from its samples using the following interpolation function [121]-[123]

$$g(t) = \frac{\sin(2 \cdot \pi \cdot B \cdot t)}{2 \cdot \pi \cdot B \cdot t} \tag{61}$$

4.1.1 QUANTIFICATION OF CONTINUOUS AMPLITUDE SIGNALS

A digital signal is essentially a sequence of numbers in which each sample is represented by a finite number of digits.

The process of converting a discrete time signal of continuous amplitude into a digital signal, that is, to express each sample of the analogue signal by means of a finite number of digits is called quantification. The error in the denotation of the continuous value of the signal by a finite set of discrete values is called quantification error [119].

The quantification process will be introduced through an example. Consider the discrete time signal:

$$x(n) = 0.5^n \quad n \geq 0 \tag{62}$$

that comes from sampling the analogue signal $x(t) = 0.5^t$, $t \geq 0$ with a sampling frequency $F_s = 1\,\text{Hz}$. The signal $x(t)$ needs n digits to get a sample of $x(n)$ without error. Obviously, any computer cannot process this signal with absolute precision since the number of digits that a computer can manage is finite.

However, let us assume that it is taken only one significant digit. To remove the remaining digits they can directly be removed, which is referred to truncation or the most significant closer number with on digit, which is known as rounding, can approximate them to the value of the sample. The allowed values in the digital signal are called quantification levels, whereas the distance Δ, between two quantification levels is called resolution.

A rounding quantifier assigns each sample of $x(n)$ the nearest quantification level whereas a truncation quantifier assigns the quantification level immediately below the taken sample. The quantification error in the case of the rounding quantification is in the interval [119]

$$-\frac{\Delta}{2} \leq e(n) \leq \frac{\Delta}{2} \tag{63}$$

that is, the instantaneous quantification error cannot exceed half the value of the resolution.

If x_{min} and x_{max} denote the maximum and minimum values that $x(n)$ can take, whereas L is the number of quantification levels, then the resolution is defined as [119]

$$\Delta = \frac{x_{\max} - x_{\min}}{L-1} \tag{64}$$

where x_{max} - x_{min} is defined as the dynamic range of the signal. Notice that if the dynamic range is preset, an increase in the number of quantification levels results in an increase of the resolution leading to a decrease in the quantification error of the quantifier improving the accuracy. In practice, the quantification levels are fixed, and then by adjusting the dynamic range the quantification error can be reduced.

The quantification of analogue signals is an irreversible process and always results in a loss of information, producing an ambiguity in the measurement of magnitude values of the signal, since a continuous signal in magnitude many elements have the same image since all samples at a distance less than $\frac{\Delta}{2}$ from certain level are assigned with the same value.

4.1.2 QUANTIFICATION OF SINUSOIDAL SIGNALS

Fig. 43 shows the sampling and quantification process of a harmonic oscillator $x(t) = A \cdot \sin(\Omega \cdot t)$ where rectangular mesh is used for the sampling and quantification of the signal. The horizontal lines denote the quantification levels of the magnitude, whereas the vertical lines denote the time values where a sample of the signal is sampled.

From an analogue signal, $x(t)$ is acquired a discrete time signal $x(nT)$ by the sampling process and finally after the quantification process a discrete amplitude signal $x_c(nT)$ is generated

If the sampling frequency F_s satisfies the sampling theorem, the only error in the analogue to digital conversion process will be the quantification. The quantification error will at every moment

$$e(t) = x(t) - x_c(t) \tag{65}$$

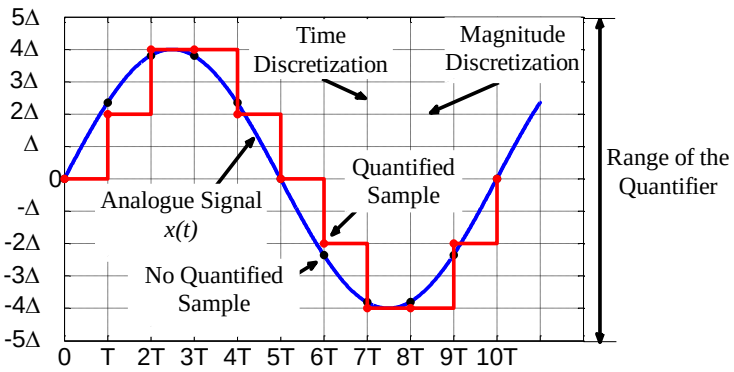

Fig. 43 Sampling and quantification of a sinusoidal signal.

whose evolution is almost linear between two sampling points. Furthermore, the average power of the quadratic error is computed as

$$P_{err} = \frac{1}{2\delta}\int_{-\delta}^{\delta} e^2(t)\cdot dt = \frac{1}{\delta}\int_{0}^{\delta} e^2(t)\cdot dt \tag{66}$$

Since $e(t) = \left(\frac{\Delta}{2\delta}\right)\cdot t$, $-\delta \le t \le \delta$, then

$$P_{err} = \frac{1}{\delta}\int_{0}^{\delta}\left(\frac{\Delta}{2\delta}\right)^2 t^2\cdot dt = \frac{\Delta^2}{12} \tag{67}$$

If the quantifier has b accuracy bits, the resolution is $\Delta = \frac{2\cdot A}{2^b}$. Then

$$P_{err} = \frac{A^2}{3\cdot 2^{2b}} \tag{68}$$

On the other hand, the power of an analogue signal is

$$P_x = \frac{1}{T}\int_{0}^{T} A\cdot\sin(\Omega\cdot t) = \frac{A^2}{2} \tag{69}$$

The quality of the analogue-digital converters is measured in terms of SQNR (signal to quantification noise ratio), that provides the relationship between the power of the signal and noise

$$SQNR = \frac{P_x}{P_{err}} = \frac{3}{2}\cdot 2^{2b} \tag{70}$$

Relation that if it is expressed in decibels is

$$SQNR(dB) = 10\cdot\log_{10}(SQNR) = 1.76 + 6.02\cdot b \tag{71}$$

That means that the SQNR increases approximately 6 dB per bit added in the acquisition system [119].

4.2 CODIFICATION OF QUANTIFIED SAMPLES

In the quantification process in an analogue to digital converter, it assigns a unique binary number at each quantification level. If it has *L* quantification levels that will require at least *L* different binary levels with a word length of *b* bits there are $2\cdot b$ different binary numbers, that is, a word length of *b* bits has $2^b \ge L$ ó $b \ge \log_2(L)$ therefore, if it is set the number of the needed quantification levels, it can be computed the necessary number of bits for the analogue-digital converter.

5 SUMMARY AND CONCLUSIONS OF THE CHAPTER

In this chapter, it has been developed the basic concepts for a proper signal acquisition.

The bases of a good signal acquisition are based on the right selection of the sampling frequency, whose value determines the highest frequency component that can be displayed on a spectrum of the acquired signal. The right selection of the sampling frequency avoids the problem of aliasing.

The importance of the time of signal acquired was also discussed in this chapter. Its selection allows the setting of the desired frequency resolution on a current spectrum regardless of the sampling frequency.

The difference between analogue and digital signals has also been discussed. Knowing the difference between them allows the application of certain processing techniques only valid for digital signals, encouraging the understanding of the techniques used in them.

In this chapter it has been demonstrated that if the highest frequency contained in an analogue signal $x(t)$ is $F_{max} = B$ and the signal is sampled with a sampling frequency $F_s > 2 \cdot F_{max}$, then $x(t)$ can entirely be reconstructed from its samples using the following interpolation function [121]-[123]

$$g(t) = \frac{\sin(2 \cdot \pi \cdot B \cdot t)}{2 \cdot \pi \cdot B \cdot t} \tag{71}$$

CHAPTER VI: EXTRACTION OF THE FAULT COMPONENT. SIGNAL FILTERING AND SIGNAL FREQUENCY SHIFTING

1 INTRODUCTION

In this chapter discusses the techniques used for the several pretreatments to extract the fault components of acquired current signals for the diagnosis of electric machines.

The chapter is structured into two sections: (i) signal filtering and (ii) signal frequency shifting.

The first part of the chapter develops the three filtering methods used for the extraction of the different fault components. The filtering methods used in this thesis are: (i) the Discrete Wavelet Transform (ii) the Wavelet Packet Transform and (iii) a new filtering method proposed by the author called Spectral Filter or filtering in the frequency domain.

The second part of this chapter develops two techniques for the signal shifting of the frequency components in the frequency spectrum. The techniques used for the frequency shifting are: (i) the technique based on the Frequency Displacement Theorem and (ii) the Hilbert transform.

Finally it is presented the conclusions of this chapter.

The main sources used for the elaboration of this chapter were [59], [61], [62], [66], [113], [114], [138]-[140].

2 SIGNAL FILTERING

The application of different filtering techniques allows the extraction of a priori hidden information of a signal.

In this section is introduced three filtering techniques used for the extraction of the necessary information from the signal for the diagnosis of electrical machines by: the Discrete Wavelet Transform, the Wavelet Packet Transform, and the Spectral Filter based on the properties of the Discrete Fourier Transform.

In the following sections the three techniques are introduced, describing how they have to be applied its advantages and inconveniences.

First the Wavelet Transform is introduced since it is one of the methods more currently used for the signal filtering.

Secondly, it is introduced the use of the Wavelet Packet Transform since it is based on the Discrete Wavelet filters, and therefore, once the filtering process with the Discrete Wavelet filters has been understood, the understanding of the operation of the Wavelet Packet filters is immediate.

Lastly it is introduced a new method of filtering, the Spectral Filter. The spectral filter is proposed as an alternative to the Wavelet and Wavelet Packet filters. The filters in the frequency domain are based on the properties of the Discrete Fourier Transform and can easily be applied to the acquired waves due to its digital nature.

2.1 WAVELET TRANSFORM

2.1.1 INTRODUCTION

The most common way of denoting the signals is in a time-amplitude although in the engineering field the signals need to be transformed to other domains (time-frequency, frequency, etc.) to carry out a more complex analysis.

Transforms allow the identification of certain hidden information in the signal through the switch of domains. The selection of the transform to be applied is based on the information that is needed to be extracted of the acquired signal and each techniques has its particular advantages and inconveniences.

The signal frequency content is one of the most important elements in digital signal processing, and it is in this area where the Fourier Transform is the most used technique for the computation of the signal frequency spectrum.

However, the Fourier transform has a major drawback that, although it allows the computation of the signal frequency spectrum, it gives no information of when the frequencies occur.

In several fields of science such as medicine, it is required the time analysis of non-stationary signals such as electrocardiograms, electromyography, etc. in both time and frequency simultaneously, that is, it is mandatory a time-frequency signal representation.

To solve this problem, the first proposed solution was the Short Time Fourier Transform (STFT). Short Time Fourier Transform is a modification of the Fourier Transform since the STFT splits a non-stationary signal into smaller intervals, which may be assumed stationary by the signal convolution with fixed width windows. After this split of the signal it is applied the Fourier Transform to each of the previously performed divisions composing the STFT.

The main drawback of the STFT is the use of fixed width windows, then according to the Heisenberg uncertainty's principle is impossible to determine with great precision a particular frequency at a specific time. However, it can be determined the frequency range at a time interval. This raises the problem of frequency and time resolution.

Assuming a stationary signal, the use of a narrow window implies a poor frequency resolution, and then it is difficult to know what the exact values of signal frequencies are in the small taken time interval.

If the window's width is increased, the frequency resolution improves at the expense of a reduction in the temporal resolution, that is, it is better known the frequency value at the expense of not knowing the time at which they occur.

Another drawback of the selection of wide windows is that they can violate the principle of stationary condition. Therefore, it must be reached a compromise on the wide of the window. After selecting the window's width, the frequency and time resolution are fixed for all frequencies and resolutions that are wanted to be observed.

The Wavelet Transform solves that problem to some extent. Unlike the Short Time Fourier Transform, which analyses the signal with a fixed width window, the Wavelet Transform uses narrow windows for high frequencies and wide windows for low frequencies. This results in a multiresolution analysis since the signal is analysed at different resolutions depending on the studied frequencies. Thanks to the multi-resolution analysis the Heisenberg uncertainty's principle is not violated.

Multiresolution analysis carried out by the Wavelet Transform is performed so as the frequency to be analysed increases, the time resolution increase while reducing the frequency resolution, whereas the frequency to be analysed decreases the frequency resolution improves, worsening the resolution in time, that is, a high frequency can be located more accurate in time than a low frequency whereas the value of a low frequency can be determined more accurately than the value of a high frequency.

Fig. 44 shows the structure of the time-frequency plane for four different types of transforms. Fig. 44.a. symbolises the structure of the time-frequency plane used for the analysis in the time domain where it can be seen that it gives no information on the frequency at any instant, whereas Fig. 44.b shows the time-frequency plane structured according to a transform in the frequency domain where it is seen that it gives no time information of the signal at any time. In Fig. 44.c shows the organization of the time-frequency plane of the STFT, where it is depicted that this transform has a fixed resolution for any instant of time and any frequency, whereas in Fig. 44.d shows the structure of the time-frequency plane for the Wavelet Transform where it is seen that its resolution in time and frequency is variable based on the value of the observed frequency.

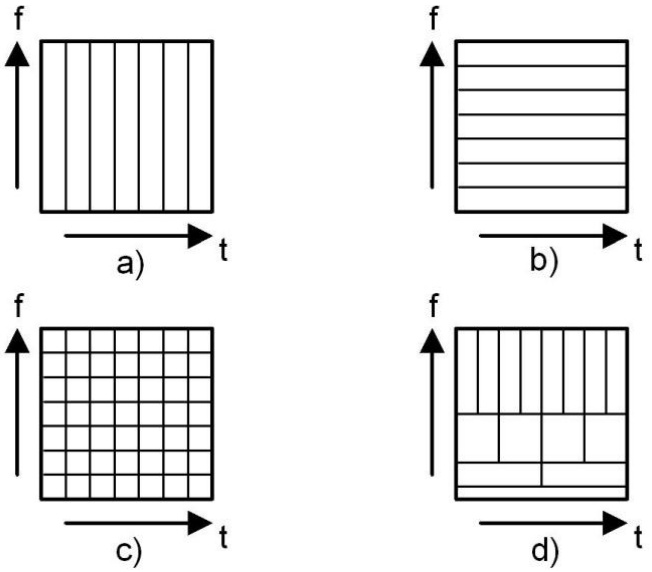

Fig. 44 Time-frequency planes for: a) Time domain b) Frequency domain c) Short Time Fourier Transform d) Wavelet Transform

To recapitulate, at this point it can be affirmed that the transform of a signal is another way of denoting a signal, since the information contained in the original signal does not change when it is applied the transform on it. Moreover, the Wavelet Transform performs a transformation from the time domain to the time-frequency domain and it has been developed to overcome the drawbacks of the Short Time Fourier Transform, which can also be used for analysis of non-stationary signals, although with a constant resolution for all frequencies, whereas the Wavelet Transform allows multiresolution analysis.

2.1.2 CONTINUOUS WAVELET TRANSFORM

A wave is defined as a function of time or space; whereas the wavelets are defined as waves located with its energy concentrated in time or in space, and are perfectly suitable for transient analysis. One of the main differences between the Wavelet Transform and the Fourier Transform or the Short Time Fourier transform is that whereas the Wavelet Transform uses finite energy waves, the other two use infinite energy signals.

Wavelet Transform analysis is similar to that performed with the Short Time Fourier Transform since the signal is multiplied by a wavelet function similar to the multiplication by a window in the STFT, computing the Wavelet Transform for each generated segment. Yet and in contrast to the STFT, for the application of the Wavelet Transform the window's width varies with each frequency range having for higher frequencies good time resolution and low frequency resolution whereas for low frequencies occurs the opposite effect.

The Continuous Wavelet Transform is defined by (72) where $x(t)$ is the analysed signal and $\psi(t)$ is the mother wavelet or base function. All the Wavelet functions in the transform are derived from the mother wavelet through a translation –shifting the wave- and scaling -expanding or compressing.

$$X_{WT}(\tau, z) = \frac{1}{\sqrt{|z|}} \int x(t) \cdot \psi^* \left(\frac{t-\tau}{z} \right) dt \tag{72}$$

The mother wavelet that generates all the rest of the base functions is determined based on predetermined criteria that determine the desired features in the wavelet function. The shifting parameter τ associates the position of the Wavelet function as it goes through the analyzed signal that corresponds with the time information of the Wavelet Transform. The calling parameter z is defined as $z=1/f$ and corresponds with the frequency information. The scaling expands and compresses the signal. Large values of the scaling parameter -low frequencies- expands the signal, favouring the observation of the information in the signal frequency domain, whereas small values -high frequencies- compresses the signal, favouring more accurate resolution in time domain. It must be taken into account that the Wavelet transform performs the convolution between the signal and the base function.

The discretization of the continuous wavelet transform enables its computation by computers since it is computed by sampling the time-scale level. The sampling frequency can be changed according to the scale factor

without violating the sampling theorem that states that the sampling frequency to reconstruct a signal must be at least twice the maximum frequency of the original signal. Therefore, the more the value of the scaling parameter increases -lower frequencies-, the more the sampling frequency can be reduced in order to reduce the number of computations performed.

2.1.3 DISCRETE WAVELET TRANSFORM

The computation of each of the necessary wavelets for the implementation of the CWT can require a lot of time and resources according to the required resolution and length of the wave. To reduce the computational cost is developed the Discrete Wavelet Transform which is based on a sub-band code that allows a fast computation of the Wavelet Transform, then its implementation is easy with low computational cost.

The DWT bases were established in 1976 when the discrete-time signal decomposition techniques began to be developed [113]. Similar works to the discrete time signal decomposition were conducted in the field of audio signal transmission that were given the name of sub-band coding.

In 1983, a similar technique to the sub-band coding was developed and took the name of pyramidal coding [114]. At the end of the eighties, there were introduced enhancements to these two codes that resulted in some efficient multiresolution signal analysis schemes.

In the CWT signals are analysed using a set of functions which are related to each other by basic operations of translation and scaling. In the case of the DWT, the time-frequency denotation of a digital signal is computed by digital filtering techniques by passing the signal to be analysed through digital filters that separate the different frequencies to be observed in a series of filter stages.

2.1.4 MULTIRESOLUTION BANK FILTER ANALYSIS

Filters are one of the most elements used in the function processing of both analogue and digital functions. Wavelets can be programmed through a rescaled iteration of filters. The signal resolution, which is a measure of the amount of details of information that the signal contains, is determined by the number of filtering operations to which the signal undergoes.

The DWT is computed by a succession of low-pass and high-pass filters in the discrete signal domain signal as shown in Fig. 45 that are called Mallat algorithm or Mallat decomposition tree [138]. Its significance lies in the way that the continuous time multiresolution method is connected with discrete time filters. In Fig. 45, the signal is denoted by $x[n]$, where n is an integer. The low pass filter is denoted by L whereas the high-pass filters are denoted by H. For each level of decomposition a high-pass filter produces a signal detail, $d[n]$, whereas the low pass filter associated with it computes approximations, $a[n]$. Furthermore, in each decomposition step each filter enables to pass half the frequency of the previous stage filters doubling thus the frequency resolution in every stage of filtering, what results in a halving of the uncertainty in the determination of the frequency.

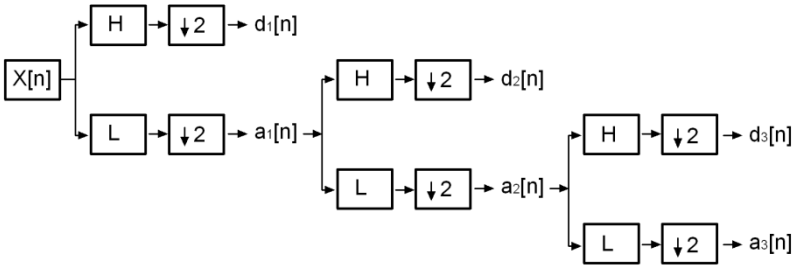

Fig. 45 DWT tree decomposition. Level 3

On the other hand and according to the sampling theorem, if the signal has a maximum frequency f_{max} there will be needed $2 \cdot f_{max}$ samples to reconstruct it, but after each filtering step, the frequency is halved, then the first stage goes from f_{max} to $f_{max}/2$ thereby enabling no loss of information by taking half of the samples of the signal. This decimate reduces the computational cost of the computation of the DWT.

The filtering process and decimation continues until it is reached the desired level of decomposition considering that the maximum value of decomposition depends on the length of the analysed signal. The DWT of the original signal is computed by concatenating all the coefficients $a[n]$ y $d[n]$ starting from the last decomposition level.

Fig. 46 shows the reconstruction tree of the original signal from the Wavelet coefficients previously computed. The reconstruction is basically the reverse process of the signal decomposition. The process of signal reconstruction is to combine the approximation and detail of each filter stage by two synthesis filters -one low band pass and other high band pass- while doubling the sampling frequency of the signal. This process runs in reverse to the decomposition tree until reconstructing the original signal.

2.1.5 WAVELET TRANSFORM FILTERING

One of the main applications of the Wavelet transform is the filtering of signals through the properties discussed for the multiresolution analysis.

The Discrete Wavelet Transform acts as a dyadic filter as it is shown in [61], [137], [138] where the bandwidth of each filter depends on the sampling frequency of the signal filter and also on the Wavelet decomposition level.

That is, for each interval of the signal, the DWT decomposes the original signal into a sum of wavelet signals (an approximation a_n and a n number of details d_j) [138]

$$I = a_n + d_n + d_{n-1} + ... + d_2 + d_1 \tag{73}$$

Each wavelet signal -a_n or d_j- is associated with a particular frequency band, that is, the wavelet signal shows the evolution of the frequency components of the original signal in the frequency range extracted by the wavelet filter [66], [137].

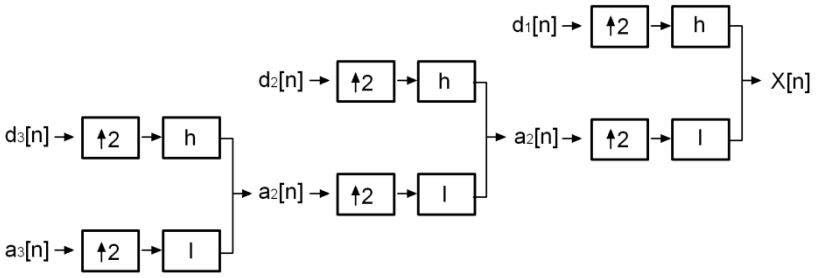

Fig. 46 DWT reconstruction tree. Level 3.

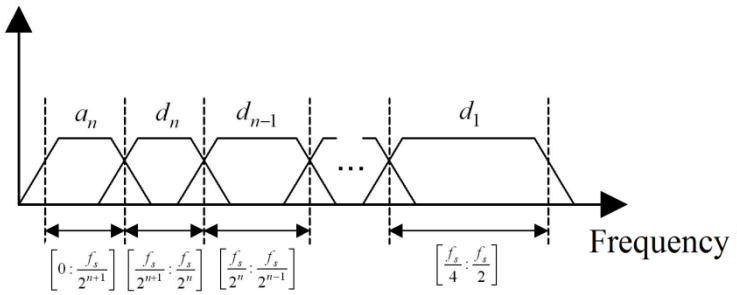

Fig. 47 Dyadic DWT filter decomposition

In particular, if f_s is the sampling frequency, d_j will be the detail that contains the information of the signal corresponding to the frequency band in the interval [66]

$$f\left(d_j\right) \in \left[\frac{f_s}{2^{j+1}}, \frac{f_s}{2^j}\right] \tag{74}$$

Whereas the approximation a_n will contain the low frequencies of the signal corresponding to the interval [66]

$$f\left(a_n\right) \in \left[0, \frac{f_s}{2^{n+1}}\right] \tag{75}$$

Therefore, the DWT performs the filtering as it is shown in Fig. 47. Notice that the Wavelet filter is not ideal, resulting in an overlap between the filtering bands [61], [62] causing some distortion in the waves if the boundaries of the bands are close to a large enough signal component.

The Wavelet Transform has the property of linearity, and hence the details and approximations can be combined to create the frequency band that satisfies the required needs for the diagnostic process.

The procedure for the extraction of a particular frequency band using the smallest filter band is introduced in the following lines.

Assume that $B_{sig} = \left[0, \frac{f_s}{2}\right]$ is the frequency range of a signal *x* sampled at a frequency f_s from which the frequency interval $B_{teo} = [f_1, f_2]$ with $f_1 < f_2$ is to be extracted.

The lowest order approximation that will contain the interval B_{teo} will be that which contains the frequency f_2 whose decomposition order is computed by:

$$nC = \text{int}\left[\frac{\log \frac{f_s}{f_2}}{\log(2)} - 1\right] \tag{76}$$

If it is extracted the signal component that corresponds to the approximation $x_{fil}(t) = a_{nC}(t)$, it will only contain the frequencies within the range $B' = \left[0, \frac{f_s}{2^{1+nC}}\right]$ where it is obviously fulfilled that $B' \subseteq B_{teo}$

The next step is to remove as much as possible of the low frequencies. That is performed by determining the order of the higher approximation that does not contain f_1 through:

$$nNC = \text{int}\left[\frac{\log \frac{f_s}{f_1}}{\log(2)}\right] \tag{77}$$

To remove the low frequency band it should be subtracted the approximation that does not contains f_1 from the approximation that contains the frequency band B_{teo}, then the filtered signal is:

$$CF_{fil}^{DWT}(t) = a_{nC}(t) - a_{nNC}(t) \tag{78}$$

The frequency band of the filtered signal will be:

$$B_{real}^{DWT} = \left[\frac{f_s}{2^{1+nNC}}, \frac{f_s}{2^{1+nC}}\right] \tag{79}$$

that satisfies $B_{real}^{DWT} \subseteq B_{teo}$, that is it has been achieved the split of the lowest frequency band that contains the specific frequency band with the subtraction of two wavelet approximations.

However, despite having met the proposed goal, the filtering with the Discrete Wavelet Transform has the drawback that the frequency bands are predetermined by the selection of the sampling frequency, thus preventing the control of the band to be extracted what usually causes that the frequency bands of the extracted signal are too large.

2.2 WAVELET PACKET TRANSFORM

Multiresolution analysis based on wavelet theory allows the decomposition of a signal through the subdivisions shown in the previous section, but this process has the disadvantage that high frequency bands have a very high uncertainty in frequency.

To solve this problem the Wavelet Packet Transform is developed. The Wavelet Packet Transform involves the application of a filter bank similar to those previously used in the original decomposition generating, from every detail of the original signal, a new approach, and a new detail [59]. Thus is achieved a complete homogeneous decomposition of the signal in bands as accurate as desired, as it is shown in Fig. 48.

The reconstruction of a signal decomposed by the Wavelet Packet Transform follows the same procedure that undergoes the signal to be reconstructed with the discrete wavelet transform.

2.2.1 WAVELET PACKET TRANSFORM FILTERING

The DWT filtering has the drawback that once set a sampling frequency, the filter bands are fixed and may not be adequate to perform the filtering process, the only way to modify them it is by varying the sampling frequency, which requires again to the acquisition of the signal what is generally not feasible. Therefore, the Wavelet Packet filtering is developed, since it offers the advantage of being able to select the maximum bandwidth for all the filter stages as it is shown in Fig. 49, regardless of the sampling frequency.

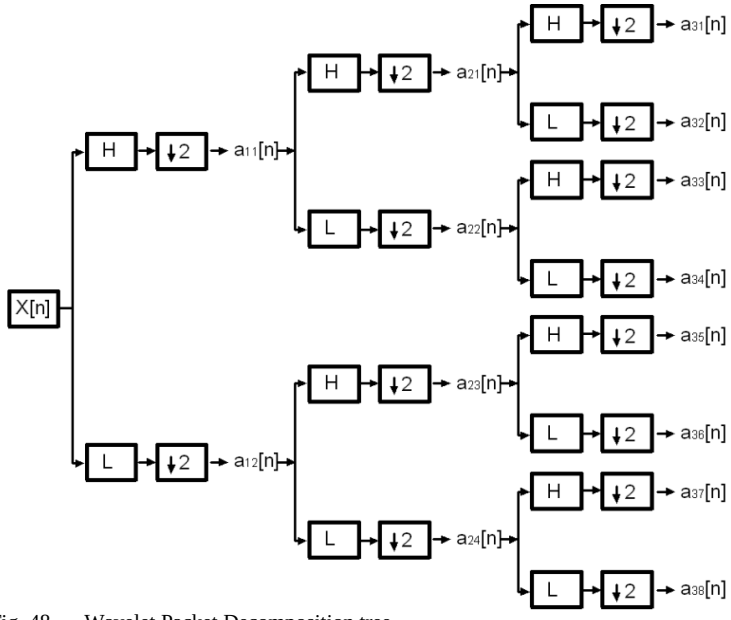

Fig. 48 Wavelet Packet Decomposition tree

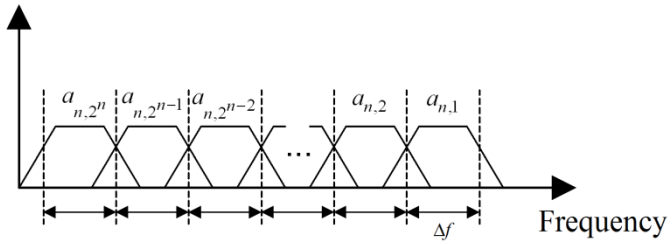

Fig. 49 Frequency band Wavelet Packet decomposition

That is, the Wavelet Packet Transform allows the decomposition of original signal in a finite number of sub-signals that have the same constant bandwidth value for all of them

$$I = \sum_{i=1}^{2^n} a_{n,i} \tag{80}$$

The main advantage of the Wavelet Packet versus the Discrete Wavelet filtering is that it can limit the maximum range of the band pass filter although it cannot determine its boundary values beforehand.

The extraction process of the same frequency band as in the previous case is initiated by selecting the maximum value of frequency increase that expands the frequency band to be extracted, both for its lower and upper values, that is, it is intended the extraction of the frequency band $B_{teo} = [\, f_{\min}, f_{\max} \,]$ and it should be set the maximum frequency increase to create a new interval $B'^{WP}_{teo} = [\, f_{\min} + \Delta f, f_{\max} + \Delta f \,]$. The value of Δf yields the minimum decomposition order that does not contain Δf by (81)

$$n_{\Delta f} = \operatorname{int}\left[\frac{\log \dfrac{f_s}{\Delta f}}{\log(2)} \right] \tag{81}$$

With the computed decomposition order calculated $n_{\Delta f}$ it is determined the effective frequency increase that will increase the limits of the bands of the designed filter:

$$d = \frac{f_s}{2^{1+n_{\Delta f}}} \tag{82}$$

Finally it is computed the width of the bands extracted by the Wavelet Packet according to (83) that meets the condition $B'^{WP}_{teo} \subseteq B^{WP}_{real} \subseteq B_{teo}$:

$$B_{real} = [\, k_{\inf} \cdot d, k_{\max} \cdot d \,] \tag{83}$$

With

$$\begin{aligned} k_{\inf} &= \operatorname{int}\left(\frac{f_{\min}}{d} \right) \\ k_{\sup} &= \operatorname{int}\left(\frac{f_{\max}}{d} + 1 \right) \end{aligned} \tag{84}$$

where the filtered signal is

$$CF_{fil}^{WP}(t) = \sum_{k_{\min}}^{k_{\max}} a_i \tag{85}$$

2.3 SPECTRAL FILTER

Recall that a finite energy aperiodic signal has a continuous frequency spectrum. Let us assume the discrete time aperiodic signal $x(n)$, whose Fourier Transform is

$$X(\omega) = \sum_{n=-\infty}^{\infty} x(n) \cdot e^{-j \cdot \omega \cdot n} \tag{86}$$

Suppose that $X(\omega)$ is periodically sampled with frequency spacing $\Delta\omega$ in radians between successive samples. Since $X(\omega)$ is periodic with period $2 \cdot \pi$, there will be only needed to take samples of the fundamental period. For convenience, it is taken N equally spaced samples in the range $0 \leq \omega \leq 2 \cdot \pi$, spaced $\Delta\omega = \frac{2 \cdot \pi}{N}$.

Firstly, there will be studied the effect of the selection of the number of samples in the frequency domain N.

If (86) is computed with $\omega = \frac{2 \cdot \pi \cdot k}{N}$ then

$$X\left(\frac{2 \cdot \pi \cdot k}{N}\right) = \sum_{n=-\infty}^{\infty} x(n) \cdot e^{-j \cdot \frac{2 \cdot \pi \cdot k \cdot n}{N}} \tag{87}$$

summation (87) can be subdivided into an infinite number of summations, each containing N terms. Thereby

$$\begin{aligned} X\left(\frac{2 \cdot \pi \cdot k}{N}\right) = \ldots + \sum_{n=-N}^{-1} x(n) \cdot e^{-j \cdot \frac{2 \cdot \pi \cdot k \cdot n}{N}} + \sum_{n=-N}^{-1} x(n) \cdot e^{-j \cdot \frac{2 \cdot \pi \cdot k \cdot n}{N}} + \\ + \sum_{n=-N}^{-1} x(n) \cdot e^{-j \cdot \frac{2 \cdot \pi \cdot k \cdot n}{N}} + \ldots = \\ = \sum_{l=-\infty}^{\infty} \sum_{n=lN}^{lN+N-1} x(n) \cdot e^{-j \cdot \frac{2 \cdot \pi \cdot k \cdot n}{N}} \end{aligned} \tag{88}$$

Changing the inner summation index from n to n-lN and exchanging the order of summations, there is

$$X\left(\frac{2 \cdot \pi \cdot k}{N}\right) = \sum_{n=0}^{N-1} \left[\sum_{l=-\infty}^{\infty} x(n - lN) \right] \cdot e^{-j \cdot \frac{2 \cdot \pi \cdot k \cdot n}{N}} \tag{89}$$

where

$$x_p(n) = \sum_{l=-\infty}^{\infty} x(n - lN) \tag{90}$$

is computed by periodically repeating $x(n)$ every N samples. Thus $x(n)$ is clearly periodic with fundamental period N. Therefore, $x(n)$ can be expanded in Fourier series as

$$x_p(n) = \sum_{k=0}^{N-1} c_k \cdot e^{j \cdot \frac{2 \cdot \pi \cdot k \cdot n}{N}} \tag{91}$$

where the Discrete Fourier coefficients are

$$c_k = \frac{1}{N} \sum_{n=0}^{N-1} x_f(n) \cdot e^{-j \cdot \frac{2 \cdot \pi \cdot k \cdot n}{N}} \tag{92}$$

if it is compared (89) with (92), there is

$$c_k = \frac{1}{N} X\left(\frac{2 \cdot \pi \cdot k}{N}\right) \tag{93}$$

hence

$$x_p(n) = \frac{1}{N} \sum_{k=0}^{N-1} X\left(\frac{2 \cdot \pi \cdot k}{N}\right) \cdot e^{j \cdot \frac{2 \cdot \pi \cdot k \cdot n}{N}} \tag{94}$$

Equation (94) gives the reconstruction of the periodic signal $x_p(n)$ from the samples of the spectrum $X(\omega)$. However, this does not mean that one can reconstruct $X(\omega)$ or $x(n)$ from the samples of $x_p(n)$. To achieve that it is studied the relationship between $x_p(n)$ and $x(n)$.

The succession of values $x_p(n)$ is the periodic extension of the values $x(n)$ as it is indicated in (90). It is trivial that $x(n)$ can be reconstructed from $x_p(n)$ if there is no aliasing in the time domain, that is, if $x(n)$ is limited in time to a shorter duration than the fundamental period, $x_p(n)$.

The described situation is shown in Fig. 50. Without loss of generality it can be considered that a finite duration sequence of $x(n)$ which is different from zero in the interval $0 \le n \le L-1$. In Fig. 50shows that when $N \ge L$

$$x(n) = x_p(n) \quad 0 \le n \le N-1 \tag{95}$$

therefore $x(n)$ can be reconstructed from $x_p(n)$ with no ambiguity.

On the other hand if $N < L$ $x(n)$ cannot be reconstructed from its periodic extension due to aliasing in the time domain.

Thus it can be concluded that the spectrum of a aperiodic discrete-time signal of finite duration can exactly be reconstructed from the samples at the frequencies $\omega = \frac{2 \cdot \pi \cdot k}{N}$, if $N \ge L$.

The procedure involves the computation of $x_p(n)$, $n = 0,1,2,...N-1$, from (94) and then

$$x(n) = \begin{cases} x_p(n) & 0 \le n \le N-1 \\ 0 & \text{any other case} \end{cases} \tag{96}$$

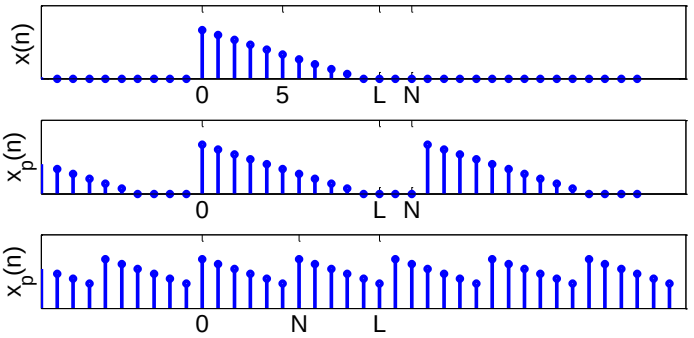

Fig. 50 Reconstruction of a digital signal. a) Original signal. b) $x_p(n)$ signal that allows the reconstruction of the original signal with no ambiguity. c) $x_p(n)$ signal that does not allow the reconstruction of the original signal due to aliasing in the time domain.

In general, when it is taken a series of equally spaced frequency samples $X\left(\frac{2\cdot\pi\cdot k}{N}\right)$ they do not uniquely denote the original sequence $x(n)$ where $x(n)$ is of finite duration. In fact, the opposite effect occurs, since a series of samples in frequency $X\left(\frac{2\cdot\pi\cdot k}{N}\right)$ correspond to a periodic sequence $x_p(n)$ of period N where $x_p(n)$ is a version of $x(n)$ with aliasing in time.

When a sequence $x(n)$ is of finite duration and $L \le N$ then $x_p(n)$ is simply a periodic repetition of $x(n)$ where $x_p(n)$ is the only period given by

$$x_p(n) = \begin{cases} x(n) & 0 \le n \le L-1 \\ 0 & L \le n \le N-1 \end{cases} \tag{97}$$

Thus if it is taken a series of frequency samples $X\left(\frac{2\cdot\pi\cdot k}{N}\right)$ it denotes the unequivocal finite duration sequence $x(n)$ since it holds that $x(n) \equiv x_p(n)$ in a fundamental period. Therefore, the original finite duration sequence $x(n)$ can be computed from the frequency samples $X\left(\frac{2\cdot\pi\cdot k}{N}\right)$ by (94).

That is, a finite duration sequence $x(n)$ whose length is L, then $x(n) = 0$ for $n < 0$ and $n \ge L$ with a Fourier Transform

$$X(\omega) = \sum_{n=0}^{L-1} x(n)\cdot e^{-j\cdot\omega\cdot n} \quad 0 \le \omega \le 2\cdot\pi \tag{98}$$

where the upper and lower indices of the summation reflects the fact that $x(n) = 0$ is out of range $0 \le n \le L-1$.

If $X(\omega)$ is sampled at equally spaced frequencies $\omega = \frac{2 \cdot \pi \cdot k}{N}$ where $N \geq L$ there is a series of samples such as

$$X(k) = X\left(\frac{2 \cdot \pi \cdot k}{N}\right) = \sum_{n=0}^{L-1} x(n) \cdot e^{-j\frac{2 \cdot \pi \cdot k \cdot n}{N}}$$
$$X\left(\frac{2 \cdot \pi \cdot k}{N}\right) = \sum_{n=0}^{N-1} x(n) \cdot e^{-j\frac{2 \cdot \pi \cdot k \cdot n}{N}} \quad (99)$$

where the upper summation index can be increased from $L-1$ to $N-1$ since $x(n) = 0$ for $n \geq L$.

Equation (99) transforms the sequence $\{x(n)\}$, whose length is $L \leq N$, into a frequency samples sequence $\{X(k)\}$ whose length is N. Since the frequency samples are computed by evaluating the Fourier transform $X(\omega)$ at a set of N discrete frequencies and equally spaced, the relationship (99) is called the Discrete Fourier Transform of $x(n)$. Moreover, the relation that allows the reconstruction of $x(n)$ from the frequency samples

$$x(n) = \frac{1}{N} \sum_{k=0}^{N-1} X(k) \cdot e^{j \cdot \frac{2 \cdot \pi \cdot k \cdot n}{N}} \quad (100)$$

which is called the inverse discrete Fourier transform enables the spectral filtering.

2.3.1 SPECTRAL FILTERING

The DFT filtering, spectral filter, allows the extraction of any band of frequencies, regardless of the selected sampling frequency with no transition zones (Fig. 51), improving the accuracy of the filtering process if it is compared to the DWT or WP filters.

One of the drawbacks of the spectral filter is that its resolution is dependent on the total time of the acquired wave according to

$$res = \frac{1}{t_{total}} \quad (100)$$

To achieve resolutions of 0.1 Hz order, it is necessary to acquire waves of at least 10 seconds.

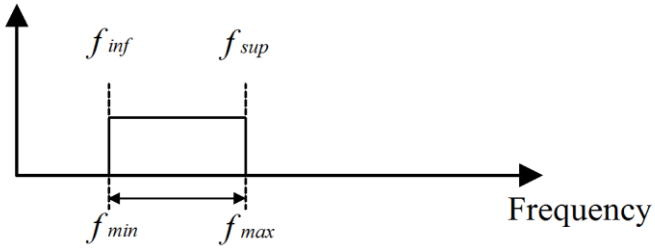

Fig. 51 Extraction of a frequency band through the spectral filter

Another drawback of the spectral filter is that its use is only valid once the waveform has completely been acquired. The use of spectral filter is not applicable in systems that must be monitored in real time.

The extraction of a frequency band with the spectral filter begins with the selection of the limits of the band to be extracted. The only restriction to be applied is the maximum resolution that can be achieved, depending on the total taken time taken of the wave according to (100).

Once the limits to be extracted, f_{min} y f_{max}, have been chosen, is applied to the wave the DFT, transforming a time domain signal the frequency domain.

After that, it will be enough select all the coefficients corresponding to the frequencies for the band to be filtered and apply the Inverse Discrete Fourier Transform to compute the filtered signal in the time domain.

2.4 EXAMPLE: DECOMPOSITION OF A CHIRP WAVE B MEANS OF THE DWT, WP AND SPECTRAL FILTER

A chirp signal is a wave that its frequency increases or decreases with time. If the increase (or decrease) of the instantaneous frequency of the chirp wave varies linearly with time is known by the name of linear Chirp.

Fig. 52 shows the evolution over time of a wave with a linear chirp, whose instantaneous frequency rate increases at 50 Hz/sec, for one second starting from the frequency 0 Hz

In this section, a linear Chirp 10 seconds long that starts from the frequency of 0 Hz, whose instantaneous rate of instantaneous frequency is 50 Hz/second, sampled at 1 kHz is decomposed through the DWT, WP and Spectral filter, showing the differences between them.

The chosen sampling frequency of 1 kHz allows the monitoring of frequencies up to 500 Hz, according to the Nyquist theorem. That value corresponds to the maximum frequency of the linear chirp waveform analyzed.

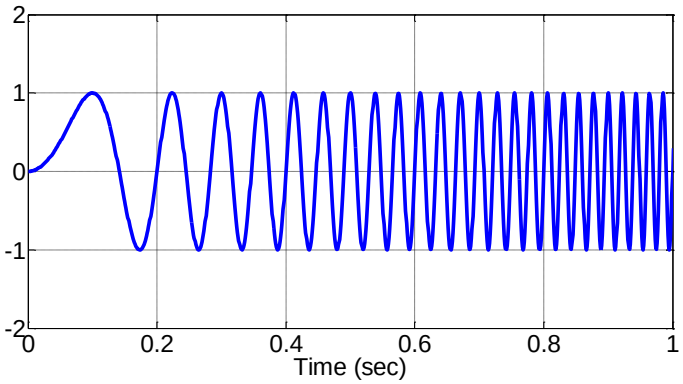

Fig. 52 Chirp wave $x = \sin(50 \cdot \pi \cdot t^2)$ in the range [0, 1] seconds.

The decomposition of a signal using the filters based on the Wavelet Transform (DWT and WP filter) is completely defined by the sampling frequency and the order of decomposition. Furthermore, the decomposition intervals of the spectral filter can be chosen by the user with a maximum frequency resolution equal to the inverse the total acquired signal time, being the maximum observable frequency determined by the Nyquist theorem.

As a result of the sampling frequency of 1 kHz, the maximum observable frequency for the three filters is 500 Hz according to the Nyquist Theorem.

The order of the decomposition chosen for the decomposition of the signal by the DWT and WP filter is 3. The frequency bands that can be extracted with both filters are shown in Table 13.

The acquired time waveform is 10 seconds. Thus, the maximum frequency resolution of the spectral filter takes the value of 1/10 = 0.1 Hz. To demonstrate the flexibility of the spectral filter, there are taken eight completely random intervals to be extracted from the linear chirp signal under study (Table 13).

TABLE 13. DECOMPOSITION INTERVALS THROUGH THE DWT, WP AND SPECTRAL FILTER

Filter	**Decomposition**	**Lower Limit**	**Upper Limit**	**Time Lower Limit**	**Time Upper Limit**
DWT	A3	0	62.5	0	1.25
	D3	62.5	125	1.25	2.5
	D2	125	250	2.5	5
	D3	250	500	5	10
WP	A31	0	62.5	0	1.25
	A32	62.5	125	1.25	2.5
	A33	125	187.5	2.5	3.75
	A34	187.5	250	3.75	5
	A35	250	312.5	5	6.25
	A36	312.5	375	6.25	7.5
	A37	375	437.5	7.5	8.75
	A38	437.5	500	8.75	10
Spectral Filter	1er Interval	0	20	0	0.4
	2º Interval	20	100	0.4	2
	3er Interval	100	150	2	3
	4º Interval	150	160	3	3.2
	5º Interval	160	360	3.2	7.2
	6º Interval	360	400	7.2	8
	7º Interval	400	430	8	8.6
	8º Interval	430	500	8.6	10

The number of intervals for the decomposition of the signal by the spectral filter is eight, but it may have been taken any other value. This fact also applies to the frequency ranges extracted.

The decomposition of the linear chirp waveform by the DWT filter is shown in Fig. 53. The extracted signal is shown in blue, while the black vertical lines delimit the extracted interval limits. Notice that the frequency bands extracted increase their frequency in quadratic progression.

The decomposition of the linear chirp waveform by the WP filter is shown in Fig. 54 for the same decomposition order of the filter than for the DWT. The main difference between the two decompositions is that the bandwidth of the filter are constant for the WP where all of them have the same width than the smaller band that the DWT decomposition takes DWT.

The overlap between the frequency bands extracted in both decompositions is more than evident and, especially noticeable between D2 and D1 details for the DWT decomposition and between the intervals A34 and A35 for the WP decomposition.

Finally, Fig. 55 shows the decomposition of the linear chirp waveform by the spectral filter. The main differences between the spectral filter and filters based on wavelet transform are: (i) its flexibility in selecting the number of bands and frequencies to extract and (ii) the small overlap between the extracted frequency bands.

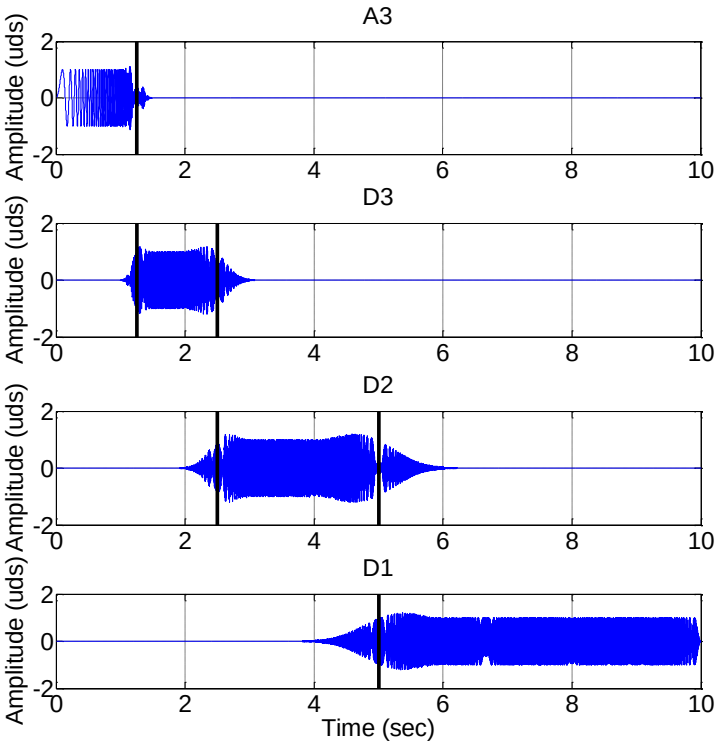

Fig. 53 DWT decomposition of the Chirp wave $x = \sin(50 \cdot \pi \cdot t^2)$. Decomposition order 3.

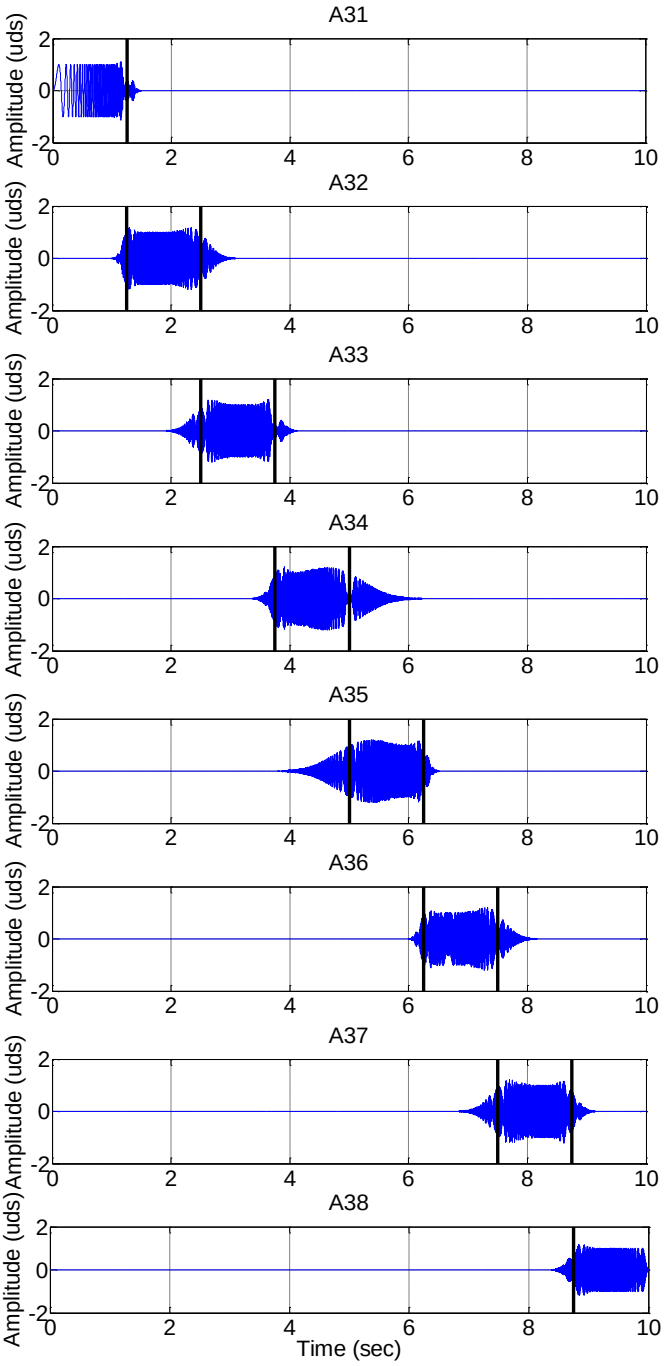

Fig. 54 WP Transform decomposition of the Chirp wave $x = \sin(50 \cdot \pi \cdot t^2)$. Decomposition order 3.

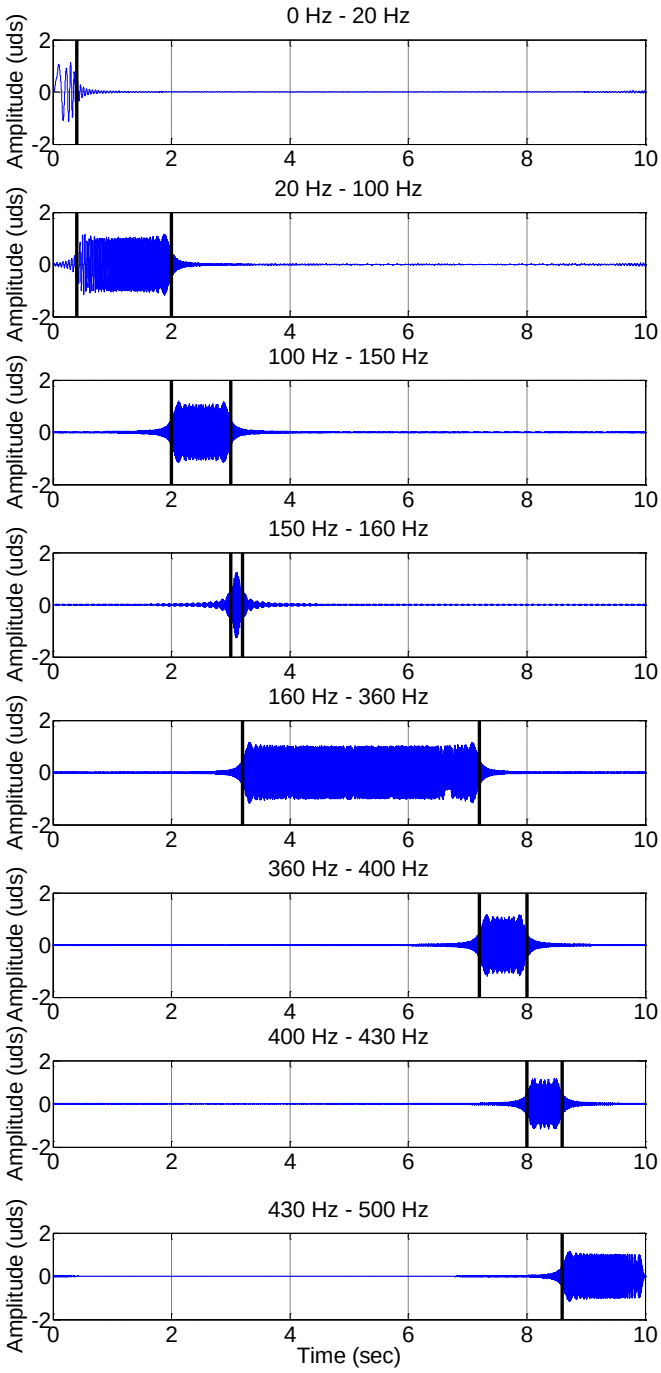

Fig. 55 Spectral Filter decomposition of the Chirp wave $x = \sin(50 \cdot \pi \cdot t^2)$.

3 FREQUENCY SHIFTING

3.1 INTRODUCTION

The frequency shifting is a very efficient technique in the digital signal processing, and can be applied to both real and complex signals. It comprises of shifting the frequency components of a wave to be analysed from the original position in the spectrum to the desired position in the frequency spectrum that facilitates the extraction in a subsequent filtering step.

One advantage of the frequency shifting in the analogue domain is that fixed frequency filters can be used as super-heterodyne receivers. In digital systems, frequencies are shifted to the centre of the base band filter [139].

3.2 DISPLACEMENT FREQUENCY THEOREM (DIFT)

The Displacement Frequency Theorem (DiFT) is widely used in information processing. The Displacement Frequency Theorem is valid for real and complex signals [139]. Mathematically if

$$\mathcal{F}\left[f(t) \right] = \mathrm{F}(\omega) \tag{101}$$

then

$$\mathcal{F}\left[f(t) \cdot e^{-j\omega_0 \cdot t} \right] = \mathrm{F}(\omega - \omega_0) \tag{102}$$

in frequency

$$\mathcal{F}\left[f(t) \cdot e^{-j2\cdot\pi\cdot f_0 \cdot t} \right] = \mathrm{F}(f - f_0) \tag{103}$$

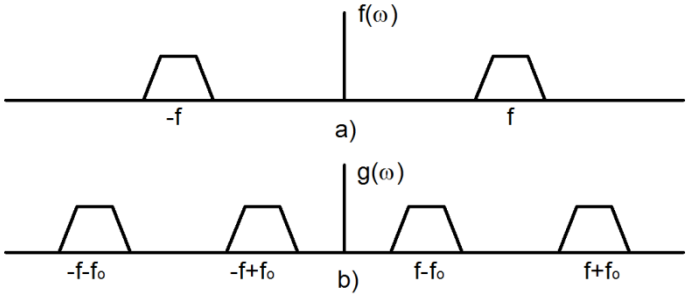

Fig. 56 Displacement in frequency of the spectral components by the Displacement Frequency Theorem. a) Original spectrum. b) Spectrum after the application of the Displacement Frequency Theorem.

Fig. 56.a shows the frequency spectrum of the signal *f*(*t*) and Fig. 56.b shows the spectrum $g(t) = \mathrm{Re}\left(f(t) \cdot e^{-j2\cdot\pi\cdot f_0 \cdot t} \right)$, that is, the spectrum has been shifted in frequency.

The proof of the Displacement Frequency Theorem is shown in the following lines.

If

$$i(t)=\sum_{i=1}^{N}A_i(t)\cdot\cos\left(\omega_i(t)\cdot t+\varphi_i(t)\right) \tag{104}$$

is a random wave with a finite number of harmonics *N*.

Applying the Euler fundamental relationship, equation (104) can be denoted as:

$$i(t)=\sum_{i=1}^{N}A_i(t)\cdot\frac{e^{i\cdot\left(\omega_i(t)\cdot t+\varphi_i(t)\right)}+e^{-i\cdot\left(\omega_i(t)\cdot t+\varphi_i(t)\right)}}{2} \tag{105}$$

Multiplying by $e^{-i\cdot\omega'(t)\cdot t}$ (105) is:

$$i'(t)=i(t)\cdot e^{-i\cdot\omega'(t)\cdot t}=\sum_{i=1}^{N}\frac{A_i(t)}{2}\cdot\frac{e^{i\cdot\left(\omega_i(t)\cdot t+\varphi_i(t)-\omega'(t)\cdot t\right)}+e^{-i\cdot\left(\omega_i(t)\cdot t+\varphi_i(t)+\omega'(t)\cdot t\right)}}{2} \tag{106}$$

Applying again the Euler fundamental relationship

$$i'(t)=\sum_{i=1}^{N}\frac{A_i(t)}{2}\cdot\left\{\begin{array}{l}\cos\left[\left(-\omega_i(t)-\omega'(t)\right)\cdot t-\varphi_i(t)\right]+i\cdot\sin\left[\left(-\omega_i(t)-\omega'(t)\right)\cdot t-\varphi_i(t)\right]+\\ \cos\left[\left(-\omega_i(t)-\omega'(t)\right)\cdot t-\varphi_i(t)\right]+i\cdot\sin\left[\left(-\omega_i(t)-\omega'(t)\right)\cdot t-\varphi_i(t)\right]\end{array}\right\} \tag{107}$$

Rearranging in real and imaginary part:

$$i'(t)=\sum_{i=1}^{N}\frac{A_i(t)}{2}\cdot\left\{\begin{array}{l}\cos\left[\left(\omega_i(t)-\omega'(t)\right)\cdot t+\varphi_i(t)\right]+\cos\left[\left(-\omega_i(t)-\omega'(t)\right)\cdot t-\varphi_i(t)\right]+\\ i\cdot\left[\sin\left[\left(\omega_i(t)-\omega'(t)\right)\cdot t+\varphi_i(t)\right]+\sin\left[\left(-\omega_i(t)-\omega'(t)\right)\cdot t-\varphi_i(t)\right]\right]\end{array}\right\} \tag{108}$$

Finally,

$$\boxed{i''(t)=\mathrm{Re}\left(i'(t)\right)=\frac{1}{2}\cdot\sum_{i=1}^{N}A_i(t)\cdot\left\{\cos\left[\left(\omega_i(t)-\omega'(t)\right)\cdot t+\varphi_i(t)\right]+\cos\left[\left(\omega_i(t)+\omega'(t)\right)\cdot t+\varphi_i(t)\right]\right\}} \tag{109}$$

The application of the frequency shifting causes that the frequency components of the wave are shifted forward and backward a frequency equal to the value of the frequency shifting and its amplitude is halved.

The application of the Displacement Frequency Theorem is illustrated by its application to a known synthetic wave.

Let us take the function

$$x(t)=10\cdot\cos\left(2\cdot\pi\cdot100\cdot t\right)+10\cdot\cos\left(2\cdot\pi\cdot300\cdot t\right) \tag{110}$$

The graphical representation of (110) is shown in Fig. 57.a. Function (110) has only two harmonic components at 100 and 300 Hz. Fig. 57.b shows the Fourier spectrum of (110) where there are the two frequency components of (110).

There is applied to (110) a 50 Hz frequency shifting, that is

$$g(t)=\mathrm{Re}\left(x(t)\cdot e^{j2\cdot\pi\cdot50\cdot t}\right) \tag{111}$$

displaying the result of the displacement in Fig. 58. Fig. 58.a shows how the signal has been modified in time, whereas in Fig. 58.b shows the new Fourier spectrum of the shifted signal.

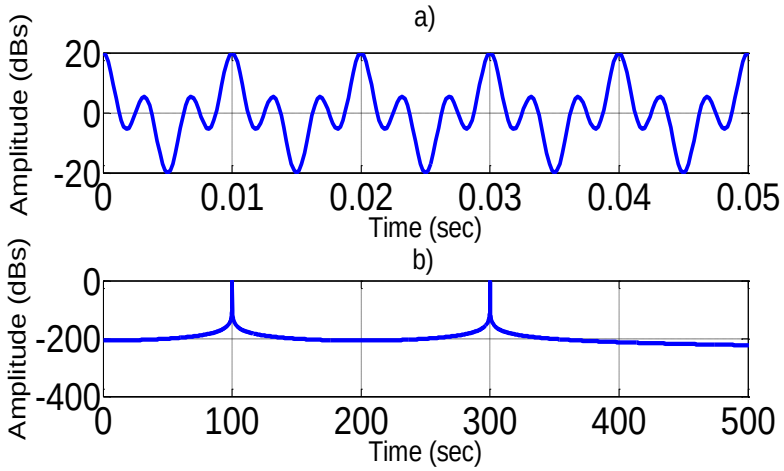

Fig. 57 a) Function $x(t) = 10 \cdot \cos(2 \cdot \pi \cdot 100 \cdot t) + 10 \cdot \cos(2 \cdot \pi \cdot 300 \cdot t)$. b) Fourier Transform of $x(t)$.

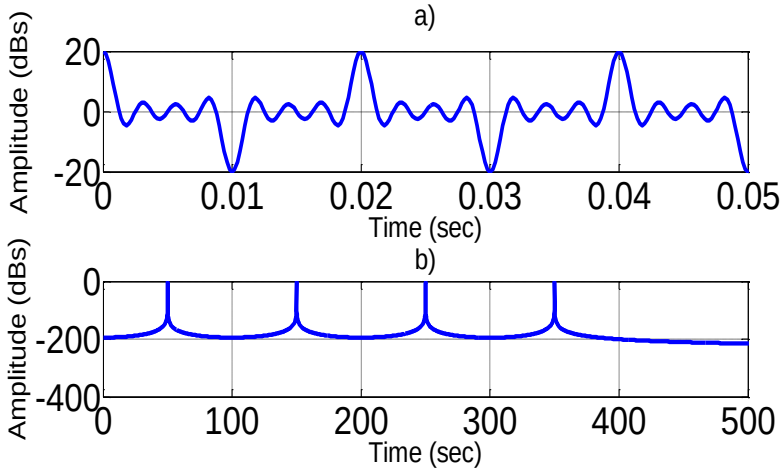

Fig. 58 a) Signal in the time domain after the application of the Displacement Frequency Theorem. b) Fourier Transform of the signal

As it was demonstrated before, the shifted signal by the Displacement Frequency Theorem shifts each harmonic forward and backward the indicated hertz value, doubling the wave harmonics Fig. 58.b. The absolute amplitude of each harmonic is halved. This does not alter the representation in the Fourier spectrum since the harmonics are normalized by the maximum value of amplitude of all harmonic, value that is also halved when the Displacement Frequency Theorem is applied. Furthermore, the information contained in a random harmonic is not altered by the frequency shifting performed since it has only been shifted its frequency in the spectrum.

The main drawback of the technique of the Displacement Frequency Theorem is that it doubles the amount of harmonic that the shifted wave contains. That can cause unwanted overlaps and consequently mistakes when the analysis of the shifted signal is performed.

Another drawback of the use of the Displacement Frequency Theorem is that it is not able to set a variable predominant frequency in the spectrum at a fixed position by a single operation. If it is wanted to perform such action, the computational cost is high, since the signal must be split into small intervals to perform as many shiftings as many divisions made to set a frequency component at a fixed frequency.

3.3 HILBERT TRANSFORM (HT)

The Hilbert transform is a signal analysis technique recently introduced in the field of diagnostics of electrical machines with an increased use [57], [130]-[132], for both analyses of steady and non-steady state signals.

The Hilbert Transform is defined as a convolution with the function $1/t$, as it is shown in the following equation [140]:

$$HT\left(x\left(t\right)\right)=y\left(t\right)=\frac{1}{\pi\cdot t}\times x\left(t\right)=\frac{1}{\pi}\int_{-\infty}^{+\infty}\frac{x\left(\tau\right)}{t-\tau}d\tau \tag{112}$$

The divergence at $t=\tau$ is allowed taking the Cauchy principal value of the integral. Combining the function $x\left(t\right)$ and its HT comes the called analytical signal (AS) defined as:

$$\vec{x}\left(t\right)=x\left(t\right)+j\cdot y\left(t\right)=A\left(t\right)\cdot e^{j\cdot\theta\left(t\right)} \tag{113}$$

Where

$$A\left(t\right)=\sqrt{x^2\left(t\right)+y^2\left(t\right)} \tag{114}$$

$$\Phi\left(t\right)=\arctan\left(x\left(t\right)/y\left(t\right)\right) \tag{115}$$

Where $A\left(t\right)$ is the instantaneous amplitude of $\vec{x}\left(t\right)$, that shows how the energy of $x\left(t\right)$ varies in time, and $\Phi\left(t\right)$ is the instantaneous phase of $\vec{x}\left(t\right)$.

The main properties of the Hilbert transform and the analytic signal are:

- The HT of a trigonometric function $x(t)$ is itself with phase shifting of 90°, that is, it transforms sines to cosines and vice versa. The spectrum of a signal which the HT has been applied has the same amplitude and frequency as the original signal, but the phase of each frequency component is shifted 90°.
- The analytical signal $\vec{x}\left(t\right)=x\left(t\right)+j\cdot HT\left(x\left(t\right)\right)$ has only one frequency band when the Fourier transform is computed, that means that the amplitudes of the negative frequency components are 0. HT holds all positive frequency components of the original signal but removes the negative ones, doubling the DC component of the original signal.
- All the low frequencies of the original signal are in the amplitude $A(t)$, whereas the high frequencies are in phase $\Phi(t)$ of the analytical signal.

The square module of the analytical signal creates a ripple in time wave that shifts the predominant frequency to the coordinate origin of the frequency spectrum of the wave where the Hilbert transform is applied the, transforming it to a DC component. The remaining wave frequencies at

which the transform has been applied are shifted backward the value of the predominant frequency, as it is concluded from the following demonstration.

If

$$i(t)=\sum_{i=1}^{i=n}\alpha_i\cdot\cos\left(\omega_i\cdot t+\varphi_i\right) \tag{116}$$

is a random wave with *n* harmonics.

The application of the Hilbert transform leads to

$$HT\left(i(t)\right)=\sum_{i=1}^{i=n}\alpha_i\cdot\sin\left(\omega_i\cdot t+\varphi_i\right) \tag{117}$$

Then the analytic signal will be,

$$s(t)=i(t)+j\cdot HT\left(i(t)\right)=\sum_{i=1}^{i=n}\alpha_i\cdot\cos\left(\omega_i\cdot t+\varphi_i\right)+\sum_{i=1}^{i=n}\alpha_i\cdot\sin\left(\omega_i\cdot t+\varphi_i\right) \tag{118}$$

The module of the analytic signal will take the value of,

$$\left|s(t)\right|=\sqrt{\mathrm{Re}^2\left(s(t)\right)+\mathrm{Im}^2\left(s(t)\right)} \tag{119}$$

where the real part is:

$$\mathrm{Re}^2\left(s(t)\right)=\sum_{i=1}^{i=n}\alpha_i^2\cdot\cos^2\left(\omega_i\cdot t+\varphi_i\right)+\sum_{i=1}^{i=n}\alpha_i\cdot\cos\left(\omega_i\cdot t+\varphi_i\right)\cdot\sum_{\substack{j=1\\j\neq i}}^{i=n}\alpha_j\cdot\cos\left(\omega_j\cdot t+\varphi_j\right) \tag{120}$$

Whereas the imaginary part will take the value of:

$$\mathrm{Im}^2\left(s(t)\right)=\sum_{i=1}^{i=n}\alpha_i^2\cdot\sin^2\left(\omega_i\cdot t+\varphi_i\right)+\sum_{i=1}^{i=n}\alpha_i\cdot\sin\left(\omega_i\cdot t+\varphi_i\right)\cdot\sum_{\substack{j=1\\j\neq i}}^{i=n}\alpha_j\cdot\sin\left(\omega_j\cdot t+\varphi_j\right) \tag{121}$$

Then, $\mathrm{Re}^2\left(s(t)\right)+\mathrm{Im}^2\left(s(t)\right)$ will take the value of

$$\begin{aligned}\mathrm{Re}^2\left(s(t)\right)+\mathrm{Im}^2\left(s(t)\right)&=\sum_{i=1}^{i=n}\alpha_i^2\cdot\cos^2\left(\omega_i\cdot t+\varphi_i\right)+\\&+\sum_{i=1}^{i=n}\alpha_i\cdot\cos\left(\omega_i\cdot t+\varphi_i\right)\cdot\sum_{\substack{j=1\\j\neq i}}^{i=n}\alpha_j\cdot\cos\left(\omega_j\cdot t+\varphi_j\right)+\\&+\sum_{i=1}^{i=n}\alpha_i^2\cdot\sin^2\left(\omega_i\cdot t+\varphi_i\right)+\\&+\sum_{i=1}^{i=n}\alpha_i\cdot\sin\left(\omega_i\cdot t+\varphi_i\right)\cdot\sum_{\substack{j=1\\j\neq i}}^{i=n}\alpha_j\cdot\sin\left(\omega_j\cdot t+\varphi_j\right)\end{aligned} \tag{122}$$

Rearranging equation (122):

$$\mathrm{Re}^2\left(s(t)\right)+\mathrm{Im}^2\left(s(t)\right)=\sum_{i=1}^{n}\alpha_i\cdot\left(\cos^2\left(\omega_i\cdot t+\varphi_i\right)+\sin^2\left(\omega_i\cdot t+\varphi_i\right)\right)+$$

$$\sum_{i=1}^{n}\alpha_i\cdot\left(\cos\left(\omega_i\cdot t+\varphi_i\right)\cdot\sum_{\substack{j=1\\j\neq i}}^{n}\alpha_j\cdot\cos\left(\omega_j\cdot t+\varphi_j\right)+\sin\left(\omega_i\cdot t+\varphi_i\right)\cdot\sum_{\substack{j=1\\j\neq i}}^{n}\alpha_j\cdot\sin\left(\omega_j\cdot t+\varphi_j\right)\right) \quad (123)$$

$$=\sum_{i=1}^{n}\alpha_i^2+\sum_{i=1}^{n}\alpha_i\cdot\sum_{\substack{j=1\\j\neq i}}^{n}\alpha_j\cdot\left(\cos\left(\omega_i\cdot t+\varphi_i\right)\cdot\cos\left(\omega_j\cdot t+\varphi_j\right)+\sin\left(\omega_i\cdot t+\varphi_i\right)\cdot\sin\left(\omega_j\cdot t+\varphi_j\right)\right) \quad (124)$$

$$=\sum_{i=1}^{n}\alpha_i^2+\sum_{i=1}^{n}\alpha_i\sum_{\substack{j=1\\j\neq i}}^{n}\alpha_j\cdot\left(\cos\left(\omega_i\cdot t+\varphi_i-\left(\omega_j\cdot t+\varphi_j\right)\right)\right) \quad (125)$$

$$=\sum_{i=1}^{n}\alpha_i^2+\sum_{i=1}^{n}\alpha_i\sum_{\substack{j=1\\j\neq i}}^{n}\alpha_j\cdot\left(\cos\left(\left(\omega_i-\omega_j\right)\cdot t-\left(\varphi_j-\varphi_j\right)\right)\right) \quad (126)$$

Then,

$$\left|s(t)\right|=\sqrt{\sum_{i=1}^{n}\alpha_i^2+\sum_{i=1}^{n}\alpha_i\sum_{\substack{j=1\\j\neq i}}^{n}\alpha_j\cdot\left(\cos\left(\left(\omega_i-\omega_j\right)\cdot t-\left(\varphi_j-\varphi_j\right)\right)\right)} \quad (127)$$

An squaring the module to remove the square root:

$$\left|s(t)\right|^2=\sum_{i=1}^{n}\alpha_i^2+\sum_{i=1}^{n}\alpha_i\sum_{\substack{j=1\\j\neq i}}^{n}\alpha_j\cdot\left(\cos\left(\left(\omega_i-\omega_j\right)\cdot t-\left(\varphi_j-\varphi_j\right)\right)\right) \quad (128)$$

Since $\cos(x)=\cos(-x)$, then

$$\boxed{\left|s(t)\right|^2=\sum_{i=1}^{n}\alpha_i^2+2\cdot\sum_{i=1}^{n}\alpha_i\sum_{j=i+1}^{n}\alpha_j\cdot\left(\cos\left(\left|\left(\omega_i-\omega_j\right)\cdot t-\left(\varphi_j-\varphi_j\right)\right|\right)\right)} \quad (129)$$

The application of the Hilbert transform for the frequency shifting is shown in the following example.

If there is the function

$$x(t)=10\cdot\cos\left(2\cdot\pi\cdot50\cdot t\right)+0.1\cdot\cos\left(2\cdot\pi\cdot49\cdot t\right) \quad (130)$$

The graphical representation of (130) is shown in Fig. 59.a. Function (130) has only two harmonic components at 49 and 50 Hz with an amplitude ratio 1/100. This waveform is similar to the problem that occurs when trying to separate an electromechanical or electromagnetic harmonic in the case of rotor asymmetries in induction electric machines. In Fig. 59.b is shown the Fourier spectrum of (130) which confirms the existence of the harmonics located at 49 and 50 Hz.

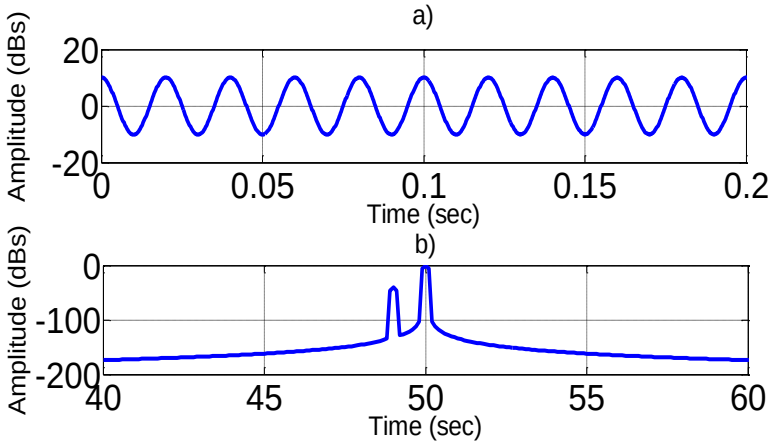

Fig. 59 Depiction of function (130). a) Time domain b) Fourier spectrum

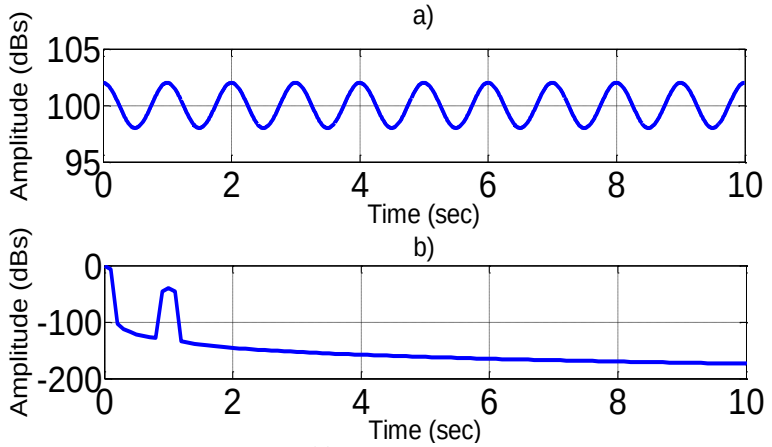

Fig. 60 Square analytical signal of function (130) a) Time domain. b) Fourier spectrum

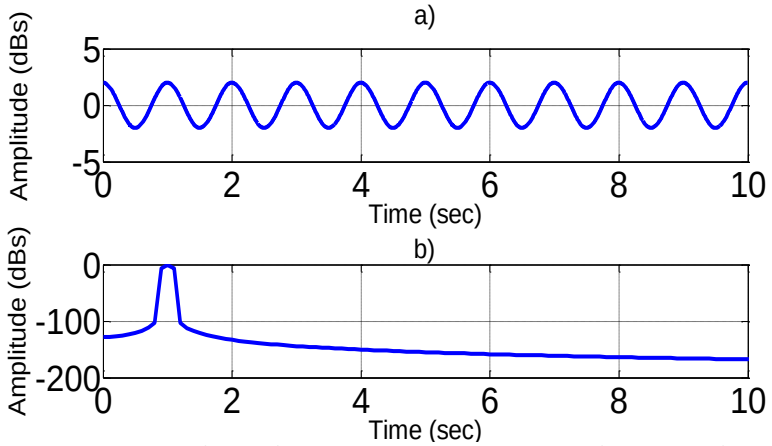

Fig. 61 Extraction of close frequency components through the frequency shifting by the Hilbert Transform and a high pass band filter (removal of the DC component). a) Time domain b) Fourier spectrum.

Applying the Hilbert Transform to the signal (130) is computed its analytic signal and, squared its module there is computed the signal obtained shown in Fig. 60.a that corresponds to the squared analytical signal. Fig. 60.b shows the Fourier spectrum of the signal of Fig. 60.a.

The comparison of the Fourier spectrum of Fig. 59.b with the spectrum of Fig. 60.b shows that the frequency components of the signal have been shifted backwards the value of the predominant frequency, that is 50 Hz .

Thus, the frequency components shown in Fig. 59.b at 49 and 50 Hz, change its location positions -1 Hz and 0 Hz. Since there is not possible to have negative frequencies in real waves, it is taken the absolute value of the frequency components, thus the real values that corresponds to the shifted frequency will be 1 Hz for frequency component of 49 Hz and 0 Hz for frequency component of 50 Hz.

Finally, to split the two components is enough to apply a high-pass filter to remove the DC component of the signal as it is shown in Fig. 61.

The main advantage of the implementation of the Hilbert Transform for the frequency shifting is that it automatically sets the greatest amplitude component to zero hertz -DC component of the transformed signal-, irrespective of the value of frequency, shifting, at the same time, the rest of the components to the same extent, which does not alter the relative frequency distance between the component with the greatest amplitude and the other components.

However, the major drawback of the Hilbert transform is that it does not allows the control of the frequency shifting of the frequency components to a particular frequency region of the plane since the process is automatically performed by shifting the greatest amplitude component provided to the 0 Hz region of the spectrum.

4 SUMMARY AND CONCLUSIONS OF THE CHAPTER

In the current chapter has been introduced the different techniques for filtering and shifting the frequency components.

Among the evaluated filtering techniques it has been shown that, the filtering based on the Wavelet Transform has its basis on the dyadic filter banks. That causes the disadvantage that once fixed the sampling frequency of the signal, the computed filter bank by the application of the Wavelet Transform has a fixed value.

The second technique introduced is the filtering technique based on Wavelet Packet Transform, technique that theoretically allows the selection of bands as small as wanted thus allowing overcoming the problem posed by the filters based on the Wavelet Transform.

Finally, it has been introduced new filtering method, which has not been used so far in the field of diagnosis, based on the properties of the Discrete Fourier Transform, valid for digital signals, which allows a much more effective filter than the one performed by Wavelet Transform or Wavelet Packet Transform since it has no transition zones.

On the other hand, in the second part of the chapter it has been shown the properties of the frequency shifting by the Displacement Frequency Theorem and by the Hilbert Transform.

The Displacement Frequency Theorem enables the shifting of any frequency component to any region of the frequency spectrum in a simple manner, with the drawback that it is not able to set a variable frequency to a specific point of the spectrum through a single operation, and it doubles the amount of harmonics contained in the shifted wave.

Finally, it has been shown that the application of the Hilbert Transform shifts the predominant frequency component, irrespective of its frequency value, to the region of 0 Hz of the frequency spectrum. The advantage of the Hilbert Transform is that it allows shifting of greater amplitude signal component as the DC component. A disadvantage, the Hilbert Transform has is that the frequency shifting is not controlled since the Hilbert Transform always sets the greatest amplitude component of the signal to zero hertz

CHAPTER VII: COMPUTATION OF THE INSTANTANEOUS FREQUENCY

1 INTRODUCTION

The concept of instantaneous frequency and its computation methods and applications of this physical quantity has been the subject of many research papers in different fields in recent decades [141]-[145]. In the area of time-frequency analysis, the instantaneous frequency proves to be a useful tool for the study of transient signals.

The computation of the instantaneous frequency by conventional methods (Park's vector or analytic signal computed by the Hilbert Transform) require the derivation of the phase of a complex signal, computed from the analysed real signal [141]-[143].

In recent years, new methods have been developed based on the energy of the signal to compute the instantaneous frequency from time-frequency distributions as CWT or WVD. However, these methods require considerable computational resources. By contrast, in [144] and [145] there have been proposed several methods for the extraction of the instantaneous frequency, using the Teager-Kaiser operator that have the great advantage over the previous methods that their computational resources are very low.

The instantaneous frequency is a function that displays for each time step a single frequency value of the analyzed signal. It should be noticed that although given a signal, the instantaneous frequency could always be computed (using algorithms such as those outlined below), this magnitude has a physical meaning only when the signal is monocomponent. For this reason in the following chapters is only computed the instantaneous frequency of fault components of the current extracted through a suitable extraction process.

2 COMPUTATION OF THE INSTANTANEOUS FREQUENCY THROUGH THE HILBERT TRANSFORM

The conventional methods for the computation of the instantaneous frequency are based on the derivative of the phase of the signal [141]-[143]. This relationship is easily observed in complex signals.

However, for real signals it must be applied a transformation that allows the computation of the phase for a real acquired signal. Among the possible transforms, two have usually performed it: the Park's vector and the Hilbert Transform.

The use of Park's vector is dismissed in this work due to the need of the acquisition of three currents to compute the phase of the real acquired current, whereas the Hilbert transform only requires one current.

When the Hilbert Transform is applied to a real signal, it is computed the analytical signal as: $s(t) = x(t) + jHT\{x(t)\} = a(t) \cdot e^{j\phi(t)}$ where $HT\{x(t)\}$

is the Hilbert transform of $x(t)$ (introduced in Chapter VI, Section 3.3.3), defining the instantaneous frequency as the derivative of the phase of the analytical signal [146]:

$$\omega(t) = \frac{d\phi(t)}{dt} \tag{131}$$

In discrete analysis, there are several ways to compute the instantaneous frequency, depending on the approach taken for the derivative. If the derivative is taken forward, the instantaneous frequency for the discrete case is defined as [142]:

$$f(n) = \frac{1}{2 \cdot \pi}\left(\phi(n+1) - \phi(n)\right) \tag{132}$$

where $\phi(n)$ is the value of the discrete phase for the instant n and $f(n)$ is the derivative of the phase in Hertz/sample. Finally, it will be enough multiplying by sampling frequency to compute the instantaneous frequency in hertz

$$IF(n) = f_s \cdot f(n) \tag{133}$$

3 COMPUTATION OF THE INSTANTANEOUS FREQUENCY THROUGH THE TEAGER-KAISER OPERATOR

Teager-Kaiser operator allows the computation of the instantaneous frequency of a real signal without requiring any previous transformation.

This condition relaxes the hardware requirements for the implementation of the Teager-Kaiser operator in electronic devices for the computation of the instantaneous frequency.

The Teager operator applied to a real function is defined as:

$$\Psi\{x(t)\} = x'^2(t) - x(t) \cdot x''(t) \tag{134}$$

which is used to measure the amount of energy that is needed to create an oscillating wave [147]. Its discrete version is defined as

$$\Psi\{x(n)\} = x^2(n) - x(n+1) \cdot x(n-1) \tag{135}$$

In [144] and [145] Teager operator is used for analysis of speech signals, where several methods are proposed to split the amplitude from frequency components of signals with modulated amplitude and frequency.

The instantaneous frequency by Teager-Kaiser operator can be computed through three approaches: DESA I, DESA I-a and DESA II [145].

The DESA I approach (Discrete time Energy Separation Algorithm I) is computed through:

$$\Omega(n) \approx \arccos\left(1 - \frac{\Psi\{y(n)\} + \Psi\{y(n+1)\}}{4 \cdot \Psi(x(n))}\right) \tag{136}$$

where $y(n) = x(n) - x(n-1)$.

If it is taken the asymmetrical derivatives, the DESA I method is slightly modified and it becomes DESA I-a method whose equation is [145]:

$$\Omega(n) \approx \arccos\left(1 - \frac{\Psi\{x(n) - x(n-1)\}}{2 \cdot \Psi(x(n))}\right) \tag{137}$$

The third computation method proposed in [145] is known as DESA II and its equation is

$$\Omega(n) \approx \arccos\left(1 - \frac{\Psi\{x(n+1) - x(n-1)\}}{2 \cdot \Psi(x(n))}\right) \tag{138}$$

Equations (136), (137) and (138) are in radians/sample then to convert them to hertz the following relation will be applied

$$IF(n) = \frac{f_s}{2 \cdot \pi} \cdot \Omega(n) \tag{139}$$

where IF is in hertz.

The use of the different possible approaches for the computation of the instantaneous frequency through the Teager-Kaiser operator, DESA I, DESA-Ia, or DESA II produces similar results and there are no significant enough changes between the different approaches [145]. The selection of one or another approach is based on the type of the chosen device to implement the computation of the instantaneous frequency through the Teager-Kaiser algorithm. On the other hand, it must also be taken into account the availability of the points taken for the computation since the approaches DESA I and DESA II require future points, whereas DESA-Ia approach only requires the current and previously points.

4 SUMMARY AND CONCLUSIONS OF THE CHAPTER

This chapter introduces four different algorithms that allow the computation of the instantaneous frequency for a real signal based on the Hilbert Transform and the Teager-Kaiser operator.

The first introduced algorithm is based on the computation of the derivative of the phase of the analytic signal computed from the analysed current signal.

The remaining introduced algorithms are based on the Teager-Kaiser operator, and there are three options: DESA I, DESA I-a and DESA II. There are not significant enough differences in the computation of the instantaneous frequency when the three Teager-Kaiser options are compared with each other.

Applying the methodology based on the Hilbert transform for the computation of the instantaneous frequency requires more hardware requirements than the computation of the instantaneous frequency through the Teager-Kaiser operator.

CHAPTER VIII: OBJECTIVE DIAGNOSTIC PARAMETERS

1 INTRODUCTION

This chapter introduces the different objective diagnostic parameters used in this thesis. The chapter is structured into three distinct sections: (i) computation of the energy parameter of the fault component, (ii) computation of the linear regression parameters and (iii) computation of the similitude coefficient.

The computation of the energy is carried out through two different methods: (i) computation in the time domain (conventional) and (ii) computation in the frequency domain, in virtue of the Plancherel's Theorem, that is proposed in this thesis.

Regarding the linear regression parameters, its computation is based on the method of least squares. In this section it is introduced the equations for the computation of the slope and the y-intercept in this thesis for adjust a straight line at a given point cloud, which in our case is the set of points (*s*, *IF*) from the extracted fault component from the measured current.

Finally, the third subsection discusses the need of a new coefficient (similitude coefficient) to assess the degree of failure of the machine since the statistical regression coefficients (Pearson, Spearman and Kendall) do not satisfactorily respond to the needs of the process of diagnosis, then the chapter concludes with the proposition of a new similitude coefficient which is an original contribution of this thesis.

2 FAULT INDICATORS BASED ON THE COMPUTATION OF THE ENERGY

The computation of the energy of the fault component is a well-known indicator in the field of electric machines, both for the evaluation of the severity of the fault and for the diagnosis itself [90], [93].

The review of the literature shows that the computation of the energy of the fault component has been performed so far in the time domain, as a direct result of the treatment of the fault components in the time domain. The computation of the energy comprises the sum of the squares of each of the acquired samples of a wave whose energy is to be evaluated.

This process is relatively simple, but its computational cost can be very high for the case when the number of acquired points of the wave to analyse is very high.

In this thesis, the computation of the energy is performed through the classical methodology in the time domain and through a new proposed methodology in this thesis that allows the computation of the energy in the frequency domain based on the application of the Plancherel's Theorem [134].

Details of each of the two quantifications of energy are shown in the following subsections.

2.1 COMPUTATION OF THE ENERGY IN THE TIME DOMAIN

The procedure for the evaluation of the severity of the failure in the time domain is carried out by the computation of the energy of the frequency band wherein the fault evolves, normalised by the value of the total energy contained in the signal to be analysed.

To enable the quantification of the energy of the fault component, the first step is its extraction from the rest of components without interest, with filters as it was explained in the preceding chapters.

Once the fault has been extracted the assumed fault component at the filtering stage, the energy of the fault component is computed according to the equation

$$E_{CF\_T} = \sum_{i=1}^{N} CF_i^2 \tag{140}$$

where CF is a discrete signal comprised by the components of the frequency band wherein the fault component to study evolves.

The total energy of the signal is analogously computed through

$$E_{S\_T} = \sum_{i=1}^{N} S_i^2 \tag{141}$$

Finally, the indicator for the determination and quantification of the severity of failure of the machine failure in % is computed by dividing (140) between (141) leading to

$$E_{Nor\_T} = \frac{E_{CF\_T}}{E_{S\_T}} \cdot 100 \tag{142}$$

The normalised energy value computed in (142) enables the comparison and evaluation of the state of an electrical machine irrespective of its operating mode, since the signal energy has been normalised by the total energy value in the same time window.

2.2 COMPUTATION OF THE ENERGY IN THE FREQUENCY DOMAIN

Plancherel's Theorem is the result of the harmonic analysis conducted by Michel Plancherel in 1910 [135]. Plancherel's Theorem shows that the integral of the square module of a function is equal to the integral of the square modulus of the frequency spectrum, enabling the computation of the energy of a signal in both the time and frequency domain through the equation:

$$\|s\|^2 = \int_{-\infty}^{+\infty} |s(t)|^2 \, dt = \frac{1}{2 \cdot \pi} \cdot \int_{-\infty}^{+\infty} |S(\omega)|^2 \, d\omega \tag{143}$$

Thus, if the frequency spectrum is normalised by the maximum amplitude value of the spectrum, it will be enough to add the amplitudes of the desired

frequencies for the computation of the signal energy in the diagnostic interval according to

$$E_{Nor\_F} = \frac{\sum_{f=f_{\inf}}^{f=f_{\sup}} \left| FFT\left(i(f)\right)\right|}{\sum_{f=0}^{f=F} \left| FFT\left(i(f)\right)\right|} \tag{144}$$

where f_{sup} is the upper limit of the frequency band from the extraction of the fault component and f_{inf} the lower limit in the same interval. The value of F corresponds to the maximum frequency of the computed Fourier spectrum and its value is function of the sampling frequency according to

$$F = \frac{f_s}{2} \tag{144}$$

3 LINEAR REGRESSION

Linear regression analysis is a statistical technique developed for the study of the relationship between variables that suits a wide variety of fields such as sociological, economic, physical, etc.

For two variables -simple regression- and also for more than two variables -multiple regression- the linear regression analysis can be performed to explore and quantify the relationship between a dependent variable called '*y*' and one or more variables , called x_1, x_2, x_3, ..., x_N and also to develop a linear equation for predictive purposes.

A scatter diagram gives a fair idea about the kind of relationship between two variables. However, a scatter diagram allows a quick first impression of type of relationship, its use to quantify this relationship has serious drawbacks: the relationship between two variables is not always perfect or null, in fact any of these extreme cases does not usually occur. That is why it is needed the computation of objective parameters to quantify the degree of relationship between the dependent and independent variable [148].

All function as

$$y = m \cdot x + b \tag{145}$$

depicts a straight line, where x and y are variables whereas m the slope of the line, and b, the y-intercept, have constant values.

The relationship shown in (145) is rarely accurate to be adjusted to any point cloud, otherwise it is an approach in which have been omitted many minor variables. Equation (145) shows a linear relationship, and it contains only a single explanatory variable, receiving the name of simple linear relationship. Assume now that there are N observations of the variable *'y'* [y_1, y_2, y_3, ..., y_N] and the corresponding observations of *'x'* [x_1, x_2, x_3, ..., x_N]; the slope m is computed according to

$$m = \frac{\sum_{i=1}^{N}(y_i - \bar{y})\cdot(x_i - \bar{x})}{\sum_{i=1}^{N}(x_i - \bar{x})^2} \tag{146}$$

Whereas *b* is computed through (145), that is

$$b = \bar{y} - m\cdot\bar{x} \tag{147}$$

Dividing numerator and denominator (146) by *N* comes

$$m = \frac{\frac{\sum_{i=1}^{N}(y_i - \bar{y})\cdot(x_i - \bar{x})}{N}}{\frac{\sum_{i=1}^{N}(x_i - \bar{x})^2}{N}} = \frac{\mathrm{cov}(x,y)}{\mathrm{var}(y)} \tag{148}$$

4 SIMILITUDE COEFFICIENT

Once the performance of least squares method has been performed is desirable to have an indicator to measure the degree of accuracy between the computed model and the measured data.

In the literature there are several indicators for the measure of the adjust, among them the Pearson correlation coefficient, the Spearman correlation coefficient and Kendall correlation coefficient are the more noteworthy [149].

The Pearson correlation coefficient measures the linear association between two variables. The value of the correlation coefficient evolves between -1 and 1, where the sign indicates the direction of the relation -negative for the inverse relation, positive for a direct relation- whereas its absolute value indicates the strength or degree of correlation, the largest value -the closer to one- indicates that the relationship is stronger whereas values close to 0 indicate that there is no linear relationship between the variables. The Pearson correlation coefficient is given by the equation [149]

$$\rho_{x,y} = \frac{\sigma_{xy}}{\sigma_x \cdot \sigma_y} \tag{149}$$

where σ_{xy} is the covariance of (x,y), σ_x is the standard deviation of the variable *x* and σ_y is the standard deviation of the variable *y*.

The Spearman correlation coefficient is a non-parametric version of the Pearson correlation coefficient that is based on data ranges rather than actual values. The Spearman coefficient is appropriate for ordinal data and for data grouped in intervals that does not meet the assumption of normality. The Spearman coefficient values vary from -1 to 1, wherein the coefficient sign indicates the direction of the relationship, as in the Pearson coefficient, whereas the absolute value of the correlation coefficient indicates the strength

of the relationship between variables. The absolute values closer to one indicate that the relationship is stronger in the same way as in the previous case. The computation of the Spearman correlation coefficient is performed through [149]

$$\rho = 1 - \frac{6 \cdot \sum_{i=1}^{N+1} D_i^2}{N \cdot \left(N^2 - 1\right)} \tag{150}$$

where D is the difference between the corresponding statistical $\left(D_i = x_i - y_i\right)$ and N the number of couples.

The Kendall coefficient is a measure for ordinal non-parametric variables or ranges that take into account the case when two variables have the same value. The sign of the coefficient indicates the direction of the relationship, as the two previous coefficients, and its absolute value indicates the magnitude thereof, so that the higher absolute value are, the stronger the relationship. The values vary between -1 and 1. Kendall coefficient is computed according to the following equation [149]

$$\tau = \frac{n_c - n_d}{\sqrt{\left(n_0 - n_1\right) \cdot \left(n_0 - n_2\right)}} \tag{151}$$

Where

$$n_0 = \frac{n \cdot \left(n-1\right)}{2}$$

$$n_1 = \sum_{i=1}^{N+1} \frac{t_i \left(t_i - 1\right)}{2}$$

$$n_2 = \sum_{j=1}^{N+1} \frac{u_j \left(u_j - 1\right)}{2}$$

n_c = Number of concordant pairs

n_d = Number of discordant pairs

t_i = Number of tied values in the i^{th} group of ties for the first quantity

u_j = Number of tied values in the j^{th} group of ties for the second quantity

In short, for normally distributed quantitative variables the Pearson correlation coefficient will be the chosen one, whereas if the data are not normally distributed or have categories in order, it will be selected the Spearman or Kendall correlation coefficient, since they measure the association between rank orders.

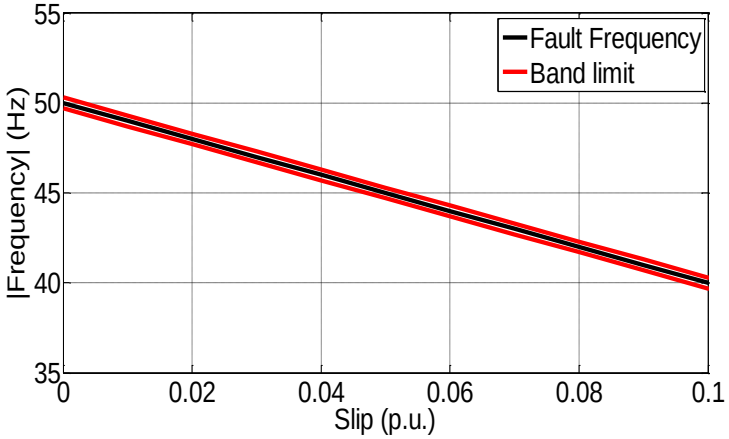

Fig. 62 Band limits for the similitude coefficient for the evolution of a rotor asymmetry fault.

However, the three correlation coefficients share the same problem since they evaluate the linear correlation between variables but no its position on the plane what can cause false positives in the diagnosis of electric machines when using these indicators.

To solve this problem, the author proposes a new coefficient, the similitude coefficient, which quantifies the amount of points that are within a tolerance band close to the theoretical line of evolution of the instantaneous frequency of the fault component. The range of the proposed similitude coefficient is bounded on the range [0,1], where values close to 1 mean that the analysed point cloud corresponds uniquely to the theoretical straight whereas the farther of 1 the similitude coefficient is, the fewer points follow the theoretical pattern. The expression of the similitude coefficient is

$$S = \frac{1}{N} \cdot \sum_{i=1}^{N} y(s_i) \begin{cases} y(s_i) = 1 \rightarrow \left| y(s_i) \right| < m \cdot s_i + c \pm \dfrac{0.3 \cdot m}{100} \\ y(s_i) = 0 \rightarrow \text{ For any other case} \end{cases} \quad (152)$$

The user, based on his particular application, sets the selection of the band limits. On the other hand, the author of this thesis proposes a band limits based on an increase of ± 0.3% of the theoretical value of the slope the frequency of the fault to be analysed, value that despite being conveniently small provides satisfactory results preventing false positive diagnosis.

5 SUMMARY AND CONCLUSIONS OF THE CHAPTER

In this chapter, it has been introduced two methods for computation of the fault indicator based on the computation of the energy. The first computes the energy of the fault component in the time domain whereas the second proposed method, which is an original contribution of this work, performs the computation of the energy in the frequency domain.

The method based on the computation of the energy in the time domain is the conventional method used in the current technical literature.

Furthermore, it is proposed the computation of the energy in the frequency domain through the direct application of the Plancherel's Theorem, computation that is faster and more efficient than the one performed in the time domain.

Secondly, it has been introduced the equations for the computation of the regression parameters based on the least squares method. Parameters, which together with the energy indicator and the similitude coefficient, guarantee the correct diagnosis of the electrical machine.

Finally, due the difficulties that the linear regression coefficients in the literature pose, it is introduced a new similitude coefficient that objectively determines the state of the machine, meeting the particular needs of the proposed diagnostic technique in this thesis.

The development of a completely objective coefficient allows the automation and application of the proposed methodology in automatic systems and/or without the supervision of human beings, increasing the reliability of the diagnostic methodology since it is not directly dependent on the decision of an operator.

CHAPTER IX: ROTOR ASYMMETRY. VALIDATION OF THE PROPOSED METHODOLOGY

1 INTRODUCTION

The validation of the methodology for the diagnosis of rotor asymmetries takes place in this chapter under the assumption that the machine can be found on symmetric state (healthy state) or with an asymmetry in the rotor winding (machine in faulty state).

The validation has been performed by testing two wound rotor induction machines. The first one is a universal machine whose stator and rotor are set to operate as wound rotor induction machine. The second is a commercial wound rotor induction machine.

This chapter is structured into two parts, depending on the fault components analysed for the detection of the rotor asymmetry: (i) Harmonic Main Components (HMC) and (ii) the High Order Harmonic Components (HOHC).

The detection of the asymmetry through the main components is subdivided into two sections, one for each tested machine, where the universal machine is tested working as generator whereas the commercial machine is tested working either as generator or motor. Fig. 63 summarizes the tests performed and the techniques used for the validations.

The diagnosis of the rotor asymmetry through the high order harmonic components is only validated on the universal machine in generating

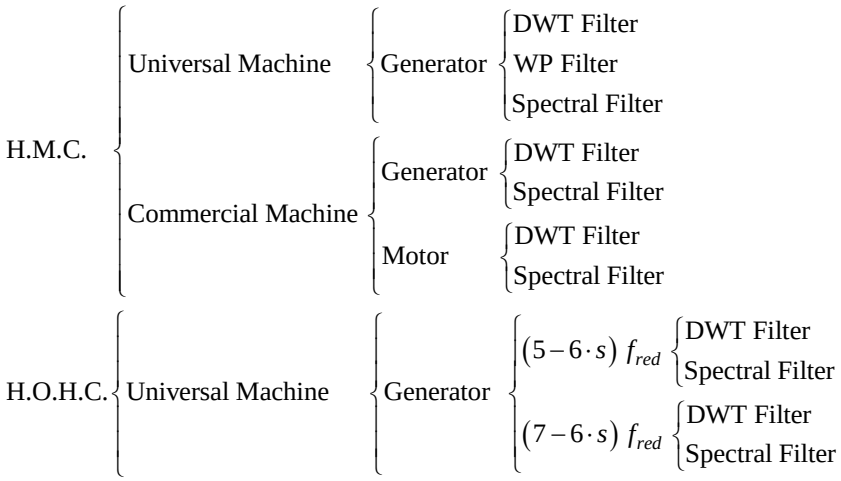

Fig. 63 Scheme of the performed tests for the validation of the methodology for the diagnosis of rotor asymmetries.

operation, studying the fault harmonics associated with the components of order $(5-6\cdot s)\cdot f_{red}$ and $(7-6\cdot s)\cdot f_{red}$.

The scheme of the proposed methodology for the detection of faults in electrical machines is developed in each of the sections of this chapter according to the scheme outlined in Chapter IV: (i) signal acquisition, (ii) extraction of the fault component, (iii) computation of the energy of the fault component, (iv) computation of the instantaneous frequency and (v) diagnostic decision.

The first stage of the diagnostic methodology corresponds to the signal acquisition. At this stage the current and speed signal are acquired in the non-stationary regime. The value of the sampling frequency and the total time of the acquired signals are also set at this stage.

The extraction of the fault component from the acquired current is performed by the application of each of the three proposed filters, (i) DWT, (ii) WP or (iii) Spectral filter whose theoretical features are developed in the Chapter VI.

Then the energy of the extracted fault component is computed in the time or the frequency domain depending on the filtering method used for the extraction of the fault component.

If value of the computed energy is below a preset threshold energy value by the user, the process is stopped since it is considered that the machine is in healthy state.

Otherwise, the process continues with the computation of the instantaneous frequency of the fault component to determine the origin of the increase of the energy. Knowing the origin of the energy extracted from the fault component prevents false positive diagnosis that can only occur if the diagnosis is exclusively based on the criterion of the increase of the energy.

The computation of the instantaneous frequency can be carried out through the two methods described in Chapter VI: (i) the classical method based on Hilbert Transform or (ii) the Teager-Kaiser operator.

The last step comprises the computation of the objective diagnostic parameters: the linear regression parameters (slope and y-intercept) and the similitude coefficient that together with the value previously computed energy, determine the status of the machine.

Each of the stages of the proposed methodology are detailed for universal machine diagnostics when the analysis of the main fault components is carried out at the machine working as generator.

The methodology can be interchangeably applied to machines working as either motor or generator, as it is demonstrated in the analysis of the commercial machine.

Finally, the diagnosis through the high order components is validated on the universal machine. The diagnostic process is detailed in this section again highlighting the slight differences in diagnosis between the diagnosis through the main components and the high order components.

2 MAIN FAULT HARMONICS

Main fault rotor asymmetry harmonics are located in the frequency spectrum closest to the fundamental current harmonic and are governed by (Chapter III):

$$f_{mag} = (1-2\cdot s)\cdot f_{red} \quad (153)$$

$$f_{mec} = (1+2\cdot s)\cdot f_{red} \quad (154)$$

The aim of the proposed methodology in this thesis is to isolate the frequency band where these harmonic components evolve, compute its energy, and determine if the extracted energy is due to a rotor asymmetry or other phenomena, through the computation of the instantaneous frequency.

The extraction process of the frequency bands can be carried out through a DWT filter, a WP filter or a Spectral filter (in frequency domain). The extraction of the components through each of the mentioned filters is detailed in the following subsections.

The validation of the proposed methodology is performed through several tests on the two tested machines.

The first one is a universal machine set as wound rotor induction machine working as generator.

The second is a 15 hp commercial wound rotor induction machine tested working either as generator or as motor.

The application of the methodology is carried out systematically for the diagnosis of the universal machine, commenting the intermediate results for each one of the studied cases. Thereafter, the methodology is applied directly to the commercial machine showing the results.

2.1 UNIVERSAL MACHINE

The tested machine in this section is a universal machine, with one pair of poles set as three-phase wound rotor induction machine whose features can be found in Annex I.

The scheme of the electrical circuit of the test rig for the validation of the fault is shown in Fig. 64. Due to practical constraints, the rotor windings have been used as primary winding (stator), connecting them to an electric supply network of 160 V and 50 Hz. The stator windings were short-circuited working as secondary winding.

The rotor asymmetry fault is performed by connecting a number of additional resistors, which have values between 4.15 and 0.07 Ohm, in series with one phase of the stator -secondary winding- to simulate the rotor asymmetry with different degrees of severity.

The tested machine is directly coupled to a DC machine which imposes the tested machine to operate above its synchronous speed forcing it working as generator.

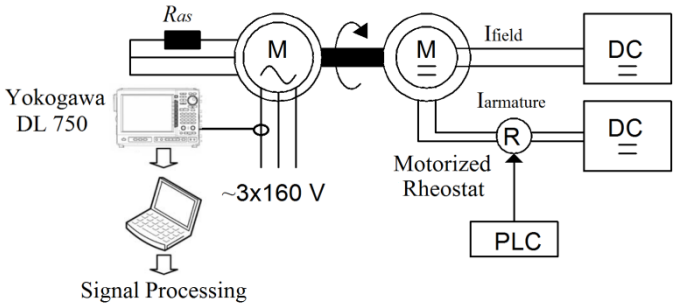

Fig. 64 Scheme of the test rig for the validation of the rotor asymmetry on the universal machine.

Fig. 65 Picture of the test bed for the test of the universal machine, set as wound rotor induction machine, in non-stationary stochastic conditions for the rotor asymmetry fault.

The field current of the DC machine is controlled through a motorised rheostat that is controlled by a PLC.

This assembly allows the control and programming of variations of fixed sequences in the field current of the machine, what consequently produces fixed speed fluctuations in the tested machine, thereby facilitating the analysis of the several tests for different degrees of severity since the machine is always subjected to the same non-stationary regime.

The line current of the primary winding -rotor- connected in delta is acquired with a clamp and the speed is acquired through an encoder of 360 pulses per revolution. Both the clamp and the encoder are connected to a digital oscilloscope 750 Yokogawa DL that has some analogue digital acquisition cards of 16 bits.

The digital oscilloscope is connected through an intranet to a personal computer that processes the signal captured. The sampling frequency chosen for the tests is set to 5 kHz.

The features of the auxiliary devices (clamp and encoder) as well as the features of the digital oscilloscope can be found in Annex II.

2.1.1 DIAGNOSIS BASED ON THE EXTRACTION OF THE FAULT COMPONENTS THROUGH A DWT FILTER

The diagnostic process starts imposing a fixed non-stationary regime, which is the same for all the tests carried out, with a fixed sequence of speed fluctuations shown in Fig. 66.a. The acquisition of the speed allows the knowledge of evolution of slip during all the transient process (Fig. 66.b).

The direct consequence of the non-stationary speed is that the acquired current cannot be analysed through the techniques developed for the steady state such as FFT. Fig. 67 shows the evolution of the acquired current as result of the speed oscillations shown in Fig. 66.a, when the machine is subjected to the maximum rotor asymmetry caused by the addition of a resistor in series in the secondary windings $R_a = 4.15\ \Omega$.

Once both signals -speed and current- have been acquired, the extraction of the fault component is performed.

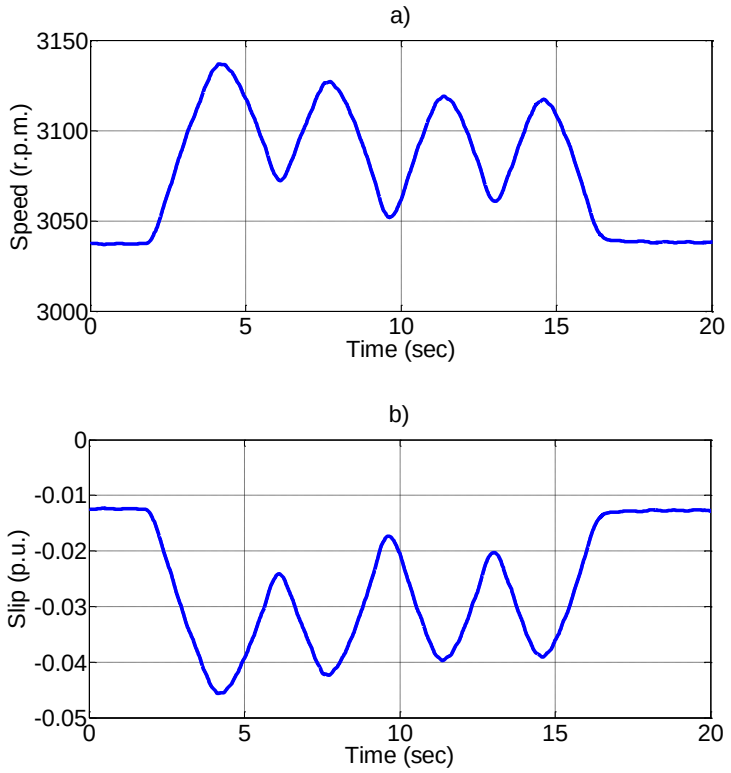

Fig. 66 a) Acquired non-stationary speed for the diagnosis of a wound rotor induction machine working as generator with a rotor asymmetry b) Evolution of the slip as a consequence of the non-stationary speed regime

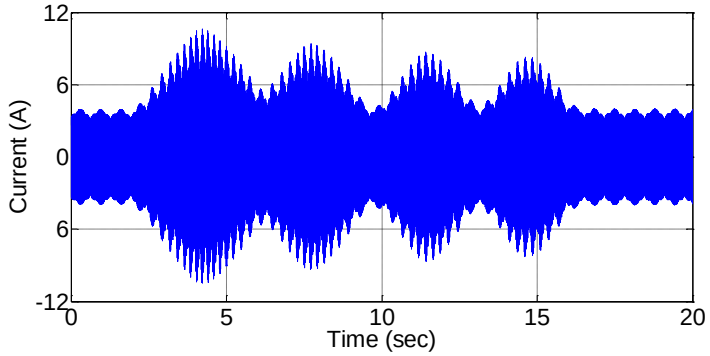

Fig. 67 Acquired stator current for the diagnosis of a rotor asymmetry. Machine working as generator in non-stationary conditions, rotor asymmetry fault (R_a = 4.15 Ω).

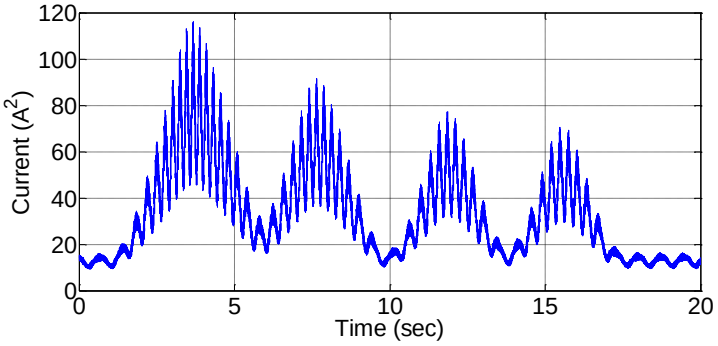

Fig. 68 Square module of the analytic signal of the acquired signal. Machine working as generator in non-stationary conditions, rotor asymmetry fault (R_a = 4.15 Ω)

The first step for the extraction of the fault component through a DWT filter when it is intended to diagnose a rotor asymmetry is to shift the fundamental frequency from 50 Hz to 0 Hz, what simultaneously shifts the fault components to the low frequency region of the spectrum.

The frequency shifting can be performed through the Frequency Displacement Frequency Theorem (DiFT) or Hilbert Transform (HT), since both are equivalent procedures. For simplicity, in this chapter will be performed the frequency shifting through the HT.

The frequency shifting through the Hilbert Transform is achieved using as a diagnostic signal the square modulus of the analytic signal of the current (Fig. 68) (Chapter VI - 3.3).

After the frequency shifting, the fault component is extracted through the filtering of the computed signal by means of a DWT filter.

Due to the imposed speed fluctuations to the tested machine, the slip is in the range [-0.057, -0.014] (see Fig. 66.b), whereas the fault components to be extracted are located in the range [51.42, 55.70] Hz for the component governed by $(1-2\cdot s)\cdot f_{red}$ and in the range [44.30, 48.58] Hz for the component governed by $(1+2\cdot s)\cdot f_{red}$. After the application of the frequency shifting, the frequency of these components are transformed into $2\cdot s\cdot f_{red}$ and $2\cdot s\cdot f_{red}$ what origins an unique component (due to the lack of physical meaning of the

negative frequency) whose frequency is $2 \cdot s \cdot f_{red}$. In the performed tests, the unique fault component, in the diagnostic signal, is included in the frequency range [1.42, 5.70] Hz (see Chapter VI - 3).

The order of the approximations that allow the extraction of the fault harmonic component are a_8 and a_{11}, as a direct result of the application of (76) and (77) (Chapter VI - 2.1.5) with a sampling frequency of 5 kHz and since the component to be extracted is bounded in the range [1.42, 5.70] Hz. The evolution in time of the a_8 and a_{11}components is shown in Fig. 69:

$$nC = \text{int}\left[\frac{\log\frac{f_s}{f_2}}{\log(2)} - 1\right] = \text{int}\left[\frac{\log\frac{5000}{5.70}}{\log(2)} - 1\right] = 8 \tag{155}$$

$$nNC = \text{int}\left[\frac{\log\frac{f_s}{f_1}}{\log(2)}\right] = \text{int}\left[\frac{\log\frac{5000}{1.42}}{\log(2)}\right] = 11 \tag{156}$$

Subtracting the approach a_{11} from the approach a_8 is computed the signal shown in Fig. 70 which contains only the frequencies contained in the range [1.22, 9.77] Hz (79) (Chapter VI - 2.1.5), range in which the fault component belongs. As there is no any other significant component in that range can be considered that Fig. 70 reproduces the time evolution of the fault component for a machine with a rotor asymmetry (R_a = 4.15 Ω) subjected to the non-stationary regime defined by Fig. 66.

Once the fault component has been isolated from other harmonic components with no interest for the diagnosis, its energy is computed.

If the value of the energy does not exceed the preset energy threshold, the diagnostic process ends since the machine is in healthy state.

If the extracted fault component exceeds the preset threshold value of energy, the diagnostic process proceeds to determine whether the origin of the detected increase of the energy is due to a rotor asymmetry. Notice that the computed value of energy does not provide information on the origin of increase of the energy and, thus, its use solely as a fault indicator is not reliable since the increase of energy can be due to a rotor asymmetry or other causes (loading conditions, voltage, noise, etc.) causing false positives.

The computation of the instantaneous frequency of the fault component allows the determination of the origin of the energy, preventing the uncertainty in the diagnosis.

The computation of the instantaneous frequency can be performed through the conventional method based on the HT (Fig. 71.a) or through the Teager-Kaiser operator (Fig. 71.b). Because of the inherent derivative operation for the computation of the instantaneous frequency, the result contains high frequency noise (Fig. 71, blue line) irrespective of the method

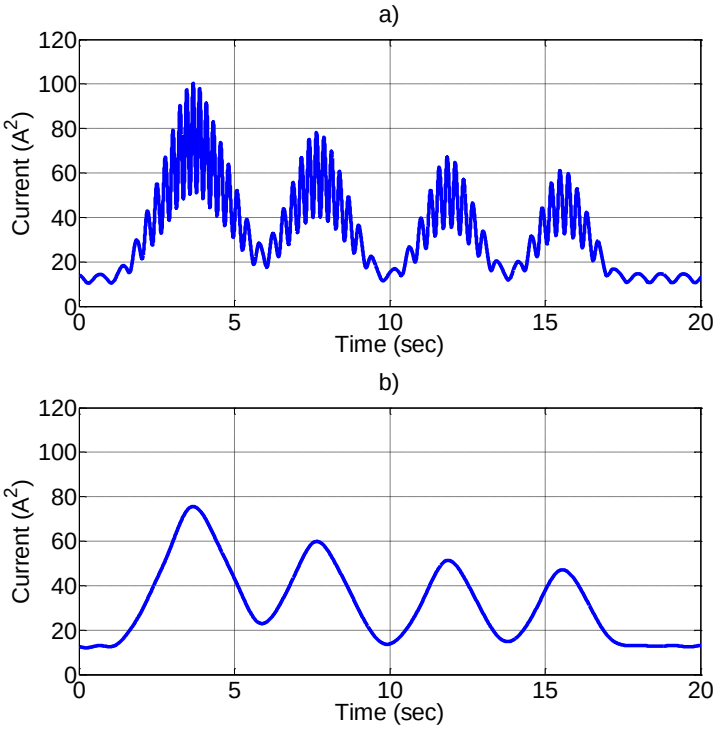

Fig. 69 DWT filtering process of the current signal a) a_8 approximation b) a_{11} Approximation

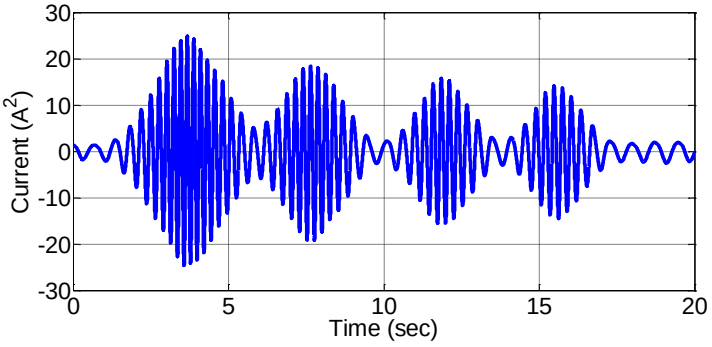

Fig. 70 Fault component of the universal machine with a rotor asymmetry (R_a = 4.15 Ω) working as generator.

for its computation. The high frequency noise is exclusively due to the computation process and therefore it must be suppressed to not affect the result of the diagnosis. The suppression of the high frequency noise is achieved through a low pass filter to the original instantaneous frequency signal, achieving an instantaneous frequency signal whose evolution is smoother (Fig. 71, red line).

After the removal of the high frequency noise, the two computed evolutions of the instantaneous frequency, through the classical method (Hilbert Transform) and through the Teager-Kaiser operator (Fig. 72), are

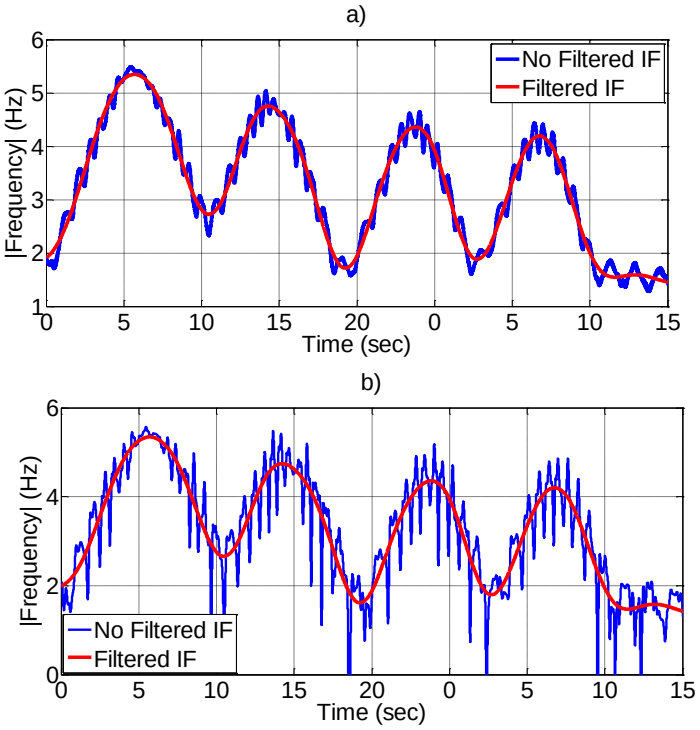

Fig. 71 Evolution of the Instantaneous Frequency (IF) for the fault component a) Classical method b) Teager-Kaiser Operator. Blue line, not filtered If. Red line, filtered IF.

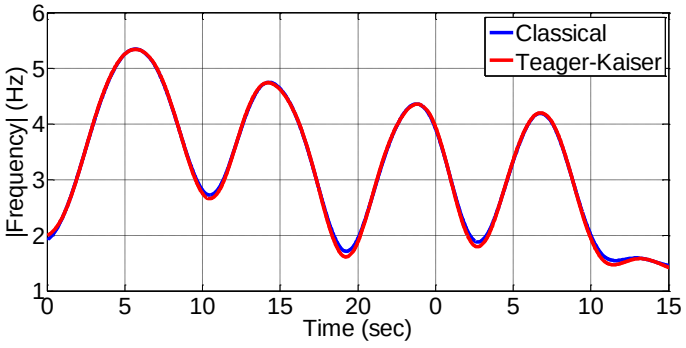

Fig. 72 Comparison of the evolution of the instantaneous frequency computed through the classical method (blue line) and through the Teager-Kaiser operator.

compared, concluding that the evolution of the instantaneous frequency is independent of the technique for its computation. The selection of one or other method of computation is based on the technical limitations of the available hardware.

The evolution of the instantaneous frequency shown in Fig. 72 does not follow any characteristic pattern in the time domain due to the stochastic evolution of speed. However, as it has already been demonstrated the

depiction of the instantaneous frequency in the slip domain follows an independent pattern of the fluctuations in speed.

Therefore, the evolution of the instantaneous frequency shown in Fig. 72 is depicted in the slip domain in Fig. 73.a (black line) where it overlaps with its theoretical evolution (red line). The comparison of both evolutions allows the determination of the origin of the energy contained in the fault component where there are two possible cases: (i) the evolution of the computed instantaneous and theoretical frequency overlap (Fig. 73.a and Fig. 73.b) or (ii) the evolution of the instantaneous frequency does not conform to the theoretical evolution (Fig. 73.c).

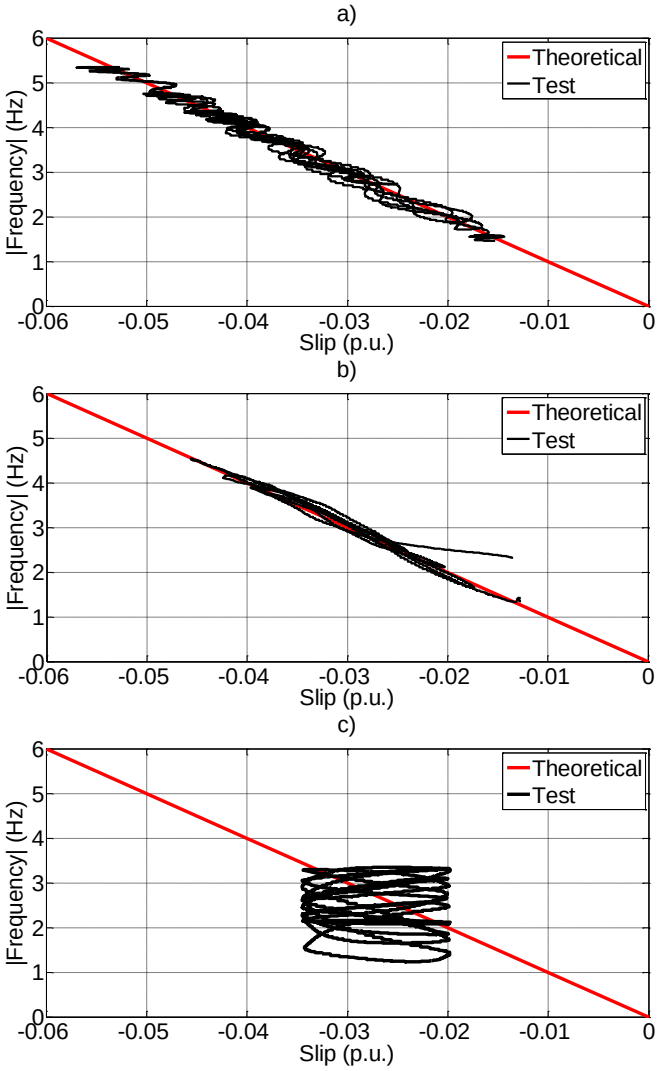

Fig. 73 Instantaneous frequency in the slip domain. Computed evolution (black line), Theoretical evolution (red line) a) Machine with rotor asymmetry (R_a = 4.15 Ω) b) Healthy machine c) Healthy machine, in non-stationary regime with high speed fluctuations.

Fig. 73.a shows the depiction of the instantaneous frequency in the slip domain for a machine with an asymmetry in its secondary winding caused by the connection of a resistor in series with a phase of the secondary winding whose value is 4.15 Ω, increasing the resistance of one phase of the secondary winding respect to the healthy state a 94.33% when the machine is subjected to the fluctuations in the speed shown in Fig. 66.a.

The value of the energy of the fault component for the case shown in Fig. 73.a is 4.129% compared to the total energy of the non-stationary analysed regime.

In Fig. 73.a is seen how the computed instantaneous frequency overlaps the rotor asymmetry theoretical pattern thereby indicating that the energy of the extracted fault component is mainly due to a rotor asymmetry.

Secondly, Fig. 73.b shows the depiction of the instantaneous frequency for a healthy machine.

The value of the energy is 0.005% compared to the total energy of non-stationary analysed regime.

In Fig. 73.b is also shown that the instantaneous frequency overlaps the rotor asymmetry theoretical pattern. This is due to the high precision of performed filtering process. As a direct consequence, the proposed method is capable of extracting the intrinsic asymmetry component of the machine due to manufacturing tolerances.

Finally, in Fig. 73.c is seen the case of a healthy machine subjected to a high-speed fluctuation (Fig. 74).

The frequency of the speed oscillation has been chosen to increase the energy in the band where the fault component evolves despite the machine is in healthy state. As a direct result of this action, the computed energy for this test is 0.092% compared to the total energy of the non-stationary analysed regime.

If the diagnostic criteria were only based on the energy parameter, the value of energy would cause false positive diagnosis since that would entail an increase of the energy, compared to the healthy machine, of one order of magnitude.

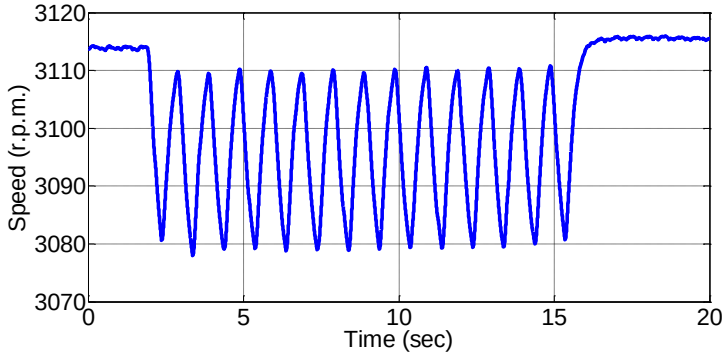

Fig. 74 High-speed fluctuation that causes an increase in the energy in the frequency band where the fault component evolves despite the machine is healthy.

However, the computation of the instantaneous frequency allows the right diagnosis of the machine, since it will be enough to look at the evolution of the instantaneous frequency (Fig. 73.c) to determine that the origin of the increase of the energy is not caused by a rotor asymmetry since the computed evolution of the instantaneous frequency does not overlap with the theoretical evolution pattern.

Thus, it can be concluded that the energy from the extracted fault component consequence of the speed variations shown in Fig. 74 is not due to a rotor asymmetry avoiding a false positive diagnosis.

A drawback of the graphical methods for the diagnosis is to set when the computed and theoretical evolution overlap enough to consider the machine in faulty state. To avoid this uncertainty, the fault diagnostic criterion is set so that when the similarity coefficient value is close to one, the linear regression values are similar to the theoretical and the value of the energy exceeds the preset threshold, the machine will be considered in faulty state.

In any other case, it cannot be asserted with absolutely certainty that the machine is affected by a rotor asymmetry, since the increase of the energy could be due to any other cause not considered.

Finally, to determine the efficacy of the method, eight more tests are performed changing the severity of the fault, but with the same speed profile (Fig. 66.a) in all cases to facilitate the comparison of results. Table 14 shows the results of all the tests conducted ranging from asymmetries that correspond with increases in the rotor winding resistance of 1.62% to 94.33%.

Notice that the value of the energy of the fault component increases as the severity of the fault increases (tests A1 - A9, Fig. 75). Fig. 75 depicts the evolution of severity fault indicator E_t function of the degree of asymmetry, characterised by increase of resistance of the faulty phase in % of the healthy state resistance. This figure shows the consistency of the proposed fault indicator based on the computation of energy.

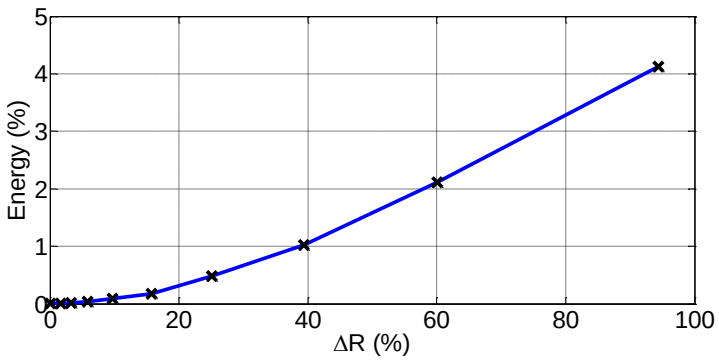

Fig. 75 Evolution of the energy of the rotor asymmetry fault component for the universal machine set as wound rotor induction machine working as generator, function of the increase of resistor in the rotor winding.

The first column of Table 14 refers to the performed test, whereas the second, *R*, provides the value of the resistor, in ohms, connected in series with the secondary to cause the rotor asymmetry. The third column, ΔR, shows the increase in percentage of the added series resistance respect to the rated value of resistance of the secondary phase of the machine. In the fourth column, *S*, is shown the proposed similitude coefficient proposed. The fifth, *m*, and sixth, *b*, columns show the target values of the linear regression, whereas the seventh column, E_t, denotes the relative value of the energy of the extracted fault component when it is computed in the time domain over the total energy of the acquired current signal in the test. The last column shows the time, in seconds, required to process the data on a PC whose features are given in Annex II.

TABLE 14. OBJECTIVE DIAGNOSTIC PARAMETERS OF ROTOR ASYMMETRY WHEN THE FAULT COMPONENT HAS BEEN EXTRACTED THROUGH A DWT FILTER. WOUND ROTOR INDUCTION UNIVERSAL MACHINE WORKING AS GENERATOR.

Test	R	ΔR	S	m	b	E_t	**Computation time**
	Ω	%				%	s
Theoretical				-100	0		
Healthy			1.000	-100.08	0.029	0.005	0.29
A1	0.07	1.62	1.000	-99.79	-0.009	0.010	0.31
A2	0.14	3.29	0.889	-83.39	0.560	0.019	0.29
A3	0.26	5.85	0.968	-98.52	0.000	0.041	0.27
A4	0.43	9.67	1.000	-100.41	-0.022	0.092	0.28
A5	0.69	15.73	0.996	-98.87	0.017	0.179	0.29
A6	1.10	25.11	1.000	-99.26	0.020	0.480	0.28
A7	1.73	39.38	1.000	-98.82	0.056	1.025	0.29
A8	2.64	60.03	0.997	-98.40	0.058	2.109	0.31
A9	4.15	94.33	0.958	-98.12	0.037	4.129	0.29
AA			0.278	-1.92	2.433	0.092	0.30

In any case, the use of the energy parameter is not significant enough to make a reliable diagnosis of the machine since the computation of the energy of the fault component provides no information about its origin, and it may cause false positive diagnosis as it would be in the case of test AA if the energy indicator were the unique parameter taken into account to determine the state of the machine. According to the energy of the fault component in the AA test, the machine would be affected by a rotor asymmetry of 9.67% despite being in a healthy state.

Finally, the last column of Table 14 shows the required time to perform computations to diagnose the machine whose value is around 0.3 seconds. To this computation time must be added the acquisition time of the wave to determine the total required computation time.

2.1.2 DIAGNOSIS BASED ON THE EXTRACTION OF THE FAULT COMPONENTS THROUGH A WAVELET PACKET FILTER

The use of DWT filters for the extraction of the rotor asymmetry fault components is complex due to the required frequency shifting in the extraction process of the fault component. Furthermore, due to such displacement, the main fault components overlap and cannot be split from each other.

To overcome these drawbacks, the filters based on the Wavelet Packet Transform will be evaluated since this transform, a priori, seems very appropriate, since it theoretically allows the extraction of both main fault components independently and with no frequency shifting.

The diagnostic process based on the Wavelet Packet starts again with the acquisition of the non-stationary speed (Fig. 66.a) and current of the machine (Fig. 67). From the previous section comes that the slip is bounded in the range [-0.057, -0.014], whereas the fault components are located at [51.42, 55.70] Hz for the component $(1-2\cdot s)\cdot f_{red}$ and [44.30, 48.58] Hz for the component $(1+2\cdot s)\cdot f_{red}$.

After the acquisition of the current and the location of the fault components in their respective frequency ranges, it is set the maximum bandwidth of the fundamental band of the WP filter bank, whose maximum width will be:

$$\Delta f = \min\left(\left| f_{red} - f_{(1-2\cdot s)\cdot f_{red}} \right|, \left| f_{red} - f_{(1+2\cdot s)\cdot f_{red}} \right|\right) \tag{157}$$

Substituting in (157), then

$$\Delta f = \min\left(\left|50-\left[51.42,55.70\right]\right|,\left|50-\left[44.30,48.58\right]\right|\right) = 1.42 \text{ Hz} \tag{158}$$

After the computation of the maximum bandwidth of the WP filter bank, it is computed the minimum value of the WP decomposition filter that satisfies (158), applying (81) (Chapter VI - 2.2.1), which leads to :

$$n_{\Delta f} = \text{int}\left[\frac{\log\frac{f_s}{\Delta f}}{\log(2)}\right] = \text{int}\left[\frac{\log\frac{5000}{1.42}}{\log(2)}\right] = 11 \tag{159}$$

The value of the actual bandwidth is set by applying the decomposition of order $n_{\Delta f}$ computed by (82)

$$d = \frac{f_s}{2^{1+n_{\Delta f}}} = \frac{5000}{2^{1+11}} = 1.22 \text{ Hz} \tag{160}$$

Thus, the fundamental bandwidth of the WP filter bank takes a value of 1.22 Hz, which theoretically prevents the overlap between the fault components and the fundamental frequency component.

Finally, it is necessary to compute the number and position of the filter banks to be taken from the WP decomposition for the extraction of the frequency band in which are contained the fault components.

The computation of the minimum and maximum position of the filter bank to be taken to extract the fault component $(1-2\cdot s)\cdot f_{red}$ will be (84):

$$k_{\inf} = \text{int}\left(\frac{f_{\min}}{d}\right) = \text{int}\left(\frac{51.42}{1.22}\right) = 42$$
$$k_{\sup} = \text{int}\left(\frac{f_{\max}}{d} + 1\right) = \text{int}\left(\frac{55.70}{1.22} + 1\right) = 46 \quad (161)$$

Whereas for the fault component $(1+2\cdot s)\cdot f_{red}$ is

$$k_{\inf} = \text{int}\left(\frac{f_{\min}}{d}\right) = \text{int}\left(\frac{44.30}{1.22}\right) = 36$$
$$k_{\sup} = \text{int}\left(\frac{f_{\max}}{d} + 1\right) = \text{int}\left(\frac{48.58}{1.22} + 1\right) = 40 \quad (162)$$

The position of the filter banks computed through (161) and (162) allow the extraction of the frequency bands

$$B_{(1-2\cdot s)\cdot f_{red}} = [42\cdot 1.22, 46\cdot 1.22] = [51.26, 56.15] \text{ Hz}$$
$$B_{(1+2\cdot s)\cdot f_{red}} = [36\cdot 1.22, 40\cdot 1.22] = [43.94, 48.82] \text{ Hz} \quad (163)$$

that contain the fault components.

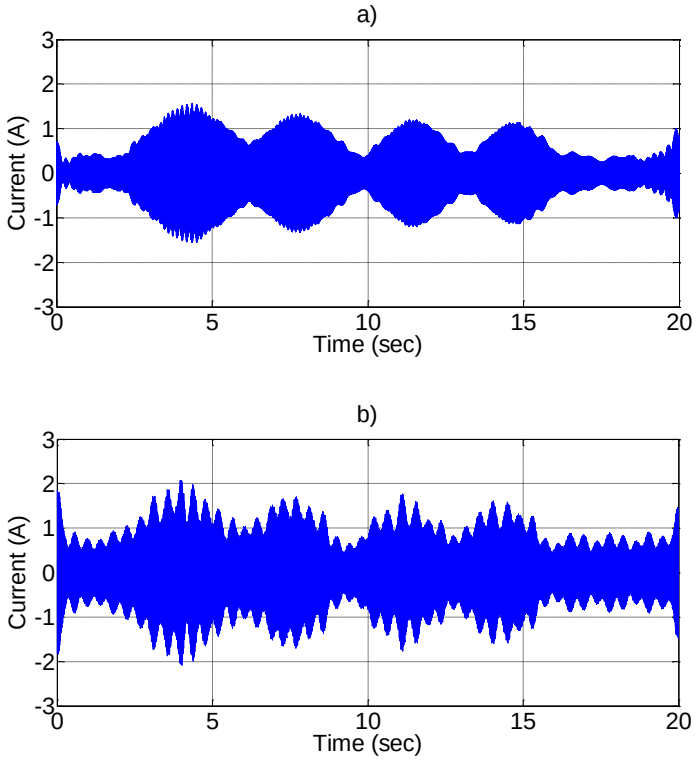

Fig. 76 Fault components extracted through the WP filter. Universal machine working as generator in non-stationary conditions, rotor asymmetry fault (R_a = 4.15 Ω).. a) Harmonic fault component $(1-2\cdot s)\cdot f_{red}$ b) Harmonic fault component $(1+2\cdot s)\cdot f_{red}$

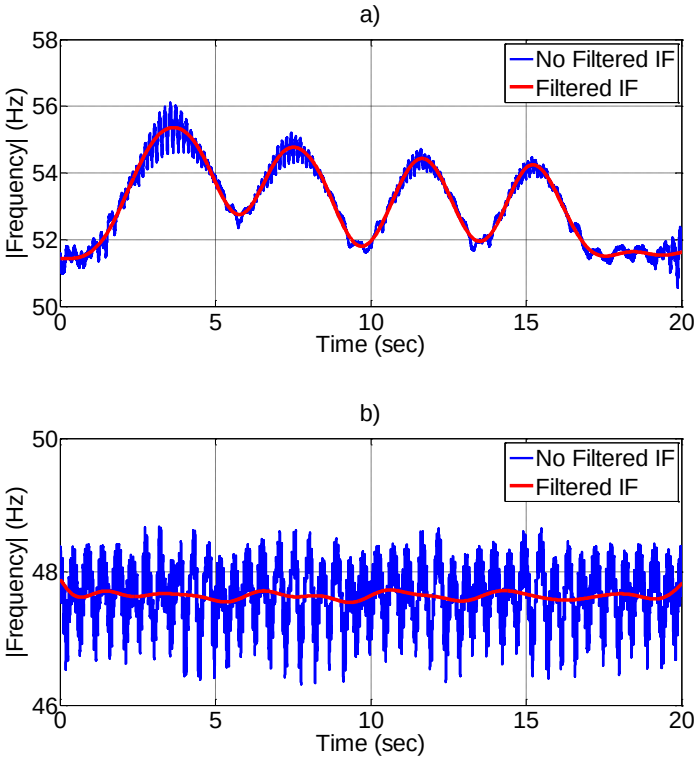

Fig. 77 Instantaneous frequency in the time domain for the fault component extracted through a WP filter. Universal machine working as generator in non-stationary conditions, rotor asymmetry fault (R_a = 4.15 Ω).. a) Harmonic fault component (1-2·*s*)·f_{red} b) Harmonic fault component (1+2·*s*)·f_{red}

The evolution of the fault component (1-2·*s*)·f_{red} extracted with a WP filter is shown in Fig. 76.a whereas the fault component (1+2·*s*)·f_{red} is shown in Fig. 76.b.

After the extraction of the fault components it is computed the value of the energy of each of them and, in the case of the preset energy threshold is exceeded, it is performed the determination of the origin of the increase of the energy.

The computation of the instantaneous frequency is analogously performed as in the previous section and the result is shown in Fig. 77 in the time domain.

Since the depiction of the instantaneous frequency lacks of any pattern in the time domain, it is mandatory its depiction in the slip domain (Fig. 78).

Fig. 78.a shows the evolution of the instantaneous frequency versus the slip for the component (1-2·*s*)·f_{red} where it is seen that this component follows the theoretical rotor asymmetry pattern. This fact is also confirmed by the computed objective values since S = 0.989, m' =-97.97 y b' = 50.06, that ensure that the computed energy of that component is due to a rotor

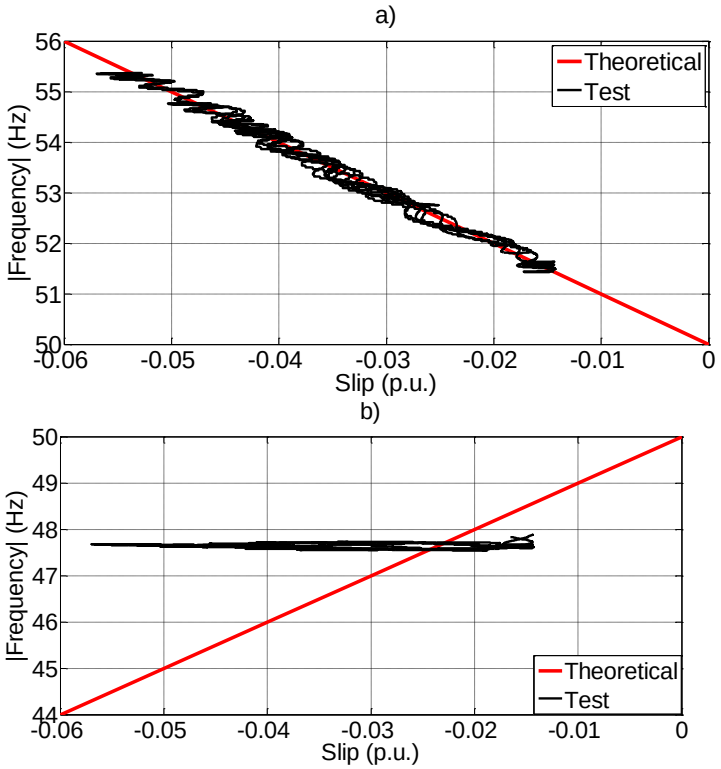

Fig. 78 Instantaneous frequency in the slip domain for the fault component extracted through a WP filter. Universal machine working as generator in non-stationary conditions, rotor asymmetry fault (R_a = 4.15 Ω).. a) Harmonic fault component (1-2·s)·f_{red} b) Harmonic fault component (1+2·s)·f_{red}

asymmetry and therefore if it exceeds the preset energy threshold, the machine will be diagnosed as in faulty state.

However, Fig. 78.b shows that the evolution of the component (1+2·s)·f_{red} does not overlap the theoretical fault pattern what implies that the energy of that component is not due to a rotor asymmetry.

The ambiguity that comes from Fig. 78 creates uncertainty in the diagnosis of the machine since the machine, at a given time, can only be diagnosed in a single state (symmetrical or asymmetrical).

The resolution of the uncertainty created by the divergence of the result in Fig. 78, is performed by the computation of the frequency response of the WP filter for the extraction of the fault component (Fig. 79), where it is shown that the response of the filter for the extraction of the component (1+2·s)·f_{red} (Fig. 79, blue line) allows 27.74% of the fundamental component in the frequency band where only the component (1+2·s)·f_{red} should be, fact that distorts the result.

Furthermore, the filter response for the component (1-2·s)·f_{red} (Fig. 79, red line) only allows 2.13% of the fundamental component in the frequency band where only component (1-2·s)·f_{red} should be, value that is not enough to distort the component (1-2·s)·$f_{red.}$

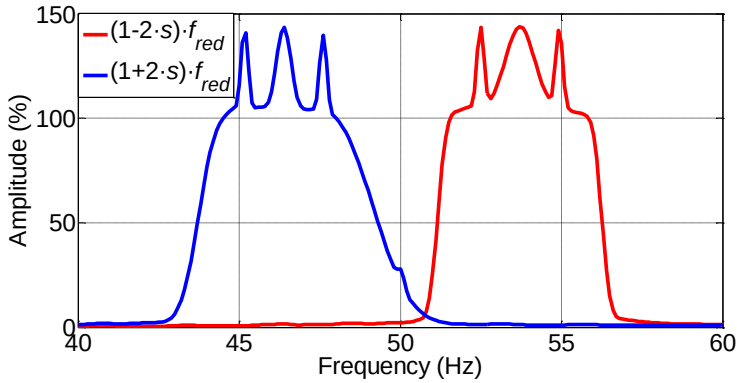

Fig. 79 Frequency response of the designed WP filter for the extraction of the fault components of rotor asymmetry for the universal machine for the tests A5-A9 and AA. Frequency response for the component $(1+2\cdot s)\cdot f_{red}$ (blue line), frequency response for the component $(1-2\cdot s)\cdot f_{red}$ (red line)

These facts indicate that the diagnosis performed by the fault component governed by $(1+2\cdot s)\cdot f_{red}$ is incorrect and should not be considered for the diagnosis of the machine, due to the distortion caused by the fundamental component in the extracted frequency band which should only contain the component $(1+2\cdot s)\cdot f_{red}$.

Analogously to the previous section, the study is conducted for the 11 performed tests to determine the diagnostic limits of the WP filters. The objective results of each test are shown in Table 15 for the component $(1-2\cdot s)\cdot f_{red}$ and in Table 16for the component $(1+2\cdot s)\cdot f_{red}$.

The first noteworthy result is that the values of the Table 16, which corresponds to the component $(1+2\cdot s)\cdot f_{red}$, are not significant due to the bad filtering that provides the designed WP filter (Fig. 79, blue line) as a result of its high permissiveness to allow the fundamental frequency component in the extracted frequency band.

The results of Table 15 correspond to the component $(1-2\cdot s)\cdot f_{red}$, showing that the similitude coefficient is close to 1 for tests A5-A9, what indicates that the computed energy of the fault component is due to a rotor asymmetry. However for the healthy, A1-A4 and AA tests the similitude coefficient is close to zero. The causes for a low similitude coefficient may be two: (i) the performed filtering is correct and the fault component has an energy so low that it is not predominant in the range extracted or (ii) an incorrect filtering.

Firstly, it is checked if the frequency response of the designed filter is correct. To perform it the frequency response of the designed WP filter for each test whose similitude coefficient is low (tests A1-A4 and AA) is computed.

The frequency response for the filters in the healthy, A1-A4 tests for the extraction of the component $(1-2\cdot s)\cdot f_{red}$ is shown in Fig. 80, which shows that the designed filter allows a 55.10% the fundamental component in the frequency range where the component $(1-2\cdot s)\cdot f_{red}$ evolves (Fig. 80, red line) distorting the result and preventing the use of the extracted signal from the diagnosis.

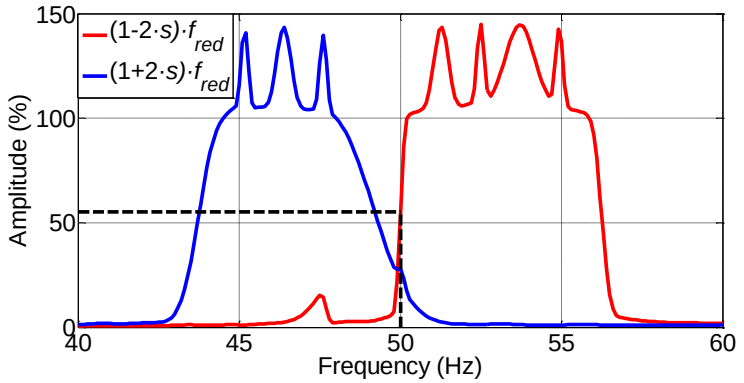

Fig. 80 Frequency response of the WP filter for the extraction of the rotor asymmetry fault for the universal machine for the tests A1-A4. Frequency response for the component $(1+2\cdot s)\cdot f_{red}$ (blue line), frequency response for the component $(1-2\cdot s)\cdot f_{red}$ (red line)

Furthermore, the frequency response of the filter for the test AA for the component $(1-2\cdot s)\cdot f_{red}$ is the same as in Fig. 79 (red line), that is, the frequency range where the component $(1-2\cdot s)\cdot f_{red}$ evolves is not distorted by the fundamental current component what enables the correct diagnosis of the machine.

The difference in the frequency response of the designed filters for the extraction of the fault components in each test is due to small differences in the speeds for the different tests, despite the device used for the automatic performance of the non-stationary regime.

The depiction of the energy function of the fault degree (Fig. 81 and Fig. 82) shows the low consistency of the energy parameter when WP performs the extraction of the fault components filters.

The representation of the energy of the fault component $(1-2\cdot s)\cdot f_{red}$ extracted through a WP filter shows high energy values (higher than 20% of the total energy of the analysed wave), for low values of rotor asymmetries, whereas for higher fault degrees, the energy of the fault component is close to 1 or 2%, confirming the distortion of the fault component by the fundamental current component.

Regarding the energy of the fault component failure $(1+2\cdot s)\cdot f_{red}$, it is noticed that its value is substantially constant and irrespective of the fault degree, preventing the performance of a correct diagnosis.

The conclusion reached after the analysis of the results of the 11 performed tests is that the use of the filters based on the WP transform due to practical difficulties, which have in their implementation, is not recommended for the extraction of the fault components of rotor asymmetry. The correct use of the filters WP requires knowing in detail, before its application for the extraction of the fault components, the frequency response of the designed filter.

This fact means that the computational cost and time necessary for the design of a WP filter to work properly has a similar order to that required to perform the whole diagnosis of a test through a DWT filter, although it is

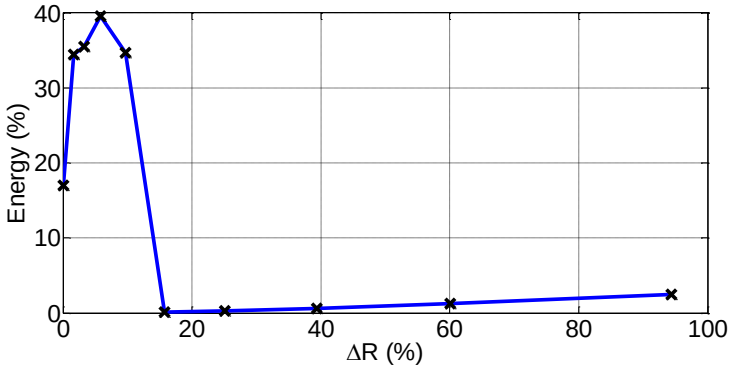

Fig. 81 Evolution of the energy for the fault component function of the increase of the resistor of a winding rotor phase for the component $(1\text{-}2\cdot s)\cdot f_{red}$. Fault components extracted through a WP filter.

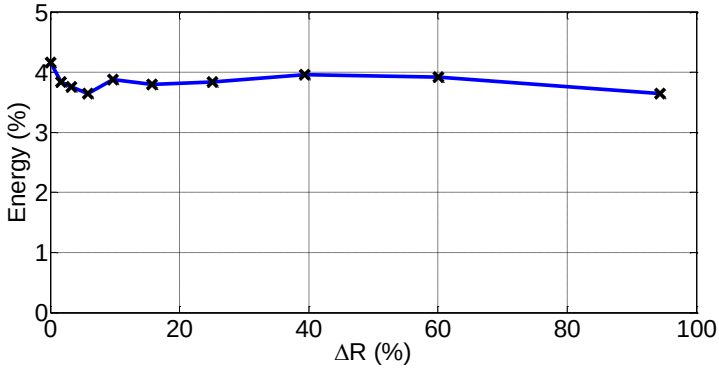

Fig. 82 Evolution of the energy for the fault component function of the increase of the resistor of a winding rotor phase for the component $(1+2\cdot s)\cdot f_{red}$. Fault components extracted through a WP filter.

mandatory a frequency shifting when the diagnosis is performed through a DWT filter.

Another drawback of the use of the WP filters is that since there are small speed changes between tests is necessary a complete recomputation of the WP filter for each test, therefore the computational cost of the implementation of the WP filters WP is inadmissible.

The disadvantages of the WP transform in the filtering process prevent its proper application in the diagnosis of electric machines. In the following sections this filtering technique will not be used due to both the high computational and temporal cost in its application which also leads to uncertain or/and inaccurate results.

TABLE 15. OBJECTIVE PARAMETERS FOR THE DIAGNOSIS OF A ROTOR ASYMMETRY THROUGH THE EXTRACTION OF THE FAULT COMPONENT $(1-2\cdot s)\cdot f_{RED}$ WITH A WP FILTER. UNIVERSAL MACHINE SET AS A WOUND ROTOR MACHINE WORKING AS GENERATOR

Test	R	ΔR	S	m	b	E_t	Computation time
	Ω	%				%	s
Theoretical				-100	0		
Healthy			0.000	1.60	50.19	16.97	0.76
A1	0.07	1.62	0.000	1.91	50.16	34.46	0.80
A2	0.14	3.29	0.000	-2.96	49.96	35.52	0.79
A3	0.26	5.85	0.000	-3.87	49.93	39.56	0.80
A4	0.43	9.67	0.000	2.59	50.18	34.69	0.79
A5	0.69	15.73	1.000	-99.41	50.01	0.116	0.79
A6	1.10	25.11	1.000	-99.15	50.03	0.270	0.78
A7	1.73	39.38	1.000	-98.80	50.05	0.593	0.81
A8	2.64	60.03	1.000	-98.36	50.06	1.232	0.81
A9	4.15	94.33	0.989	-97.97	50.06	2.465	0.81
AA			0.000	0.45	51.56	0.058	0.76

TABLE 16. OBJECTIVE PARAMETERS FOR THE DIAGNOSIS OF A ROTOR ASYMMETRY THROUGH THE EXTRACTION OF THE FAULT COMPONENT $(1+2\cdot s)\cdot f_{RED}$ WITH A WP FILTER. UNIVERSAL MACHINE SET AS A WOUND ROTOR MACHINE WORKING AS GENERATOR

Test	R	ΔR	S	m	b	E_t	Computation time
	Ω	%				%	s
Theoretical				-100	0		
Healthy			0.168	-1.66	47.62	4.16	0.76
A1	0.07	1.62	0.164	-1.56	47.60	3.84	0.80
A2	0.14	3.29	0.172	-1.65	47.59	3.76	0.79
A3	0.26	5.85	0.181	-1.52	47.59	3.65	0.80
A4	0.43	9.67	0.180	-1.59	47.60	3.88	0.79
A5	0.69	15.73	0.141	-1.37	47.60	3.80	0.79
A6	1.10	25.11	0.157	-1.51	47.60	3.84	0.78
A7	1.73	39.38	0.122	-1.09	47.63	3.96	0.81
A8	2.64	60.03	0.128	-1.28	47.61	3.92	0.81
A9	4.15	94.33	0.097	-1.34	47.59	3.65	0.81
AA			0.363	0.06	47.67	4.37	0.76

2.1.3 DIAGNOSIS BASED ON THE EXTRACTION OF THE FAULT COMPONENTS THROUGH A SPECTRAL FILTER

In the previous sections it has been performed the extraction of the fault components of rotor asymmetry rotor through the DWT and WP filters.

The drawbacks associated with them, complexity, low flexibility, high computational cost, can be solved with the spectral filter, which is based on the properties of the Discrete Fourier Transform (Chapter VI - 2.3).

The main advantages of the spectral filter are (i) high flexibility since it can select any frequency range with a resolution equal to the inverse of the sampling time, (ii) low computational cost since the filtering is based on the computation of a Discrete Fourier transform and (iii) the lack of transition bands associated with non-ideal filters.

The diagnostic process, as in the two previous cases, begins with the acquisition of speed (Fig. 66.a) and current (Fig. 67) during the non-stationary operation.

The evolution of slip and frequency of the fault components $(1-2\cdot s)\cdot f_{red}$ and $(1+2\cdot s)\cdot f_{red}$ remain unchanged from the previous sections since the analysed signals are the same. As the slip varies in the range [-0.057, -0.014], ranges $[f_{min}, f_{max}]$ that contain the frequencies of the fault components are:

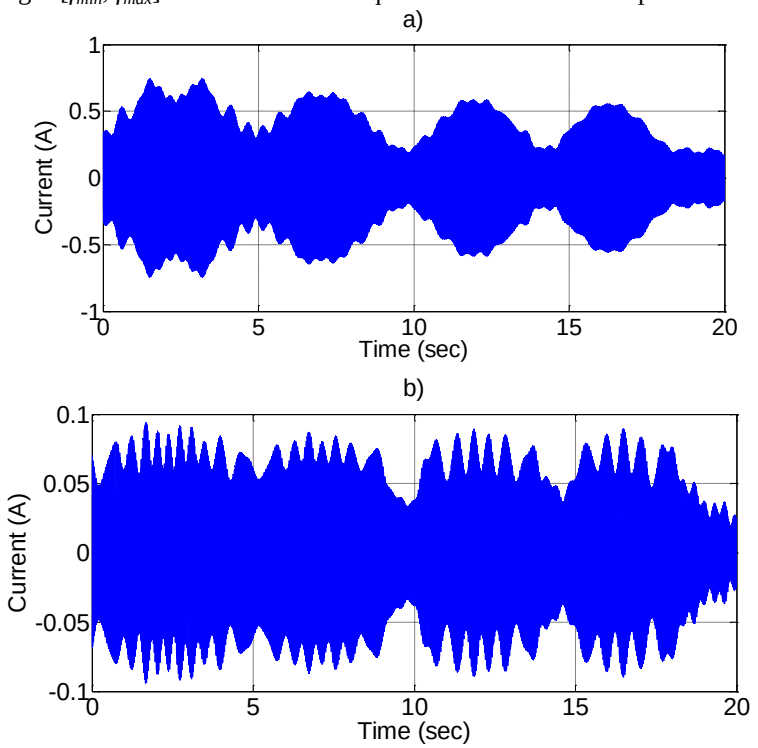

Fig. 83 Fault components extracted through the WP filter. Universal machine working as generator in non-stationary conditions, rotor asymmetry fault (R_a = 4.15 Ω). a) Harmonic fault component $(1-2\cdot s)\cdot f_{red}$ b) Harmonic fault component $(1+2\cdot s)\cdot f_{red}$

- Component $(1-2\cdot s)\cdot f_{red}$: [51.42, 55.70] Hz
- Component $(1+2\cdot s)\cdot f_{red}$: [44.30, 48.58] Hz

The resolution of the spectral filter is inversely proportional to the time of the acquired wave for the diagnosis. In this diagnosis, the captured current waveform lasts 20 seconds (Fig. 67), therefore, the maximum resolution that the width of the frequency band to be extracted through spectral filter is:

$$\Delta f = \frac{1}{t_{adq}} = \frac{1}{20} = 0.05 \text{ Hz} \tag{164}$$

that is, the frequency ranges that may be extracted will be multiples of Δf, then the following frequency ranges $[f_{inf}, f_{sup}]$ can directly extracted:

$$\begin{aligned} B_{(1-2\cdot s)\cdot f_{red}} &= [51.40, 55.70] \text{ Hz} \\ B_{(1+2\cdot s)\cdot f_{red}} &= [44.30, 48.60] \text{ Hz} \end{aligned} \tag{165}$$

The evolution of the fault component failure $(1-2\cdot s)\cdot f_{red}$ extracted through the spectral filter is shown in Fig. 83.a whereas the fault component $(1+2\cdot s)\cdot f_{red}$ is shown in Fig. 83b.

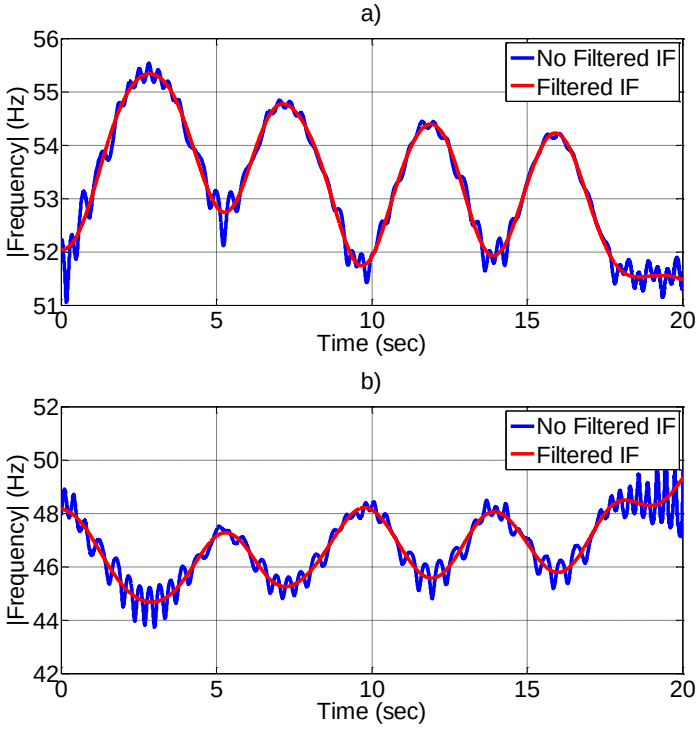

Fig. 84 Instantaneous frequency in the time domain for the fault component extracted through a spectral filter. Universal machine working as generator in non-stationary conditions, rotor asymmetry fault (R_a = 4.15 Ω).. a) Harmonic fault component $(1-2\cdot s)\cdot f_{red}$ b) Harmonic fault component $(1+2\cdot s)\cdot f_{red}$

Once the fault components have been extracted, the energy for each of them is computed and, if it exceeds the energy threshold value that determines the machine is in faulty state, the determination of the origin of the increase of energy is performed through the computation of the instantaneous frequency, whose depiction in the time domain is shown in Fig. 84.

Although the proposed filter lacks of transition bands and possesses no external components into the range to be extracted, the instantaneous frequency still has high frequency components caused by the derivation in the computation of the instantaneous frequency, which must be removed through the application of a low pass band filter.

It has already been mentioned that the depiction in the time domain of the instantaneous frequency follows no pattern, being necessary its depiction in the slip domain (Fig. 85) to determine whether the instantaneous frequency fits the characteristic theoretical fault pattern. The evolution of the computed frequency of the fault component $(1\text{-}2\cdot s)\cdot f_{red}$ in the slip domain is shown in Fig. 85.a where it is shown that it fits the theoretical asymmetry pattern.

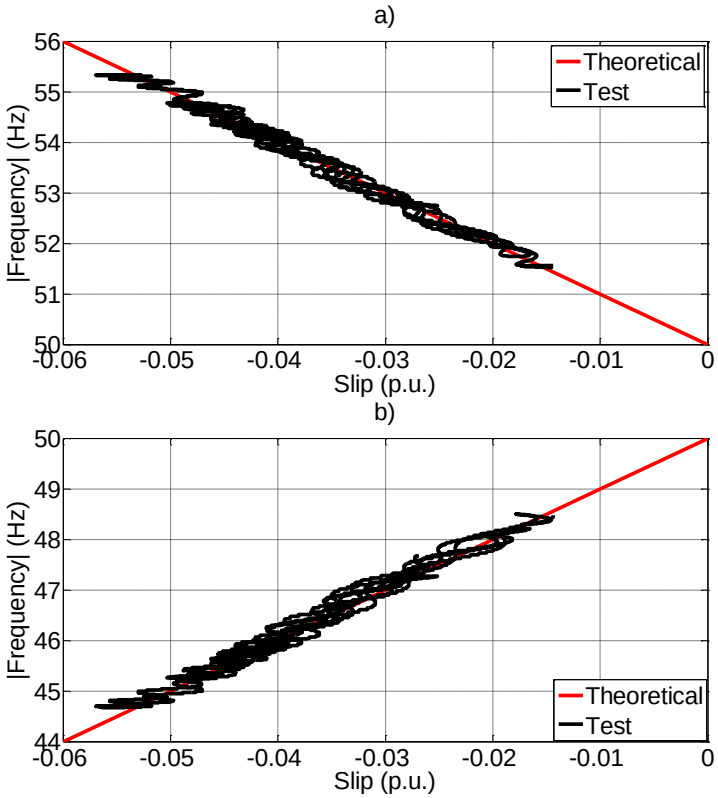

Fig. 85 Instantaneous frequency in the slip domain for the fault component extracted through a spectral filter. Universal machine working as generator in non-stationary conditions, rotor asymmetry fault (R_a = 4.15 Ω).. a) Harmonic fault component $(1\text{-}2\cdot s)\cdot f_{red}$ b) Harmonic fault component $(1+2\cdot s)\cdot f_{red}$

Fig. 85.b shows the evolution of the instantaneous frequency of the $(1+2\cdot s)\cdot f_{red}$ where it is noticed again that the evolution of the instantaneous frequency fits the fault pattern. Therefore, it is concluded that the computed value of the energy in this test is due to the rotor asymmetry, for both the component $(1-2\cdot s)\cdot f_{red}$ and for the component $(1+2\cdot s)\cdot f_{red}$. If the computed value of the energy exceeds the threshold value, the machine will be in faulty state.

The numerical results of the 11 performed tests are shown in Table 17 for the fault component $(1-2\cdot s)\cdot f_{red}$ and in Table 18 for the fault component to the $(1+2\cdot s)\cdot f_{red}$ where the energy of the fault components have been computed in the frequency domain through the application of the Plancherel's Theorem.

If the computed values of the energy in the time domain (Table 14, Fig. 75) are compared with those computed in the frequency domain (Table 17, Fig. 86) it is concluded that their magnitudes are practically identical, validating the computation of the energy in any of the two domains.

The analysis of the results for the component $(1-2\cdot s)\cdot f_{red}$ shows that the evolution of the energy indicator is practically linear and directly proportional to the degree of asymmetry of the machine. Moreover, in all the tests conducted, the similitude coefficient (S) is close to 1 and the values of the slope and y-intercept are close to the theoretical. Therefore, it will be enough to set a threshold energy value to determine when the machine is asymmetric enough to be considered in faulty state.

Just like when the diagnosis is performed through the extraction of the component through DWT filters, it is seen that the similitude coefficient for the test AA is not close to 1 and therefore determines that the value of the computed energy of the fault component is not due to a rotor asymmetry what prevents the misdiagnosis of a healthy machine with oscillating load from false positives.

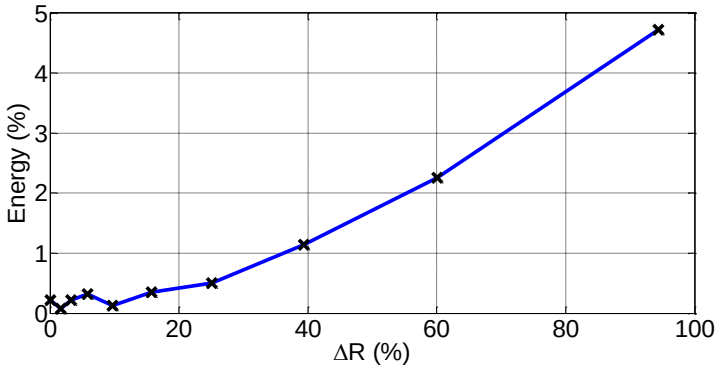

Fig. 86 Evolution of the energy for the fault component function of the increase of the resistor of a winding rotor phase for the component $(1-2\cdot s)\cdot f_{red}$. Fault components extracted through a spectral filter.

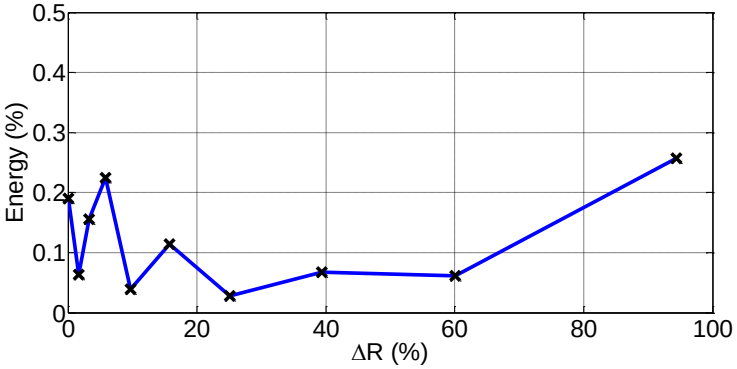

Fig. 87 Evolution of the energy for the fault component function of the increase of the resistor of a winding rotor phase for the component $(1+2\cdot s)\cdot f_{red}$. Fault components extracted through a spectral filter

TABLE 17. OBJECTIVE PARAMETERS FOR THE DIAGNOSIS OF A ROTOR ASYMMETRY THROUGH THE EXTRACTION OF THE FAULT COMPONENT $(1-2\cdot s)\cdot F_{RED}$ WITH A SPECTRAL FILTER. UNIVERSAL MACHINE SET AS A WOUND ROTOR MACHINE WORKING AS GENERATOR

Test	***R***	***ΔR***	***S***	***m***	***b***	E_f	**Computation time**
	Ω	%				%	s
Theoretical				-100	0		
Healthy			0.699	-60.57	50.74	0.217	0.16
A1	0.07	1.62	0.910	-110.51	49.61	0.074	0.16
A2	0.14	3.29	0.912	-107.19	49.73	0.218	0.16
A3	0.26	5.85	0.998	-98.16	50.04	0.320	0.16
A4	0.43	9.67	1.000	-100.40	49.98	0.131	0.16
A5	0.69	15.73	1.000	-99.38	50.01	0.354	0.17
A6	1.10	25.11	1.000	-100.03	49.99	0.499	0.17
A7	1.73	39.38	1.000	-98.63	50.05	1.137	0.17
A8	2.64	60.03	1.000	-98.93	50.03	2.254	0.17
A9	4.15	94.33	0.986	-98.61	50.03	4.724	0.17
AA			0.354	1.39	52.82	0.179	0.16

According to the evolution of the computed instantaneous frequency for the fault component $(1+2\cdot s)\cdot f_{red}$ (Fig. 85.b), it would be expected that the diagnosis of the machine is also possible through this component since the evolution of the instantaneous frequency follows the theoretical fault pattern.

However, the analysis of the energy indicator associated with the fault component $(1+2\cdot s)\cdot f_{red}$ determines that its use is inappropriate due to the non-existent relationship between the status of the machine status (healthy or faulty) and the energy level of the fault component, as it is shown in Fig. 87. The poor performance of the component $(1+2\cdot s)\cdot f_{red}$ is attributed to its small

TABLE 18. OBJECTIVE PARAMETERS FOR THE DIAGNOSIS OF A ROTOR ASYMMETRY THROUGH THE EXTRACTION OF THE FAULT COMPONENT $(1+2\cdot s)\cdot F_{RED}$ WITH A SPECTRAL FILTER. UNIVERSAL MACHINE SET AS A WOUND ROTOR MACHINE WORKING AS GENERATOR

Test	R	ΔR	S	m	b	E_f	Computation time
	Ω	%				%	S
Theoretical				-100	0		
Healthy			0.082	0.50	48.74	0.190	0.16
A1	0.07	1.62	0.248	7.90	48.62	0.063	0.16
A2	0.14	3.29	0.176	4.99	48.60	0.156	0.16
A3	0.26	5.85	0.228	16.78	48.76	0.225	0.16
A4	0.43	9.67	0.915	94.36	49.82	0.039	0.16
A5	0.69	15.73	1.000	100.97	50.07	0.114	0.17
A6	1.10	25.11	0.826	80.30	49.29	0.028	0.17
A7	1.73	39.38	0.986	99.26	49.97	0.067	0.17
A8	2.64	60.03	0.987	98.10	49.94	0.061	0.17
A9	4.15	94.33	0.931	97.66	49.97	0.257	0.17
AA			0.356	2.99	47.11	0.166	0.16

amplitude. Fig. 83 shows that the amplitude of the fault component failure $(1+2\cdot s)\cdot f_{red}$ is around 10 times smaller than the electromagnetic component $(1-2\cdot s)\cdot f_{red}$. That implies that noise or other harmonic components present in the extracted frequency range are as important as the fault harmonic component with a magnitude comparable to the fault component and thus they distort the results based on the computation of the energy of the electromechanical harmonic.

2.2 TESTS ON THE COMMERCIAL MACHINE

In this section, the proposed methodology is validated on a commercial wound rotor induction machine whose features are detailed in Appendix I.

The scheme of the electrical circuit of the test rig for the validation is shown in Fig 88. The methodology is validated through the performance of one test with healthy machine and six additional tests adding resistors in series to a rotor winding phase whose values are between 0.69 and 0.02 Ω that in percentage of the resistance of phase represents an increase of 206% and 6% respectively. An additional test where the machine is healthy and the speed is oscillating is carried out with the same purpose as in the previous section.

The commercial machine is tested in two series: (i) a generator mode (S1 closed, S2 open) and (ii) motor mode (S1 open, S2 closed). The sampling frequency is 5 kHz for both series.

2.2.1 GENERATOR MODE

For the diagnose of the commercial machine in generator mode, seven automated tests, one in healthy state and six where additional resistors and connected in series to the rotor of the tested machine, are conducted in a non-stationary stochastic regime, imposing the same speed profile (Fig. 90.a) for all of them. The machine to be tested is connected to the electrical network, in star connection, a reduced voltage of 235 V due to practical problems, since the power of the DC machine is half the power of the tested induction machine.

An additional test with oscillating speed (Fig. 90.b) is carried out with the same purpose as in the previous section.

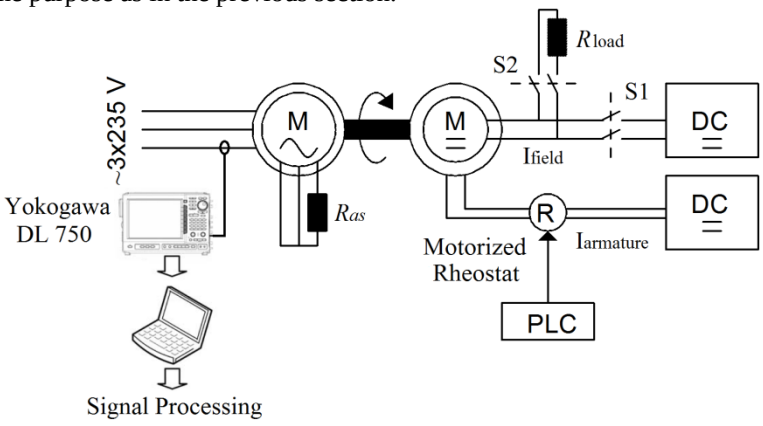

Fig. 88 Scheme of the test rig for the validation of the rotor asymmetry on the commercial wound rotor machine.

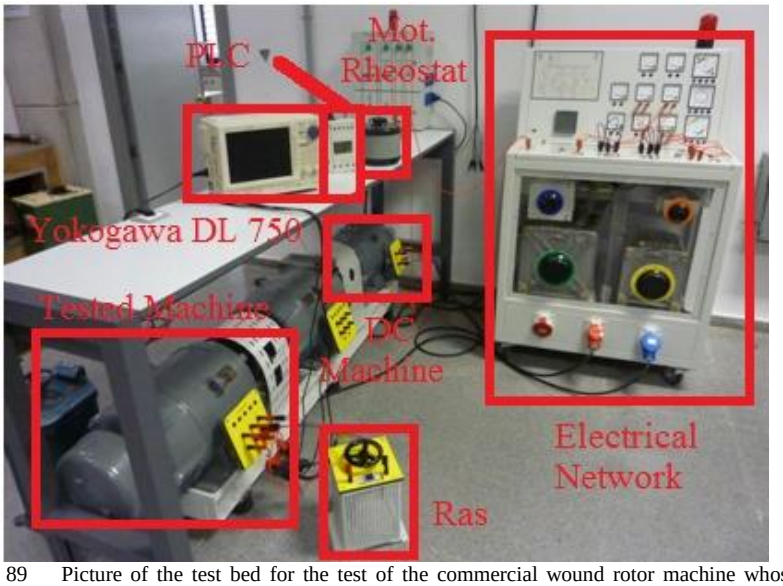

Fig. 89 Picture of the test bed for the test of the commercial wound rotor machine whose power is 11 kW.

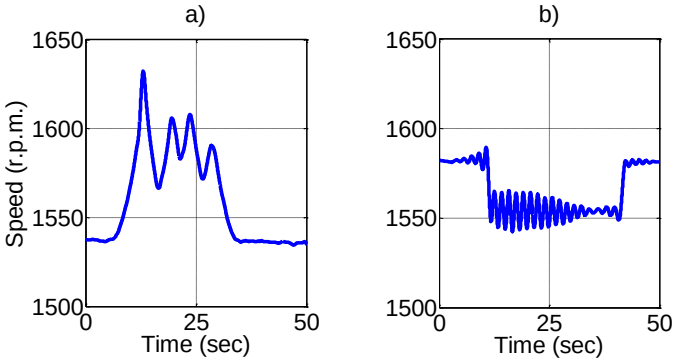

Fig. 90 Oscillating speed of the commercial wound rotor machine working as generator. a) Healthy, A1-A6 tests b) AA test.

2.2.1.1 DIAGNOSIS BASED ON THE EXTRACTION OF THE FAULT COMPONENTS THROUGH A DWT FILTER

Given the imposed speed fluctuation in the tests, the slip that the machine is subjected to evolves in the range [-0.088, -0.023], whereas the fault component $(1-2\cdot s)\cdot f_{red}$ is located in the frequency range [52.37, 58.82] Hz and the component $(1+2\cdot s)\cdot f_{red}$ evolves in [41.18, 47.63] Hz

The extraction of the fault component through a DWT filter forces to shift -50 Hz the fundamental frequency for relocate it into the frequency of 0 Hz. This action also shifts the fault components to the low frequency region of the spectrum. The frequency shifting of -50 Hz relocate both fault components in the same frequency range [2.37, 8.82] Hz. The necessary approximations for the extraction of the frequency band where the fault components are a_8 and a_{11} that allow the extraction of the frequency band [1.22, 9.76] Hz

$$nC = \text{int}\left[\frac{\log\left(\frac{5000}{8.82}\right)}{\log(2)} - 1\right] = 8 \tag{166}$$

$$nNC = \text{int}\left[\frac{\log\left(\frac{5000}{2.37}\right)}{\log(2)}\right] = 11 \tag{167}$$

After the extraction of the fault component its energy is computed and, in the event that it exceeds the threshold value, it is proceeded to the determination of the origin of the energy through the computation of the instantaneous frequency and its depiction in the slip domain.

To illustrate the method, this action is performed irrespective of the computed value of the energy for three cases: (i) fault state machine (Fig. 91), (ii) healthy machine (Fig. 92), and (iii) machine in healthy state undergoing quick speed oscillations (Fig. 93).

Fig. 91 shows the evolution of the instantaneous frequency (black line) where one resistor has been connected in series to the rotor of the machine, increasing the resistance of the phase 42% of its rated value. The evolution of the computed instantaneous frequency (black line) overlaps the theoretical instantaneous frequency (red line), indicating that the computed energy for this extracted fault component is due to a rotor asymmetry, where the severity of the fault degree is determined by the value of the energy of the fault component.

Fig. 92 shows the result for a healthy machine, where it can also be seen that the computed instantaneous frequency overlaps the theoretical instantaneous frequency.

The discrimination between the healthy or faulty machine is performed by the computed value of the energy of the extracted component, since in the case of Fig. 91, the energy of the component is 3.53% compared with the total energy of the acquired signal, whereas for the component of Fig. 92 the energy is 0.002%, which is an increase of energy of 4 orders of magnitude for the component of Fig. 91 regarding the component of Fig. 92, therefore the machine of Fig. 91 is in faulty state.

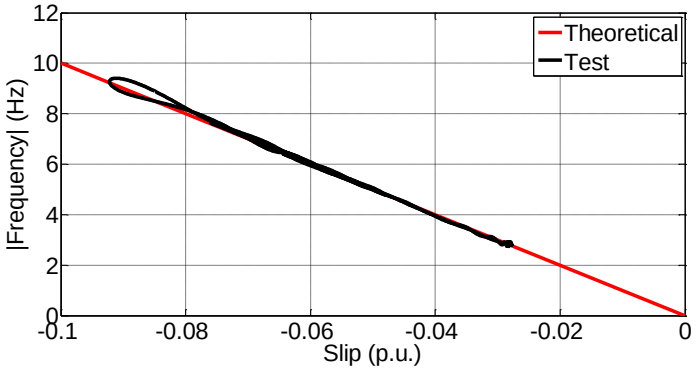

Fig. 91 Instantaneous frequency in the slip domain for the fault component (rotor asymmetry) extracted through a DWT filter. Commercial wound rotor induction machine in faulty state (R_a = 0.14 Ω), A4 test. Generator mode.

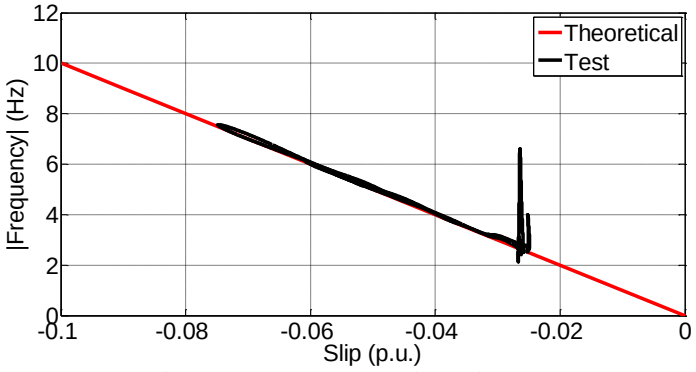

Fig. 92 Instantaneous frequency in the slip domain for the fault component (rotor asymmetry) extracted through a DWT filter. Commercial wound rotor induction machine in healthy state, healthy test. Generator mode.

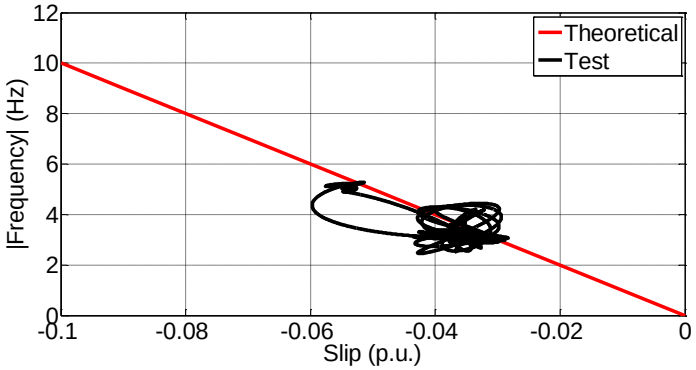

Fig. 93 Instantaneous frequency in the slip domain for the fault component (rotor asymmetry) extracted through a DWT filter. Commercial wound rotor induction machine in healthy state, AA test (oscillating speed fluctuations). Generator mode.

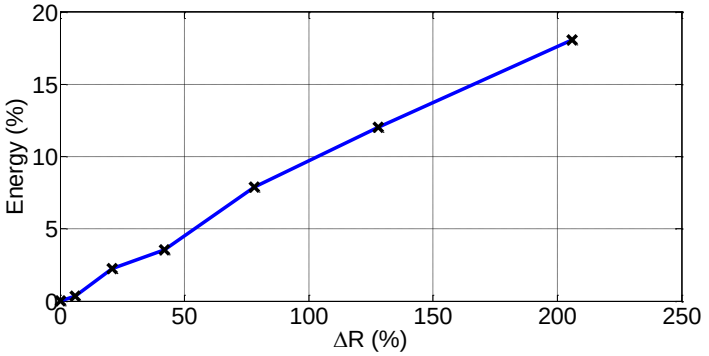

Fig. 94 Evolution of the energy of the rotor asymmetry fault component function of the increase of the fault resistance in the rotor winding.

Finally, Fig. 93 shows the evolution of the instantaneous frequency for the test where the machine is in healthy state whose speed is oscillating. The energy of the band where the fault component evolves is the order of magnitude of the healthy machine since in this case the speed oscillations produce current harmonics whose frequency does not belong to the tested range. However, if the value of the energy was high, as in the previous section, the analysis of the instantaneous frequency would allow the discrimination of the state of the machine since as it is shown in Fig. 93, the instantaneous frequency does not overlap with the theoretical pattern, indicating that the computed increase of energy is not due to a rotor asymmetry.

The numerical results of eight tests for validation of the method are shown in Table 19.

Fig. 94 shows the evolution of energy function of the degree of rotor asymmetry. It is noticed that the evolution of energy is directly proportional to the fault degree. This result agrees with the already shown for the wound rotor induction universal machine discussed in the previous section.

TABLE 19. OBJECTIVE PARAMETERS OF THE DIAGNOSIS FOR A ROTOR ASYMMETRY THROUGH THE EXTRACTION OF THE FAULT COMPONENT WITH A DWT FILTER. COMMERCIAL WOUND ROTOR INDUCTION MACHINE WORKING AS GENERATOR.

Test	R	ΔR	S	m	b	E_t	**Computation time**
	Ω	%				%	s
Theoretical				-100	0		
Healthy			0.888	-87.17	0.76	0.002	0.59
A1	0.02	6	1.000	-101.34	-0.05	0.35	0.57
A2	0.07	21	1.000	-101.02	-0.11	2.25	0.59
A3	0.14	42	0.995	-101.60	-0.16	3.53	0.59
A4	0.26	78	1.000	-101.63	-0.16	7.90	0.59
A5	0.43	128	0.961	-102.87	-0.31	12.04	0.59
A6	0.69	206	1.000	-103.28	-0.20	18.06	0.59
AA			0.404	-81.31	0.46	0.002	0.58

2.2.1.2 DIAGNOSIS BASED ON THE EXTRACTION OF THE FAULT COMPONENTS THROUGH A SPECTRAL FILTER

The diagnostic process of the machine based on the spectral filter is exactly equal to that developed for the extraction of the fault component through the DWT filter, but substituting the DWT filter stage for a filtering stage with a spectral filter.

This change allows the extraction of the frequency band more accurately, since the resolution of the spectral filter is 0.05 Hz, allowing the extraction of the frequency band [52.35, 58.85] Hz in the case of the component $(1-2\cdot s)\cdot f_{red}$ and [41.15, 47.65] Hz for the component $(1+2\cdot s)\cdot f_{red}$, bands that are clearly narrower than the extracted band through the DWT filter.

Notice that the extracted bandwidth through the spectral filter is 58.85-52.35 = 6.5 Hz wide, whereas for the DWT filter is 9.76-1.22 = 8.54 Hz wide, that fact causes a reduction of noise that distorts the extraction of the fault component, improving the accuracy of the diagnostic technique.

The results in the diagnostic process through the spectral filters are shown in Fig. 95, Fig. 96 and Fig. 97 being these figures the analogues to figures Fig. 91, Fig. 92, Fig. 93 that were the result of the diagnostic process with the use of DWT filters.

The numerical results for the eight tests performed are shown in Table 20 for the component $(1-2\cdot s)\cdot f_{red}$, whereas the results for the component $(1+2\cdot s)\cdot f_{red}$ are shown in Table 21

The depiction of the energy of the extracted fault components is shown in Fig. 98 for the component $(1-2\cdot s)\cdot f_{red}$ and in Fig. 99 for the component $(1+2\cdot s)\cdot f_{red}$.

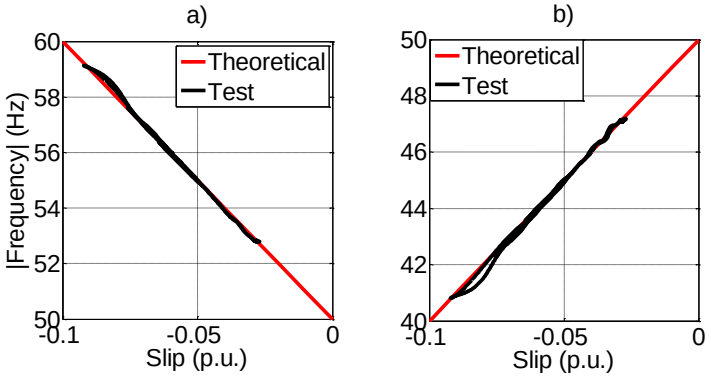

Fig. 95 Instantaneous frequency versus the slip for the extracted fault components through a spectral filter. Commercial machine in faulty state ($R_a = 0.14\ \Omega$), rotor asymmetry, A4 test. Generator mode. A) Fault component $(1-2\cdot s)\cdot f_{red}$ b) Fault Component $(1+2\cdot s)\cdot f_{red}$

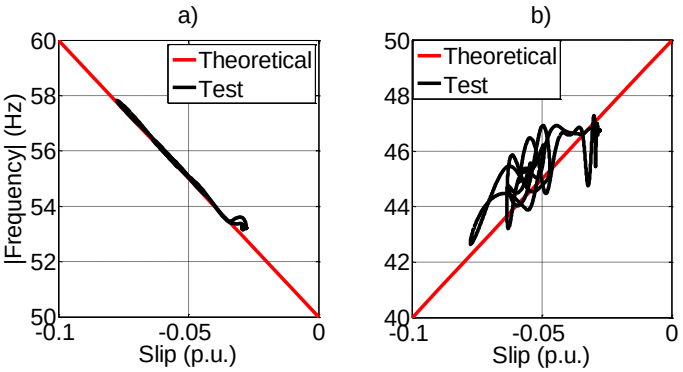

Fig. 96 Instantaneous frequency versus the slip for the extracted fault components through a spectral filter. Commercial machine in healthy state, healthy test. Generator mode. A) Fault component $(1-2\cdot s)\cdot f_{red}$ b) Fault Component $(1+2\cdot s)\cdot f_{red}$

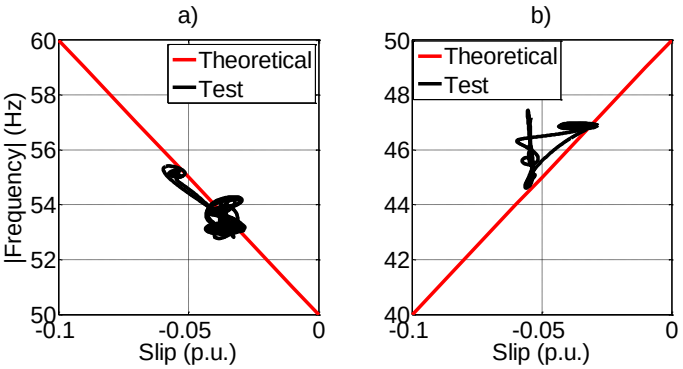

Fig. 97 Instantaneous frequency versus the slip for the extracted fault components through a spectral filter. Commercial machine in healthy state, AA test, oscillating speed fluctuations. Generator mode. A) Fault component $(1-2\cdot s)\cdot f_{red}$ b) Fault Component $(1+2\cdot s)\cdot f_{red}$

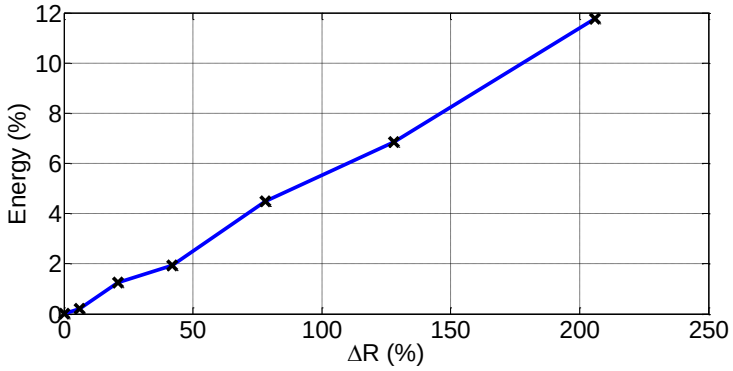

Fig. 98 Evolution of the energy of the fault component of rotor asymmetry function of the increase of the resistance in the rotor winding for the harmonic component $(1-2\cdot s)\cdot f_{red}$

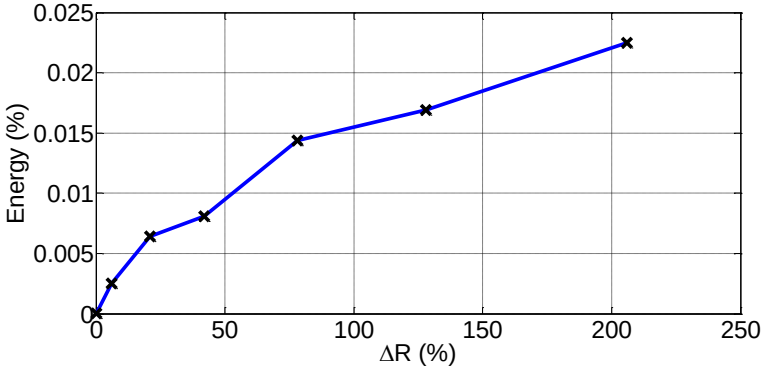

Fig. 99 Evolution of the energy of the fault component of rotor asymmetry function of the increase of the resistance in the rotor winding for the harmonic component $(1+2\cdot s)\cdot f_{red}$

Both evolutions are substantially linear and proportional to the degree of rotor asymmetry that the machine undergoes as it was pointed out in the previous sections. Like when the machine universal was tested, the evolution of the energy of the component $(1+2\cdot s)\cdot f_{red}$ is less uniform than the component $(1-2\cdot s)\cdot f_{red}$. This is because the amplitude of the component $(1+2\cdot s)\cdot f_{red}$ in test conditions is much smaller than the electromagnetic component, and therefore the results are much more affected by noise and other components in the analysed band.

Computation times in this series of tests are greater than in the test for the universal machine, since the acquired time of the signal is longer and therefore the amount of processed points.

TABLE 20. OBJECTIVE PARAMETERS OF THE DIAGNOSIS FOR A ROTOR ASYMMETRY THROUGH THE EXTRACTION OF THE FAULT COMPONENT $(1-2\cdot s)\cdot F_{RED}$ WITH A SPECTRAL FILTER. COMMERCIAL WOUND ROTOR INDUCTION MACHINE WORKING AS GENERATOR

Test	R	ΔR	S	m	b	E_f	Computation time
	Ω	%				%	s
Theoretical				-100	50		
Healthy			0.973	-90.71	50.37	0.0009	0.41
A1	0.02	6	1	-101.12	49.95	0.202	0.41
A2	0.07	21	0.994	-100.58	49.90	1.254	0.42
A3	0.14	42	0.996	-101.36	49.83	1.932	0.41
A4	0.26	78	1	-101.45	49.81	4.494	0.42
A5	0.43	128	0.994	-102.86	49.84	6.864	0.44
A6	0.69	206	1	-103.01	49.76	11.765	0.40
AA			0.230	-30.30	52.88	0.0009	0.43

TABLE 21. OBJECTIVE PARAMETERS OF THE DIAGNOSIS FOR A ROTOR ASYMMETRY THROUGH THE EXTRACTION OF THE FAULT COMPONENT $(1+2\cdot s)\cdot F_{RED}$ WITH A SPECTRAL FILTER. COMMERCIAL WOUND ROTOR INDUCTION MACHINE WORKING AS GENERATOR

Test	R	ΔR	S	m	b	E_f	Computation time
	Ω	%				%	s
Theoretical				100	50		
Healthy			0.076	62.33	49.34	$3.60\cdot10^{-5}$	0.42
A1	0.02	6	0.809	101.22	49.84	$2.50\cdot10^{-3}$	0.41
A2	0.07	21	0.893	101.08	49.88	$6.40\cdot10^{-3}$	0.43
A3	0.14	42	0.955	98.22	49.81	$8.10\cdot10^{-3}$	0.42
A4	0.26	78	0.871	101.54	49.91	$1.44\cdot10^{-2}$	0.43
A5	0.43	128	0.976	102.71	50.06	$1.69\cdot10^{-2}$	0.44
A6	0.69	206	0.986	103.04	50.14	$2.25\cdot10^{-2}$	0.41
AA			0.086	1.85	47.18	$1.00\cdot10^{-4}$	0.40

As a consequence of the low value of the energy of the fault component governed by $(1+2\cdot s)\cdot f_{red}$ on the conditions under the tests are performed, their use is not recommended for the diagnosis of rotor asymmetries. Furthermore, it should be noticed that the fault component $(1+2\cdot s)\cdot f_{red}$ is affected by the inertia of the system and, therefore, the results will be function of it. This fact is verified by the comparison of the results in the previous section for the universal machine (low inertia) in wound rotor configuration (Fig. 87) with the results for the commercial wound rotor induction machine (Fig. 99).

2.2.2 MOTOR MODE

The application of the methodology is also possible in motor mode. For the validation of the motor case, in the assembly shown in Fig. 88 the DC

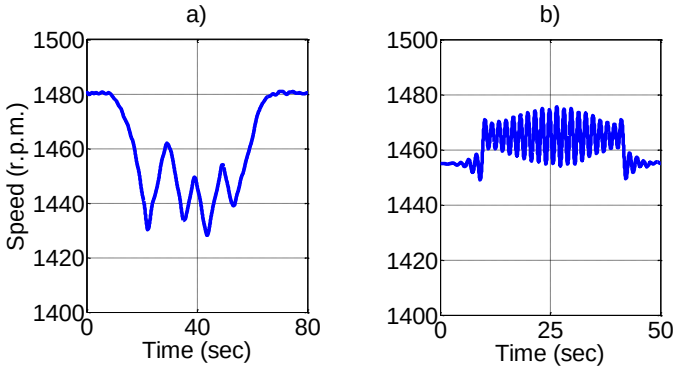

Fig. 100 Non-stationary speed imposed to the commercial machine for the motor tests. a) Healthy, A1-A6 tests b) AA tests

machine works as a generator feeding an external resistor. The machine to be tested is connected to the network, in star connection, a reduced voltage of 235 V due to practical problems, since the power of the DC machine is half the power of the tested induction machine.

Eight tests in non-stationary stochastic conditions are carried out in this section to validate the methodology. The series of tests performed is the same as in the previous section.

The speed profile imposed on the first seven tests is shown in Fig. 100.a, whereas in Fig. 100.b is shown the speed imposed for oscillating speed test, analogous to those already shown for the generator case (previous section).

2.2.2.1 DIAGNOSIS BASED ON THE EXTRACTION OF THE FAULTS COMPONENTS THROUGH A DWT FILTER

The imposed speed fluctuations to the machine cause the slip that the machine is subjected is bounded in the range [0.1, 0.0481], what imposes frequencies of the fault components bounded in the range [45.19, 49] Hz for the component $(1-2\cdot s)\cdot f_{red}$ and [51, 54.81] Hz for the component $(1+2\cdot s)\cdot f_{red}$.

The application of frequency shifting to bring the fundamental component at 0 Hz shifts the two fault components to the frequency range [1, 4.81] Hz. The approximations necessary for the extraction of the fault component are la a_9 and a_{12} that allow the extraction of the frequency band [0.61, 4.88] Hz

$$nC = \text{int}\left[\frac{\log\left(\frac{5000}{4.85}\right)}{\log(2)} - 1\right] = 9 \tag{168}$$

$$nNC = \text{int}\left[\frac{\log\left(\frac{5000}{1}\right)}{\log(2)}\right] = 12 \tag{169}$$

The results when the machine operates in motor mode are similar to those already mentioned when the machine operates in generator mode.

Fig. 101 shows the depiction of the instantaneous frequency for a machine with an increase of the resistance in one of the rotor phases of 42%. The fact that the instantaneous frequency overlaps the theoretical pattern indicates that the computed energy is due to the machine is affected by rotor asymmetry and if this value exceeds the preset threshold value established to consider the machine as in faulty state, the machine will be diagnosed as in faulty state.

Fig. 102 shows the evolution of the instantaneous frequency for a component of a machine in healthy state where it is shown that it does not overlap with the theoretical pattern, then the energy contained in the fault component is not due to rotor asymmetry.

Regardless of the evolution of the instantaneous frequency, it should be noticed that the value of the energy of the fault component shown in Fig. 102 is the lowest of them all, since it corresponds to the healthy machine, and therefore it would not have exceeded the energy threshold value

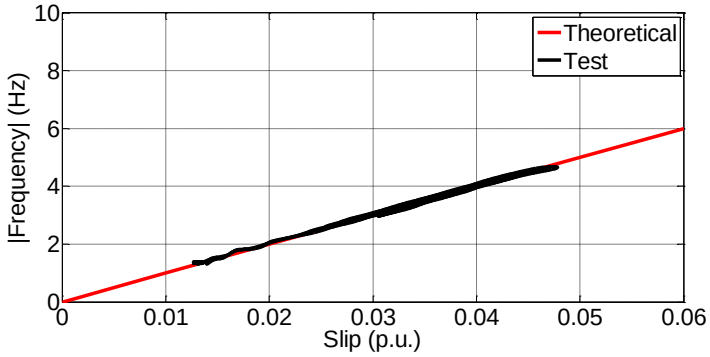

Fig. 101 Instantaneous frequency in the slip domain for the fault component (rotor asymmetry) extracted through a DWT filter. Commercial wound rotor induction machine in faulty state (R_a = 0.14 Ω), A3 test. Motor mode.

making unnecessary to compute the evolution of the instantaneous frequency.

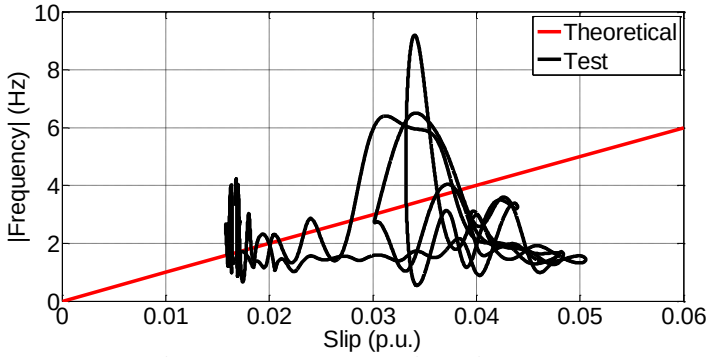

Fig. 102 Instantaneous frequency in the slip domain for the fault component (rotor asymmetry) extracted through a DWT filter. Commercial wound rotor induction machine in healthy state, healthy test. Motor mode.

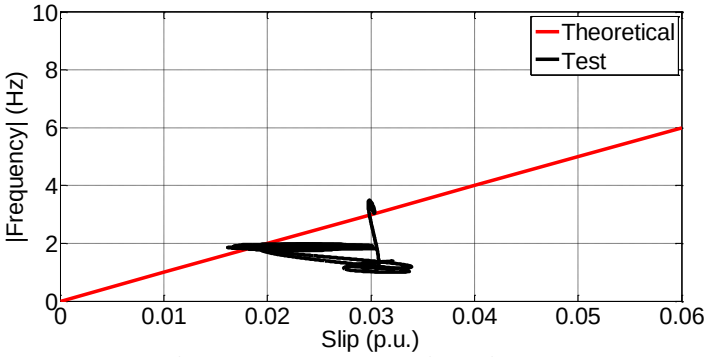

Fig. 103 Instantaneous frequency in the slip domain for the fault component (rotor asymmetry) extracted through a DWT filter. Commercial wound rotor induction machine in healthy state, AA test (oscillating speed fluctuations). Motor mode.

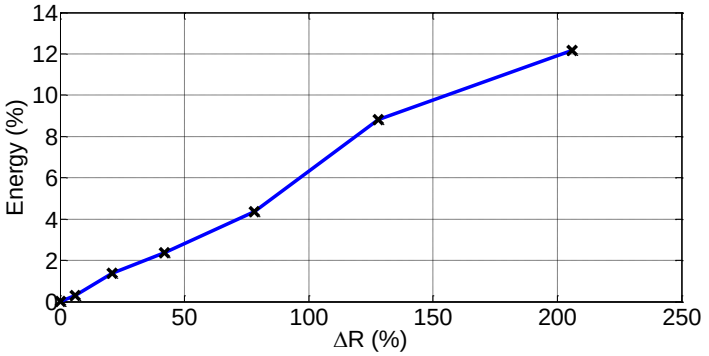

Fig. 104 Evolution of the energy of the rotor asymmetry fault component function of the increase of the fault resistance in the rotor winding.

Finally, Fig. 103 shows the evolution of the instantaneous frequency for the oscillating speed fluctuation. The use of the instantaneous frequency correctly discriminates the state of the machine since even though the energy of the frequency band is high, Fig. 103 shows that the instantaneous frequency of the fault component does not follow the theoretical pattern, indicating that the increase in energy is not due to a rotor asymmetry and therefore the machine is in a healthy state.

The numerical result of the eight tests is shown in Table 22, where it can be seen that the similitude coefficient value is low for the two tests in which the machine is in healthy state (test 'healthy' and 'AA') whereas it takes values close to 1 for test where there was a rotor asymmetry, thereby allowing the correct diagnosis of the rotor asymmetry once a minimum energy value above which it is considered that the fault exists is established.

The evolution of energy indicator as in the previous cases is practically linear and proportional to the degree of asymmetry in the machine as shown in Fig. 104.

TABLE 22. OBJECTIVE PARAMETERS OF THE DIAGNOSIS FOR A ROTOR ASYMMETRY THROUGH THE EXTRACTION OF THE FAULT COMPONENT WITH A DWT FILTER. COMMERCIAL WOUND ROTOR INDUCTION MACHINE WORKING AS MOTOR

Test	R	ΔR	S	m	b	E_t	Computation time
	Ω	%				%	s
Theoretical				100	0		
Healthy			0.109	1.41	2.34	0.0025	0.98
A1	0.02	6	1.000	89.40	0.26	0.303	0.96
A2	0.07	21	1.000	102.15	-0.11	1.369	0.99
A3	0.14	42	1.000	90.89	0.18	2.372	0.98
A4	0.26	78	1.000	92.05	0.18	4.368	0.98
A5	0.43	128	1.000	98.40	0.06	8.821	1.00
A6	0.69	206	0.986	93.34	0.10	12.180	1.01
AA			0.326	-13.76	2.16	0.36	0.64

The linear behaviour of the energy with the degree of asymmetry is consistent with the previous results when the machine is operating on generator mode.

2.2.2.2 DIAGNOSIS BASED ON THE EXTRACTION OF THE FAULT COMPONENT THROUGH A SPECTRAL FILTER

The diagnosis of the machine working as motor through the extraction of the fault components through a spectral filter is performed by replacing the DWT filter for the extraction of the fault components with a spectral filter as it is done for the diagnosis of the machine in generator mode.

This change in the filter allows the extraction of both fault components independently (without a frequency shifting of the components) since the spectral filter allows the extraction of the frequency band [45.15, 49] Hz and [51, 54.85] Hz directly. Recall that the frequency components for the speed oscillations imposed by the non-stationary stochastic system are contained in the frequency bands [45.19, 49] and [51, 54.81] Hz respectively.

The depiction of solution when the extraction of the fault components is performed by the spectral filter is shown in Fig. 105, Fig. 106, and Fig. 107 these figures are analogues to those for the diagnosis of the machine when the extraction of the fault component is performed by a DWT filter (Fig. 101, Fig. 102 and Fig. 103).

The conclusions reached after the analysis of the eight performed tests in motor mode match those already stated for the case of the DWT filter and exposed in the previous section, Notice, again, the linear evolution of the energy of the fault component function of the degree of asymmetry that the machine is subjected Fig. 108 for the component $(1-2\cdot s)\cdot f_{red}$ and Fig. 109 for component $(1+2\cdot s)\cdot f_{red}$). In this test is also shown a lower energy for the component $(1+2\cdot s)\cdot f_{red}$ and therefore less reliable than when the diagnosis is based on this component.

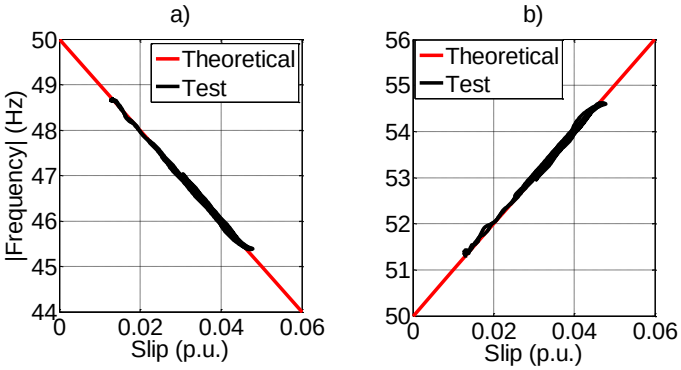

Fig. 105 Instantaneous frequency versus the slip for the extracted fault components through a spectral filter. Commercial machine in faulty state ($R_a = 0.07\ \Omega$), rotor asymmetry, A2 test. Generator mode. A) Fault component $(1-2\cdot s)\cdot f_{red}$ b) Fault Component $(1+2\cdot s)\cdot f_{red}$

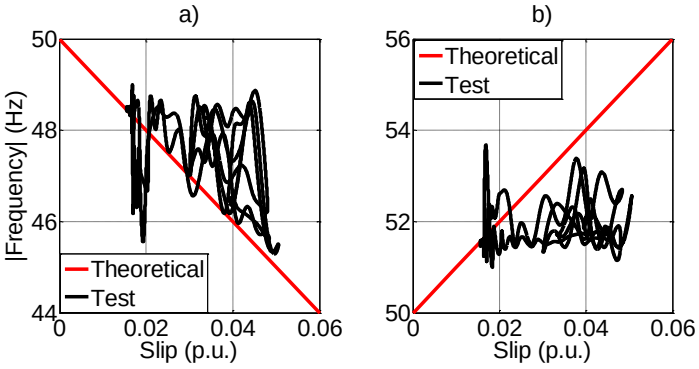

Fig. 106 Instantaneous frequency versus the slip for the extracted fault components through a spectral filter. Commercial machine in healthy state, healthy test. Generator mode. A) Fault component $(1-2\cdot s)\cdot f_{red}$ b) Fault Component $(1+2\cdot s)\cdot f_{red}$

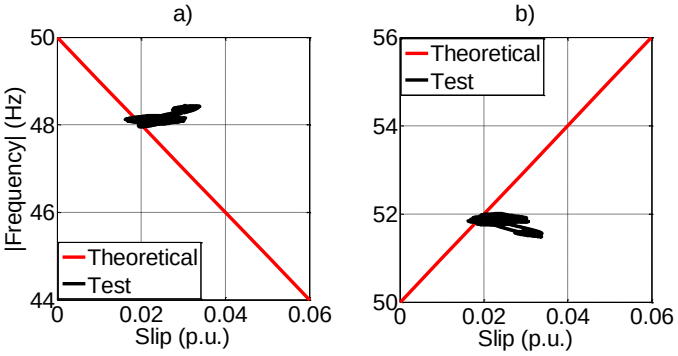

Fig. 107 Instantaneous frequency versus the slip for the extracted fault components through a spectral filter. Commercial machine in healthy state, AA test, oscillating speed fluctuations. Generator mode. A) Fault component $(1-2\cdot s)\cdot f_{red}$ b) Fault Component $(1+2\cdot s)\cdot f_{red}$

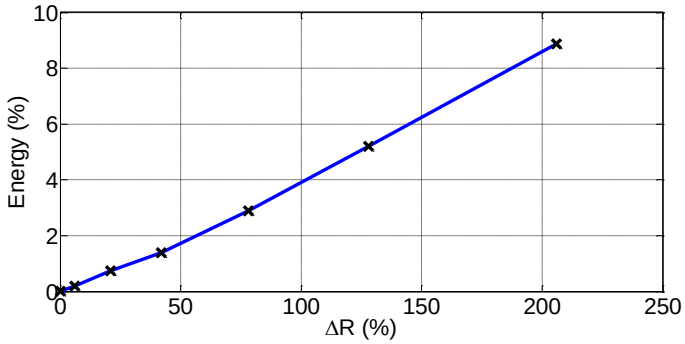

Fig. 108 Evolution of the energy of the fault component of rotor asymmetry function of the increase of the resistance in the rotor winding for the harmonic component $(1-2\cdot s)\cdot f_{red}$

TABLE 23. OBJECTIVE PARAMETERS OF THE DIAGNOSIS FOR A ROTOR ASYMMETRY THROUGH THE EXTRACTION OF THE FAULT COMPONENT $(1-2\cdot s)\cdot f_{RED}$ WITH A SPECTRAL FILTER. COMMERCIAL WOUND ROTOR INDUCTION MACHINE WORKING AS MOTOR

Test	***R***	***ΔR***	***S***	***m***	***b***	***E_f***	**Computation time**
	Ω	%				%	s
Theoretical				-100	50		
Healthy			0.254	-39.91	48.77	0.0049	0.69
A1	0.02	6	1.000	-88.92	49.72	0.185	0.65
A2	0.07	21	1.000	-102.64	50.01	0.740	0.65
A3	0.14	42	1.000	-91.57	49.81	1.392	0.68
A4	0.26	78	0.955	-92.64	49.75	2.890	0.68
A5	0.43	128	1.000	-98.83	49.86	5.198	0.67
A6	0.69	206	1.000	-92.52	49.88	8.880	0.63
AA			0.291	18.68	47.71	0.084	0.63

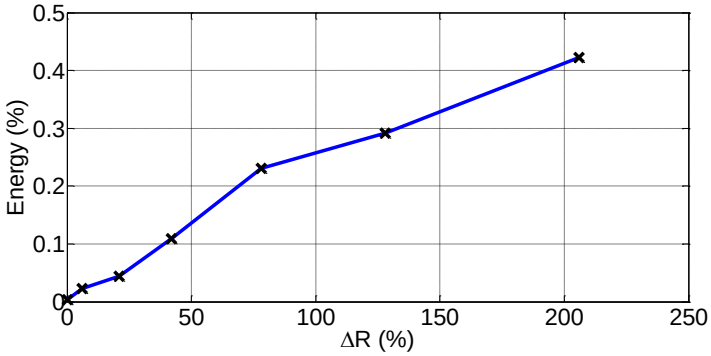

Fig. 109 Evolution of the energy of the fault component of rotor asymmetry function of the increase of the resistance in the rotor winding for the harmonic component $(1+2\cdot s)\cdot f_{red}$

TABLE 24. OBJECTIVE PARAMETERS OF THE DIAGNOSIS FOR A ROTOR ASYMMETRY THROUGH THE EXTRACTION OF THE FAULT COMPONENT $(1+2\cdot s)\cdot F_{RED}$ WITH A SPECTRAL FILTER. COMMERCIAL WOUND ROTOR INDUCTION MACHINE WORKING AS MOTOR

Test	R	ΔR	S	m	b	E_f	Computation time
	Ω	%				%	s
Theoretical				100	50		
Healthy			0.214	8.97	51.57	0.0036	0.69
A1	0.02	6	1.000	89.33	50.26	0.0225	0.67
A2	0.07	21	1.000	102.34	49.96	0.0441	0.67
A3	0.14	42	1.000	89.57	50.19	0.1089	0.61
A4	0.26	78	0.889	92.64	50.28	0.2304	0.68
A5	0.43	128	1.000	97.90	50.18	0.2916	0.6
A6	0.69	206	1.000	93.74	50.09	0.4225	0.63
AA			0.277	-20.61	52.30	0.0576	0.65

Additionally, there is seen a reduction in the computation time compared with the time required to perform the diagnosis with DWT filters despite it is provided more information on the performed diagnosis.

3 HIGH ORDER FAULT COMPONENTS

In some cases due to the particular conditions of operation of induction machines, the diagnosis in the spectral region where the main fault components evolve cannot be performed, due to contamination caused by the fundamental current component or other phenomena.

When such a situation occurs, those methodologies based on the analysis of the main fault components are disabled.

To avoid this inconvenience and/or to reaffirm the diagnosis, in this section the proposed methodology for the diagnosis of rotor asymmetries through the main fault component, is adapted to carry out the same diagnosis on the high order fault components associated with the components $(5-6\cdot s)\cdot f_{red}$ and $(7-6\cdot s)\cdot f_{red}$.

The adaptation of the already introduced methodology for the diagnosis of machines through the higher-order components is simple. Despite this and due to the differences found between the diagnostic process through the main and the high order components, it is developed again the implementation of the diagnostic method in detail for the extraction of the high order fault components associated with the component $(5-6\cdot s)\cdot f_{red}$.

After application of the methodology to the component $(5-6\cdot s)\cdot f_{red}$ the methodology is applied to the diagnosis of a machine through the high order fault components whose frequency is $(7-6\cdot s)\cdot f_{red}$.

The diagnosis of the electric machine through the high order components is performed on the universal machine working as generator. The speed and current waves are the same than in the section 2.1. of this chapter.

3.1 FAULT COMPONENTS OF ORDER (5-6·s)·FRED

The high order fault harmonic of rotor asymmetry associated with the frequency component $(5-6\cdot s)\cdot f_{red}$ are governed by the equations (Chapter III):

$$\begin{aligned} f_{(5-4\cdot s)\cdot f_{red}} &= (5-4\cdot s)\cdot f_{red} \\ f_{(5-8\cdot s)\cdot f_{red}} &= (5-8\cdot s)\cdot f_{red} \end{aligned} \tag{170}$$

The main characteristic of these two components is that they are symmetrical respect to the component $(5-6\cdot s)\cdot f_{red}$ at a distance of $2\cdot s\cdot f_{red}$ at any instant.

The extraction of both fault components is performed through filters (DWT, and spectral WP) used for the extraction of the main fault components.

3.1.1 DIAGNOSIS BASED ON THE EXTRACTION OF THE FAULT COMPONENTS THROUGH A DWT FILTER

The diagnostic process through the higher order components starts from the same signals -speed (Fig. 66.a) and current (Fig. 66.b)- for the diagnosis through the main fault components.

However in this section, there will not be extracted the components $(1-2\cdot s)\cdot f_{red}$ and $(1+2\cdot s)\cdot f_{red}$, but the goal is the extraction of the fault components $(5-4\cdot s)\cdot f_{red}$ and $(5-8\cdot s)\cdot f_{red}$.

As a consequence of the speed fluctuation that the machine is subjected during the test, the slip is bounded on the range [-0.057, -0.014], which leads to the fault components $(5-4\cdot s)\cdot f_{red}$ y $(5-8\cdot s)\cdot f_{red}$ are bounded in the frequency range [252.8, 261.4] and [255.6, 272.8] Hz respectively, whereas the healthy component $(5-6\cdot s)\cdot f_{red}$ is bounded in the range [254.2, 267.1] Hz.

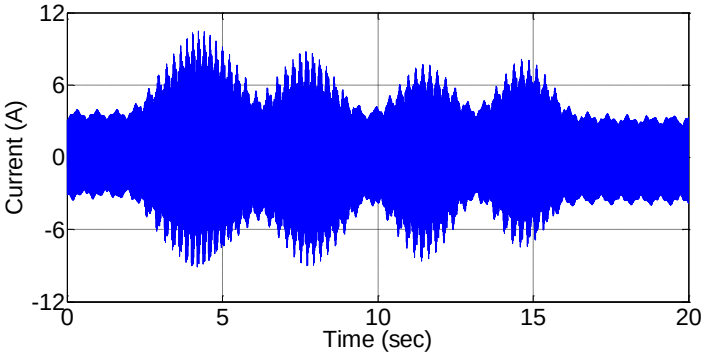

Fig. 110 Current signal after the frequency shifting of -250 Hz.

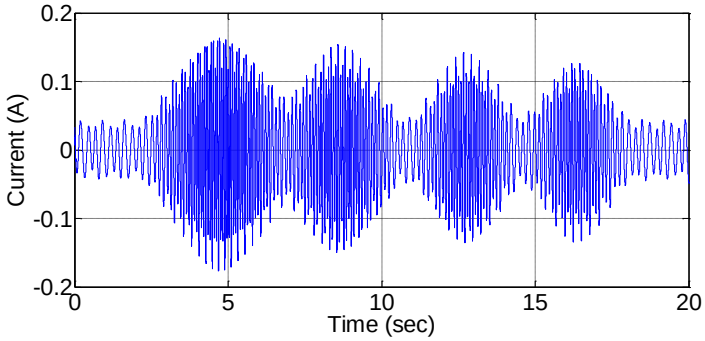

Fig. 111 Current signal that only contains the harmonic components $(5\text{-}4\cdot s)\cdot f_{red}$, $(5\text{-}6\cdot s)\cdot f_{red}$ and $(5\text{-}8\cdot s)\cdot f_{red}$

The extraction process of the fault components begins with the frequency shifting of -250 Hz of all components similar to the performed shifting for the diagnosis of the main fault components.

The frequency shifting could be carried out by Hilbert transform or the DiFT for the case of main fault components. However, for the case of high order components, the displacement can only be performed through the DiFT.

The current signal after the frequency shifting is shown in Fig. 110. The frequency shifting performed shifts the components $(5\text{-}4\cdot s)\cdot f_{red}$, $(5\text{-}6\cdot s)\cdot f_{red}$. and $(5\text{-}8\cdot s)\cdot f_{red}$ to the low frequency region, where each of them is bounded in the range [2.8, 11.4], [4.2, 17.1] and [5.6, 22.8] Hz respectively.

Recall that the purpose of the frequency shifting is the extraction of the fault components governed by $(5\text{-}4\cdot s)\cdot f_{red}$ and $(5\text{-}8\cdot s)\cdot f_{red}$, whose frequencies evolves at the ranges determined by the fluctuation of the imposed speed by the non-stationary regime. Similarly to what occurred with the main fault components and the main current component, these frequency ranges are partly overlapping with the range corresponding to the component $(5\text{-}6\cdot s)\cdot f_{red}$ that prevents the extraction of these components from a direct filtering process.

Once the frequency shifting has been performed, it is necessary the extraction of the three studied components $(5\text{-}4\cdot s)\cdot f_{red}$, $(5\text{-}6\cdot s)\cdot f_{red}$. and $(5\text{-}8\cdot s)\cdot f_{red}$ from the other current components. This action is conducted by a DWT filter containing the minimum and maximum frequency of the three studied components. The adequate approximations are the a_6 and a_{10}, since they allow the extraction of the frequency range [2.44, 39.06] Hz

$$nC = \text{int}\left[\frac{\log\frac{f_s}{f_2}}{\log(2)} - 1\right] = \text{int}\left[\frac{\log\frac{5000}{22.8}}{\log(2)} - 1\right] = 6 \qquad (171)$$

$$nNC = \text{int}\left[\frac{\log\frac{f_s}{f_1}}{\log(2)}\right] = \text{int}\left[\frac{\log\frac{5000}{2.8}}{\log(2)}\right] = 10 \qquad (172)$$

The signal extracted from the filter stage is shown in Fig. 111, signal that only contains the harmonic components $(5\text{-}4\cdot s)\cdot f_{red}$, $(5\text{-}6\cdot s)\cdot f_{red}$ and $(5\text{-}8\cdot s)\cdot f_{red}$.

At this point it has been succeeded in the extraction of the three studied components $(5\text{-}4\cdot s)\cdot f_{red}$, $(5\text{-}6\cdot s)\cdot f_{red,}$ and $(5\text{-}8\cdot s)\cdot f_{red}$, from the other current components. The problem that arises is that the component $(5\text{-}6\cdot s)\cdot f_{red}$ is present both when the machine is in healthy state and when it is in faulty state, being the predominant component in the range of extracted frequencies.

This fact far from being a drawback, allows the extraction of the fault components through the Hilbert Transform.

The application of the Hilbert Transform shifts all components of a signal the value of the predominant frequency of the wave at each instant, which applied to the studied wave will cause a shift in the frequency equal to $(5\text{-}6\cdot s)\cdot f_{red}$, fixing the component $(5\text{-}6\cdot s)\cdot f_{red}$ at 0 Hz and the associated fault components, $(5\text{-}4\cdot s)\cdot f_{red}$ and $(5\text{-}8\cdot s)\cdot f_{red}$, at a distance $2\cdot s\cdot f_{red}$ Hz each instant, that is, the components $(5\text{-}4\cdot s)\cdot f_{red}$ and $(5\text{-}8\cdot s)\cdot f_{red}$ will be bounded on the frequency range [1.4, 5.7] Hz.

The implementation of the Hilbert transform to the signal of Fig. 111 is shown in Fig. 112, which has a high similarity to Fig. 68, since that signal is the equivalent to the signal for the diagnostic process of the main fault components for the diagnosis of high order components.

From this step, the diagnostic process is analogue to the process already discussed for the diagnosis of the main fault components.

The extraction of the fault components $(5\text{-}4\cdot s)\cdot f_{red}$ and $(5\text{-}8\cdot s)\cdot f_{red}$ whose frequency evolution coincides after the applied transformations will be

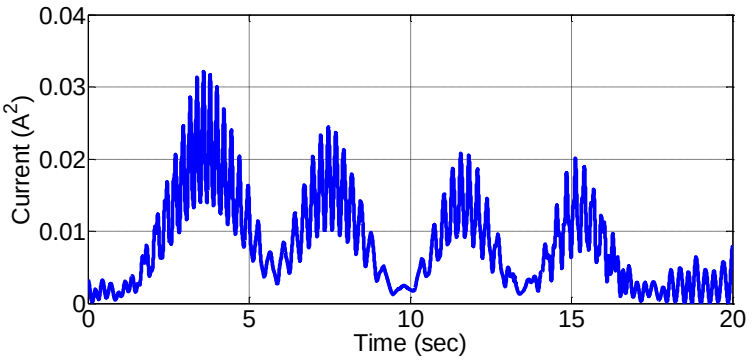

Fig. 112 Square analytical signal after the implementation of the Hilbert Transform to the signal of Fig. 111.

performed through a DWT filter whose approximations will be a_8 and a_{11} since they cover the frequency range [1.22, 9.76] Hz

$$nC = \text{int}\left[\frac{\log\frac{f_s}{f_2}}{\log(2)} - 1\right] = \text{int}\left[\frac{\log\frac{5000}{5.7}}{\log(2)} - 1\right] = 8 \tag{173}$$

$$nNC = \text{int}\left[\frac{\log\frac{f_s}{f_1}}{\log(2)}\right] = \text{int}\left[\frac{\log\frac{5000}{1.4}}{\log(2)}\right] = 11 \tag{174}$$

Fig. 113 shows the evolution in the time domain of the approximation a_8, whereas in Fig. 114 is shown the evolution of the component a_{11}. The difference between the two approaches, a_8-a_{11}, allows the extraction of the frequency range in which is bounded the sought fault component sought, component that is shown in Fig. 115.

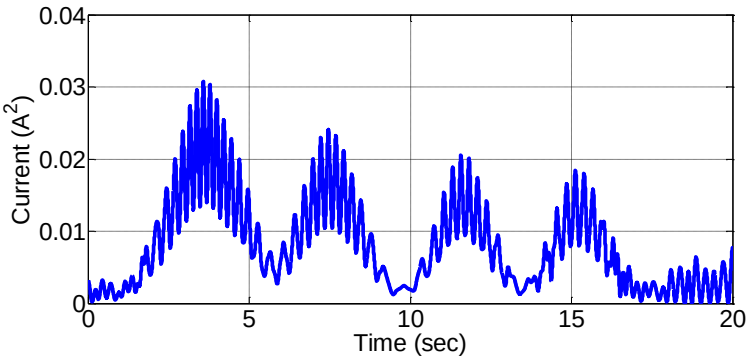

Fig. 113 Evolution of the approximation a_8 in the time domain.

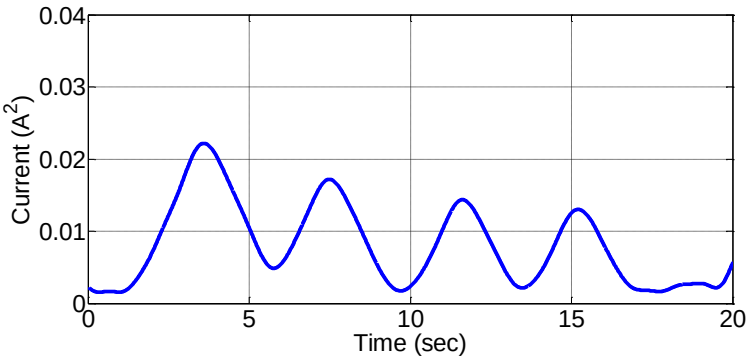

Fig. 114 Evolution of the component a_{11} in the time domain.

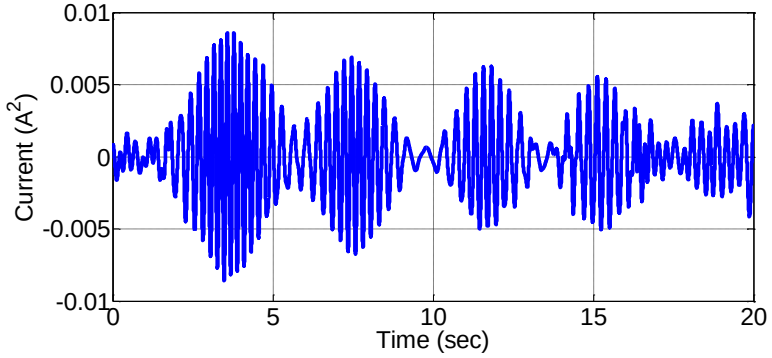

Fig. 115 High order fault component of rotor asymmetry extracted through a DWT filter (a_8-a_{11}) associated with the harmonic frequency component $(5\text{-}4\cdot s)\cdot f_{red}$ and $(5\text{-}8\cdot s)\cdot f_{red}$. Universal machine with rotor asymmetry (R_a = 4.15 Ω). Generator mode.

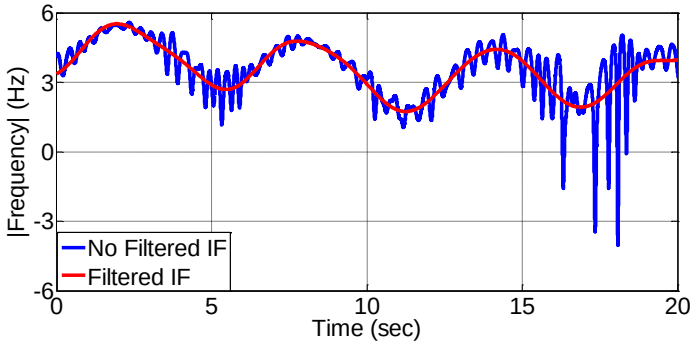

Fig. 116 Evolution of the instantaneous frequency in the time domain for the high order fault components associated with the components $(5\text{-}4\cdot s)\cdot f_{red}$ and $(5\text{-}8\cdot s)\cdot f_{red}$ in the universal machine working as generator with a rotor asymmetry.

As in the case of the main fault components, it is computed the energy of the extracted fault component and if it exceeds the preset energy threshold that determines the faulty state, the computation of the instantaneous frequency to determine the origin of the fault component is carried out.

The computation of the instantaneous frequency is a process that results in a wave of high frequency noise (Fig. 116, blue line) is therefore necessary a filtering stage, with a low pass filter, to remove unwanted high order components that results in an smoother instantaneous frequency (Fig. 116, red line).

The depiction of the instantaneous frequency in the slip domain is shown Fig. 117 for the case of a machine with rotor (R_a = 4.15 Ω) in generator mode. In Fig. 118 depicts the case of a healthy machine and finally Fig. 119 shows the instantaneous frequency in the case of healthy machine under oscillating speeds.

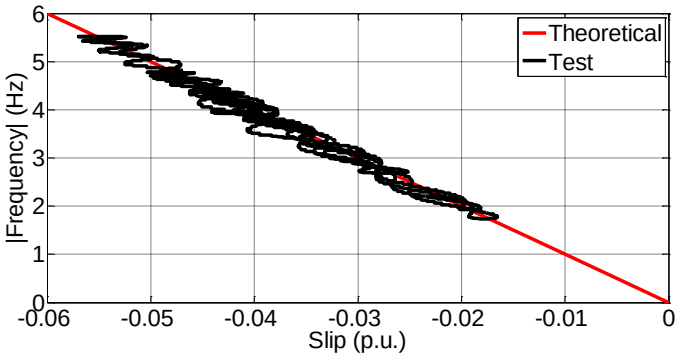

Fig. 117 Evolution of the instantaneous frequency in the slip domain for the rotor fault component associated with the components $(5\text{-}4\cdot s)\cdot f_{red}$ and $(5\text{-}8\cdot s)\cdot f_{red}$ for a machine in rotor asymmetry state ($R_a = 4.15\ \Omega$) working as generator. A9 test.

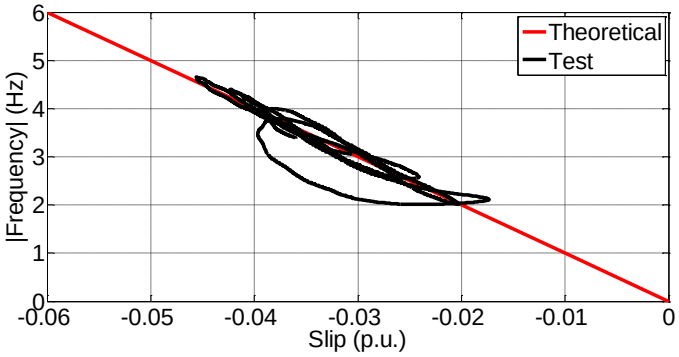

Fig. 118 Evolution of the instantaneous frequency in the slip domain for the rotor fault component associated with the components $(5\text{-}4\cdot s)\cdot f_{red}$ and $(5\text{-}8\cdot s)\cdot f_{red}$ for a machine in healthy state working as generator. Healthy test.

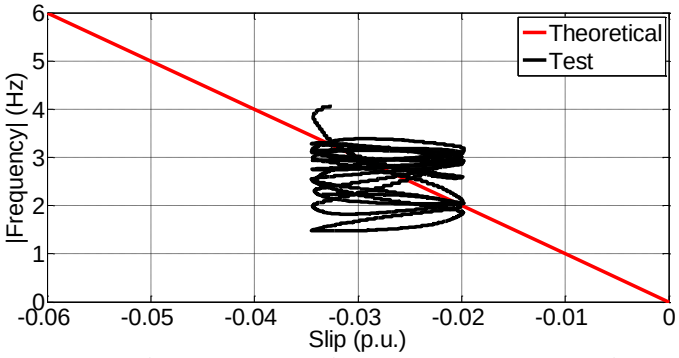

Fig. 119 Evolution of the instantaneous frequency in the slip domain for the rotor fault component associated with the components $(5\text{-}4\cdot s)\cdot f_{red}$ and $(5\text{-}8\cdot s)\cdot f_{red}$ for a machine in healthy state working as generator. Healthy machine under oscillating speed fluctuations. AA test

TABLE 25. OBJECTIVE PARAMETERS OF DIAGNOSIS FOR A ROTOR ASYMMETRY THROUGH THE EXTRACTION OF THE FAULT COMPONENT ASSOCIATED WITH $(5-6\cdot s)\cdot f_{RED}$ WITH A DWT FILTER. UNIVERSAL MACHINE SET AS WOUND ROTOR MACHINE WORKING AS GENERATOR

Test	R	ΔR	S	m	b	E_t	Computation time
	Ω	%				%	s
Theoretical				-100	0		
Healthy			0.858	-97.05	0.04	$1.48\cdot10^{-7}$	0.45
A1	0.07	1.62	0.523	-8.42	3.17	$7.39\cdot10^{-7}$	0.45
A2	0.14	3.29	0.432	-37.28	2.36	$1.85\cdot10^{-6}$	0.44
A3	0.26	5.85	0.437	-27.40	2.61	$5.94\cdot10^{-7}$	0.46
A4	0.43	9.67	0.695	-68.36	1.18	$8.16\cdot10^{-7}$	0.45
A5	0.69	15.73	1.000	-100.11	-0.03	$2.87\cdot10^{-6}$	0.44
A6	1.10	25.11	0.710	-78.35	0.80	$9.09\cdot10^{-6}$	0.43
A7	1.73	39.38	0.989	-98.63	0.05	$2.15\cdot10^{-5}$	0.45
A8	2.64	60.03	0.988	-99.07	0.03	$4.60\cdot10^{-5}$	0.45
A9	4.15	94.33	0.951	-97.58	0.04	$9.93\cdot10^{-5}$	0.43
AA			0.348	-7.39	2.46	$6.09\cdot10^{-6}$	0.43

The considerations to the results (Table 25) are equivalent to those already discussed for the diagnosis of the machine through the main fault components.

On the other hand, the depiction of energy function of the degree of rotor asymmetry of the machine (Fig. 120) still evolves linearly and directly proportional to the degree of rotor asymmetry, similar to the result when the diagnosis is performed with the main fault components.

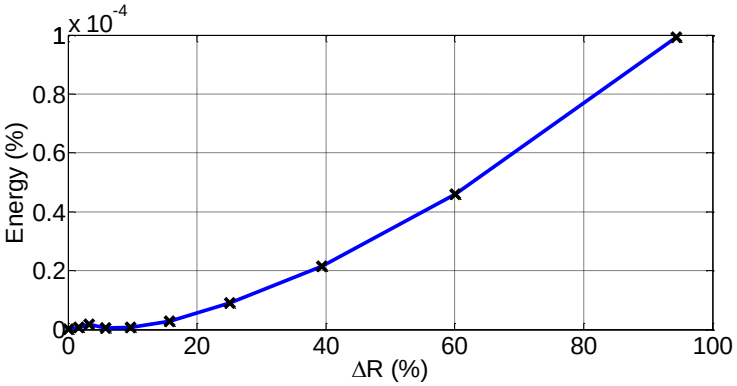

Fig. 120 Evolution of the energy for the rotor fault component function of the increase of the resistance in the rotor winding for the fault components associated with the harmonics $(5-4\cdot s)\cdot f_{red}$ and $(5-8\cdot s)\cdot f_{red}$

This fact confirms that the diagnosis performed with the high order components associated with the component $(5\text{-}6\cdot s)\cdot f_{red}$ is correct and consistent enough to be performed without fearing of inconsistent results due to the small amount of energy associated with the high order components.

3.1.2 DIAGNOSIS BASED ON THE EXTRACTION OF THE FAULT COMPONENTS THROUGH A WP FILTER

In this case, the use of WP filters for direct extraction of the fault components is not possible since the evolution of the component $(5\text{-}6\cdot s)\cdot f_{red}$ overlaps with the evolution of the components $(5\text{-}4\cdot s)\cdot f_{red}$ and $(5\text{-}8\cdot s)\cdot f_{red}$.

The only way to perform the extraction of these components is to shift them to the low frequency region and applying the Hilbert transform.

The performance of these actions shifts the faults components close to frequencies whose values is 0 Hz where the response of the WP and DWT filters is identical what causes no differences between the application either methodology.

3.1.3 DIAGNOSIS BASED ON THE EXTRACTION OF THE FAULT COMPONENTS THROUGH A SPECTRAL FILTER

The extraction of the fault components associated with the component $(5\text{-}6\cdot s)\cdot f_{red}$ through the spectral filtering follows the same steps as those for extraction of the fault components through DWT filter where that filtering process is replaced by a spectral filter.

The main advantage of the spectral filter is the reduction of extraction bands compared to those used with the DWT filter, improving the accuracy in the computation.

If the extracted band with DWT filter are analysed, it comes that the first band extracted, the one that extracts the components of higher order with respect to other signal components, is [2.44, 39.06] Hz whereas the spectral filter achieves a band of [2.8, 22.8] Hz that is much narrower than the one of the DWT filter.

Besides in the second filtering, the one that extracts the components $(5\text{-}4\cdot s)\cdot f_{red}$ and $(5\text{-}8\cdot s)\cdot f_{red}$ from the component $(5\text{-}6\cdot s)\cdot f_{red}$, the DWT filter needs to extract the band [1.22, 9.76] Hz whereas the spectral filter only requires [1.4, 5.7] Hz improving the accuracy again.

The rest of the needed computations for the diagnosis are equal to those already shown in the previous section.

Fig. 121, Fig. 122 and Fig. 123show the results with the spectral filter that correspond to the same tests for the case analysed with the DWT filter whose depiction is shown in Fig. 117, Fig. 118and Fig. 119

The numerical results are shown in Table 26. The considerations made for the previous section also apply to this section.

Another advantage of the spectral filters compared with the DWT filters is the reduction of required time to perform the diagnostic process, since the required time for spectral filters is 0.32 seconds whether for the DWT filters the diagnosis requires 0.42 seconds.

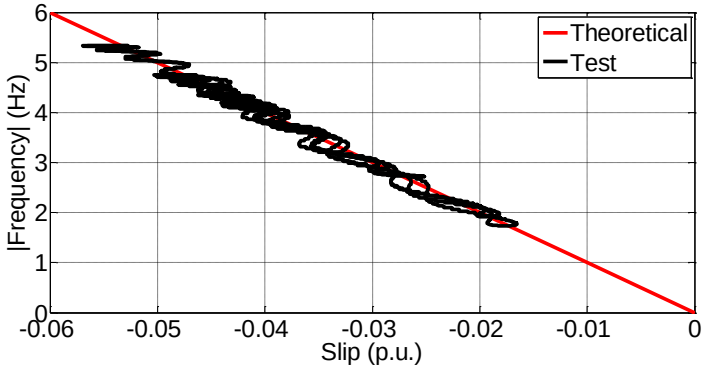

Fig. 121 Evolution of the instantaneous frequency in the slip domain for the rotor asymmetry fault component associated with $(5\text{-}4\cdot s)\cdot f_{red}$ and $(5\text{-}8\cdot s)\cdot f_{red}$ for a machine with rotor asymmetry (R_a = 4.15 Ω) working as generator extracted through a spectral filter. A9 test.

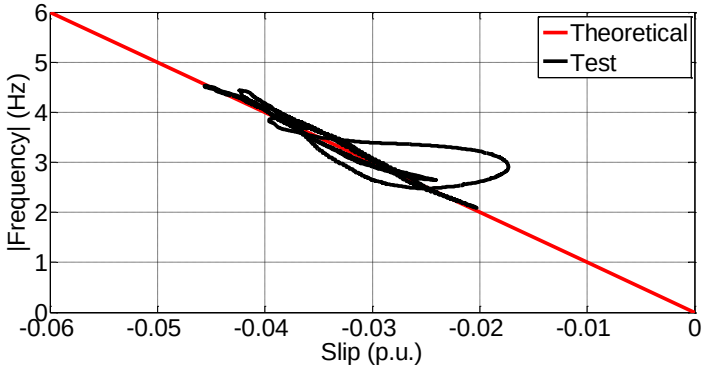

Fig. 122 Evolution of the instantaneous frequency in the slip domain for the rotor asymmetry fault component associated with $(5\text{-}4\cdot s)\cdot f_{red}$ and $(5\text{-}8\cdot s)\cdot f_{red}$ for a machine in healthy state extracted through a spectral filter. Healthy test.

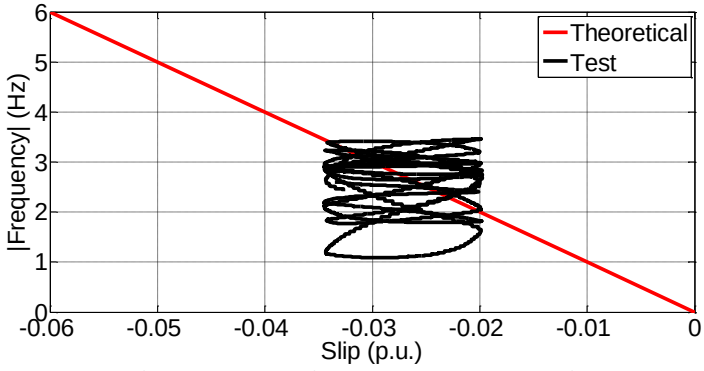

Fig. 123 Evolution of the instantaneous frequency in the slip domain for the rotor asymmetry fault component associated with $(5\text{-}4\cdot s)\cdot f_{red}$ and $(5\text{-}8\cdot s)\cdot f_{red}$ for a machine in healthy state extracted through a spectral filter. AA test.

TABLE 26. OBJECTIVE PARAMETERS FOR THE DIAGNOSIS OF A ROTOR ASYMMETRY THROUGH THE EXTRACTION OF THE FAULT COMPONENT ASSOCIATED WITH $(5-4\cdot s)\cdot F_{RED}$ AND $(5-8\cdot s)\cdot F_{RED}$ WITH A SPECTRAL FILTER. UNIVERSAL MACHINE AS WOUND ROTOR MACHINE WORKING AS GENERATOR

Test	***R***	***ΔR***	***S***	***m***	***b***	E_t	**Computation time**
	Ω	%				%	s
Theoretical				-100	0		
Healthy			0.863	-78.70	0.82	$1.34\cdot10^{-7}$	0.32
A1	0.07	1.62	0.465	-49.78	1.50	$4.58\cdot10^{-8}$	0.29
A2	0.14	3.29	0.510	-64.61	1.12	$8.29\cdot10^{-8}$	0.30
A3	0.26	5.85	0.660	-74.06	0.83	$2.58\cdot10^{-7}$	0.31
A4	0.43	9.67	1.000	-99.12	0.02	$7.81\cdot10^{-7}$	0.30
A5	0.69	15.73	1.000	-99.96	-0.02	$2.59\cdot10^{-6}$	0.30
A6	1.10	25.11	1.000	-99.91	-0.01	$7.76\cdot10^{-6}$	0.31
A7	1.73	39.38	1.000	-98.63	0.06	$2.01\cdot10^{-5}$	0.31
A8	2.64	60.03	1.000	-98.45	0.06	$4.44\cdot10^{-5}$	0.27
A9	4.15	94.33	0.984	-98.02	0.04	$9.14\cdot10^{-5}$	0.31
AA			0.293	1.63	2.64	$1.85\cdot10^{-6}$	0.29

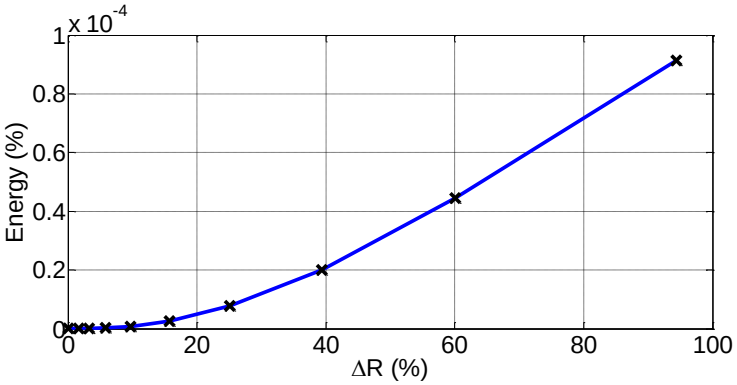

Fig. 124 Evolution of the energy for the rotor fault component function of the increase of the resistance in the rotor winding for the fault components associated with the harmonics $(5-4\cdot s)\cdot f_{red}$ and $(5-8\cdot s)\cdot f_{red}$

3.2 HIGH ORDER FAULT COMPONENT OF ORDER (7-6·s)·FRED

The high order fault harmonics of rotor asymmetry associated with the frequency component $(7\text{-}6\cdot s)\cdot f_{red}$ are governed by the equations (Chapter III):

$$\begin{aligned} f_{(7-4\cdot s)\cdot f_{red}} &= (7-4\cdot s)\cdot f_{red} \\ f_{(7-8\cdot s)\cdot f_{red}} &= (7-8\cdot s)\cdot f_{red} \end{aligned} \quad (175)$$

The characteristics of both components are analogues to the equivalent fault components for the diagnosis of the machine through the high order components associated with the component $(5\text{-}6\cdot s)\cdot f_{red}$ except that the initial frequency shifting must be -350 Hz.

Since the extraction of the fault components is identical to that performed in the previous subsection, the following sections only shown the results of the diagnostic process through the fault components associated with component $(7\text{-}6\cdot s)\cdot f_{red}$.

3.2.1 DIAGNOSIS BASED ON THE EXTRACTION OF THE FAULT COMPONENTS THROUGH A DWT FILTER

The diagnostic process begins again with the signals -speed (Fig. 66.a) and current (Fig. 67)- used to carry out the diagnosis through the main fault components and the associated components with the $(5\text{-}6\cdot s)\cdot f_{red}$ component.

Due to the oscillations in speed that the machine is subjected, the slip is bounded in the range [-0.057, -0.014],that causes that the fault components $(7\text{-}4\cdot s)\cdot f_{red}$ and $(7\text{-}8\cdot s)\cdot f_{red}$ are bounded in the frequency range [352.8, 361.4] and [355.6, 372.8] Hz respectively, whereas the healthy component $(7\text{-}6\cdot s)\cdot f_{red}$ is bounded in the range [354.2, 367.1] Hz.

The extraction process begins with shifting -350 Hz all components of the acquired current signal, what shifts the components under consideration $(7\text{-}4\cdot s)\cdot f_{red}$, $(7\text{-}6\cdot s)\cdot f_{red}$. and $(7\text{-}8\cdot s)\cdot f_{red}$ to the low frequency region where each of them is bounded in the range [2.8, 11.4], [4.2, 17.1] and [5.6, 22.8] Hz respectively, frequency ranges that match with those obtained for the components $(5\text{-}4\cdot s)\cdot f_{red}$, $(5\text{-}6\cdot s)\cdot f_{red}$. and $(5\text{-}8\cdot s)\cdot f_{red}$, therefore that entails that the diagnostic process is exactly the same from this step.

To avoid unnecessary repetitions, there are only shown the results for the case of the diagnosis of the machine through the fault components associated with $(7\text{-}6\cdot s)\cdot f_{red}$.

Fig. 125 shows the result of the diagnosis when the machine has a rotor asymmetry caused by adding in series a resistance whose value is R_a = 4.15 Ω through the fault components associated with $(7\text{-}6\cdot s)\cdot f_{red}$ component. This result is similar to that achieved with the components associated with components $5\text{-}6\cdot s)\cdot f_{red}$ that is shown in Fig. 117.

Fig. 126 shows the result of the diagnosis of the healthy machine through the components associated with the component $(7\text{-}6\cdot s)\cdot f_{red}$ where it is shown that the computed frequency does not match the theoretical frequency pattern. This result is similar to that shown in Fig. 118 for the components of order $(5\text{-}6\cdot s)\cdot f_{red}$.

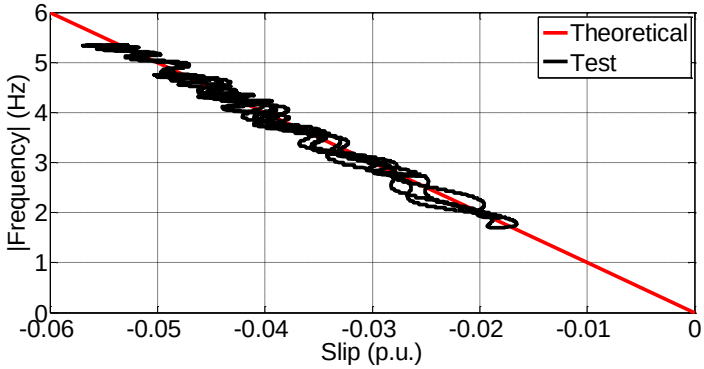

Fig. 125 Evolution of the instantaneous frequency in the slip domain for the rotor asymmetry fault component associated with $(7\text{-}4\cdot s)\cdot f_{red}$ and $(7\text{-}8\cdot s)\cdot f_{red}$ for a machine with rotor asymmetry (R_a = 4.15 Ω) working as generator extracted through a DWT filter. A9 test

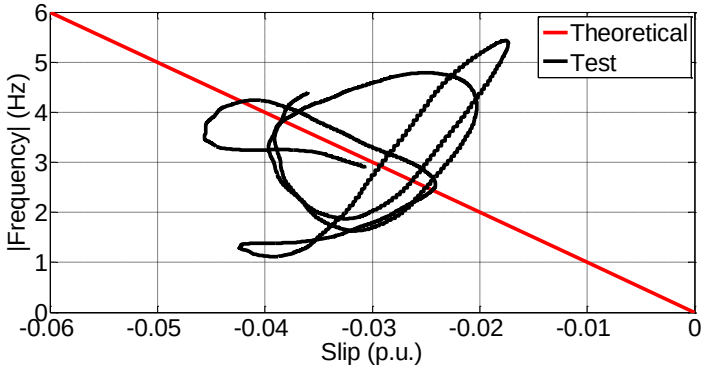

Fig. 126 Evolution of the instantaneous frequency in the slip domain for the rotor asymmetry fault component associated with $(7\text{-}4\cdot s)\cdot f_{red}$ and $(7\text{-}8\cdot s)\cdot f_{red}$ for a machine in healthy state extracted through a DWT filter. Healthy test.

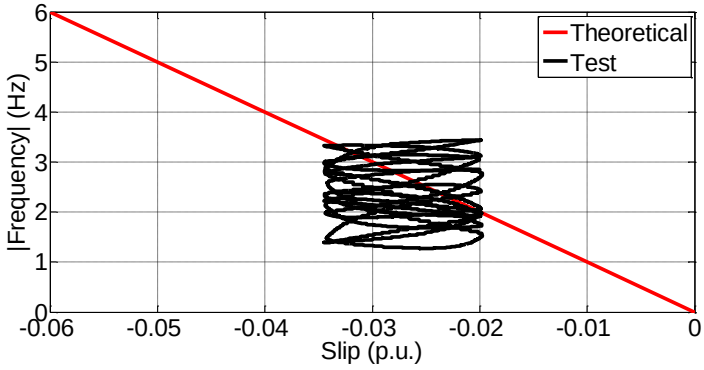

Fig. 127 Evolution of the instantaneous frequency in the slip domain for the rotor asymmetry fault component associated with $7\text{-}4\cdot s)\cdot f_{red}$ and $(7\text{-}8\cdot s)\cdot f_{red}$ for a machine in healthy state extracted through a DWT filter. AA test

Finally, Fig. 127 shows the evolution of the instantaneous frequency for the machine when it is subjected to high speed oscillations associated with the component $(7\text{-}6\cdot s)\cdot f_{red}$ after the diagnostic process. The corresponding result is shown in Fig. 119.

The considerations discussed for the components $(5\text{-}6\cdot s)\cdot f_{red}$ are valid for components of order $(7\text{-}6\cdot s)\cdot f_{red}$ due to its complete analogy.

TABLE 27. OBJECTIVE PARAMETERS FOR THE DIAGNOSIS OF A ROTOR ASYMMETRY THROUGH THE EXTRACTION OF THE FAULT COMPONENT ASSOCIATED WITH $(7\text{-}4\cdot s)\cdot F_{RED}$ AND $(7\text{-}8\cdot s)\cdot F_{RED}$ WITH A DWT FILTER. UNIVERSAL MACHINE AS WOUND ROTOR MACHINE WORKING AS GENERATOR

Test	R	ΔR	S	m	b	E_t	Computation time
	Ω	%				%	s
Healthy			0.165	52.20	4.79	$7.69\cdot10^{-6}$	0.47
A1	0.07	1.62	0.337	-24.75	2.60	$7.11\cdot10^{-6}$	0.44
A2	0.14	3.29	0.429	-23.41	2.54	$2.35\cdot10^{-6}$	0.49
A3	0.26	5.85	0.538	-8.40	3.36	$1.30\cdot10^{-5}$	0.45
A4	0.43	9.67	0.809	-40.33	2.19	$7.73\cdot10^{-6}$	0.45
A5	0.69	15.73	0.885	-81.90	0.66	$7.44\cdot10^{-6}$	0.44
A6	1.10	25.11	0.714	-87.29	0.54	$1.28\cdot10^{-5}$	0.49
A7	1.73	39.38	0.844	-96.98	0.11	$2.29\cdot10^{-5}$	0.45
A8	2.64	60.03	0.775	-85.74	0.59	$4.55\cdot10^{-5}$	0.49
A9	4.15	94.33	0.954	-97.98	0.04	$6.90\cdot10^{-5}$	0.46
AA			0.275	-1.71	2.35	$1.94\cdot10^{-6}$	0.43

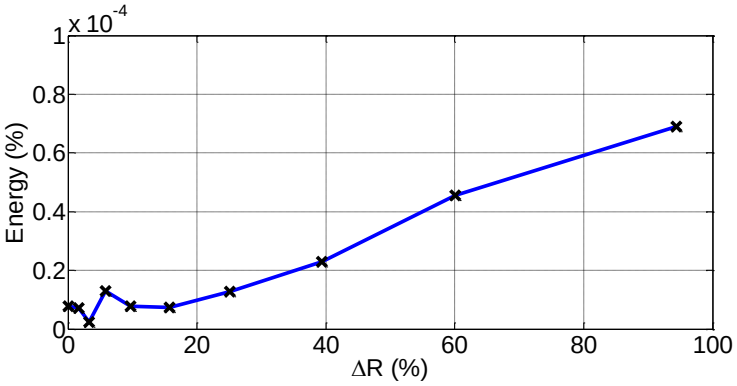

Fig. 128 Evolution of the energy for the rotor fault component function of the increase of the resistance in the rotor winding for the fault components associated with the harmonics $(7\text{-}4\cdot s)\cdot f_{red}$ and $(7\text{-}8\cdot s)\cdot f_{red}$ extracted with a DWT filter.

The numerical results of the 11 performed tests are shown in Table 27. The conclusion drawn from the analysis is that the diagnosis of the machine through the fault components associated with the component $(7\text{-}6\cdot s)\cdot f_{red}$ is only possible if the asymmetry degree is much higher than the diagnosis performed through the main or order $(5\text{-}6\cdot s)\cdot f_{red}$ components because of the small amplitude of the fault components. The diagnosis of electrical machines through the high order components associated with the component $7\text{-}6\cdot s)\cdot f_{red}$ is possible for imbalances of 94.33% in its phases (test A9), since the rest of tests cannot achieve a correct diagnose of the machine even though the evolution of the energy component required is linear and proportional to the degree of rotor asymmetry of the machine (Fig. 128).

3.2.2 DIAGNOSIS BASED ON THE EXTRACTION OF THE FAULT COMPONENTS THROUGH A SPECTRAL FILTER

Finally, it is shown the results of the diagnosis of the electric machine through the analysis of the fault components associated with the component $(7\text{-}6\cdot s)\cdot f_{red}$ extracted with a spectral filter.

The results of the diagnosis are shown in Fig. 129, Fig. 130 and Fig. 131 whose analogue results, which were performed with DWT filters, are those shown in Fig. 125, la Fig. 126 and Fig. 127.

Moreover, the analogue results for the fault component of order $(5\text{-}6\cdot s)\cdot f_{red}$ are shown in Fig. 121, la Fig. 122 and Fig. 123.

The numerical results of the 11 performed tests show that the diagnosis of the electrical machine through the fault components associated with fault component $(7\text{-}6\cdot s)\cdot f_{red}$ through a spectral filter is as accurate and effective as the diagnosis performed with the fault components associated with the component $(5\text{-}6\cdot s)\cdot f_{red}$ since in both cases is achieved the diagnose of a rotor asymmetry of 9.67% of the rotor winding resistance and the evolution of the energy of the fault component is linear and proportional to the degree of rotor asymmetry as it is shown in Fig. 132.

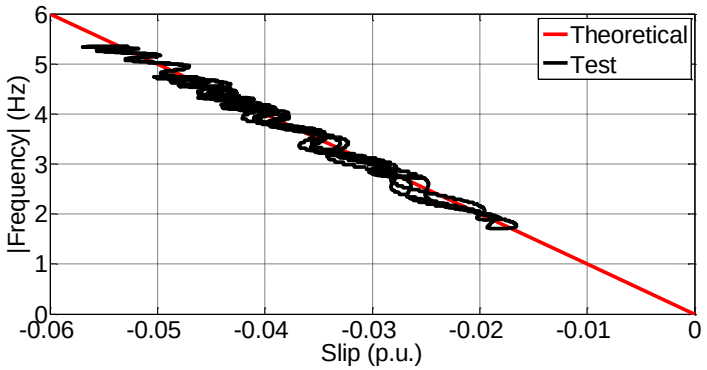

Fig. 129 Evolution of the instantaneous frequency in the slip domain for the rotor asymmetry fault component associated with $(7\text{-}4\cdot s)\cdot f_{red}$ and $(7\text{-}8\cdot s)\cdot f_{red}$ for a machine with rotor asymmetry (R_a = 4.15 Ω) working as generator extracted through a spectral filter. A9 test

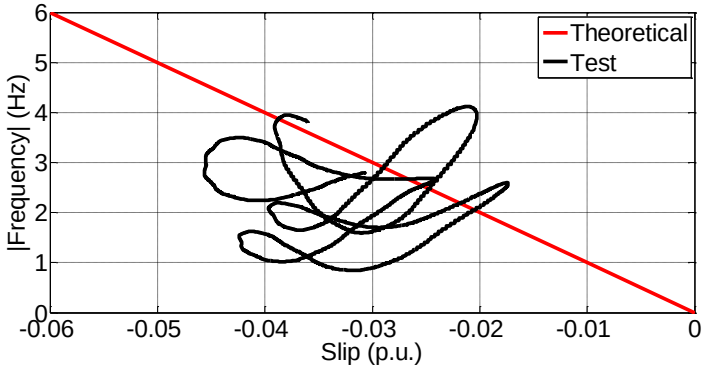

Fig. 130 Evolution of the instantaneous frequency in the slip domain for the rotor asymmetry fault component associated with $(7-4\cdot s)\cdot f_{red}$ and $(7-8\cdot s)\cdot f_{red}$ for a machine in healthy state extracted through a spectral filter. Healthy test.

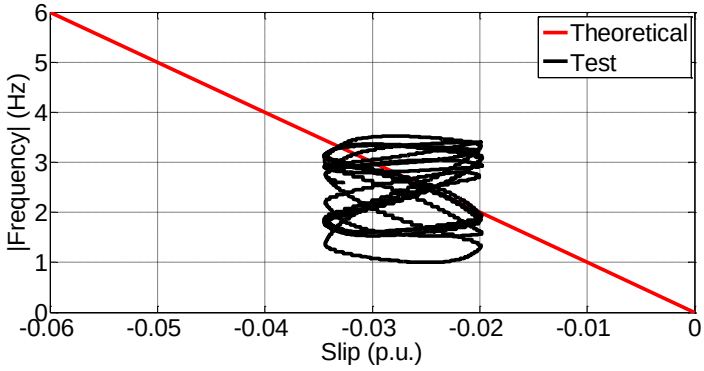

Fig. 131 Evolution of the instantaneous frequency in the slip domain for the rotor asymmetry fault component associated with $(7-4\cdot s)\cdot f_{red}$ and $(7-8\cdot s)\cdot f_{red}$ for a machine in healthy state extracted through a spectral filter. AA test.

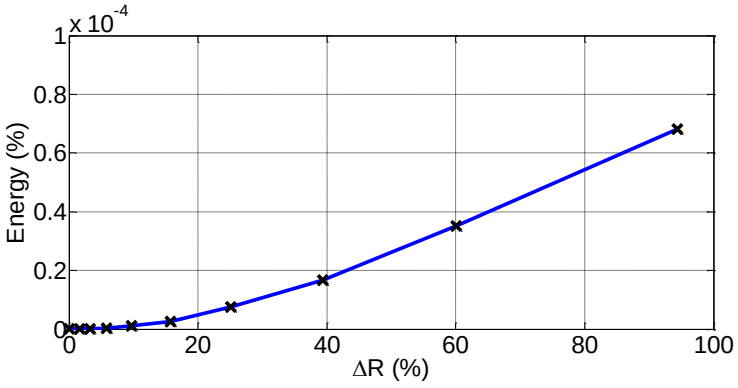

Fig. 132 Evolution of the energy for the rotor fault component function of the increase of the resistance in the rotor winding for the fault components associated with the harmonics $(7-4\cdot s)\cdot f_{red}$ and $(7-8\cdot s)\cdot f_{red}$ extracted with a spectral filter.

TABLE 28. OBJECTIVE PARAMETERS FOR THE DIAGNOSIS OF A ROTOR ASYMMETRY THROUGH THE EXTRACTION OF THE FAULT COMPONENT ASSOCIATED WITH $(7-4\cdot s)\cdot F_{RED}$ AND $(7-8\cdot s)\cdot F_{RED}$ WITH A SPECTRAL FILTER. UNIVERSAL MACHINE AS WOUND ROTOR MACHINE WORKING AS GENERATOR.

Test	R	ΔR	S	m	b	E_f	Computation time
	Ω	%				%	s
Healthy			0.147	11.44	2.70	$2.39\cdot10^{-8}$	0.28
A1	0.07	1.62	0.455	-53.65	1.56	$4.67\cdot10^{-8}$	0.28
A2	0.14	3.29	0.404	-78.19	0.55	$9.38\cdot10^{-8}$	0.30
A3	0.26	5.85	0.676	-64.49	1.22	$3.23\cdot10^{-7}$	0.32
A4	0.43	9.67	1.000	-100.30	-0.02	$1.19\cdot10^{-6}$	0.30
A5	0.69	15.73	0.997	-99.43	0.00	$2.66\cdot10^{-6}$	0.27
A6	1.10	25.11	1.000	-99.29	0.02	$7.52\cdot10^{-6}$	0.28
A7	1.73	39.38	1.000	-98.58	0.06	$1.68\cdot10^{-5}$	0.31
A8	2.64	60.03	1.000	-98.44	0.06	$3.51\cdot10^{-5}$	0.29
A9	4.15	94.33	0.971	-98.19	0.03	$6.82\cdot10^{-5}$	0.32
AA			0.287	1.85	2.56	$1.53\cdot10^{-6}$	0.29

4 SUMMARY AND CONCLUSIONS OF THE CHAPTER

In this chapter it has been validated the proposed diagnostic methodology for the detection of rotor asymmetries in induction electric machines in non-stationary stochastic regimes.

The method has been validated on two wound rotor induction machines in generator mode (universal machine) and in generator and motor mode (commercial machine).

The diagnosis was carried out through the main fault components and also with the high order fault components associated with the components $(5-6\cdot s)\cdot f_{red}$ and $(7-6\cdot s)\cdot f_{red}$.

The extraction of the fault components is carried out through three different filtering techniques: DWT, WP and spectral filtering, which is proposed in this thesis.

The extraction of the components through DWT filters has proven to give good results in the extraction of the main fault components as for the high order fault components, but with less accurate results than those obtained with spectral filters, technique that is the one that best results performs.

Despite the fact that theoretically the use of WP filters seems an ideal technique for the extraction of the fault components of rotor asymmetry, its practical application has shown that the use of WP filters should be discarded because of their complexity, high temporal and computational cost in the diagnosis of rotor asymmetries.

The computation of the instantaneous frequency has been performed using the conventional method and the Teager-Kaiser operator and there are little difference between them, then it can be concluded that the selection of

any of these two techniques for the computation of the instantaneous frequency will depend on the hardware and software available for its practical application.

The computation of the energy of the extracted fault components was performed in the time and frequency domain yielding no significant differences between them.

The diagnostic decision is made based on the analysis of the energy parameter, similitude coefficient and linear regression parameters. The use of these three parameters allows the diagnostic performance of the electric machine with a high reliability avoiding the possibility of false positives.

The global conclusions achieved in this chapter are:

- The proposed methodology in this thesis is able to diagnose the rotor asymmetry fault in electrical induction machines, regardless of its operating mode, motor or generator, in non-stationary stochastic regimes through the determination of the origin of the energy of the fault component previously extracted.
- The proposed methodology eliminates the possibility of false positives caused by phenomena that cause increases in the energy of the signal and from load or voltage fluctuations that can occur in the methods only based on the energy parameter of the fault component.
- The proposed methodology are able to perform the diagnosis of electrical machines through the analysis of the main fault components as well as the components whose order is associated with the components $(5\text{-}6\cdot s)\cdot f_{red}$ and $(7\text{-}6\cdot s)\cdot f_{red}$.
- The energy parameter of the fault component has almost a linear response versus the increase in the rotor imbalance, showing a good consistency of the methodology for the computation of the energy parameter.
- The implementation of WP filters for the extraction of the fault component is not satisfactory.
- The use of filters based on the DWT and spectral filter achieve satisfactory results in the diagnosis of the machine, being the spectral filters that require less computational cost, offering greater versatility and less complexity in their implementation.

CHAPTER X: STATOR ASYMMETRY. VALIDATION OF THE PROPOSED METHODOLOGY

1 INTRODUCTION

This chapter applies the methodology proposed in Chapter IV to the diagnosis of stator asymmetries in wound rotor induction machines working as motor or generator in stochastic regime.

The proposed method is not valid for squirrel cage rotor induction machines since it is based on the extraction of the fault components of the rotor current.

The validation of the methodology for the diagnosis of stator asymmetry is carried out under the hypothesis, similar to the previous chapter that the state machine is healthy or affected by a stator asymmetry.

This chapter is structured into two parts. The first one performs the detection of the stator asymmetry on the universal machine set as wound rotor machine introduced in Chapter IX, working as generator. The second part of the chapter is intended for the detection of the fault of the stator asymmetry in the commercial machine, which also was introduced in the previous chapter, working as motor and generator.

Fig. 133 summarizes the performed tests and the tools used for the extraction of the fault components.

In this chapter, unlike the former, the extraction of the fault components will be only carried out through the application of the filters based on DWT and spectral filter, discarding the WP filters WP for the reasons given in Chapter IX.

The computation of the energy of the fault component will be performed both in the time and in the frequency domain, comparing the computed results, as in the previous chapter.

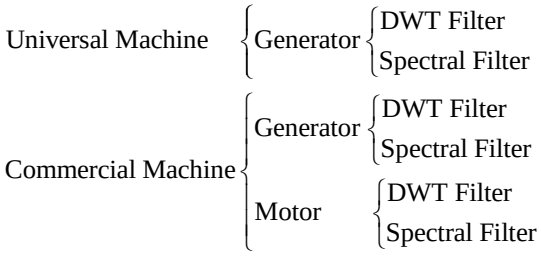

Fig. 133 Scheme of the performed test and analysis for the validation of the diagnostic methodology for the stator asymmetry

Finally, the instantaneous frequency is only computed through the method based on the Hilbert transform, since in Chapter IX was discussed that the differences in the computation of the instantaneous frequency between the classical and Teager-Kaiser operator are virtually non-existent.

The implementation of the methodology for the diagnosis of stator asymmetries is discussed in detail in section 2.1: (i) diagnosis of the universal machine working as generator, showing and discussing the partial results, similar to what was already done in Chapter IX. (ii) After the performance of the methodology, it is shown the results for the diagnosis of the tested universal machine as well as for the commercial machine.

2 VALIDATION OF THE METHODOLOGY

The stator asymmetry fault component to be extracted for the diagnosis of the machine is located on the rotor current and its evolution in the frequency spectrum is computed by (Chapter III):

$$f_{est} = (2 - s) \cdot f_{red} \tag{176}$$

The purpose of the diagnostic process is to isolate the frequency band in which the component fault evolves and compute its energy.

After the evaluation of the energy, if it does not exceed the preset threshold value, it can be ensured that the machine is not in faulty state.

In the event that the energy exceeds the preset threshold value, with the instantaneous frequency, it is determined if its origin is consequence of a stator asymmetry.

2.1 UNIVERSAL MACHINE

The tested universal machine in this chapter is the same as that tested in the previous chapter. The features of the stator and rotor winding are detailed in Annex I.

The electrical scheme of the test bed for the validation of the methodology is shown in Fig. 134. The stator is connected to the electrical network to 300 V at 50 Hz.

The stator asymmetry is performed by connecting a series of resistors whose values are among 4.15 Ω and 0.07 Ω in series with one of the stator phases.

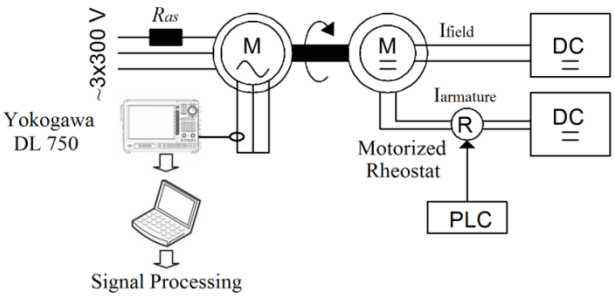

Fig. 134 Scheme of the test rig for the validation of the stator asymmetry for the universal machine

As in the previous chapter, the tested machine is coupled to a DC machine, controlled by a PLC, which forces the generator operation of the tested machine. By using the PLC that controls the excitation of the DC machine, the performed tests are automated tests facilitating the comparison of the results, since the machine is subjected to the same speed profile for all the test series.

The rotor current -secondary- is measured with a clamp and the speed is acquired by an encoder. Both the clamp and the encoder are connected to a digital oscilloscope 750 Yokogawa DL that has an analogue-to-digital conversion acquisition card of 16 bits. The digital oscilloscope is connected through an intranet to a personal computer that processes the signal captured. Unlike the rotor asymmetry tests, the selected sampling frequency is set to 2 kHz in order to demonstrate that the no influence of the value of the sampling frequency in the diagnosis.

The features of the auxiliary switchgear (clamp and encoder) and the digital oscilloscope are found in Annex II.

2.1.1 DIAGNOSIS BASED ON THE EXTRACTION OF THE FAULT COMPONENTS THROUGH A DWT FILTER

The diagnostic process begins imposing a non-stationary regime characterized by a fluctuating speed shown in Fig. 135.a. The acquisition of the speed allows to know the evolution of slip for all non-stationary process Fig. 135.b.

Analogously to the cases already studied for the rotor asymmetries, the acquired rotor current cannot be analysed by techniques developed for the steady state due to its transient nature.

The acquired rotor current, whose result comes from the fluctuations in speed shown in Fig. 135.a is shown in Fig. 136. The current in Fig. 136 corresponds to a machine subjected to a stator asymmetry caused by the connection in series of resistance whose value is R_a = 4.15 Ω in one the phases of the stator winding of the machine.

Once both signals -speed and current- have been acquired, it is proceeded with the extraction of the fault component.

Due to fluctuations in speed at which the machine is subjected in the speed transient, the slip evolves in the range [-0.04, -0.012] (see Fig. 135.b), whereas the fault component to be extracted is located in the range [100.65, 102.05] Hz (176).

The extraction of the frequency band in which the fault evolves is performed through the approximations a_3 and a_4 of a DWT filter as a consequence of the sampling frequency of 2 kHz with which it has been acquired the rotor current to be analyzed, and since the fault component is bounded in the range [100.65, 102.05] Hz:

$$nC = \text{int}\left[\frac{\log\frac{f_s}{f_2}}{\log(2)} - 1\right] = \text{int}\left[\frac{\log\frac{2000}{102.05}}{\log(2)} - 1\right] = 3 \qquad (177)$$

$$nNC = \text{int}\left[\frac{\log\frac{f_s}{f_1}}{\log(2)}\right] = \text{int}\left[\frac{\log\frac{2000}{100.65}}{\log(2)}\right] = 4 \tag{178}$$

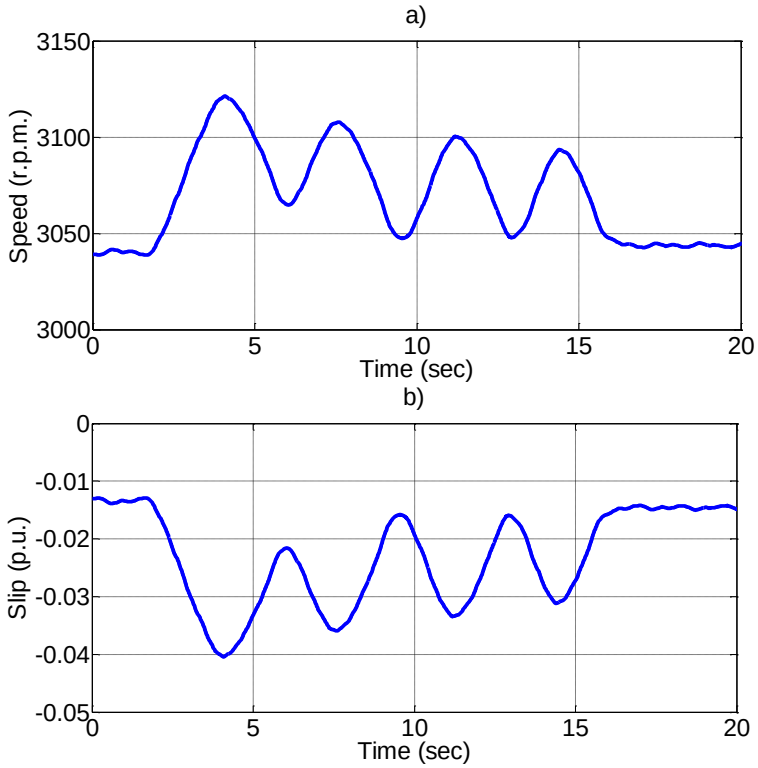

Fig. 135 a) Acquired non-stationary speed regime b) Slip evolution

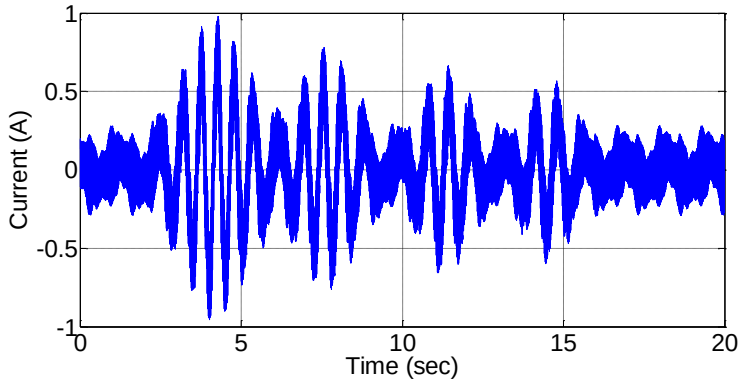

Fig. 136 Acquired current in the non-stationary stochastic regime. Universal machine working as generator in non-stationary stochastic conditions, stator asymmetry fault (R_a = 4.15 Ω)

Fig. 137.a shows the evolution in time of the approximation a_3, whereas Fig. 137.b shows the evolution in time of the approximation a_4. The difference of both approaches (a_3-a_4) allows the computation of the sought fault component since its difference only contains the frequency range [62.5, 125] Hz. The evolution in time of extracted fault component is shown in Fig. 138.

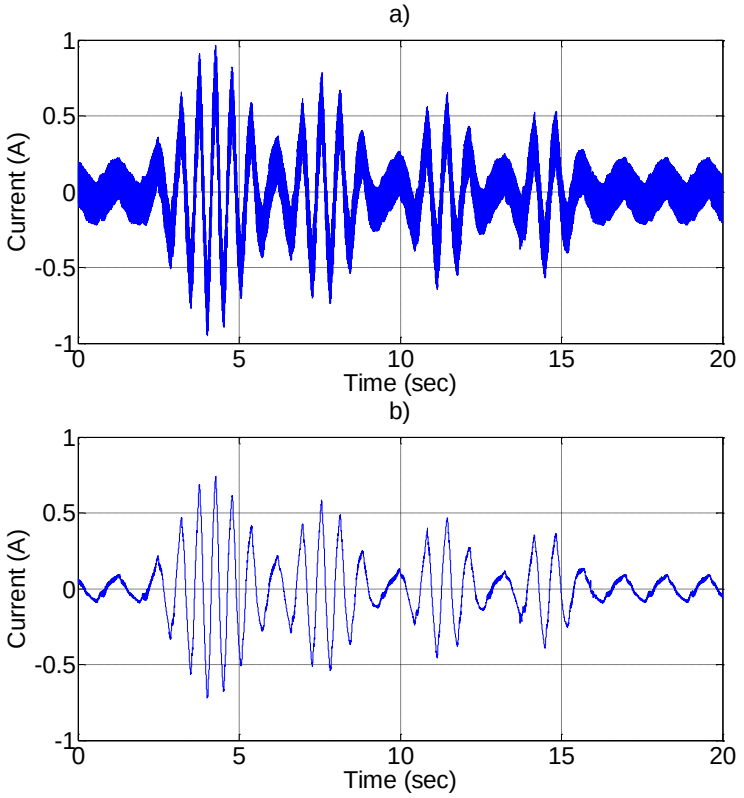

Fig. 137 Filtering DWT process of the signal. a) a_3 approximation b) a_4 approximation

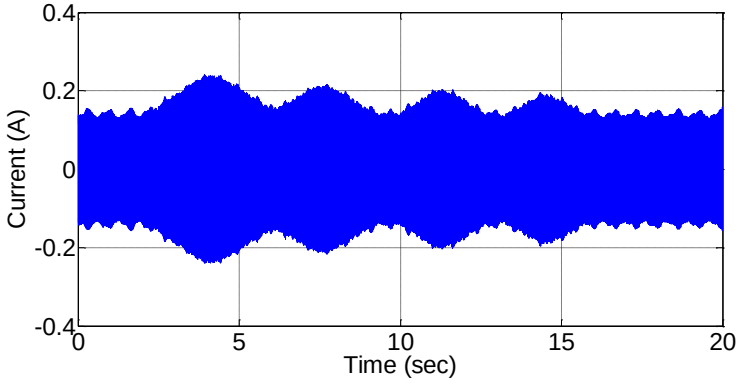

Fig. 138 Extracted stator asymmetry fault component. Machine with a stator asymmetry (R_a = 4.15 Ω) working as generator.

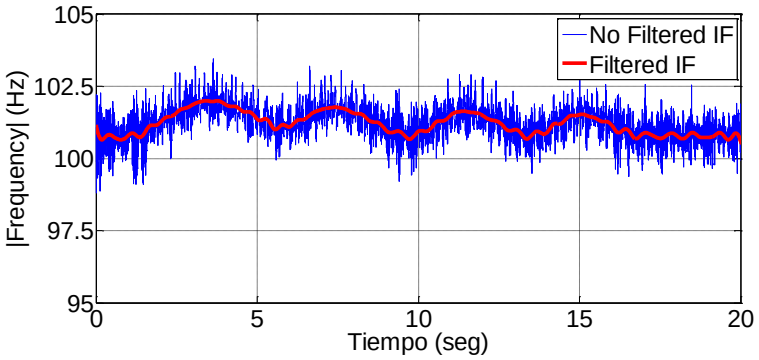

Fig. 139 Evolution of the instantaneous frequency of the stator asymmetry fault component in the time domain extracted through a DWT filter

After the extraction of the fault component, it is computed its energy. In the event that the computed energy does not exceed the preset energy threshold, the diagnostic process is stopped since the machine is in healthy state.

Otherwise, if the machine exceeds the threshold value, it is necessary to compute the instantaneous frequency of the fault component to determine whether the origin of the detected energy is consequence of the stator asymmetry.

The evolution of the instantaneous frequency of the extracted fault component in the time domain Fig. 138 is shown in Fig. 139. In it is seen again in the high frequency noise due to the derivation operation in the computation process (blue line). The removal of these high frequency components is performed using a low pass filter. The process for the removal of high frequency components is identical to that already performed and described in Chapter IX.

The evolution of the instantaneous frequency does not follow any pattern in the time domain but it does when it is plotted versus the slip.

In Fig. 140, is shown the depiction of the computed instantaneous frequency of the extracted fault component versus the slip (black line) and the theoretical evolution (red line), showing that the evolution of the computed instantaneous frequency matches the theoretical evolution, indicating that the origin of energy of the extracted fault component is due to a stator asymmetry.

The feasibility of the methodology for the detection of stator asymmetries is demonstrated through the diagnosis of the studied universal machine. Ten tests in a non-stationary regime are performed, modifying the degree of severity of the fault caused by connecting different resistors in series (see Table 29) in one phase of the stator of the tested machine with the aim of determining the minimum value of asymmetry that can be diagnosed through the application of the proposed methodology.

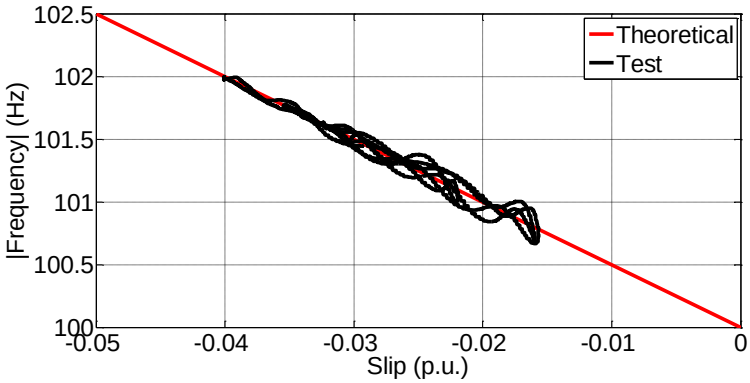

Fig. 140 Instantaneous frequency in the slip domain for the stator asymmetry fault component. Computed evolution (black line), theoretical evolution (red line), for a machine with stator asymmetry (R_a = 4.15 Ω). Extraction of the fault component through a DWT filter

TABLE 29. OBJECTIVE PARAMETERS FOR THE DIAGNOSIS OF A STATOR ASYMMETRY THROUGH THE EXTRACTION OF THE FAULT COMPONENT WITH A DWT FILTER. UNIVERSAL MACHINE AS WOUND ROTOR MACHINE WORKING AS GENERATOR

Test	***R***	***ΔR***	***S***	***m***	***b***	E_t	**Computation time**
	Ω	%				%	s
Theoretical				-50	100		
Healthy			0.991	-51.03	99.96	0.462	0.67
A1	0.07	1.62	0.917	-51.00	99.97	0.372	0.69
A2	0.14	3.29	0.992	-50.82	99.98	0.360	0.68
A3	0.26	5.85	0.998	-51.11	99.99	0.410	0.66
A4	0.43	9.67	1.000	-50.05	100.01	0.593	0.64
A5	0.69	15.73	1.000	-50.61	99.99	0.960	0.68
A6	1.10	25.11	1.000	-50.44	99.98	1.392	0.68
A7	1.73	39.38	1.000	-50.34	99.98	2.310	0.68
A8	2.64	60.03	1.000	-49.96	99.99	4.752	0.64
A9	4.15	94.33	1.000	-49.58	100.01	9.548	0.66

The analysis of the results reveals that the method is capable of diagnosing stator asymmetries that increase 15.73% of the stator winding resistance (test A5), since the value of the energy of the fault component is 107% greater than the energy value of the fault component when the machine is in a healthy state. Furthermore, the similitude coefficient (*S*) takes the value of 1, and the linear regression parameters are close to the theoretical parameters (m_{A5} = -50.61, m_{Theo} = -50; b_{A5} = 99.99, b_{Theo} = 100) indicating

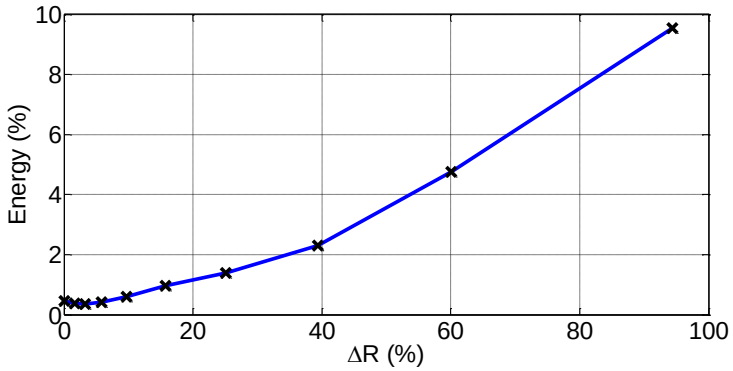

Fig. 141 Evolution of the energy of the fault component function of the increase of the resistance in the stator winding

with no doubt that the computed energy from the extracted fault component for the test A5 is a direct result of the stator asymmetry.

Fig. 141 shows the evolution of energy function of the degree of stator asymmetry that the analyzed machine is subjected.

The conclusion drawn from Fig. 141 is that the almost linear and directly proportional evolution of the energy of to the fault component related to the value of the resistor connected in series to the stator winding of the machine to produce failure, confirming the good consistency of the proposed methodology for the diagnosis of electrical machines in non-stationary stochastic regimes.

2.1.2 DIAGNOSIS BASED ON THE EXTRACTION OF THE FAULT COMPONENTS THROUGH A SPECTRAL FILTER

The use of the DWT filters for the extraction of the fault component of the rotor current implicitly carries the acceptance of errors in the filtering of the fault component failure due to non-ideality of the DWT filters.

This fact may lead to a misdiagnosis at certain times. To minimize errors in the extraction of the fault components is proposed the use of the spectral filter, as in Chapter IX, due to their advantages for the extraction of the fault components.

The diagnosis of a stator asymmetry through the extraction of the fault component with a spectral filter is performed identically to the diagnostic process introduced in the previous section but substituting the DWT filter stages for spectral filter stages.

The result of this change in the filter used is that whereas DWT filters allow the extraction of the frequency band [62.5, 125] Hz, whose width is 62.5 Hz, the spectral filters allow the extraction of the frequency band [100.65, 102.05] Hz, whose width is 1.4 Hz. The width of the extracted frequency band through the spectral filter is much smaller than the width of the band extracted through the DWT filter, fact that minimizes the possibility of making errors (since the band is narrower the likelihood of unintended components is reduced) and, therefore, improving the accuracy and reliability of the results.

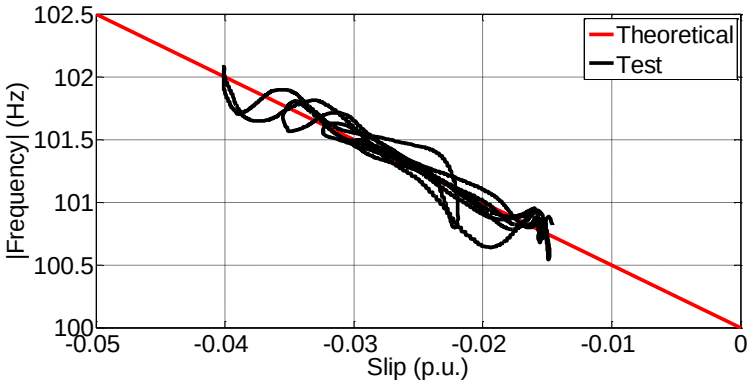

Fig. 142 Instantaneous frequency in the slip domain for the stator asymmetry fault component. Computed evolution (black line), theoretical evolution (red line), for a machine with stator asymmetry (R_a = 4.15 Ω). Extraction of the fault component through a spectral filter.

All the considerations already discussed in the previous section apply to this section since the diagnostic process is equivalent.

Fig. 142 shows the result after processing the same signal as in the previous section, replacing the DWT filter stages by spectral filter stages.

The numerical results of the ten tests are shown in Table 30, where it is shown that the proposed methodology is capable of diagnosing stator asymmetries that increase 15.73% the resistance of the stator winding phases, since the energy of the fault component of the test A5 is 135.29% greater than the energy of the fault component of the healthy test. Furthermore, the similitude coefficient (S) takes the value of 0.987 (very close to one), and the linear regression parameters are close to the theoretical parameters (m_{A5} = -47.59, m_{Theo} = -50; b_{A5} = 100.06, b_{Theo} = 100) indicating with no doubt that energy from the extracted fault component in the test A5 is a direct result of the stator asymmetry stator of the studied machine.

The use of the spectral filters reduces the required time to perform the diagnostic process, as in the case of applying the DWT filters for the diagnosis of the stator asymmetries are needed around 0.65 seconds, whereas if the diagnosis is performed through the spectral filters, the computational cost is reduced to 0.40 seconds.

Both in Table 30 and in Table 29 is noted a slight reduction in the computed energy for the tests A1, A2, A3 (small asymmetry) related to the healthy test. This behaviour is attributed to the existence of a small intrinsic asymmetry in the healthy machine, which in this case is compensated by connecting additional resistors of small value.

In an analogue manner to that used in the previous section, Fig. 143 shows the evolution of the energy of the fault component function of the degree of asymmetry imposed on the analysed machine.

TABLE 30. OBJECTIVE PARAMETERS FOR THE DIAGNOSIS OF A STATOR ASYMMETRY THROUGH THE EXTRACTION OF THE FAULT COMPONENT WITH A SPECTRAL FILTER. UNIVERSAL MACHINE AS WOUND ROTOR MACHINE WORKING AS GENERATOR

Test	R	ΔR	S	m	b	E_f	**Computation time**
	Ω	%				%	s
Theoretical				-50	100		
Healthy			1.000	-49.08	100.01	0.102	0.39
A1	0.07	1.62	0.981	-48.32	100.04	0.096	0.40
A2	0.14	3.29	0.962	-48.27	100.05	0.096	0.40
A3	0.26	5.85	0.992	-48.52	100.06	0.102	0.41
A4	0.43	9.67	0.967	-48.66	100.04	0.160	0.39
A5	0.69	15.73	0.987	-47.59	100.06	0.240	0.38
A6	1.10	25.11	1.000	-47.48	100.06	0.303	0.40
A7	1.73	39.38	0.993	-47.49	100.05	0.563	0.38
A8	2.64	60.03	0.982	-47.68	100.04	1.166	0.39
A9	4.15	94.33	0.987	-48.47	100.03	2.372	0.39

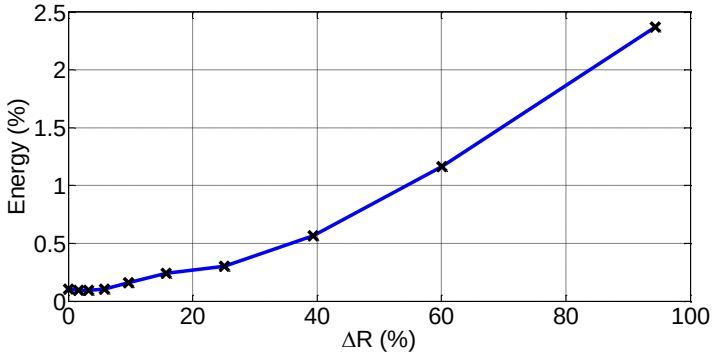

Fig. 143 Evolution of the energy of the fault component function of the increase of the resistance in the stator winding

The depiction of the energy versus the value of the resistor connected in series to the stator winding to cause the failure has the same character as that shown in the previous section (almost linear and directly proportional to the degree of asymmetry).

However, the absolute value of the energy of the extracted fault component through the spectral filter is approximately four times smaller than the value of the energy in the case of the extraction through the DWT filter.

This fact is justified by the reduction in the bandwidth of the extracted fault component (1.4 Hz for spectral filters in front of the 62.5 Hz for DWT filters) that provides the use of spectral filters.

The reduction of the extracted bandwidth extracted implies the reduction of energy due to the suppression of low energy components not related to the fault and therefore they do not alter the performed diagnosis.

2.2 COMMERCIAL MACHINE

The tested commercial wound rotor machine in this chapter is the same as that in the previous chapter. The features of its stator winding and rotor are detailed in Annex I.

The electrical scheme of the test bed for the validation of the fault is shown in Fig. 144. The supply voltage to the stator of the machine is 235 V (star) due to the restriction imposed by the DC machine coupled to it.

The stator asymmetry failure is produced by connecting in series a series of resistors, whose values are between 0.69 and 0.07 Ω, to one of the stator phases.

The chosen sampling frequency for the acquisition of the waves was set in this second case in 5 kHz to show its not influence in the diagnostic process.

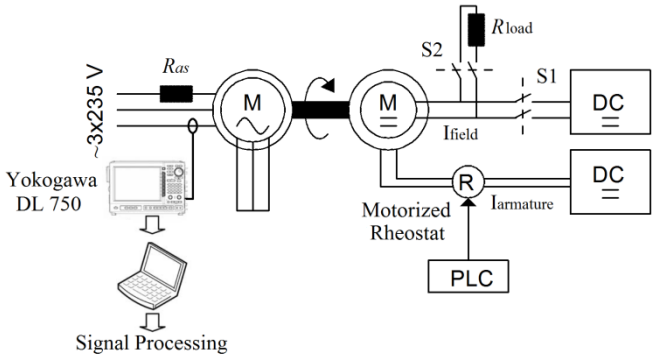

Fig. 144 Scheme of the test rig for the validation of the stator asymmetry for the commercial wound rotor induction machine.

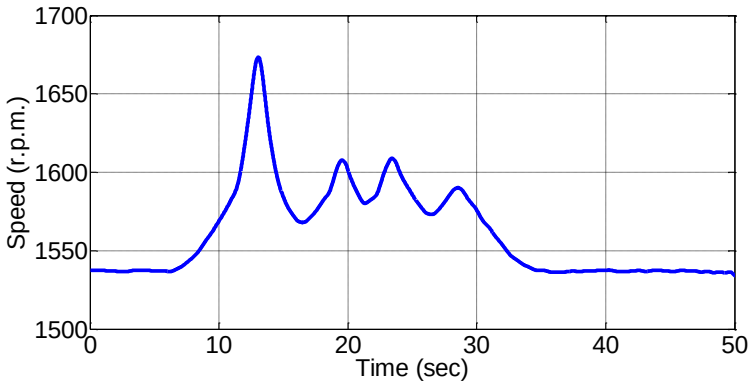

Fig. 145 Imposed non-stationary speed for the tests of stator asymmetry for the commercial machine working as generator.

2.2.1 GENERATOR MODE

The diagnosis of the commercial machine working as generator is carried out through the performance of six standard tests: one in healthy state and the remaining five in faulty state with different degrees of severity.

The tests are carried out in non-stationary stochastic conditions imposing the same speed fluctuation profile for all tests (Fig. 145).

2.2.1.1 DIAGNOSIS BASED ON THE EXTRACTION OF THE FAULT COMPONENTS THROUGH A DWT FILTER

Given the speed profile imposed on the tests, the slip, which the machine is subjected, is in the range [-0.12, -0.023], whereas the fault component $(2\text{-}s)\cdot f_{red}$ is located in the range of frequencies [101.13, 105.78] Hz.

The extraction of the frequency band in which the fault evolves is performed by the approximations a_4 and a_5 of a DWT filter since the sampling frequency is 5 kHz and the fault component is bounded in the range [101.13, 105.78] Hz

$$nC = \text{int}\left[\frac{\log\frac{f_s}{f_2}}{\log(2)} - 1\right] = \text{int}\left[\frac{\log\frac{5000}{105.78}}{\log(2)} - 1\right] = 4 \tag{179}$$

$$nNC = \text{int}\left[\frac{\log\frac{f_s}{f_1}}{\log(2)}\right] = \text{int}\left[\frac{\log\frac{5000}{101.13}}{\log(2)}\right] = 5 \tag{180}$$

The extracted frequency band through the DWT filter corresponds to the frequency range [78.13, 156.25] Hz, range that contains the evolution of the frequency of the fault component.

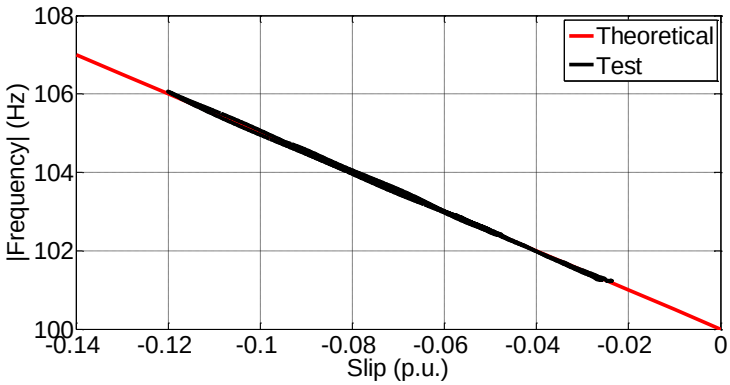

Fig. 146 Instantaneous frequency of the fault component in the slip domain extracted through a DWT filter. Commercial machine with a stator asymmetry R_a = 0.07 Ω, A1 test. Generator mode

After extraction of the fault component its energy is computed and, if it exceeds the preset threshold value, it is proceeded to the computation of the instantaneous frequency for the determination of the origin of the energy of the fault component.

The process of computation of the instantaneous frequency is similar to that already performed in the previous section.

Fig. 146 shows the result of the diagnosis of a machine with a stator asymmetry caused by the connection in series of a resistor whose values is R_a = 0.07 Ω. In it is shown how computed evolution (black line) overlaps with the theoretical evolution (red line). That indicates that the origin of the computed energy of the extracted fault component is due to a stator asymmetry.

Six tests were performed with different degrees of stator asymmetry to carry out the validation of the proposed methodology.

According to the absolute value of the energy of the computed fault components, it is concluded that the proposed method is able to diagnose increases of 206% of the nominal stator resistance, since in the tests A1-A4, the value of the energy of the fault component is less than the value of energy of the fault component for the healthy machine (Table 31).

However, the parabolic depiction of the value of the energy versus the value of the fault resistance connected in series with the stator windings caused a further investigation to explain the evolution of energy shown in Fig. 147.

The first causes that were investigated to explain the parabolic evolution of energy of the fault component was to determine if there was an intrinsic asymmetry in the stator windings. This fact was unlikely since, according to the results (Table 31, Fig. 147), the inherent asymmetry in one of the stator windings should be 80%.

TABLE 31. OBJECTIVE PARAMETERS FOR THE DIAGNOSIS OF A STATOR ASYMMETRY THROUGH THE EXTRACTION OF THE FAULT COMPONENT WITH A DWT FILTER. COMMERCIAL WOUND ROTOR MACHINE WORKING AS GENERATOR

Test	R	ΔR	S	m	b	E_t	**Computation time**
	Ω	%				%	s
Theoretical				-50	100		
Healthy			1.00	-50.53	99.96	0.221	1.18
A1	0.07	21	1.00	-50.47	99.99	0.116	1.16
A2	0.14	42	1.00	-50.99	99.99	0.102	1.22
A3	0.26	78	1.00	-50.42	100.00	0.078	1.21
A4	0.43	128	1.00	-50.43	99.99	0.168	1.22
A5	0.69	206	1.00	-50.25	99.99	0.624	1.18

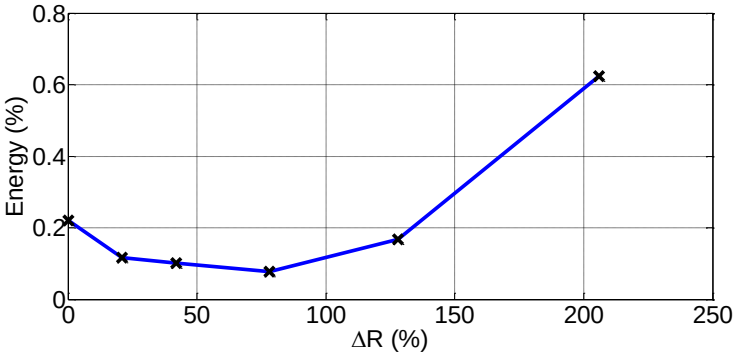

Fig. 147 Evolution of the energy of the fault component function of the increase of the resistance in the stator winding

In spite of that, measurements of the resistances of each of the stator phases are taken. The resistance values were 0.3342 Ω for phase A, 0.3305 Ω for phase B and 0.3433 Ω for phase C.

After measuring the resistance values of each of the phases is concluded that the maximum difference between the value of phase resistors (phase A vs. C phase) is less than 5% (in particular it takes the value of 3.8%). Thus, the hypothesis of 80% intrinsic asymmetry is entirely discarded.

The following action taken to determine the parabolic origin of energy component was to determine if the contact resistance (whose value is not linear and is highly dependent on good contact between the terminal of the resistor and the wiper) was responsible for the parabolic behaviour.

To solve the proposed problem, the rheostat that creates the imbalance was tested with several loads and, the position of the wiper was changed at least three times per position. The measures taken determined that the rheostat was not the responsible for the parabolic evolution of the energy.

Finally, the last action taken was to measure the voltage at the stator terminals of the tested machine tested when the rheostat was connected. The measure of the voltage at the terminals determined that the machine was not only subjected to an imbalance of resistance in its phase (there was only one rheostat connected) but was also subjected to a voltage imbalance because of the connection of the rheostat.

Notice that the minimum value of the resistance of the rheostat is 0.07 Ω what is 20.59% of the phase resistance of the machine and, consequently, causes a voltage imbalance in the machine that should be taken into account for the diagnosis.

The conclusion of all the performed process is that the fault components for the wound rotor induction machine of 15 CV working as generator do not follow the expected linear evolution because of the stator asymmetry and the voltage imbalance.

2.2.1.2 DIAGNOSIS BASED ON THE EXTRACTION OF THE FAULT COMPONENTS THROUGH A SPECTRAL FILTER

Due to problems associated with the use of the DWT filters and to discard a bad filtering as the cause that produces the parabolic evolution of energy in the previous subsection, it is proposed the application of the method with the spectral filter. In this subsection the results of the performed diagnostic process are directly shown since the diagnostic process carried out is identical to that performed in the previous section substituting the DWT filter stages by spectral filter stages.

The use of the spectral filters allow the extraction of the frequency band [101.12, 105.78] Hz, reducing the width of the extracted range with a DWT filter and consequently minimizing errors and increasing the accuracy of the method.

Fig. 148 shows the evolution of the instantaneous frequency of the extracted fault component in the previous section through a spectral filter, where it is shown that its evolution overlaps with the theoretical evolution as in the previous case.

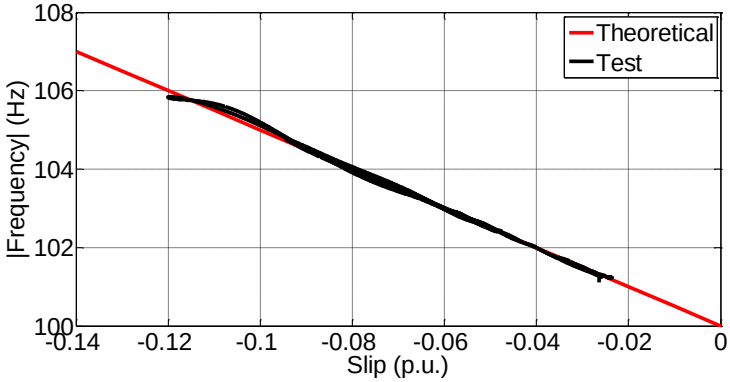

Fig. 148 Instantaneous frequency of the fault component in the slip domain extracted through a spectral filter. Commercial machine with a stator asymmetry R_a = 0.07 Ω, A1 test. Generator mode.

TABLE 32. OBJECTIVE PARAMETERS FOR THE DIAGNOSIS OF A STATOR ASYMMETRY THROUGH THE EXTRACTION OF THE FAULT COMPONENT WITH A SPECTRAL FILTER. COMMERCIAL WOUND ROTOR MACHINE WORKING AS GENERATOR

Test	R	ΔR	S	m	b	E_f	Computation time
	Ω	%				%	s
Theoretical				-50	100		
Healthy			1.00	-50.41	99.97	0.053	0.81
A1	0.07	21	1.00	-50.37	100.00	0.029	0.82
A2	0.14	42	1.00	-51.02	99.99	0.026	0.80
A3	0.26	78	1.00	-50.11	100.01	0.020	0.80
A4	0.43	128	1.00	-50.18	100.00	0.040	0.79
A5	0.69	206	1.00	-50.22	99.99	0.152	0.79

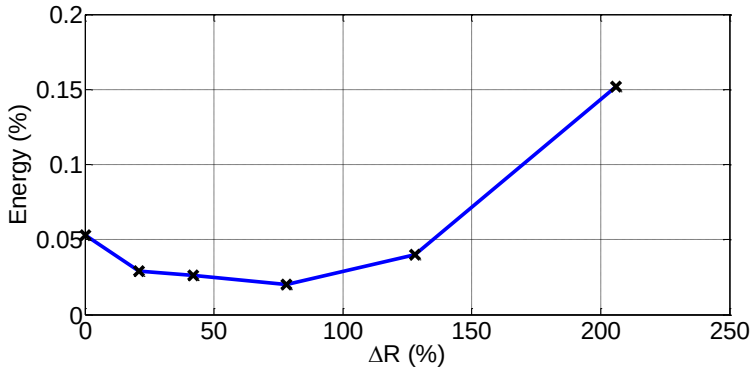

Fig. 149 Evolution of the energy of the fault component function of the increase of the resistance in the stator winding

The numerical results of the six tests are shown in Table 32 and its depiction is in Fig. 149. The extraction of the fault component was performed through using spectral filters replacing the DWT filters used in the previous section.

The conclusion drawn from the analysis of the results after conducting the diagnosis through the spectral filter is that the filtering stage has no influence on the parabolic evolution of energy of the extracted fault component.

This fact confirms that the hypothesis introduced in the previous section, which justified the parabolic evolution of energy of the fault component failure, is certain.

2.2.2 MOTOR MODE

The application of the methodology is also possible under motor mode conditions. In this case, the assembly shown in Fig. 144, the DC machine works as a generator feeding an external resistor. The tested machine under is connected to the electrical network, star connection, at the reduced voltage of 235 V due to practical problems imposed by the DC machine (its power is 50% of the power of the tested commercial machine).

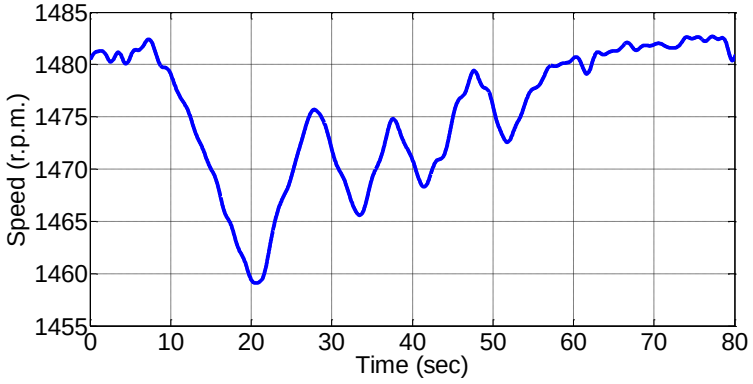

Fig. 150 Imposed non-stationary speed for the tests of stator asymmetry for the commercial machine working as motor

Six tests are performed in non-stationary stochastic conditions characterized by fluctuating speed Fig. 150 for the validation of the method. The performed tests are similar to those already mentioned for the previous section where the was working as a generator.

To avoid the effect of the voltage imbalance discussed in the previous section, a resistance of 0.26 Ω is connected to each of the stator windings of the machine thereby reducing the effect of the voltage imbalance.

2.2.2.1 DIAGNOSIS BASED ON THE EXTRACTION OF THE FAULT COMPONENTS THROUGH A DWT FILTER

The imposed speed fluctuations to the machine cause that the slip, which the machine is subjected, is located in the range [0.011, 0.027], then the frequency of the fault component is in the range [98.64, 99.42] Hz.

The extraction of the frequency band in which is contained the fault component is conducted through a DWT filter. The approximations necessary for the extraction of the frequency band are the a_4 and a_5 as the sampling rate used for the acquisition of the waves is 5 kHz and the fault component is bounded on the range [98.64, 99.42] Hz

$$nC = \text{int}\left[\frac{\log\frac{f_s}{f_2}}{\log(2)} - 1\right] = \text{int}\left[\frac{\log\frac{5000}{99.42}}{\log(2)} - 1\right] = 4 \tag{181}$$

$$nNC = \text{int}\left[\frac{\log\frac{f_s}{f_1}}{\log(2)}\right] = \text{int}\left[\frac{\log\frac{5000}{98.64}}{\log(2)}\right] = 5 \tag{182}$$

The DWT filter approximations employed for extraction of the frequency band of the fault component extract the frequency range [78.13, 156.25] Hz of the analysed current, range where the fault component evolves.

Fig. 151 shows the evolution of the instantaneous frequency of the extracted fault component of current when the machine is subjected to an imbalance in the stator of R_a = 0.69 Ω. In it is noted that the computed and theoretical evolution overlap, indicating that the origin of the computed energy is due to a stator asymmetry.

The numerical results of the six tests are shown in Table 33 that shows that the methodology is able to determine, in all the studied cases, that the energy of the fault component is due to the stator asymmetry, allowing the diagnosis of asymmetries that increase from 21% of the resistance of one phase of the stator winding.

The evolution of the energy of the fault component is shown in Fig. 152 where it can be observed that it has a direct behaviour related to the value of the fault resistance connected in series with the stator winding (the greater the asymmetry, the greater the energy of the extracted fault component).

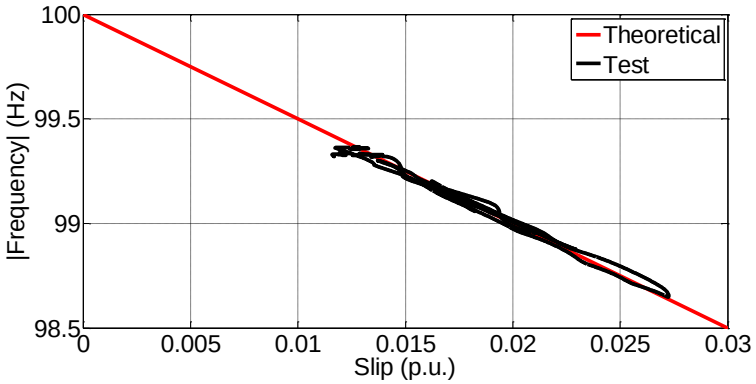

Fig. 151 Instantaneous frequency of the fault component in the slip domain extracted through a DWT filter. Commercial machine with a stator asymmetry R_a = 0.69 Ω, A5 test. Motor mode

TABLE 33. OBJECTIVE PARAMETERS FOR THE DIAGNOSIS OF A STATOR ASYMMETRY THROUGH THE EXTRACTION OF THE FAULT COMPONENT WITH A DWT FILTER. COMMERCIAL WOUND ROTOR MACHINE WORKING AS MOTOR

Test	***R***	***ΔR***	***S***	***m***	***b***	E_t	**Computation time**
	Ω	%				%	s
Theoretical				-50	100		
Healthy			1.00	-48.49	99.98	0.116	0.82
A1	0.07	21	1.00	-49.90	100.00	0.203	0.76
A2	0.14	42	1.00	-48.93	99.99	0.423	0.80
A3	0.26	78	1.00	-49.90	100.03	1.082	0.84
A4	0.43	128	1.00	-47.30	99.95	1.638	0.78
A5	0.69	206	1.00	-45.60	99.91	7.398	0.78

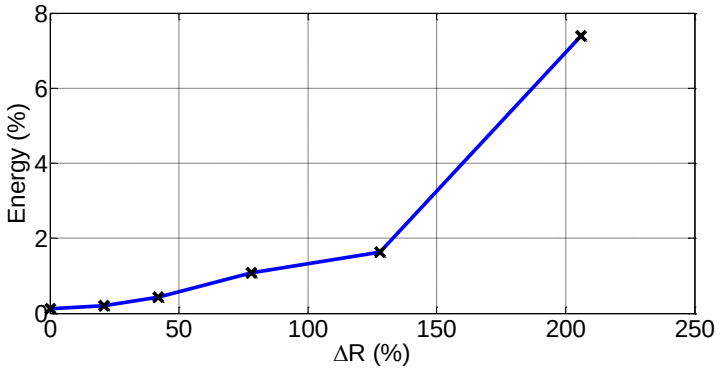

Fig. 152 Evolution of the energy of the fault component function of the increase of the resistance in the stator winding

2.2.2.2 DIAGNOSIS BASED ON THE EXTRACTION OF THE FAULT COMPONENTS THROUGH A SPECTRAL FILTER

Finally, the diagnostic process performed through the DWT filters is performed again replacing the DWT filter stages by spectral filter stages, analogue to the previous sections.

The extracted frequency band with the spectral filter takes the values of [98.64, 99.43] Hz, improving the quality of the extracted range regarding the use of the DWT filters.

Fig. 153 shows the same result as shown in Fig. 151 but in this case the fault component is extracted with the application of the spectral filter. The differences between the two figures are almost non-existent.

The numerical results of the six tests are shown in Table 34 reaching the same conclusions as those given for the diagnosis of the fault through the extraction of the fault component with the DWT filters.

The use of spectral filters has again a faster computation time. In the case of test A5, the diagnosis with the DWT filters required 0.78 seconds (see Table 33) whereas the diagnosis of the same test through the spectral filter has required only 0.50 seconds (see Table 34).

The use of the spectral filters in the proposed methodology allows a reduction in diagnostic time of 39% over the time required for the diagnosis with DWT filters. This fact, together with the lower requirement level programming of the methodology and hardware, make the use of spectral filters the ideal tool for the extraction of the fault components.

The evolution of the energy of the fault component is shown in Fig. 154, where it is shown that its evolution is direct function of the increase in the asymmetry caused to the machine (the greater asymmetry, the greater energy in the fault component) as it was already shown for the extraction of the fault component with the DWT filters.

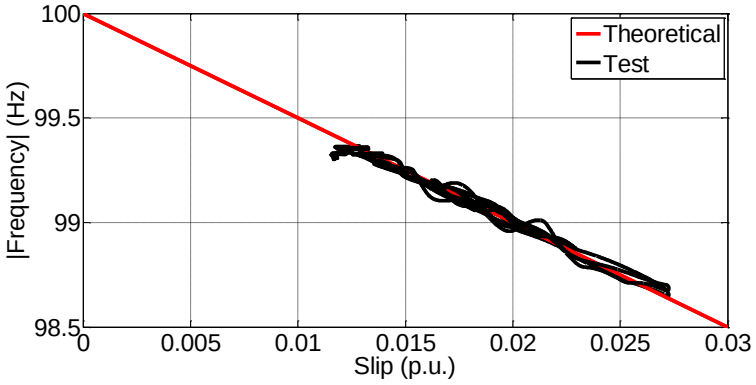

Fig. 153 Instantaneous frequency of the fault component in the slip domain extracted through a spectral filter. Commercial machine with a stator asymmetry R_a = 0.69 Ω, A5 test. Motor mode

Finally, it should be noticed that the use of spectral filters reduce the absolute value of the energy of the fault component, as it was for the case of the previous sections, since the extracted bandwidth by this filtering technique is much smaller than the extracted bandwidth with the use of the DWT filters.

TABLE 34. OBJECTIVE PARAMETERS FOR THE DIAGNOSIS OF A STATOR ASYMMETRY THROUGH THE EXTRACTION OF THE FAULT COMPONENT WITH A SPECTRAL FILTER. COMMERCIAL WOUND ROTOR MACHINE WORKING AS MOTOR

Test	R	ΔR	S	m	b	E_f	**Computation time**
	Ω	%				%	s
Theoretical				-50	100		
Healthy			1.00	-48.40	99.98	0.026	0.50
A1	0.07	21	1.00	-49.49	99.99	0.048	0.51
A2	0.14	42	1.00	-48.67	99.98	0.102	0.53
A3	0.26	78	1.00	-49.50	100.02	0.250	0.49
A4	0.43	128	1.00	-47.17	99.95	0.397	0.54
A5	0.69	206	1.00	-44.72	99.90	1.796	0.50

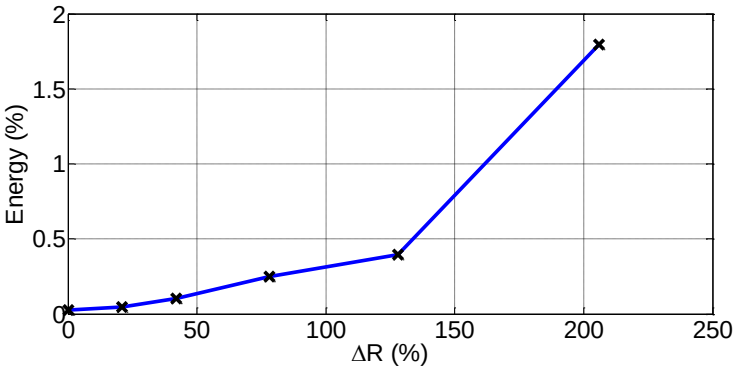

Fig. 154 Evolution of the energy of the fault component function of the increase of the resistance in the stator winding extracted with a spectral filter.

3 SUMMARY AND CONCLUSIONS OF THE CHAPTER

In this chapter it has been demonstrated the feasibility of the diagnosis of stator asymmetries in wound rotor induction machines rotor through the proposed methodology applied to the rotor current.

The diagnosis is carried out in non-stationary stochastic conditions for both motor and generator mode, on a universal machine set as wound rotor induction machine and on a commercial wound rotor induction machine rotor of 11 kW power.

The extraction of the fault component of stator asymmetry is performed through the DWT and spectral filters.

The diagnostic criterion, as in the previous chapter, is based on the analysis of the computed objective parameters of energy, similitude coefficient and linear regression reducing the likelihood of false positives.

The main conclusions of this chapter are:

- The proposed methodology is able to diagnose stator asymmetries in wound rotor induction machines through the analysis of one of its rotor currents, for any operating mode in stochastic regimes.
- The sampling frequency does not influence the diagnostic process provided it meets the Nyquist's criterion.
- – In contrast to the results of the previous chapter, the diagnosis of the stator asymmetry is insensitive to the filtering method (DWT or spectral), since it is able to correctly diagnose asymmetries of the order of 20% in the stator winding.
- Despite the insensitivity of the results function of the selected filter, the use of the spectral filter is preferred over the DWT filter since its use requires lower computational cost than the use of the DWT filters an order between 30% and 50%.
- The use of the spectral filters reduces the absolute amount of energy of the extracted fault component compared with the use of the DWT filters due to the smaller width of the extracted frequency band that can be extracted with them.
- The percentage change of the energy compared to the total energy of the signal is independent of the method for the extraction of the fault component.
- The evolution of the energy of the fault component is not as linear as that for the rotor asymmetry.
- The effect of an incipient fault can lead to an increase or decrease in the energy parameter when the tested machine has a constructive stator asymmetry due to tolerances in the manufacturing process.

CHAPTER XI: MIXED ECCENTRICITY. VALIDATION OF THE PROPOSED METHODOLOGY

1 INTRODUCTION

The two previous chapters focused on the study of rotor (Chapter IX) and stator asymmetry fault (Chapter X).

This chapter will study the application of the proposed methodology for the diagnosis of mixed eccentricity in induction machines.

The demonstration of the feasibility of the technique of diagnosis of mixed eccentricity is performed by conducting a series of tests on squirrel cage rotor induction machines and wound rotor induction machines in stochastic regimes, operating in generator and motor mode in healthy state and in a state of mixed eccentricity.

For each machine two prototypes were set, one as machine with mixed eccentricity and the other as healthy machine. In the prototype machine with fault the mixed eccentricity is achieved by replacing the original bearings for an eccentric accurate bearing system, as described in the following sections. The prototype machine of healthy machine is an identical machine, where it is also replaced its bearings for a new system equal to the faulty machine, but in this case without eccentricity. This ensures that the differences detected in the tests are only due to the eccentricity and not due to constructive differences caused by the manipulation of the bearings.

Each pair of machines is tested in motor and generator operation demonstrating the independence of the methodology against the regime of operation. Within each mode, there are two different tests with different duration and speed profiles. Thus, it is demonstrated the independence of the methodology against t duration of the analyzed transient and the evolution of the load which the machine is subjected. Finally, each test is analysed by extracting the fault component through a DWT or a spectral filter, showing the differences between them.

In total eight cases are analysed to validate the diagnostic methodology for the fault of mixed of eccentricity. Each case consists of two tests: (i) test of the healthy machine and (ii) test of the machine with mixed eccentricity.

The first four tests are carried out on the squirrel cage rotor induction machine; the first two correspond to generator operation and the last two to motor mode. The structure is repeated for the four tests corresponding to the wound rotor induction machine.

Finally, each case is analyzed by the DWT and the spectral filters.

A scheme cases performed and analyzed for the validation of the methodology is summarised in Fig. 155.

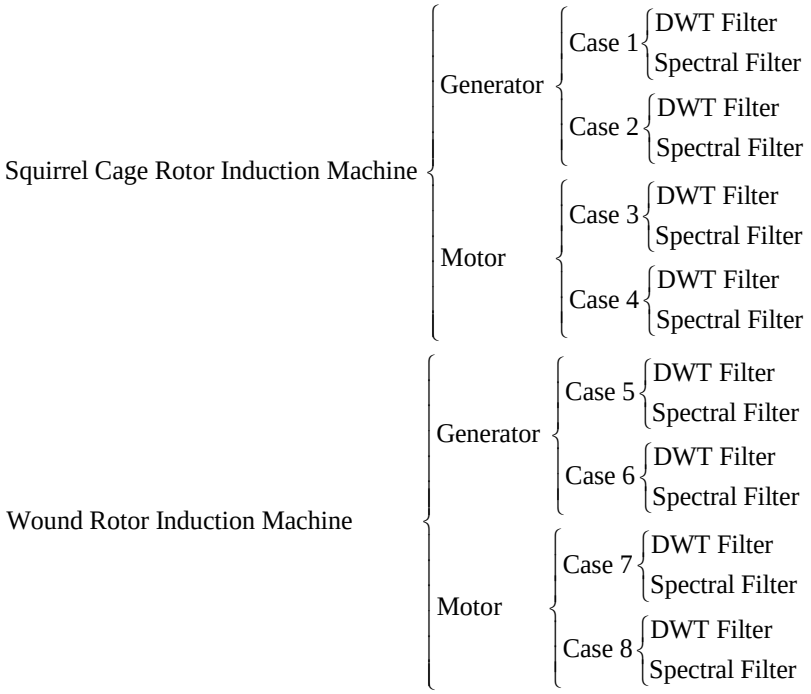

Fig. 155 Scheme of the test and analysis performed for the validation of the methodology for the mixed eccentricity

2 VALIDATION OF THE METHODOLOGY

The fault component of mixed eccentricity evolves in the frequency region of the stator current (Chapter III):

$$f_{exc} = f_{red} - \frac{f_{red}}{p}(1-s) \tag{183}$$

The aim is to isolate the frequency band that contains the fault component, compute its energy and determine if its origin is mixed due to the mixed eccentricity.

In the event that the computed energy exceeds the preset threshold with the instantaneous frequency is determined if the origin of energy of the extracted fault component is because of the mixed eccentricity.

2.1 SQUIRREL CAGE ROTOR INDUCTION MACHINE

Tests conducted to validate the method are carried out on a commercial squirrel cage rotor induction machine working either as generator or motor connected to the network at a voltage of 230 V (delta) at 50 Hz, whose characteristics are shown in Annex I.

Two squirrel cage rotor induction machines are tested to validate the method. The first machine has its original bearings replaced by two bearing

with smaller outer diameter and larger inner diameter that together with two concentric bearing houses perfectly couple the new bearing to the shaft and end bell. A similar action is carried out on the second machine but this time the two precision eccentric bearing houses to attach the new bearing to the shaft and the end bell.

The eccentric bearing houses were mechanised with a 0.15 mm eccentricity for the outer bearing house and 0.25mm eccentricity for the inner bearing house. These values lead to a static eccentricity of 30% and 50% of dynamic eccentricity on the machine. A scheme of the bearing system is shown in Fig. 156. In Fig. 157 is shown a picture of the original bearing and the new bearing with the eccentric bearing houses to create the eccentricity.

The electrical scheme of the test bed for the tests of the squirrel cage rotor induction machines is shown Fig. 158. The tested machine is coupled to another asynchronous machine, whose features are similar to the tested machine, that forces the operation of the machine to be tested above its synchronous speed (generator mode) or load machine (motor mode). In any case, the speed that the tested machine undergoes is controlled by the auxiliary machine.

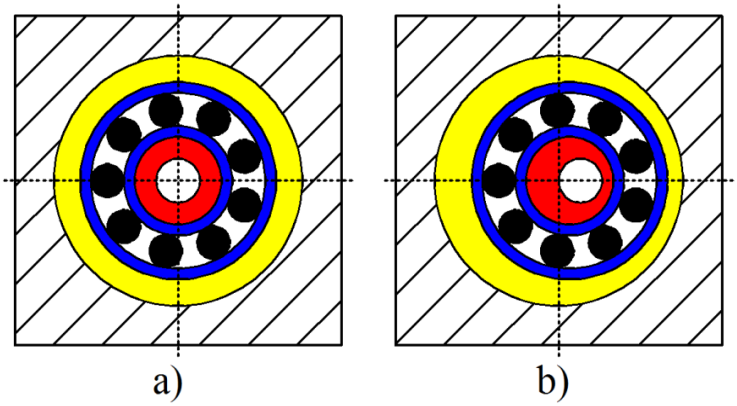

Fig. 156 Scheme of the bearings to achieve the mixed eccentricity failure. A) Bearing with concentric bearing houses b) Bearing with eccentric bearing houses

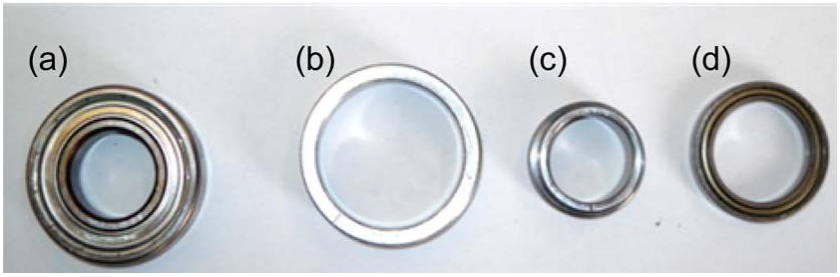

Fig. 157 Picture of the bearings and bearing houses to create the mixed eccentricity failure. A) Original bearing b) Outer eccentric bearing house c) Inner eccentric bearing house d) New bearing

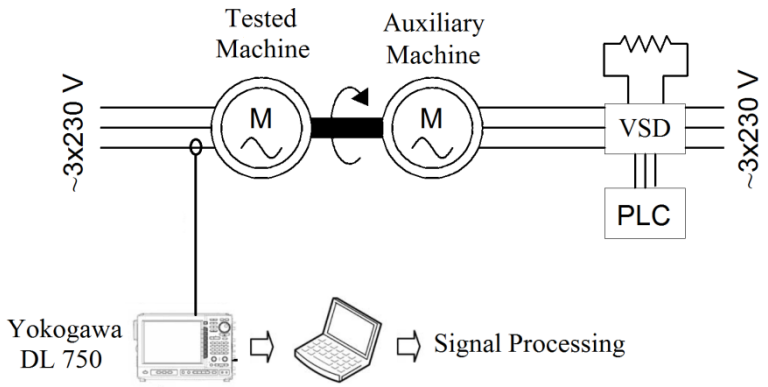

Fig. 158 Electrical scheme of the test bed for the validation of the methodology of diagnosis of mixed eccentricity.

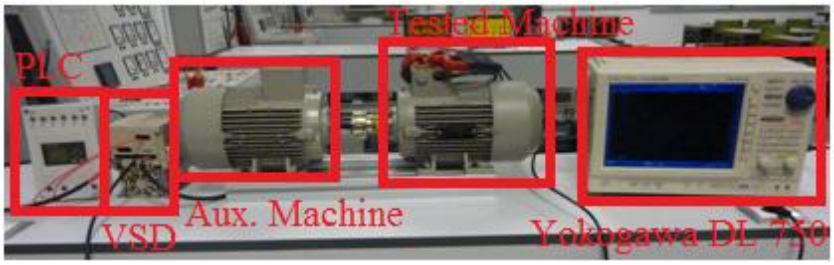

Fig. 159 Picture of the test bed for the test of the squirrel cage rotor induction machine with mixed eccentricity.

The auxiliary machine is controlled by a VSD who is also controlled by a PLC. This configuration allows the setting of fixed sequences in the speed allowing tests on the machine under non-stationary conditions with the same speed profile for all tests, facilitating the comparison of the results.

The stator current is measured with a clamp and the speed is taken by a encoder. Both devices are connected to a digital oscilloscope DL Yokohama 750 that has a 16 bit AD acquisition card. The oscilloscope is connected via an intranet to a PC where the acquired signals are processed. The sampling frequency used in the tests was 5 kHz.

The features of the auxiliary switchgear (clamp and encoder) and digital oscilloscope can be found in Annex II.

Since the diagnostic process is very similar for all tests of this chapter introduces in detail the diagnosis of squirrel cage rotor induction machine for case 1, whereas for the remaining tests the testing conditions are summarised in the Table 37 and the results in Table 38. The graphical results for case 2, case 3, and case 4 are respectively shown in Fig. 166, Fig. 167 and Fig. 168.

2.1.1 SQUIRREL CAGE ROTOR INDUCTION MACHINE: CASE 1

In Case 1, the machine is subjected to the velocity profile shown in Fig. 160. Fig. 161shows the evolution of the fluctuation of the stator current

due to the imposed speed on the machine. The duration of the stochastic regime is 20 seconds.

The diagnosis of the machine is performed through the extraction of the fault components through DWT filters or spectral filters. The results are shown in the following sections.

2.1.1.1 DIAGNOSIS BASED ON THE EXTRACTION OF THE FAULT COMPONENTS THROUGH A DWT FILTER

Due to the imposed speed fluctuations to the machine (Fig. 160), the slip, which the machine is subjected, is bounded in the range [-0.038, -0.008], and the fault component is bounded in the frequency range [24.03, 24.80] Hz (183).

The fault component is extracted through the direct application of a DWT filter, given the absence of harmonic components close to the fault harmonics of mixed eccentricity. The necessary approximations to extract the fault component will be the a_6 and a_7 since the sampling frequency is 5 kHz and the frequencies where the component to be extracted evolves are [24.03, 24.80] Hz

$$nC = \text{int}\left[\frac{\log\frac{f_s}{f_2}}{\log(2)} - 1\right] = \text{int}\left[\frac{\log\frac{5000}{24.80}}{\log(2)} - 1\right] = 6 \qquad (184)$$

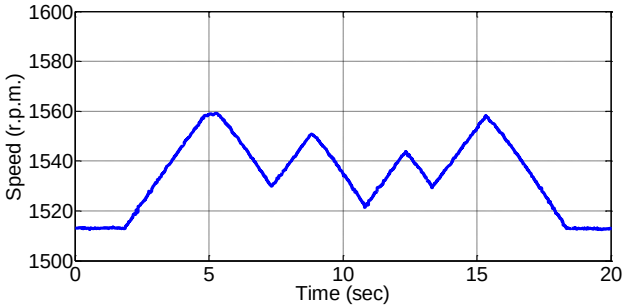

Fig. 160 Speed in the non-stationary stochastic regime for case 1. Squirrel cage rotor induction machine. Generator mode.

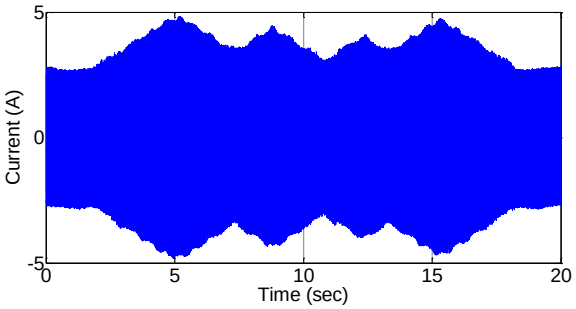

Fig. 161 Stator current consequence of the imposed speed fluctuations for case 1. Squirrel cage rotor induction machine. Generator mode.

$$nNC = \text{int}\left[\frac{\log\frac{f_s}{f_1}}{\log(2)}\right] = \text{int}\left[\frac{\log\frac{5000}{24.03}}{\log(2)}\right] = 7 \tag{185}$$

The selection of these decompositions allows the extraction of the frequency band [19.53, 39.06] Hz, band that clearly contains the desired fault component.

After extraction of fault component, its energy is computed and if it is greater than the preset threshold is necessary to compute the instantaneous frequency to determine if the origin of the energy of the fault component is due to the mixed eccentricity or other causes.

The process of computation of the instantaneous frequency is similar to that already performed in Chapters IX and X. Therefore, its computation will not be repeated in detail.

The result of applying the method is shown in Fig. 162 and Fig. 163.

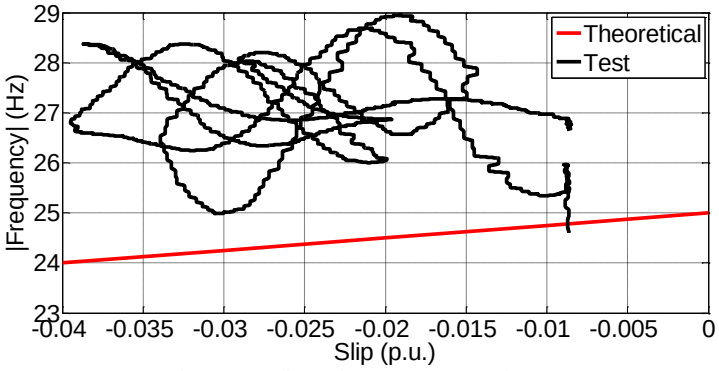

Fig. 162 Instantaneous frequency of the fault component of mixed eccentricity in the slip domain extracted through a DWT filter for case 1. Commercial squirrel cage rotor induction machine in healthy state. Generator mode.

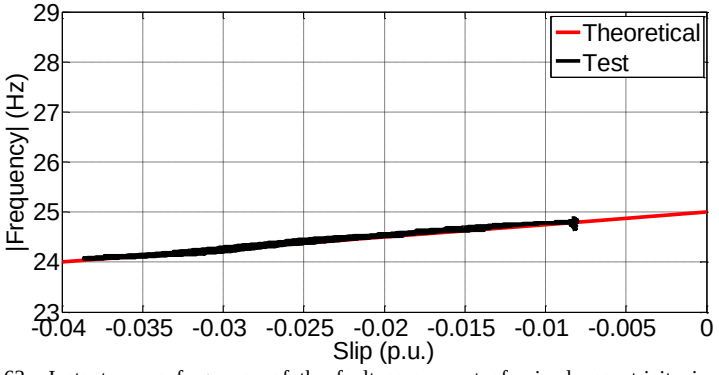

Fig. 163 Instantaneous frequency of the fault component of mixed eccentricity in the slip domain extracted through a DWT filter for case 1. Commercial squirrel cage rotor induction machine with mixed eccentricity. Generator mode.

TABLE 35. OBJECTIVE PARAMETERS FOR CASE 1. DIAGNOSIS OF A MIXED ECCENTRICITY THROUGH THE EXTRACTION OF THE FAULT COMPONENT WITH A DWT FILTER. SQUIRREL CAGE ROTOR INDUCTION MACHINE WORKING AS GENERATOR. DURATION OF THE NON-STATIONARY STOCHASTIC REGIME 20 SECONDS

Test	S	m	b	E_t	Computation time
Theoretical		25	25		
Healthy	0.01	-25.85	26.42	0.0025	0.34
Faulty	1.00	25.38	25.03	0.0441	0.35

In the first one (Fig. 162) is shown the instantaneous frequency of the extracted fault component when the machine is in a healthy state, that shows that the computed evolution (black line) clearly does not fit the theoretical evolution (red line), that is the energy of the extracted fault component is not due to a mixed eccentricity.

Fig. 163 shows the analogue result to that shown in Fig. 162 when the machine has a mixed eccentricity, showing that the evolution of the instantaneous frequency fits perfectly to the theoretical evolution, thereby determining that the energy of the extracted fault component is due to a mixed eccentricity.

The objective parameters of the diagnosis (Table 35) agree with the graphical results shown, since the similitude coefficient is practically zero in the case of a healthy test (S = 0.01), whereas taking the value of 1 for the machine with mixed eccentricity. Furthermore, the linear regression parameters are similar to the theoretical in the faulty case whereas they do not coincide for the healthy test.

Finally, if it is compare the value of the energy of the performed tests, there was an increase of one order of magnitude related to the energy value of the healthy case when the machine is under the influence of a mixed eccentricity.

The achieved results ensure that the diagnosis carried out for the detection of the mixed eccentricity through the proposed methodology is right.

2.1.1.2 DIAGNOSIS BASED ON THE EXTRACTION OF THE FAULT COMPONENTS THROUGH A SPECTRAL FILTER

The use of DWT filters force the extraction of extremely wide frequency bands ([19.53, 39.06] Hz) related to the frequency evolution of the fault components ([24.03, 24.80] Hz). This may cause the interference of unwanted harmonics in the extracted frequency band, causing an incorrect diagnosis.

This problem is solved by the use of spectral filters, as it was checked in the previous chapters, since they can extract frequency ranges narrower than the DWT filters, improving the accuracy of the diagnosis.

The results of diagnosis of mixed eccentricity for case 1, replacing the DWT filtering step performed in the previous paragraph, by spectral filtering stages are shown in the following paragraphs.

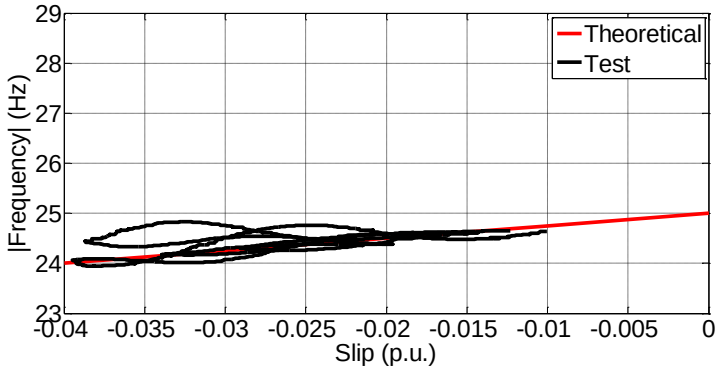

Fig. 164 Instantaneous frequency of the fault component of mixed eccentricity in the slip domain extracted through a spectral filter for case 1. Commercial squirrel cage rotor induction machine in healthy state. Generator mode..

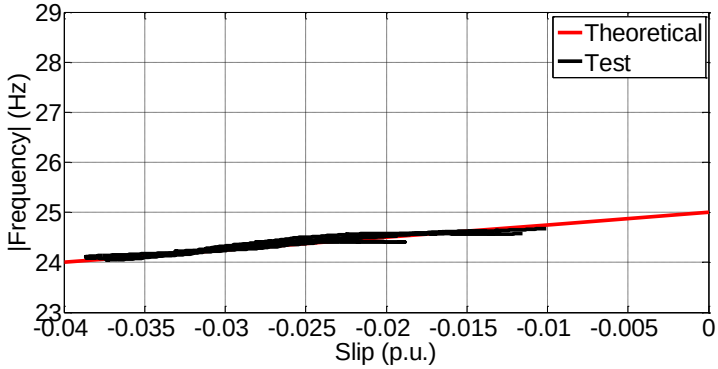

Fig. 165 Instantaneous frequency of the fault component of mixed eccentricity in the slip domain extracted through a spectral filter for case 1. Commercial squirrel cage rotor induction machine with mixed eccentricity. Generator mode.

The direct consequence of the change of filters is that the extracted bandwidth is reduced, since in the case of the DWT filters the narrowest frequency band that can be drawn is [19.53, 39.06] Hz, whereas in the case of the spectral filters the extracted frequency band takes the frequency range [24, 24.80] Hz.

The graphic results are shown in Fig. 164, in the case of healthy machine whose results with DWT filters are shown in Fig. 162, whereas in Fig. 165 is shown the result of the diagnosis of the machine with mixed eccentricity, whose results with DWT filters is shown in Fig. 163.

The objective parameters of the diagnosis (Table 36) agree with the graphical results. The first difference from the results with the DWT filters is the increase in the similitude coefficient for the case of healthy machine. This effect is a direct consequence of the filtering performed by the spectral filters since the extracted frequency band is narrower than the one extracted by the DWT filters, greatly improving the accuracy.

TABLE 36. OBJECTIVE PARAMETERS FOR CASE 1. DIAGNOSIS OF A MIXED ECCENTRICITY THROUGH THE EXTRACTION OF THE FAULT COMPONENT WITH A SPECTRAL FILTER. SQUIRREL CAGE ROTOR INDUCTION MACHINE WORKING AS GENERATOR. DURATION OF THE NON-STATIONARY STOCHASTIC REGIME 20 SECONDS

Test	S	m	b	E_f	Computation time
Theoretical		25	25		
Healthy	0.873	16.71	24.86	0.0001	0.18
Faulty	1.000	23.26	24.97	0.01	0.21

Regarding the absolute value of the computed energy, a reduction is noticed. This again is consistent with the already exposed reasoning: the extracted frequency bands are narrower, and then the value of the energy content should be smaller. This effect does not prevent the correct diagnosis of the fault since the comparison of the energy of the fault component versus energy value in healthy state energy shows an increase of two orders of magnitude.

Besides, of the advantages already discussed of spectral filters, it must also be considered its faster speed in the diagnosis process as this is reduced from 0.34 seconds, necessary for the diagnosis with DWT filters, until 0.21 seconds with the spectral filters, what is a reduction of 13% in the diagnosis time.

2.1.2 SQUIRREL CAGE ROTOR INDUCTION MACHINE: CASE 2, 3 AND 4

Table 37 summarises the test conditions of those that the squirrel cage rotor induction machines have underwent for the validation of the methodology of the mixed eccentricity fault.

The graphic results for each case are shown in Fig. 166, Fig. 167 and Fig. 168 respectively. Each of these figures consists of six figures where figure a) denotes the evolution of the speed that the tested machine has been subjected, figure b) shows the evolution of the current, figure c) shows the qualitative diagnosis for healthy machine when the fault component is extracted with a DWT filter whereas figure d) shows the corresponding result when the machine is affected by a mixed eccentricity. Figures e) and f) are the analogues to figures c) and d) when the fault component is extracted through a spectral filter.

Table 38 summarizes the numerical result (quantitative) of each of the three performed tests.

TABLE 37. CONDITIONS OF THE PERFORMED TEST FOR THE VALIDATION OF THE PROPOSED METHODOLOGY FOR THE DETECTION OF A MIXED ECCENTRICITY IN SQUIRREL CAGE ROTOR INDUCTION MACHINES

Case	Rotor	Mode	Test time	Sampling Frequency
2	Squirrel Cage	Generator	10	5 kHz
3	Squirrel Cage	Motor	20	5 kHz
4	Squirrel Cage	Motor	10	5 kHz

TABLE 38. QUANTITATIVE RESULTS FOR CASE 2, 3 AND 4 FOR THE VALIDATION OF THE METHODOLOGY FOR THE DETECTION OF A MIXED ECCENTRICITY FAULT IN SQUIRREL CAGE INDUCTION ROTOR MACHINES

Case	Filter	Fault Freq.	Extr. Freq.	Test	*S*	*m*	*b*	*E*	Comp. time
		Hz	Hz	**Theo.**		25	25	%	sec
2	**DWT**	[24.09, 24.66]	[19.53, 39.06]	**Healthy**	0	-32.33	26.34	0.0064	0.34
				Faulty	0.98	26.65	25.08	0.0576	0.35
	Spectral		[24.09, 24.66]	**Healthy**	1	21.85	24.92	0.0001	0.18
				Faulty	1	17.30	24.83	0.01	0.18
3	**DWT**	[25.84, 27.17]	[19.53, 39.06]	**Healthy**	0.13	77.66	22.11	0.0049	0.31
				Faulty	0.86	23.81	25.06	0.0289	0.33
	Spectral		[25.80, 27.20]	**Healthy**	0.99	23.87	25.07	0.0004	0.19
				Faulty	1	25.47	24.92	0.0064	0.21
4	**DWT**	[25.91, 27.17]	[19.53, 39.06]	**Healthy**	0.11	29.97	25.49	0.0049	0.30
				Faulty	1.00	26.38	24.86	0.0289	0.30
	Spectral		[25.80, 27.20]	**Healthy**	1.00	23.52	25.13	0.0004	0.18
				Faulty	1.00	21.61	25.21	0.0064	0.18

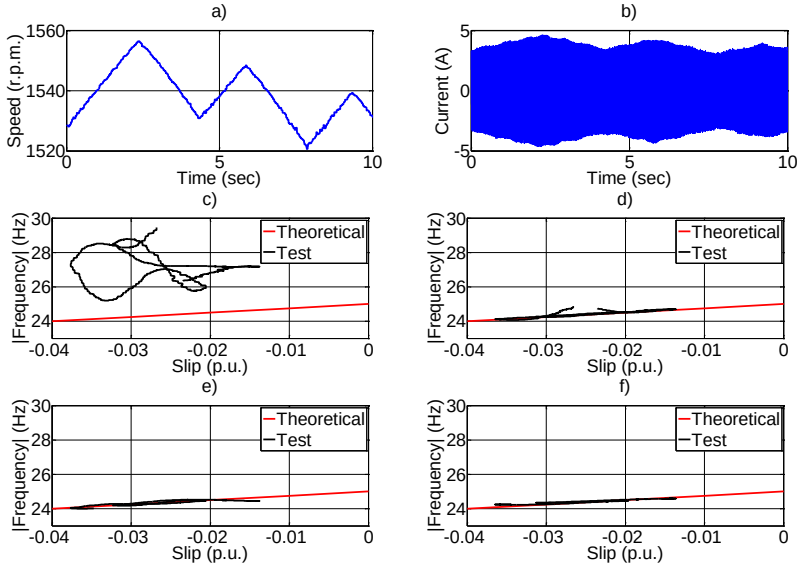

Fig. 166 Case 2: Squirrel cage rotor induction machine working as generator. a) Speed b) Current c) Instantaneous frequency for healthy machine (DWT filter) d) Instantaneous frequency for a machine with mixed eccentricity (DWT filter) e) Instantaneous frequency for a healthy machine (spectral filter) f) Instantaneous frequency for a machine with mixed eccentricity (spectral filter)

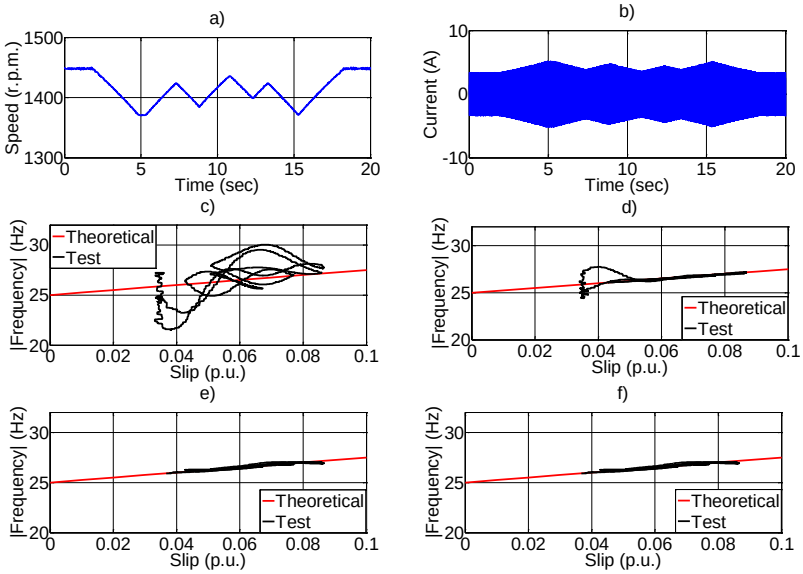

Fig. 167 Case 3: Squirrel cage rotor induction machine working as motor. a) Speed b) Current c) Instantaneous frequency for healthy machine (DWT filter) d) Instantaneous frequency for a machine with mixed eccentricity (DWT filter) e) Instantaneous frequency for a healthy machine (spectral filter) f) Instantaneous frequency for a machine with mixed eccentricity (spectral filter)

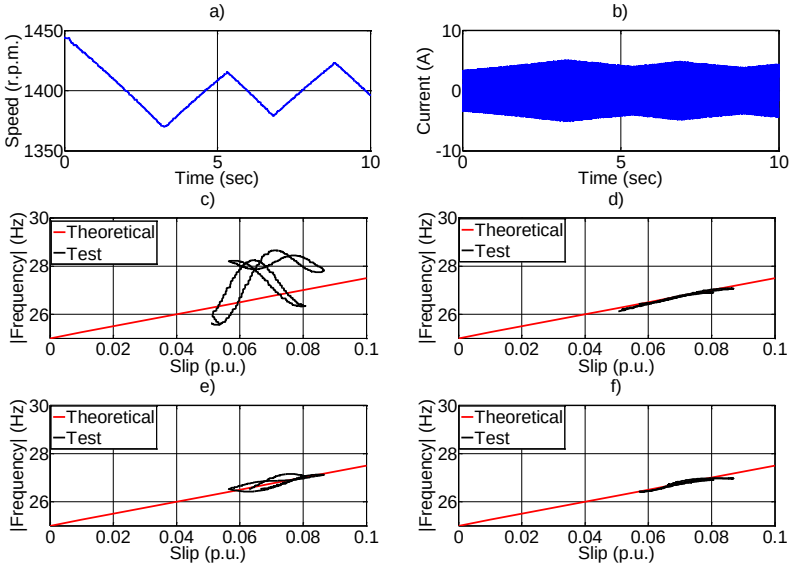

Fig. 168 Case 4: Squirrel cage rotor induction machine working as motor. a) Speed b) Current c) Instantaneous frequency for healthy machine (DWT filter) d) Instantaneous frequency for a machine with mixed eccentricity (DWT filter) e) Instantaneous frequency for a healthy machine (spectral filter) f) Instantaneous frequency for a machine with mixed eccentricity (spectral filter)

Despite the differences in the performed tests (different speed profiles, duration of the analysed transient regime of operation), the conclusions drawn from the analysis of the results are equivalent to those given above for case 1. Thus, it can be said that the methodology has been successfully validated for the diagnosis of squirrel cage rotor induction machine irrespective of the speed fluctuations, duration of the transient and operating regime.

2.2 WOUND ROTOR INDUCTION MACHINE

The methodology is also validated on wound rotor induction machines working as generator and motor. The tested machine is connected to the grid at a voltage of 230 V (delta) and 50 Hz. The features of the tested machine can be found in Annex I.

Similarly, that in the case of squirrel cage rotor induction machines, two wound rotor induction machines are tested to perform the validation. The mixed eccentricity fault is created in the same way that the already exposed for the squirrel cage rotor induction machine, that is, the original bearings of the machines are replaced by a system of bearings whose inner diameter is greater than the original diameter whereas the inner is smaller. The adjustment of these smaller bearings to the shaft and end bell of the machine is carried out by two precision bearing houses.

The bearing houses in the reference machine, healthy machine, are concentric, whereas for the machine with eccentricity have an eccentricity of 0.1 mm for both the inner and the outer bearing houses that produces a 50% of static eccentricity and a 50% of dynamic eccentricity. The arrangement of the bearings is identical to that shown in Fig. 156.

The electrical scheme of the test bed is shown in Fig. 169. The machine under test is coupled to another asynchronous machine, as in the previous case, that controls the speed of the tested machine forcing both generator and motor mode. The control of the auxiliary machine is identical to the one of previous section (connecting to the network through a VSD controlled by a PLC) therefore, it also enables the implementation of automated speed profiles facilitating the comparison of the results.

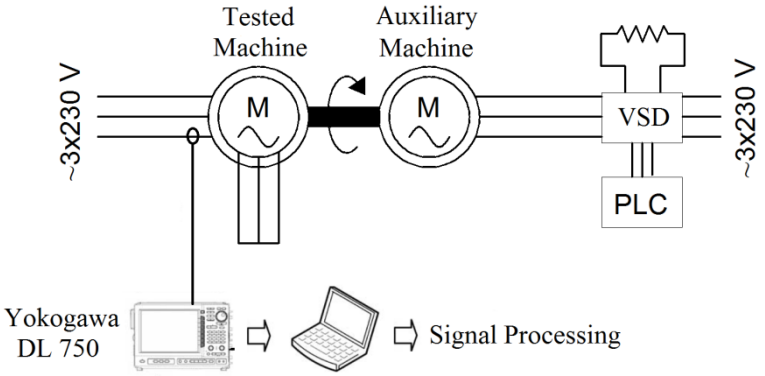

Fig. 169 Electrical scheme for the test on the wound rotor induction machine

Fig. 170 Picture of the test bed for the test of the wound rotor induction machine with a mixed eccentricity

TABLE 39. CONDITIONS OF THE PERFORMED TEST FOR THE VALIDATION OF THE PROPOSED METHODOLOGY FOR THE DETECTION OF A MIXED ECCENTRICITY IN WOUND ROTOR INDUCTION MACHINES

Case	Rotor	Mode	Test time	Sampling Frequency
5	Wound	Generator	30	5 kHz
6	Wound	Generator	10	5 kHz
7	Wound	Motor	30	5 kHz
8	Wound	Motor	10	5 kHz

TABLE 40. QUANTITATIVE RESULTS FOR CASE 5, 6, 7 AND 8 FOR THE VALIDATION OF THE METHODOLOGY FOR THE DETECTION OF A MIXED ECCENTRICITY FAULT IN WOUND ROTOR INDUCTION MACHINES

Case	Filter	Fault Freq.	Extr. Freq.	Test	*S*	*m*	*b*	*E*	Comp. time
		Hz	Hz	**Theo.**		25	25	%	sec
5	**DWT**	[24.16, 24.89]	[19.53, 39.06]	**Healthy**	0.75	37.93	25.31	0.0064	0.41
				Faulty	0.98	24.78	24.98	0.0196	0.44
	Spectral		[24.16, 24.89]	**Healthy**	1.00	23.54	24.98	0.0016	0.27
				Faulty	1.00	24.86	24.98	0.0036	0.28
6	**DWT**	[24.16, 24.78]	[19.53, 39.06]	**Healthy**	0.86	46.54	25.39	0.0081	0.28
				Faulty	0.99	26.67	25.02	0.0256	0.28
	Spectral		[24.10, 24.80]	**Healthy**	1.00	18.22	24.87	0.0016	0.19
				Faulty	1.00	25.29	24.99	0.0036	0.19
7	**DWT**	[25.14, 25.93]	[19.53, 39.06]	**Healthy**	0.46	87.92	24.76	0.0036	0.38
				Faulty	0.95	21.91	25.08	0.0324	0.40
	Spectral		[25.91, 27.17]	**Healthy**	1.00	23.91	25.03	0.0004	0.26
				Faulty	1.00	23.89	25.02	0.0036	0.26
8	**DWT**	[25.27, 25.93]	[19.53, 39.06]	**Healthy**	0.20	72.75	24.73	0.0025	0.33
				Faulty	1.00	25.55	25.00	0.0144	0.30
	Spectral		[25.20, 26.00]	**Healthy**	1.00	14.10	25.27	0.0004	0.20
				Faulty	1.00	24.82	25.00	0.0036	0.21

The signal acquisition is performed using the same equipment as in the previous cases. The sampling frequency is 5 kHz.

The scheme followed for the validation of methodology for wound rotor induction machines is the same that was followed for the squirrel cage rotor induction machine, repeating the same series of tests.

Since the methodology has no major changes when it is set on wound rotor induction machines, it is directly shown the results without going into the details, since they have been discussed in the previous section.

Analogue to the results shown for the case of squirrel cage rotor induction machines, Table 39 shows the conditions of the tests that the tested machines have been subjected, whereas Table 40 shows the quantitative results. Finally, Fig. 171-Fig. 174 show the graphical results (qualitative) for each of the performed tests in the same way as in the previous section.

The analysis of the results for the wound rotor induction machines shows no significant differences from the results for squirrel cage rotor induction machines before the different conditions to which the machines have been subjected (different speed profiles, duration of the analysed transient regime of operation).

Therefore, it can be stated that the proposed methodology is valid for the diagnosis of mixed eccentricity in wound rotor induction machines in non-stationary stochastic conditions irrespective of its functioning regime.

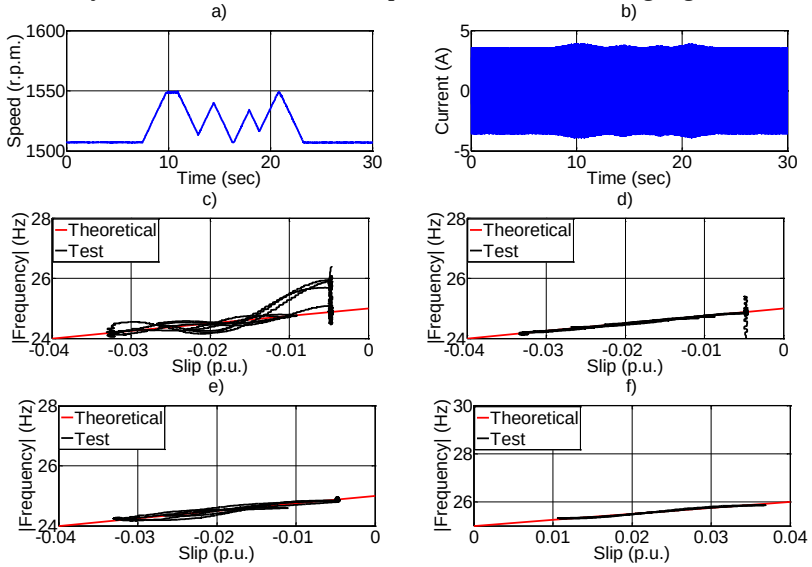

Fig. 171 Case 5: Wound rotor induction machine working as generator. a) Speed b) Current c) Instantaneous frequency for healthy machine (DWT filter) d) Instantaneous frequency for a machine with mixed eccentricity (DWT filter) e) Instantaneous frequency for a healthy machine (spectral filter) f) Instantaneous frequency for a machine with mixed eccentricity (spectral filter)

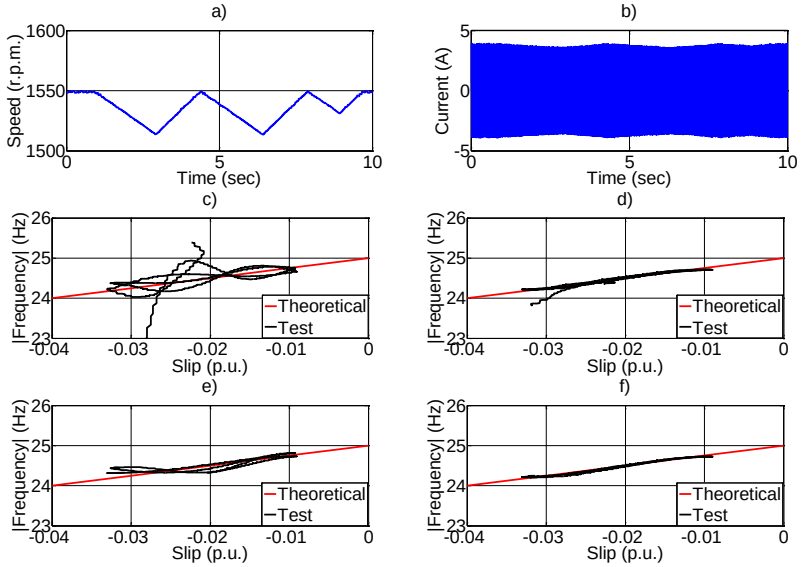

Fig. 172 Case 6: Wound rotor induction machine working as generator. a) Speed b) Current c) Instantaneous frequency for healthy machine (DWT filter) d) Instantaneous frequency for a machine with mixed eccentricity (DWT filter) e) Instantaneous frequency for a healthy machine (spectral filter) f) Instantaneous frequency for a machine with mixed eccentricity (spectral filter)

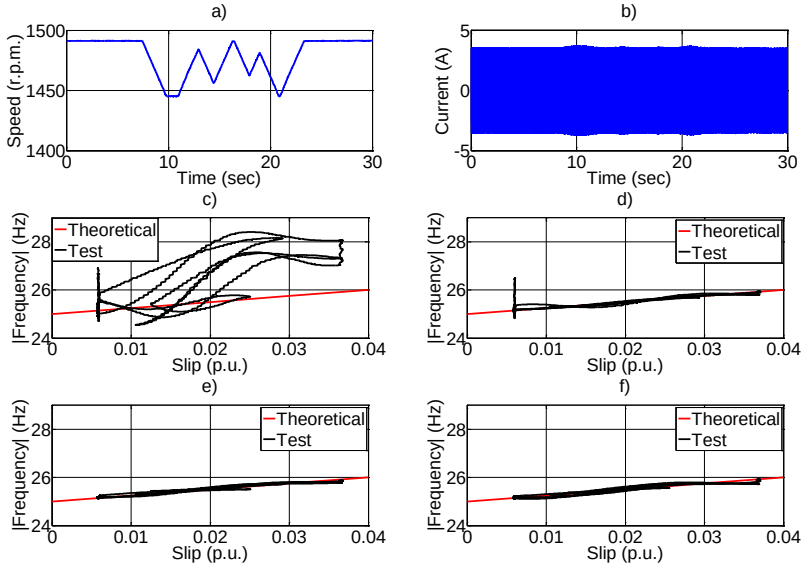

Fig. 173 Case 7: Wound rotor induction machine working as motor. a) Speed b) Current c) Instantaneous frequency for healthy machine (DWT filter) d) Instantaneous frequency for a machine with mixed eccentricity (DWT filter) e) Instantaneous frequency for a healthy machine (spectral filter) f) Instantaneous frequency for a machine with mixed eccentricity (spectral filter)

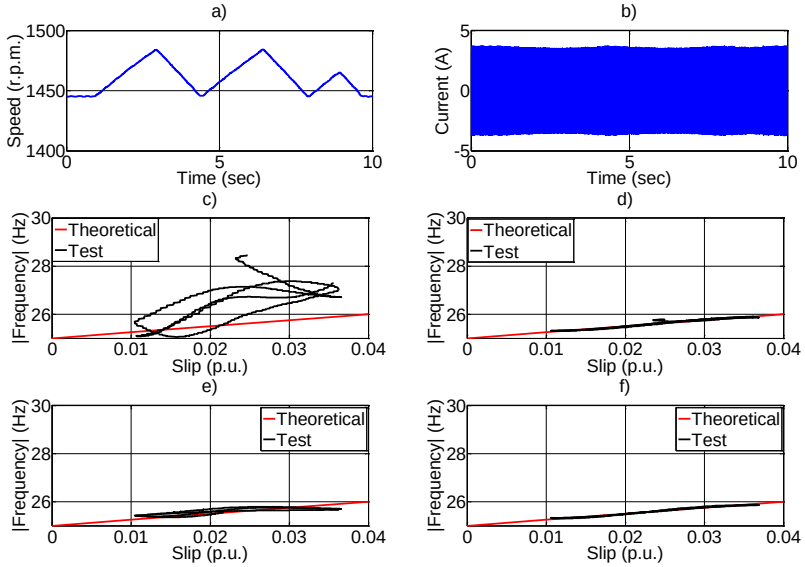

Fig. 174 Case 8: Wound rotor induction machine working as motor. a) Speed b) Current c) Instantaneous frequency for healthy machine (DWT filter) d) Instantaneous frequency for a machine with mixed eccentricity (DWT filter) e) Instantaneous frequency for a healthy machine (spectral filter) f) Instantaneous frequency for a machine with mixed eccentricity (spectral filter)

3 SUMMARY AND CONCLUSIONS OF THE CHAPTER

The correct diagnosis of the mixed eccentricity fault through the proposed methodology has been validated through multiple tests in this chapter.

The diagnosis of the mixed eccentricity has been carried out satisfactorily on four induction machines, two with squirrel cage rotor, two of wound rotor, in non-stationary stochastic regimes, working as generator or motor with mixed eccentricity and in healthy state.

This chapter has demonstrated the independence of the evolution of the speed and duration of the stochastic transient for the result of the diagnosis through the developed methodology.

The diagnosis of the mixed eccentricity shows good results irrespective of the filter (DWT or spectral) for the extraction of the fault component.

The comparison of both filtering methods shows that the spectral filters ire more accurate than the DWT filters for the extraction of the fault components due to the smaller extracted bandwidth, preventing the inclusion of unwanted components in it.

The computational cost of the spectral filters is smaller than the computational cost of the diagnosis with DWT filters, again favouring the application of spectral filters for the extraction of the fault components.

CHAPTER XII: DIAGNOSIS OF MACHINES FED FROM VSD AT STEADY AND VARIABLE FREQUENCY

1 INTRODUCTION

The proposed diagnostic methodology in this thesis has been validated in previous chapters for the diagnosis of rotor asymmetries (Chapter IX), stator asymmetries (Chapter X) and mixed eccentricity (Chapter XI) for induction machines fed directly from the electrical network operating in non-stationary stochastic regimes.

However, more and more, induction machines are supplied from Variable Speed Drives (VSD). Feeding an induction machine from those devices can be performed at constant or variable frequency according to the needs of each industrial process.

In this chapter, it is shown the ability of the methodology already discussed and validated to be adapted to the diagnosis of induction machines when they are fed from VSD, at both constant and variable frequency.

The diagnosis of electric induction machines fed from VSD is not the subject of this thesis, even though all the equations introduced have been developed as general as possible, allowing a direct application in the event that the machines are fed from VSD.

The verification of the developed technique for machines fed from VSD is performed by the analysis of a squirrel cage rotor induction machine with mixed eccentricity working as motor in non-stationary stochastic regime. To reach such goal, three tests will be performed: (i) the first diagnoses the mixed eccentricity fault in a squirrel cage rotor induction machine fed from a VSD with a constant supply frequency of 25 Hz (ii) The second test will diagnose a mixed eccentricity fault in a squirrel cage rotor induction machine fed from a VSD with variable frequency between 26 and 30 Hz at constant slip. (iii) The third diagnosed case will be a squirrel cage rotor induction machine fed from a VSD at variable frequency between 26 and 30 Hz with variable slip.

In this chapter, unlike the previous ones, the extraction of the fault components will be carried out only through the DWT filters. This decision is a consequence of the better behaviour of spectral filter, considering that if it is possible to diagnose the machine with DWT filters correctly, the use of spectral filters will improve the results.

Regarding the computation of the energy of the fault component, it is highlighted that its computation is performed only in the time domain, since the aim of this chapter is to demonstrate the possibility of the use of the methodology on machines fed from VSD, allowing an in-depth study for future work.

The fault component of mixed eccentricity that allows the diagnosis of the induction machine evolves in the frequency spectrum of stator current (Chapter III):

$$f_{exc} = f_{red} - \frac{f_{red}}{p}(1-s) \tag{186}$$

The aim of the methodology is to isolate the frequency band in which the alleged fault harmonic evolves, compute its energy and determine if its origin is due to the mixed eccentricity.

In the event that the computed energy exceeds the preset threshold, with the instantaneous frequency is determined if the origin of extracted energy of the fault component is a consequence of the mixed eccentricity or other causes.

One of the main differences between this chapter and the previous chapter is how the machines are fed since in this chapter the machines are fed from a VSD whose features can be found in Annex II.

The control of the VSD that feeds the tested machine is at voltage vs. frequency scalar control without slip compensation. The rated voltage of the tested machines is 230 V (delta) at 50 Hz Thus, the V/f has a value of

$$\frac{V}{f} = \frac{230}{50} = 4.6\,\frac{V}{Hz} \tag{187}$$

that is, the supply voltage of the machine is function of the frequency that is supplied to maintain a constant flux in the machine regardless of the frequency at which the machine operates.

2 MACHINE FED FROM A VSD AT CONSTANT FREQUENCY AND VARIABLE SLIP

The feasibility of the diagnosis through the developed technique in this thesis is carried out, first, on a squirrel cage rotor induction machine, working as motor, subjected to a stochastic regime when the machine is fed from a VSD at 25 Hz constant frequency.

The tested machines in this section are the same as those tested in the previous chapter. The features of the machines are in Annex I. The procedure followed to force the mixed eccentricity is in Chapter XI-2.1.

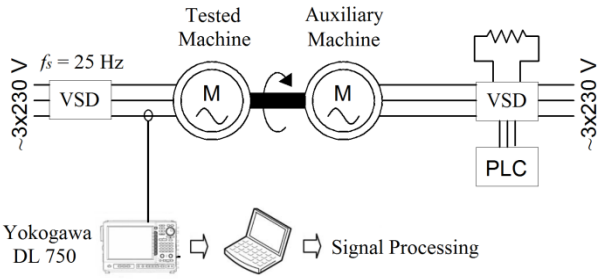

Fig. 175 Electric scheme of the test bed for the evaluation of the methodology when the machine is fed from a VSD at constant frequency.

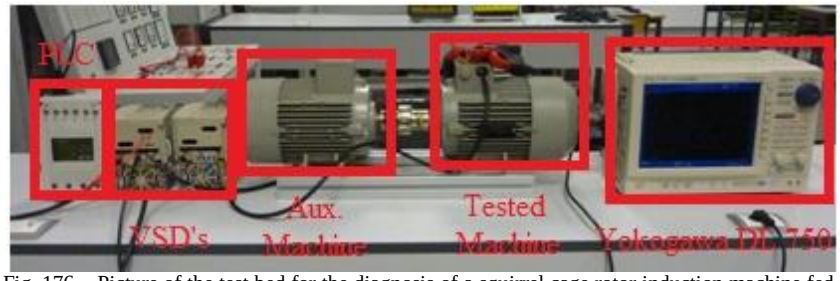

Fig. 176 Picture of the test bed for the diagnosis of a squirrel cage rotor induction machine fed from a VSD at a constant frequency with mixed eccentricity.

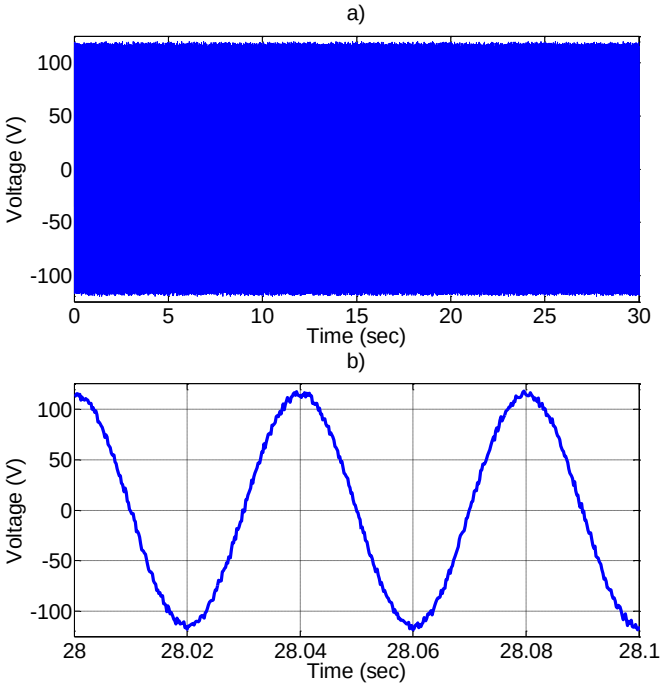

Fig. 177 Supply voltage when the machine is fed from the VSD at 25 Hz. A) General vision b) Detail

The electrical scheme for the test bed is shown in Fig. 175, whereas Fig. 176 shows a picture. The tested machine is coupled to another machine asynchronous, similar to the tested one, which allows loading it. Feeding the electrical machine at 25 Hz from the VSD means that the rms voltage supplied to the machine is 115 V rms. The evolution of the supply voltage is shown in Fig. 177.

The auxiliary machine is also fed from a VSD. The VSD is controlled through a PLC the same way as in the preceding chapters. This configuration allows programming fixed sequences in the speed profile of the tested machine under non-stationary stochastic regimes while having the same speed profile in all tests, facilitating the comparison of the results.

The stator current is measured with a clamp and the speed by an encoder. Both devices are connected to a digital oscilloscope DL Yokohama 750 that

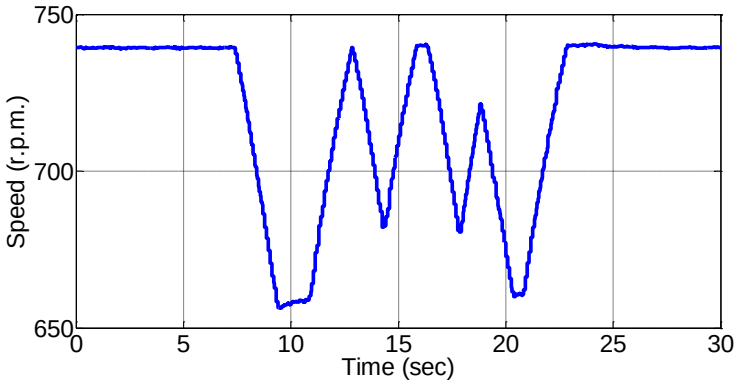

Fig. 178 Evolution of the speed in non-stationary stochastic conditions. Squirrel cage rotor induction machine working as motor fed from a VSD at 25 Hz.

has an AD 16 bit acquisition card. The oscilloscope is connected via intranet to a PC where the acquired signals are processed. The sampling frequency used in the tests was 5 kHz.

The features of the auxiliary switchgear (clamp and encoder) and digital oscilloscope can be found in Annex II.

The validation of the methodology begins imposing the speed profile shown in Fig. 178 to the tested machine. Fig. 179 shows the evolution of the stator current in the test. The acquisition time is 30 seconds.

Due to imposed speed fluctuations on the machine (Fig. 178), the slip, which the machine is subjected, is bounded in the range [0.013, 0.12], and the fault component to be extracted is in the range [12.66, 14.06] Hz (186).

The extraction of the fault component requires the DWT filter approximations a_7 and a_8 since the sampling frequency is 5 kHz and the frequency range where the fault component evolves is [12.66, 14.06] Hz (186).

$$nC = \text{int}\left[\frac{\log\frac{f_s}{f_2}}{\log(2)} - 1\right] = \text{int}\left[\frac{\log\frac{5000}{14.06}}{\log(2)} - 1\right] = 7 \tag{188}$$

$$nNC = \text{int}\left[\frac{\log\frac{f_s}{f_1}}{\log(2)}\right] = \text{int}\left[\frac{\log\frac{5000}{12.65}}{\log(2)}\right] = 8 \tag{189}$$

The selection of these decompositions allow the extraction of the frequency band [9.77, 19.53] Hz, band that contains the frequency range where fault evolves but not the fundamental component.

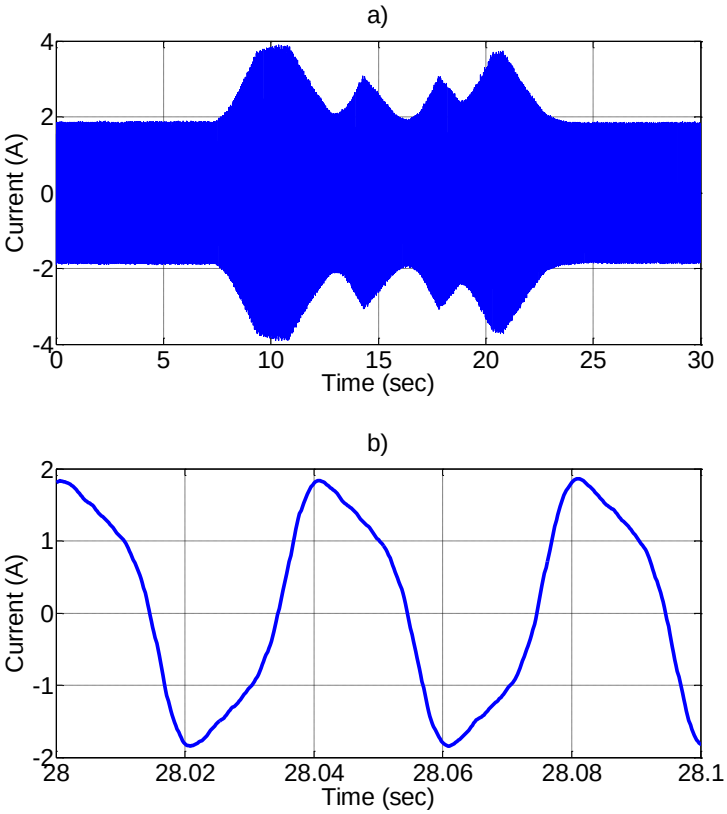

Fig. 179 Acquired stator current in non-stationary stochastic regime consequence of the imposed speed oscillations in Fig. 178 when the machine is fed from a VSD at 25 Hz. a) General vision b) Detail

As in previous chapters, after the extraction of the fault component, its energy is computed and if it exceeds the preset threshold value, it must be determined the origin of the computed energy through the computation of the instantaneous frequency.

The implementation each of the stages of the proposed methodology produces the graphic results shown in Fig. 180, for healthy machine, and Fig. 181 for a machine with mixed eccentricity.

Fig. 180 shows that the evolution of the fault component does not overlap with the theoretical pattern. This indicates that the energy of the fault component is not due to a mixed eccentricity and thus, the machine is in a healthy state.

In Fig. 181, there is seen a tendency in the evolution of the instantaneous frequency of the fault component to overlap the theoretical pattern, indicating that the energy of the fault component is because of the mixed eccentricity.

The objective parameters of diagnosis (Table 41) are consistent with graphic results, since the similitude coefficient is almost zero in the case of healthy machine (S = 0.059), whereas the value is close to 1 (S = 0.878) for the case of mixed eccentricity. On the other hand, the regression parameters

are similar to the theoretical in the case of faulty state whereas there is no similarity when the machine is in healthy state.

The value of the energy of the fault component in the case of mixed eccentricity is 625% higher than the value of the energy in the healthy case showing the viability of the method for the diagnosis when the machine is fed from a VSD at constant frequency.

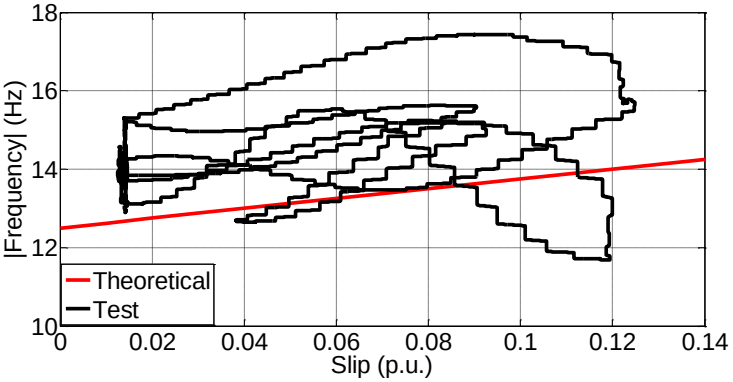

Fig. 180 Instantaneous frequency for the fault component of mixed eccentricity in the slip domain extracted through a DWT filter when the machine is fed from a VDS at 25 Hz. Commercial squirrel cage rotor induction machine in healthy state. Motor mode.

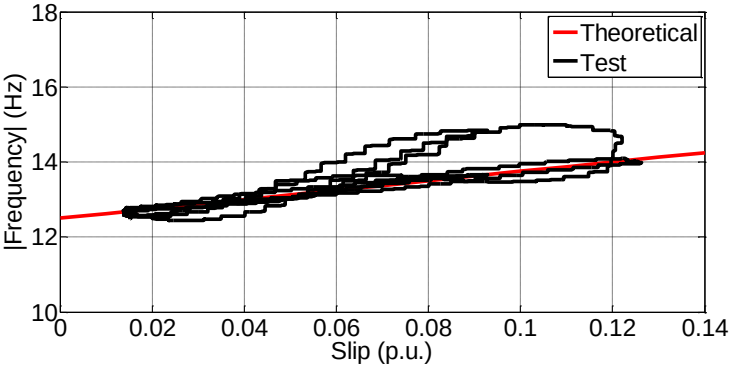

Fig. 181 Instantaneous frequency for the fault component of mixed eccentricity in the slip domain extracted through a DWT filter when the machine is fed from a VDS at 25 Hz. Commercial squirrel cage rotor induction machine with mixed eccentricity. Motor mode.

TABLE 41. OBJECTIVE PARAMETERS FOR THE DIAGNOSIS OF A MIXED ECCENTRICITY THROUGH THE EXTRACTION OF THE FAULT COMPONENT WITH A DWT FILTER. COMMERCIAL SQUIRREL CAGE ROTOR INDUCTION MACHINE FED FROM A VSD AT 25 HZ, WORKING AS MOTOR

Test	***S***	***m***	***b***	E_t	**Computation time**
Theoretical		12.5	12.5		
Healthy	0.059	0.36	10.02	0.0036	0.39
Faulty	0.878	15.21	12.44	0.0225	0.43

3 MACHINE FED FROM A VSD AT VARIABLE FREQUENCY AND CONSTANT SLIP

The application of the technique is also possible when the machine is fed from a VSD that supplies voltage at variable frequencies when the machine operates at constant slip.

In this section is tested the same machine as in the previous section, feeding it through a VSD in the frequency range of 26-30 Hz with constant slip.

To achieve a constant slip, the machine is decoupled from the auxiliary machine used in the preceding test adding a disk that increases the inertia of the system. Thus, the machine is tested in no load state and since the mechanical losses have a low enough value it is achieved a steady enough slip for the application of the methodology.

The electric scheme of the test bed is shown in Fig. 182. Fig. 183 shows a picture of the assembly.

The feeding of the machine to be tested is carried out through a VSD whose control strategy is V/f with value of 4.6 V/Hz. The machine is operated in the frequency range [26, 30] Hz and since it is operating under no load conditions, the evolution of the speed is nearly proportional to the frequency.

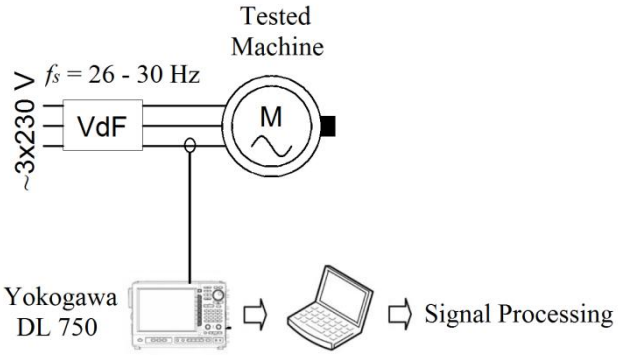

Fig. 182 Electrical scheme of the test bed for the evaluation of the methodology when the machine is fed from a VSD at variable frequency.

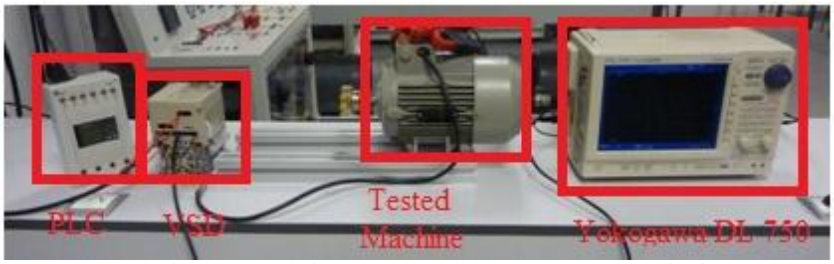

Fig. 183 Picture of the assembly of a squirrel cage rotor induction machine fed from a VSD, at variable frequency, with mixed eccentricity.

The value of the increasing/decreasing frequency ramp of the VSD was set at 2 Hz/second between the two set points (26 and 30 Hz).

Enabling and disabling the set point values was achieved by a PLC, whose features are listed in Annex II, that controls the drive with a DC voltage of 5V value The frequency inverter get shown in Fig. 184.a, whereas the PLC control signal to the converter is shown in Fig. 184.b.

The stator current is measured with a clamp and the speed by an encoder. Both devices are connected to a digital oscilloscope DL Yokohama 750 that has an AD 16 bit acquisition card. The oscilloscope is connected via intranet to a PC where the acquired signals are processed. The sampling frequency used in the test was 5 kHz.

The actual frequency evolution (Fig. 185) of the machine is computed by the extraction of the instantaneous frequency of the fundamental component of the measured current waveform in the test, shown in Fig. 186.

On the other hand, the voltage supplied to stator windings is shown in Fig. 187.

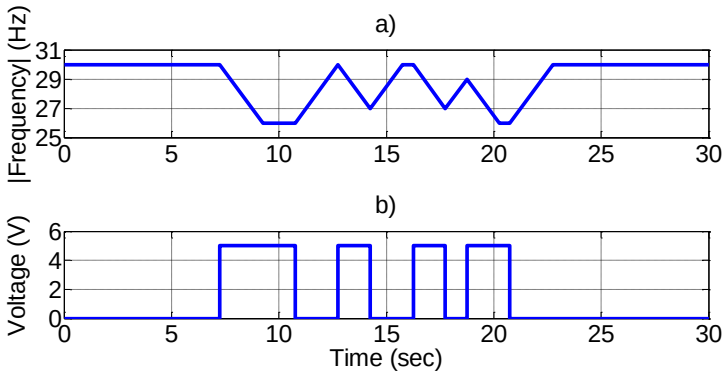

Fig. 184 a) Set points values of frequency for the VSD b) Control signal of the references of the VSD (0 V - 30 Hz; 5 V - 26 Hz).

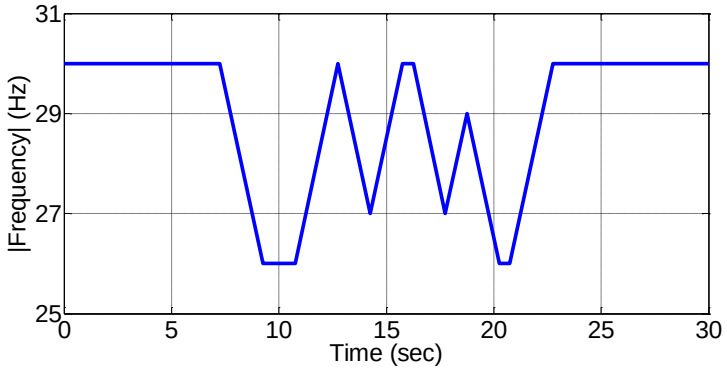

Fig. 185 Actual evolution of the fundamental frequency of the stator current

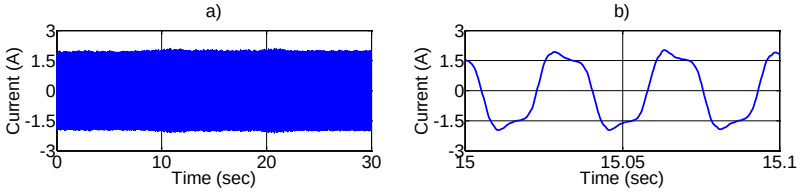

Fig. 186 Acquired stator current for a non-stationary stochastic regime consequence of the imposed frequency oscillations when it is fed from a VSD with a variable frequency in the range [26, 30] Hz at constant slip. a) General vision b) Detail

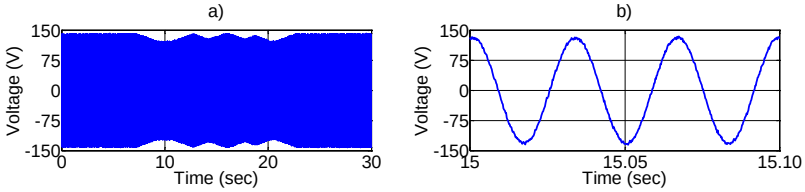

Fig. 187 a) General vision of the voltage supplied to the tested machine b) Detail

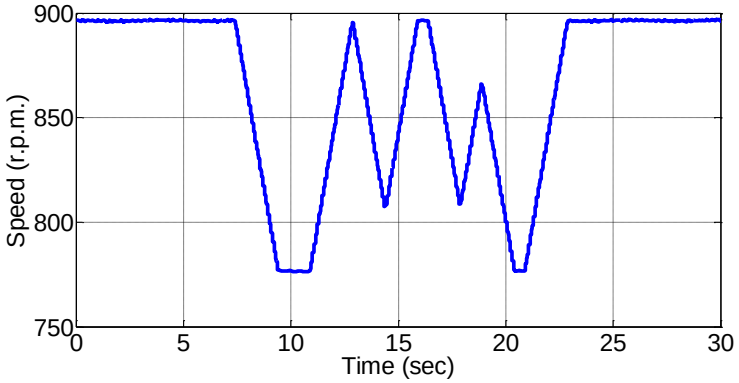

Fig. 188 Evolution of the acquired speed when the machine is fed with stochastic frequencies . Squirrel cage rotor induction machine, fed from a VSD with variable frequencies from 26 to 30 Hz.

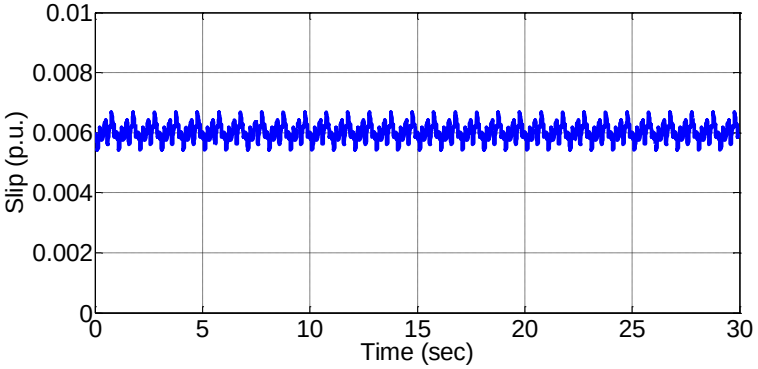

Fig. 189 Slip when the machine is fed from a VSD with variable frequency in the range [26, 30] Hz.

Fig. 188 shows the evolution of the speed during the test. Fig. 189 depicts the evolution of the computed slip from frequency and speed waves. It is noticed that the slip is almost constant throughout the stationary stochastic regime.

As a result of the frequency fluctuations that feed the machine, its operating speed is not constant working under a non-stationary stochastic regime.

The evolution of the speed is similar to the evolution of the previous sections since the same program to control the VSD that feeds the machine to be tested is used to control the speed in the previous chapters.

As a consequence of the frequency fluctuations (Fig. 185) and given that the machine operates at substantially constant slip (s = 0.006), the fault component of mixed eccentricity is bounded in the range [13.08, 15.09] Hz (186).

The extraction of the fault component requires the DWT filter approximations a_7 and a_8 as the sampling frequency is 5 kHz and the frequencies where the fault component evolves are [13.08, 15.09] Hz

The selection of these decompositions allow the extraction of the frequency band [9.77, 19.53] Hz, band that contains the frequency range where fault evolves but not the fundamental component.

As in previous chapters, after the extraction of the fault component its energy is computed and if it exceeds the preset threshold value, it must be determined the origin of the computed energy with the instantaneous frequency.

The results following the application of the diagnostic technique are introduced in Fig. 190, healthy machine, and Fig. 191, machine with mixed eccentricity.

Since in this case the slip is nearly constant, as shown in Fig. 189, it is depicted the plane instantaneous frequency-supply frequency. This depiction of the fault component using as independent variable the frequency of the fundamental component of the supply voltage is similar to that already shown in the previous chapters when the machine was fed with a constant frequency. In this section, the slip and the supply frequency swap roles since it is the slip which remains constant while the supply frequency varies.

Fig. 190 shows that the evolution of the fault component for healthy machine does not overlap with the theoretical pattern. Thus, it can be ensured that the energy of fault component is not due to a mixed eccentricity and, therefore, the machine is in a healthy state.

In Fig. 191, the evolution of the fault component tends to concentrate on the theoretical pattern. This ensures that the energy of the extracted fault component is mainly due to a mixed eccentricity and thus, if the value of the energy is high enough, it can be ensured that the machine is under a mixed eccentricity fault.

The objective parameters of the diagnosis (Table 42) are consistent with the graphic results, since the similitude coefficient is almost zero in the case of healthy machine (S = 0.227), whereas the value is 1 (S = 1) for the case of mixed eccentricity machine. On the other hand, the regression parameters are

similar to the theoretical in the case of faulty state whereas there is no similarity when the machine is in a healthy state.

The value of the energy of the fault component in the case of mixed eccentricity is two orders of magnitude greater than the value of the energy in the healthy case showing the viability of the method for the diagnosis of mixed eccentricity when the machines are fed from VSD at constant slip.

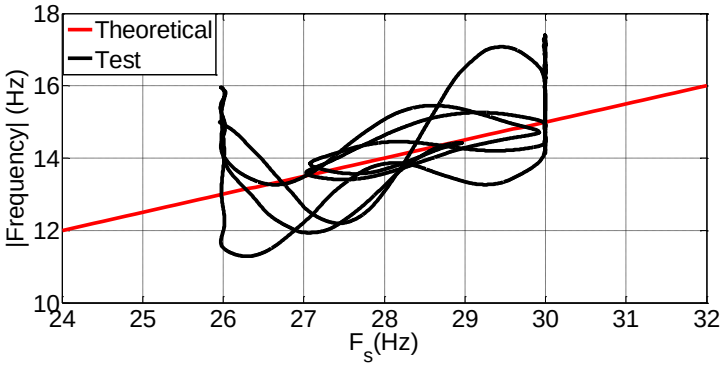

Fig. 190 Instantaneous frequency of the fault component of mixed eccentricity in the supply frequency domain extracted through a DWT filter when the machine is fed from a VSD in the frequency range 26 to 30 Hz. Commercial squirrel cage rotor induction machine in healthy state working as motor.

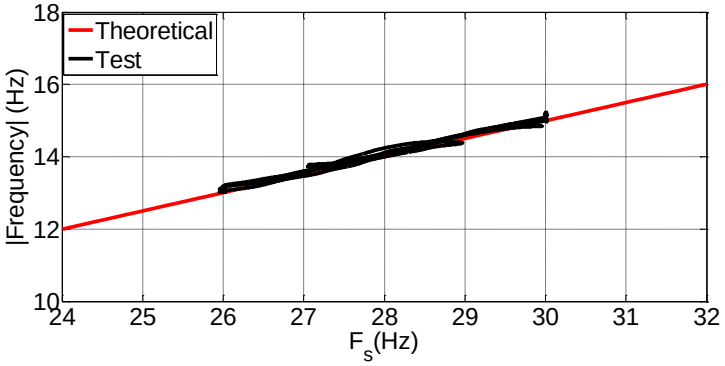

Fig. 191 Instantaneous frequency of the fault component of mixed eccentricity in the supply frequency domain extracted through a DWT filter when the machine is fed from a VSD in the frequency range 26 to 30 Hz. Commercial squirrel cage rotor induction machine with mixed eccentricity working as motor.

TABLE 42. OBJECTIVE PARAMETERS OF DIAGNOSIS FOR A MIXED ECCENTRICITY THROUGH THE EXTRACTION OF THE FAULT COMPONENT WITH A DWT FILTER. COMMERCIAL SQUIRREL ROTOR CAGE INDUCTION MACHINE FED FROM A VSD WITH VARIABLE FREQUENCY WITH CONSTANT SLIP WORKING AS MOTOR

Test	***S***	***m***	***b***	E_t	**Computation time**
Theoretical		0.503	0		
Healthy	0.227	0.706	-5.361	0.011	0.63
Faulty	1.000	0.496	0.192	0.137	0.66

4 MACHINE FED FROM A VSD AT VARIABLE FREQUENCY AND SLIP

The diagnosis of electrical induction machines fed from VSD's with variable slip and frequency is the most general possible case of diagnosis.

In this section is diagnosed a machine with mixed eccentricity fed from a VSD in the frequency range [26, 30] Hz with variable slip.

The variable slip in this section is achieved by adding a small disk to the shaft of the machine that increases enough the mechanical losses to avoid constant slip.

The electric scheme of the assembly and the test conditions are the same as those for the case when the machine was fed from a VSD with variable frequency and constant slip. Thus, the results are very similar to those discussed in the previous section as shown in Fig. 192 (speed and instantaneous frequency of the current), Fig. 193 (stator current of the tested machine) and Fig. 194 (voltage applied to the stator terminals).

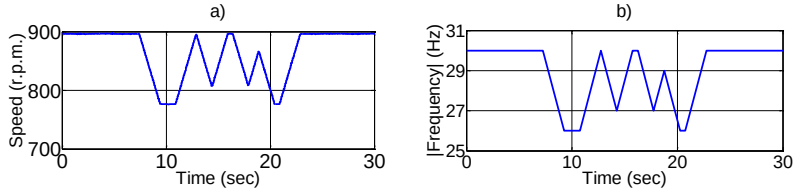

Fig. 192 a) Speed evolution b) Evolution of the instantaneous frequency of the stator current

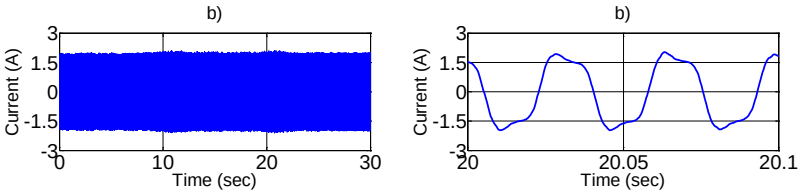

Fig. 193 Acquired stator current in non-stationary stochastic regime consequence of the imposed frequency oscillations of the supply frequency to the machine fed from VSD with a variable frequency in the range [26 ,30] Hz with variable slip. a) General vision b) Detail

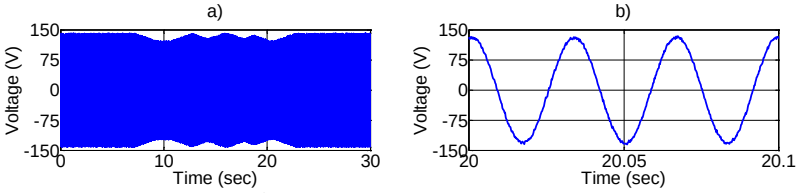

Fig. 194 a) General vision of the voltage supplied to the tested machine b) Detail

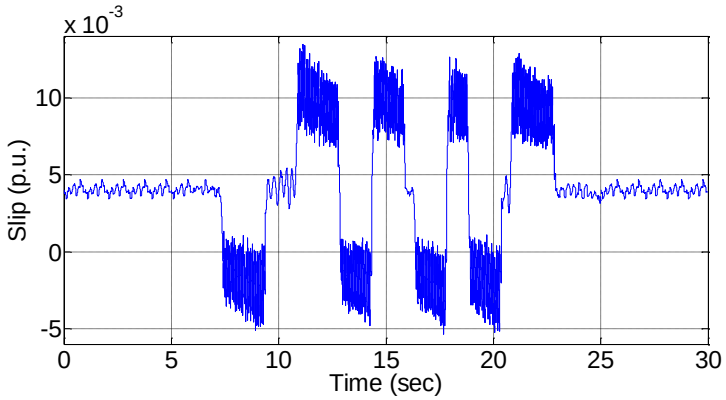

Fig. 195 Slip evolution

Unlike all the previous tests, the simultaneously non-constant features of the supply frequency (Fig. 192.b) and slip (Fig. 195) prevents the depiction of the evolution of the instantaneous frequency versus them since that depiction does not follow any pattern in any of the two domains. Thus, the characteristic values of slope and y used in the previous chapters for the diagnosis of electrical machines are meaningless.

Despite this and since it is known the value of the instantaneous frequency and the slip that the machine is subjected, it is possible the computation of the value of the theoretical instantaneous frequency by (186).

The theoretical value of the instantaneous frequency can be compared with the computed value of the alleged fault component allowing qualitatively whether the alleged fault component follows the evolution of the fault component.

Fig. 196 shows the qualitative result for healthy machine where it is seen that the actual evolution of the frequency of the alleged fault component does not follow the theoretical evolution. Fig. 197 shows the real evolution of the instantaneous frequency of the fault component, in this case it is seen that theoretical and the actual evolution overlap indicating the possibility of the existence of a mixed eccentricity fault.

Since the qualitative criterion is not enough to determine if the machine is in faulty state, Table 43 shows the results that allow the correct diagnosis of the machine and its automation.

Note that the results shown in Table 43 are identical to those for the machine fed from a variable frequency converter with slip constant (Table 42) since the slip values are quite similar (in both tests the machines are operating under no load conditions).

Another fact to highlight is the absence in Table 43 of the slope (m) and y-intercept (b) parameters since in this case they are meaningless.

The comparison of the energy values between the healthy and faults state, it is noted that the energy of the alleged fault component is an order of magnitude greater than the energy in the case of healthy machine. Furthermore, the diagnosis is confirmed since the similitude coefficient (S) takes the value of 1 for the extracted component in the event of failure and a value far away from 1 (0.227) in the case of healthy machine, indicating that

the alleged fault component in the case of fault evolves the same way as the theoretical frequency of failure, confirming the diagnosis.

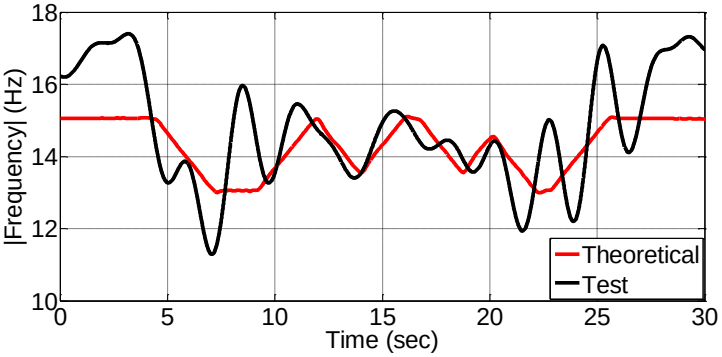

Fig. 196 Evolution of the theoretical instantaneous frequency (red line) and real (black line) for a machine fed from a VSD with variable frequency and slip in healthy state.

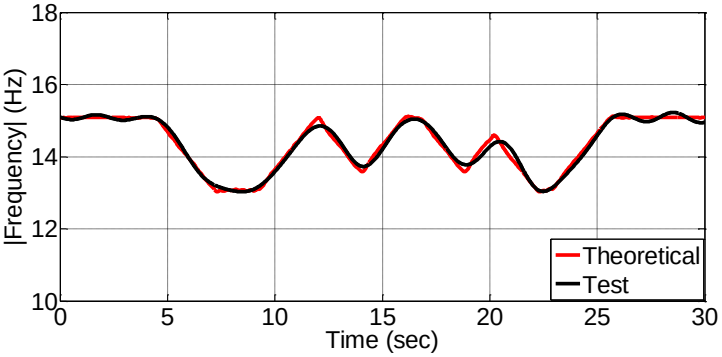

Fig. 197 Evolution of the theoretical instantaneous frequency (red line) and real (black line) for a machine fed from a VSD with variable frequency and slip with mixed eccentricity.

TABLE 43. OBJECTIVE PARAMETERS OF DIAGNOSIS FOR A MIXED ECCENTRICITY THROUGH THE EXTRACTION OF THE FAULT COMPONENT WITH A DWT FILTER. COMMERCIAL WOUND ROTOR INDUCTION MACHINE FED FROM VDS WITH VARIABLE FREQUENCY AND SLIP. WORKING AS MOTOR

Test	S	E_t	**Computation time**
Theoretical			
Healthy	0.227	0.011	0.67
Faulty	1.000	0.137	0.61

5 SUMMARY AND CONCLUSIONS OF THE CHAPTER

This chapter shows the possibility of the diagnosis of electrical machines fed from VSD at constant and variable frequency, operating under constant and variable slip conditions.

The feasibility of the application of the proposed methodology is shown with the diagnosis of a mixed eccentricity fault on three different feeding conditions.

The first test shows the possibility of the diagnosis when the machine is fed from a VSD at constant frequency operating at variable slip.

The second test shows the possibility of the diagnosis when the machine is fed from a VSD at variable frequency but the slip is constant.

Finally, the third tests exposes a diagnosis of the machine when the VSD feds the machine at variable frequency and slip.

The results shown for the first test follow the philosophy already introduced in the previous chapters to diagnose the faults of rotor and stator asymmetry and mixed eccentricity when machines are powered from the electric network at a constant frequency, showing good consistency.

For the second test there are good results following the proposed methodology in the previous chapters if it is exchanged the function of the slip for the supply frequency and vice versa.

Finally, the third test shows the possibility of the diagnosis of induction machines in the most general possible conditions (variable frequency and slip).

Despite the promising results exposed, the diagnosis of electrical induction machines fed from VSD is a field open to future research.

CHAPTER XIII: CONCLUSIONS

In this thesis it has been developed a new methodology for the diagnosis of faults in electrical induction machines operating under non-stationary stochastic conditions, based on the analysis of the evolution of the instantaneous frequency in the frequency-slip plane, which determines the origin of the energy of the alleged extracted fault component. Unlike previous works present in the state of art, the methodology avoids false positive diagnoses, as well as improves the accuracy and reliability of the already developed techniques. The development of the methodology in this thesis consisted of the following set of steps:

1.- Analysis of the fault components of rotor and stator asymmetry and mixed eccentricity in squirrel cage rotor and wound rotor induction machines, irrespective of its operation.

It has thoroughly been researched, after the study of the previous work discussed in the state of art, the evolution of the components in the currents associated with rotor and stator asymmetry and mixed eccentricity in squirrel cage rotor and wound rotor induction machines.

The evolution of the fault components in the currents are expressed through various equations that are only dependent on the slip (speed) the machine undergoes and the supply frequency.

In the case of mechanical failures (mixed eccentricity), the fault components are also dependent on the number of pairs of poles of the machine.

The derivation of the equations of faults allows knowing the time evolution of the different fault frequencies and its evolution in the slip domain.

The depiction of the evolution of the fault frequencies in the frequency slip plane describes straight lines that are independent of the supply conditions, changes in speed, load, features of the machine and has characteristic values for each kind of failure, allowing the establishment of fault patterns in non-stationary stochastic regimes of operation.

The introduced equations are valid for any regime of operation of the machine (motor and generator). Given its general character, they also provide insight into the value of the fault frequencies when the machines are fed from VSD.

The study of the fault components is not limited only to the main fault components since it has also been developed the equations for the high order fault components, which have the same general character than the main fault components.

2.- Proposition of a diagnostic method for machines working in non-stationary stochastic conditions.

It has been developed a methodology based on the analysis of the current of the machine that allows the diagnosis of electric machines in non-stationary stochastic operation through the main fault components and the high order fault components.

The introduced method for the analysis of the electrical machine has the following major improvements over previous works for the diagnosis of electrical machines in non-stationary stochastic operation:

- Unlike previous works, in this method the increase of energy is a necessary but not enough condition to determine that the machine is in faulty state.
- The depiction of the instantaneous frequency of the fault components in the slip domain allows the determination the origin of the energy of the alleged fault component, thus avoiding false positives.

3.- Proposition of a new filtering method in the frequency domain, for the extraction of the fault components.

It has been developed a new filtering method based on the properties of the discrete Fourier transform in the frequency domain, named spectral filter.

The advantages of the spectral filter compared to previously developed filters are:

- High flexibility in the selection of the number of frequency bands to be extracted, where its value is independent of the sampling frequency, unlike what happens with the filters based on the Wavelet transform.
- High flexibility in the selection of the width of the frequency bands to be extracted, where its value is independent of the sampling frequency and can take any value depending on the maximum resolution of the filter that is only dependent on the inverse of the total time of acquired waveform.
- Reduction of the overlapping between the different frequency bands, increasing the diagnostic accuracy.
- Reduction of time and hardware level requirements for the implementation of the filtering process.

4.- Proposal of new numerical indices of characterization and quantification of faults.

Because of the new filter in the frequency domain, it has been developed a technique to quantify the energy in the frequency domain because of Theorem Plancharel.

The advantages of the quantization of energy in the frequency domain are:

– Reduction of the computation times of the alleged fault components.
– Reduction of the hardware level requirements for the computation of energy for the alleged fault component.
– Enables the implementation of the proposed methodology in low cost electronic devices.

Furthermore, due to the practical difficulties of the different coefficients of linear regression in the technical literature, it has been developed a new numeric index (similitude coefficient) that facilitates the determination of the state of the machine.

The main advantages of the developed index are:

– Avoid false positive diagnoses when the frequency components have the same slope as the fault components but with different y-intercept.
– Simplifies its interpretation since it is bounded in the range [0, 1] allowing to know the degree of similarity between the theoretical pattern of the fault component and the studied fault component per unit.

5.- Other contributions

Finally, this thesis introduces the following contributions:

– Computation of the instantaneous frequency through Teager-Kaiser operator that encourages the implementation of the methodology in low cost electronic devices.
– Implementation of the coefficients of least squares linear regression to the diagnosis of electrical machines facilitating the implementation of the proposed methodology through artificial intelligence.
– Introduction of a scheme for the automation of the proposed methodology.
– Introduction to the diagnosis of electrical machines fed from VSD.

CHAPTER XIV: FUTURE RESEARCH

This thesis opens several lines of research that may be the subject of future work, because of the achieved results:

- Implementation of the proposed methodology to induction machines fed by VSD and doubled fed.
  - The main drawback of the adaptation of the methodology for the diagnosis of this kind of machines is the overlap between the fundamental frequency component and fault component due to variation of the frequency supplied by VSD.
- Validation of the developed methodology for industrial applications such as wind power generation or electric vehicles.
  - The main drawback to be solved would be the adaptation of the technique to the particular conditions of each industrial application due to the different control techniques associated with each of them.
- Adaptation of the methodology to other types of faults such as short circuits in the stator windings and bearings.
- Extension of the proposed methodology to other types of machines, such as permanent magnet synchronous machines using the speed-frequency analysis instead of sliding-frequency analysis proposed in this thesis.
- Deep study of spectral filter.
  - It should be researched the effect of overlap between bands, minimum time value of the acquired waveform for acceptable results, the effect of the sampling frequency in the filtering, etc.
- Development of portable devices or embedded diagnostic systems, because of the simplicity of the algorithms for the computation the instantaneous frequency, filtering and energy computation.

CONTRIBUTIONS

This thesis has resulted in the following contributions at the time of its printing:

Journals:

– Vedreño-Santos, F.; Riera-Guasp, M.; Henao, H.; Pineda-Sanchez, M.; Panadero-Puche, R.; "Diagnosis of Rotor and Stator Asymmetries in Wound Rotor Induction Machines under Non-Stationary Operation through the Instantaneous Frequency", Accepted for publication on Transactions on Industrial Electronics August 2013

Congress:

– Vedreño-Santos, F.; Riera-Guasp, M.; Pineda-Sanchez, M.; "Diagnosis of Induction Machines under Non-Stationary Conditions by means of the Spectral Filter", *Diagnostics for Electric Machines, Power Electronics & Drives (SDEMPED), 2013 IEEE International Symposium on*, vol., no., pp. 27-30 August 2013

– Riera-Guasp, M.; Pons-Llinares, J.; Climente-Alarcon, V.; Vedreño-Santos, F. ; Pineda-Sanchez, M.; Antonino-Daviu, J.; Puche-Panadero, R.; Perez-Cruz, J.; Roger-Folch, J.; "Diagnosis of induction machines under non-stationary conditions: Concepts and tools," *Electrical Machines Design Control and Diagnosis (WEMDCD), 2013 IEEE Workshop on*, vol, no, pp 220,231,11-12 March 2013

– Vedreno-Santos, F.; Riera-Guasp, M.; Henao, H.; Pineda-Sanchez, M., "Diagnosis of faults in induction generators under fluctuating load conditions through the instantaneous frequency of the fault components," *Electrical Machines (ICEM), 2012 XXth International Conference on*, vol., no., pp.1653,1659, 2-5 Sept. 2012

– Vedreno-Santos, F.; Riera-Guasp, M.; Henao, H.; Pineda-Sanchez, M.; Antonino-Daviu, J.A., "Diagnosis of eccentricity in induction machines working under fluctuating load conditions, through the instantaneous frequency," *IECON 2012 - 38th Annual Conference on IEEE Industrial Electronics Society*, vol., no., pp.5108,5113, 25-28 Oct. 2012

– Pons-Llinares, J.; Climente-Alarcon, V.; Vedreno-Santos, F.; Antonino-Daviu, J.; Riera-Guasp, M., "Electric machines diagnosis techniques via transient current analysis," *IECON 2012 - 38th Annual Conference on IEEE Industrial Electronics Society*, vol., no., pp.3893,3900, 25-28 Oct. 2012

REFERENCES

[1] Bonnett, A.H.; Soukup, G.C., "Analysis of rotor failures in squirrel-cage induction motors," *Industry Applications, IEEE Transactions on*, vol.24, no.6, pp.1124,1130, Nov.-Dec. 1988

[2] Bonnett, A.H.; Soukup, G.C., "Cause and analysis of stator and rotor failures in three-phase squirrel-cage induction motors," *Industry Applications, IEEE Transactions on*, vol.28, no.4, pp.921,937, Jul/Aug 1992

[3] Bonnett, A.H.; Soukup, G.C., "Rotor Failures in Squirrel Cage Induction Motors," *Industry Applications, IEEE Transactions on*, vol.IA-22, no.6, pp.1165,1173, Nov. 1986.

[4] Nandi, S.; Toliyat, H.A.; Xiaodong Li, "Condition monitoring and fault diagnosis of electrical motors-a review," *Energy Conversion, IEEE Transactions on*, vol.20, no.4, pp.719,729, Dec. 2005.

[5] Pinjia Zhang; Yi Du; Habetler, T.G.; Bin Lu, "A Survey of Condition Monitoring and Protection Methods for Medium-Voltage Induction Motors," *Industry Applications, IEEE Transactions on*, vol.47, no.1, pp.34,46, Jan.-Feb. 2011

[6] Williamson, S.; Mirzoian, K., "Analysis of Cage Induction Motors with Stator Winding Faults," *Power Apparatus and Systems, IEEE Transactions on*, vol.PAS-104, no.7, pp.1838,1842, July 1985.

[7] Kliman, G.B.; Premerlani, W.J.; Koegl, R.A.; Hoeweler, D., "A new approach to on-line turn fault detection in AC motors," *Industry Applications Conference, 1996. Thirty-First IAS Annual Meeting, IAS '96., Conference Record of the 1996 IEEE*, vol.1, no., pp.687,693 vol.1, 6-10 Oct 1996

[8] Cruz, S. M A; Cardoso, A. J M, "Stator winding fault diagnosis in three-phase synchronous and asynchronous motors, by the extended Park's vector approach," *Industry Applications, IEEE Transactions on*, vol.37, no.5, pp.1227,1233, Sep/Oct 2001.

[9] Cardoso, A. J M; Saraiva, E.S., "Computer-aided detection of air gap eccentricity in operating three-phase induction motors by Park's vector approach," *Industry Applications, IEEE Transactions on*, vol.29, no.5, pp.897,901, Sep/Oct 1993

[10] Nandi, S.; Toliyat, H.A., "Novel frequency-domain-based technique to detect stator interturn faults in induction machines using stator-induced voltages after switch-off," *Industry Applications, IEEE Transactions on*, vol.38, no.1, pp.101,109, Jan/Feb 2002

[11] Sang-Bin Lee; Tallam, R.M.; Habetler, T.G., "A robust, on-line turn-fault detection technique for induction machines based on monitoring the sequence component impedance matrix," *Power Electronics, IEEE Transactions on*, vol.18, no.3, pp.865,872, May 2003.

[12] Mirafzal, B.; Demerdash, N. A O, "On innovative methods of induction motor interturn and broken-bar fault diagnostics," *Industry*

Applications, IEEE Transactions on, vol.42, no.2, pp.405,414, March-April 2006.

[13] Stefani, A.; Yazidi, A.; Rossi, C.; Filippetti, F.; Casadei, D.; Capolino, G.-A., "Doubly Fed Induction Machines Diagnosis Based on Signature Analysis of Rotor Modulating Signals," *Industry Applications, IEEE Transactions on*, vol.44, no.6, pp.1711,1721, Nov.-dec. 2008.

[14] da Silva, A.M.; Povinelli, R.J.; Demerdash, N. A O, "Induction Machine Broken Bar and Stator Short-Circuit Fault Diagnostics Based on Three-Phase Stator Current Envelopes," *Industrial Electronics, IEEE Transactions on*, vol.55, no.3, pp.1310,1318, March 2008.

[15] Yazidi, A.; Henao, H.; Capolino, G.-A.; Betin, F.; Capocchi, L., "Experimental inter-turn short circuit fault characterization of wound rotor induction machines," *Industrial Electronics (ISIE), 2010 IEEE International Symposium on*, vol., no., pp.2615,2620, 4-7 July 2010

[16] Yazidi, A.; Henao, H.; Capolino, G.-A.; Betin, F., "Rotor inter-turn short circuit fault detection in wound rotor induction machines," *Electrical Machines (ICEM), 2010 XIX International Conference on*, vol., no., pp.1,6, 6-8 Sept. 2010

[17] Diaz, D.; Amaya, M. C.; Paz, A., "Inter-turn short-circuit analysis in an induction machine by finite elements method and field tests," *Electrical Machines (ICEM), 2012 XXth International Conference on*, vol., no., pp.1757,1763, 2-5 Sept. 2012

[18] Pusca, R.; Romary, R.; Ceban, A., "Detection of inter-turn short circuits in induction machines without knowledge of the healthy state," *Electrical Machines (ICEM), 2012 XXth International Conference on*, vol., no., pp.1637,1642, 2-5 Sept. 2012

[19] Cameron, J.R.; Thomson, W.T.; Dow, A.B., "Vibration and current monitoring for detecting air gap eccentricity in large induction motors," *Electric Power Applications, IEE Proceedings B*, vol.133, no.3, pp.155,163, May 1986.

[20] Dorrell, D.G.; Thomson, W.T.; Roach, S., "Analysis of air gap flux, current, and vibration signals as a function of the combination of static and dynamic air gap eccentricity in 3-phase induction motors," *Industry Applications, IEEE Transactions on*, vol.33, no.1, pp.24,34, Jan/Feb 1997.

[21] Milimonfared, J.; Kelk, H.M.; Nandi, S.; Minassians, A.D.; Toliyat, H.A., "A novel approach for broken-rotor-bar detection in cage induction motors," *Industry Applications, IEEE Transactions on*, vol.35, no.5, pp.1000,1006, Sep/Oct 1999.

[22] Nandi, S.; Ahmed, S.; Toliyat, H.A., "Detection of rotor slot and other eccentricity related harmonics in a three phase induction motor with different rotor cages," *Energy Conversion, IEEE Transactions on*, vol.16, no.3, pp.253,260, Sep 2001.

[23] Zhenxing Liu; Xianggen Yin; Zhe Zhang; Deshu Chen; Wei Chen, "Online rotor mixed fault diagnosis way based on spectrum analysis of

instantaneous power in squirrel cage induction motors," *Energy Conversion, IEEE Transactions on*, vol.19, no.3, pp.485,490, Sept. 2004.

[24] Xianghui Huang; Habetler, T.G.; Harley, R.G.; Wiedenbrug, E.J., "Using a Surge Tester to Detect Rotor Eccentricity Faults in Induction Motors," *Industry Applications, IEEE Transactions on*, vol.43, no.5, pp.1183,1190, Sept.-oct. 2007.

[25] Long Wu; Xianghui Huang; Habetler, T.G.; Harley, R.G., "Eliminating Load Oscillation Effects for Rotor Eccentricity Detection in Closed-Loop Drive-Connected Induction Motors," *Power Electronics, IEEE Transactions on*, vol.22, no.4, pp.1543,1551, July 2007.

[26] Drif, M.; Cardoso, A. J M, "Airgap-Eccentricity Fault Diagnosis, in Three-Phase Induction Motors, by the Complex Apparent Power Signature Analysis," *Industrial Electronics, IEEE Transactions on*, vol.55, no.3, pp.1404,1410, March 2008.

[27] Drif, M.; Cardoso, A. J M, "The Use of the Instantaneous-Reactive-Power Signature Analysis for Rotor-Cage-Fault Diagnostics in Three-Phase Induction Motors," *Industrial Electronics, IEEE Transactions on*, vol.56, no.11, pp.4606,4614, Nov. 2009.

[28] Drif, M.; Cardoso, A. J M, "Discriminating the Simultaneous Occurrence of Three-Phase Induction Motor Rotor Faults and Mechanical Load Oscillations by the Instantaneous Active and Reactive Power Media Signature Analyses," *Industrial Electronics, IEEE Transactions on*, vol.59, no.3, pp.1630,1639, March 2012

[29] Mi-Jung Kim; Byong-Kuk Kim; Ji-Woo Moon; Yun-Hyun Cho; Don-Ha Hwang; Dong-Sik Kang, "Analysis of Inverter-Fed Squirrel-Cage Induction Motor During Eccentric Rotor Motion Using FEM," *Magnetics, IEEE Transactions on*, vol.44, no.6, pp.1538,1541, June 2008

[30] Faiz, J.; Ebrahimi, B.-M.; Akin, B.; Toliyat, H.A., "Dynamic analysis of mixed eccentricity signatures at various operating points and scrutiny of related indices for induction motors," *Electric Power Applications, IET*, vol.4, no.1, pp.1,16, January 2010

[31] Nandi, S.; Ilamparithi, T.C.; Sang-Bin Lee; Doosoo Hyun, "Detection of Eccentricity Faults in Induction Machines Based on Nameplate Parameters," *Industrial Electronics, IEEE Transactions on*, vol.58, no.5, pp.1673,1683, May 2011

[32] Ceban, A.; Pusca, R.; Romary, R., "Study of Rotor Faults in Induction Motors Using External Magnetic Field Analysis," *Industrial Electronics, IEEE Transactions on* , vol.59, no.5, pp.2082,2093, May 2012

[33] Gritli, Y.; Rossi, C.; Casadei, D.; Zarri, L.; Filippetti, F., "Demagnetizations diagnosis for Permanent Magnet Synchronous Motors based on advanced Wavelet Analysis," *Electrical Machines*

(ICEM), 2012 XXth International Conference on , vol., no., pp.2397,2403, 2-5 Sept. 2012

[34] Deleroi, "Squirrel cage motor with broken bar in the rotor – Physical phenomena and their experimental assesment," *Proc. Int. Conf. Electrical Machines*, 1982

[35] Williamson, S.; Smith, A.C., "Steady-state analysis of 3-phase cage motors with rotor-bar and end-ring faults," *Electric Power Applications, IEE Proceedings B*, vol.129, no.3, pp.93,, May 1982.

[36] Kliman, G. B.; Koegl, R.A.; Stein, J.; Endicott, R. D.; Madden, M. W., "Noninvasive detection of broken rotor bars in operating induction motors," *Energy Conversion, IEEE Transactions on*, vol.3, no.4, pp.873,879, Dec 1988.

[37] Schoen, R.R.; Lin, B.K.; Habetler, T.G.; Schlag, J.H.; Farag, S., "An unsupervised, on-line system for induction motor fault detection using stator current monitoring," *Industry Applications, IEEE Transactions on*, vol.31, no.6, pp.1280,1286, Nov/Dec 1995.

[38] Bangura, J.F.; Demerdash, N.A., "Diagnosis and characterization of effects of broken bars and connectors in squirrel-cage induction motors by a time-stepping coupled finite element-state space modeling approach," *Energy Conversion, IEEE Transactions on*, vol.14, no.4, pp.1167,1176, Dec 1999

[39] Arthur, N.; Penman, J., "Induction machine condition monitoring with higher order spectra," *Industrial Electronics, IEEE Transactions on*, vol.47, no.5, pp.1031,1041, Oct 2000.

[40] Kostic-Perovic, D.; Arkan, M.; Unsworth, Peter, "Induction motor fault detection by space vector angular fluctuation," *Industry Applications Conference, 2000. Conference Record of the 2000 IEEE*, vol.1, no., pp.388,394 vol.1, 2000

[41] Kral, C.; Wieser, R.S.; Pirker, F.; Schagginger, M., "Sequences of field-oriented control for the detection of faulty rotor bars in induction machines-the Vienna Monitoring Method," *Industrial Electronics, IEEE Transactions on*, vol.47, no.5, pp.1042,1050, Oct 2000.

[42] Bellini, A.; Filippetti, F.; Franceschini, G.; Tassoni, C.; Kliman, G.B., "Quantitative evaluation of induction motor broken bars by means of electrical signature analysis," *Industry Applications, IEEE Transactions on*, vol.37, no.5, pp.1248,1255, Sep/Oct 2001

[43] Kral, C.; Pirker, F.; Pascoli, G., "Detection of rotor faults in squirrel-cage induction machines at standstill for batch tests by means of the Vienna monitoring method," *Industry Applications, IEEE Transactions on*, vol.38, no.3, pp.618,624, May/Jun 2002.

[44] Zhengping Zhang; Zhen Ren; Wenying Huang, "A novel detection method of motor broken rotor bars based on wavelet ridge," *Energy Conversion, IEEE Transactions on*, vol.18, no.3, pp.417,423, Sept. 2003.

[45] Benbouzid, M.E.H.; Kliman, G.B., "What stator current processing-based technique to use for induction motor rotor faults diagnosis?,"

Energy Conversion, IEEE Transactions on, vol.18, no.2, pp.238,244, June 2003.

[46] Cupertino, F.; De Vanna, E.; Salvatore, Luigi; Stasi, S., "Analysis techniques for detection of IM broken rotor bars after supply disconnection," *Industry Applications, IEEE Transactions on*, vol.40, no.2, pp.526,533, March-April 2004

[47] Demian, C.; Mpanda-Mabwe, A.; Henao, H.; Capolino, G.-A., "Detection of induction machines rotor faults at standstill using signals injection," *Industry Applications, IEEE Transactions on*, vol.40, no.6, pp.1550,1559, Nov.-Dec. 2004.

[48] Henao, H.; Martis, C.; Capolino, G.-A., "An equivalent internal circuit of the induction machine for advanced spectral analysis," *Industry Applications, IEEE Transactions on*, vol.40, no.3, pp.726,734, May-June 2004

[49] Bellini, A.; Franceschini, G.; Tassoni, C., "Monitoring of induction Machines by maximum covariance method for frequency tracking," *Industry Applications, IEEE Transactions on*, vol.42, no.1, pp.69,78, Jan.-Feb. 2006.

[50] Jongbin Park; Byunghwan Kim; Jinkyu Yang; Sang Bin Lee; Wiedenbrug, E.J.; Teska, M.; Han, S., "Evaluation of the detectability of broken rotor bars for double squirrel cage rotor induction motors," *Energy Conversion Congress and Exposition (ECCE), 2010 IEEE*, vol., no., pp.2493,2500, 12-16 Sept. 2010.

[51] Byunghwan Kim; Kwanghwan Lee; Jinkyu Yang; Sang-Bin Lee; Wiedenbrug, E.J.; Shah, M.R., "Automated Detection of Rotor Faults for Inverter-Fed Induction Machines Under Standstill Conditions," *Industry Applications, IEEE Transactions on*, vol.47, no.1, pp.55,64, Jan.-Feb. 2011

[52] Cabanas, M.F.; Pedrayes, F.; Melero, M.G.; Garcia, C.H.R.; Cano, J.M.; Orcajo, G.A.; Norniella, J.G., "Unambiguous Detection of Broken Bars in Asynchronous Motors by Means of a Flux Measurement-Based Procedure," *Instrumentation and Measurement, IEEE Transactions on*, vol.60, no.3, pp.891,899, March 2011

[53] Cabanas, M.F.; Pedrayes, F.; Rojas, C.H.; Melero, M.G.; Norniella, J.G.; Orcajo, G.A.; Cano, J.M.; Nuno, F.; Fuentes, D.R., "A New Portable, Self-Powered, and Wireless Instrument for the Early Detection of Broken Rotor Bars in Induction Motors," *Industrial Electronics, IEEE Transactions on*, vol.58, no.10, pp.4917,4930, Oct. 2011

[54] Kia, S.H.; Henao, H.; Capolino, G.-A., "A High-Resolution Frequency Estimation Method for Three-Phase Induction Machine Fault Detection," *Industrial Electronics, IEEE Transactions on*, vol.54, no.4, pp.2305,2314, Aug. 2007.

[55] Ayhan, B.; Trussell, H.J.; Mo-Yuen Chow; Myung-Hyun Song, "On the Use of a Lower Sampling Rate for Broken Rotor Bar Detection With DTFT and AR-Based Spectrum Methods," *Industrial*

Electronics, IEEE Transactions on, vol.55, no.3, pp.1421,1434, March 2008.

[56] Tsoumas, I.P.; Georgoulas, G.; Mitronikas, E.D.; Safacas, A.N., "Asynchronous Machine Rotor Fault Diagnosis Technique Using Complex Wavelets," *Energy Conversion, IEEE Transactions on*, vol.23, no.2, pp.444,459, June 2008.

[57] Puche-Panadero, R.; Pineda-Sanchez, M.; Riera-Guasp, M.; Roger-Folch, J.; Hurtado-Perez, E.; Perez-Cruz, J., "Improved Resolution of the MCSA Method Via Hilbert Transform, Enabling the Diagnosis of Rotor Asymmetries at Very Low Slip," *Energy Conversion, IEEE Transactions on*, vol.24, no.1, pp.52,59, March 2009

[58] Riera-Guasp, M.; Pons-Llinares, J.; Vedreno-Santos, F.; Antonino-Daviu, J.A.; Fernandez Cabanas, M., "Evaluation of the amplitudes of high-order fault related components in double bar faults," *Diagnostics for Electric Machines, Power Electronics & Drives (SDEMPED), 2011 IEEE International Symposium on*, vol., no., pp.307,315, 5-8 Sept. 2011.

[59] Bouzida, A.; Touhami, O.; Ibtiouen, R.; Belouchrani, A.; Fadel, M.; Rezzoug, A., "Fault Diagnosis in Industrial Induction Machines Through Discrete Wavelet Transform," *Industrial Electronics, IEEE Transactions on*, vol.58, no.9, pp.4385,4395, Sept. 2011.

[60] Toliyat, H.A.; Lipo, T.A., "Transient analysis of cage induction machines under stator, rotor bar and end ring faults," *Energy Conversion, IEEE Transactions on*, vol.10, no.2, pp.241,247, Jun 1995.

[61] Antonino-Daviu, J.A.; Riera-Guasp, M.; Folch, J.R.; Molina Palomares, M.P., "Validation of a new method for the diagnosis of rotor bar failures via wavelet transform in industrial induction machines," *Industry Applications, IEEE Transactions on*, vol.42, no.4, pp.990,996, July-Aug. 2006.

[62] J. Antonino-Daviu, M. Riera-Guasp, J. Roger-Folch, F. Martínez-Giménez, and A. Peris, "Application and optimization of the discrete wavelet transform for the detection of broken rotor bars in induction machines," *Applied and Computational Harmonic Analysis*, vol. 21, pp. 268-279, 2006.

[63] J. Antonino-Daviu, P. Jover, M. Riera, A. Arkkio, and J. Roger-Folch, "DWT analysis of numerical and experimental data for the diagnosis of dynamic eccentricities in induction motors," *Mechanical Systems and Signal Processing*, vol. 21, pp. 2575–2589, Feb. 2007.

[64] J. Antonino-Daviu, P. Jover Rodriguez, M. Riera-Guasp, M. Pineda-Sánchez, A. Arkkio, "Detection of Combined Faults in Induction Machines with Stator Parallel Branches through the DWT of the startup current" *Mechanical Systems and Signal Processing*, Elsevier, vol. 23, no. 7, Oct. 2009, pp. 2336-2351.

[65] Riera-Guasp, M.; Antonino-Daviu, J.A.; Roger-Folch, J.; Molina Palomares, M.P., "The Use of the Wavelet Approximation Signal as a

Tool for the Diagnosis of Rotor Bar Failures," Industry Applications, IEEE Transactions on, vol.44, no.3, pp.716,726, May-june 2008.

[66] Riera-Guasp, M.; Antonino-Daviu, J.A.; Pineda-Sanchez, M.; Puche-Panadero, R.; Perez-Cruz, J., "A General Approach for the Transient Detection of Slip-Dependent Fault Components Based on the Discrete Wavelet Transform," *Industrial Electronics, IEEE Transactions on*, vol.55, no.12, pp.4167,4180, Dec. 2008.

[67] Faiz, J.; Ebrahimi, B.-M.; Akin, B.; Toliyat, H.A., "Finite-Element Transient Analysis of Induction Motors Under Mixed Eccentricity Fault," *Magnetics, IEEE Transactions on*, vol.44, no.1, pp.66,74, Jan. 2008

[68] Pineda-Sanchez, M.; Riera-Guasp, M.; Antonino-Daviu, J.A.; Roger-Folch, J.; Perez-Cruz, J.; Puche-Panadero, R., "Instantaneous Frequency of the Left Sideband Harmonic During the Start-Up Transient: A New Method for Diagnosis of Broken Bars," *Industrial Electronics, IEEE Transactions on*, vol.56, no.11, pp.4557,4570, Nov. 2009.

[69] Pineda-Sanchez, M.; Riera-Guasp, M.; Pons-Llinares, J.; Climente-Alarcon, V.; Perez-Cruz, J., "Diagnosis of induction machines under transient conditions through the Instantaneous Frequency of the fault components," *Electrical Machines (ICEM), 2010 XIX International Conference on*, vol., no., pp.1,6, 6-8 Sept. 2010

[70] Blodt, M.; Regnier, J.; Faucher, J., "Distinguishing Load Torque Oscillations and Eccentricity Faults in Induction Motors Using Stator Current Wigner Distributions," *Industry Applications, IEEE Transactions on*, vol.45, no.6, pp.1991,2000, Nov.-dec. 2009.

[71] Pons-Llinares, J.; Antonino-Daviu, J.; Roger-Folch, J.; Morinigo-Sotelo, D.; Duque-Perez, O., "Eccentricity diagnosis in Inverter - Fed Induction Motors via the Analytic Wavelet Transform of transient currents," *Electrical Machines (ICEM), 2010 XIX International Conference on*, vol., no., pp.1,6, 6-8 Sept. 2010.

[72] Pons-Llinares, J.; Antonino-Daviu, J.A.; Riera-Guasp, M.; Pineda-Sanchez, M.; Climente-Alarcon, V., "Induction Motor Diagnosis Based on a Transient Current Analytic Wavelet Transform via Frequency B-Splines," *Industrial Electronics, IEEE Transactions on*, vol.58, no.5, pp.1530,1544, May 2011.

[73] Douglas, H.; Pillay, P.; Ziarani, A.K., "A new algorithm for transient motor current signature analysis using wavelets," *Industry Applications, IEEE Transactions on*, vol.40, no.5, pp.1361,1368, Sept.-Oct. 2004.

[74] Douglas, H.; Pillay, P.; Ziarani, A.K., "Broken rotor bar detection in induction machines with transient operating speeds," *Energy Conversion, IEEE Transactions on*, vol.20, no.1, pp.135,141, March 2005.

[75] Supangat, R.; Ertugrul, N.; Soong, W.L.; Gray, D.A.; Hansen, C.; Grieger, J., "Detection of broken rotor bars in induction motor using

starting-current analysis and effects of loading," *Electric Power Applications, IEE Proceedings* -, vol.153, no.6, pp.848,855, November 2006.

[76] Blodt, M.; Chabert, M.; Regnier, J.; Faucher, J., "Mechanical Load Fault Detection in Induction Motors by Stator Current Time-Frequency Analysis," *Industry Applications, IEEE Transactions on*, vol.42, no.6, pp.1454,1463, Nov.-dec. 2006.

[77] Kia, S.H.; Henao, H.; Capolino, G.-A., "Diagnosis of Broken-Bar Fault in Induction Machines Using Discrete Wavelet Transform Without Slip Estimation," *Industry Applications, IEEE Transactions on*, vol.45, no.4, pp.1395,1404, July-aug. 2009

[78] Kia, S.H.; Mpanda-Mabwe, A.; Ceschi, R., "Slip independent monitoring of wound-rotor induction machines," *Industrial Electronics (ISIE), 2010 IEEE International Symposium on*, vol., no., pp.1485,1490, 4-7 July 2010

[79] Briz, F.; Degner, M.W.; Garcia, P.; Bragado, D., "Broken Rotor Bar Detection in Line-Fed Induction Machines Using Complex Wavelet Analysis of Startup Transients," *Industry Applications, IEEE Transactions on*, vol.44, no.3, pp.760,768, May-june 2008.

[80] Pineda-Sanchez, M.; Riera-Guasp, M.; Antonino-Daviu, J.A.; Roger-Folch, J.; Perez-Cruz, J.; Puche-Panadero, R., "Diagnosis of Induction Motor Faults in the Fractional Fourier Domain," *Instrumentation and Measurement, IEEE Transactions on*, vol.59, no.8, pp.2065,2075, Aug. 2010

[81] Pineda-Sanchez, M.; Riera-Guasp, M.; Roger-Folch, J.; Antonino-Daviu, J.A.; Perez-Cruz, J.; Puche-Panadero, R., "Diagnosis of Induction Motor Faults in Time-Varying Conditions Using the Polynomial-Phase Transform of the Current," *Industrial Electronics, IEEE Transactions on*, vol.58, no.4, pp.1428,1439, April 2011

[82] Antonino-Daviu, J.; Aviyente, S.; Strangas, E.; Riera-Guasp, M., "A scale invariant algorithm for the automatic diagnosis of rotor bar failures in induction motors," *Industrial Electronics (ISIE), 2011 IEEE International Symposium on*, vol., no., pp.496,501, 27-30 June 2011

[83] Antonino-Daviu, J.; Riera-Guasp, M.; Pons-Llinares, J.; Jongbin Park; Sang Bin Lee; Jiyoon Yoo; Kral, C., "Detection of Broken Outer-Cage Bars for Double-Cage Induction Motors Under the Startup Transient," *Industry Applications, IEEE Transactions on*, vol.48, no.5, pp.1539,1548, Sept.-Oct. 2012.

[84] Riera-Guasp, M.; Pineda-Sanchez, M.; Perez-Cruz, J.; Puche-Panadero, R.; Roger-Folch, J.; Antonino-Daviu, J.A., "Diagnosis of Induction Motor Faults via Gabor Analysis of the Current in Transient Regime," *Instrumentation and Measurement, IEEE Transactions on*, vol.61, no.6, pp.1583,1596, June 2012

[85] Gritli, Y.; Sang Bin Lee; Filippetti, F.; Zarri, L., "Advanced diagnosis of outer cage damage in double squirrel cage induction motors under time-varying condition based on wavelet analysis," *Energy*

Conversion Congress and Exposition (ECCE), 2012 IEEE , vol., no., pp.1284,1290, 15-20 Sept. 2012

[86] Climente-Alarcon, V.; Antonino-Daviu, J.; Vedreno-Santos, F.; Puche-Panadero, R., "Vibration Transient Detection of Broken Rotor Bars by PSH Sidebands," *Industry Applications, IEEE Transactions on* , vol.PP, no.99, pp.1,1, 0

[87] Blodt, M.; Bonacci, D.; Regnier, J.; Chabert, M.; Faucher, J., "On-Line Monitoring of Mechanical Faults in Variable-Speed Induction Motor Drives Using the Wigner Distribution," *Industrial Electronics, IEEE Transactions on*, vol.55, no.2, pp.522,533, Feb. 2008.

[88] Cusido, J.; Romeral, L.; Ortega, J.A.; Rosero, J.A.; Garcia Espinosa, A., "Fault Detection in Induction Machines Using Power Spectral Density in Wavelet Decomposition," *Industrial Electronics, IEEE Transactions on*, vol.55, no.2, pp.633,643, Feb. 2008.

[89] Stefani, A.; Bellini, A.; Filippetti, F., "Diagnosis of Induction Machines' Rotor Faults in Time-Varying Conditions," *Industrial Electronics, IEEE Transactions on*, vol.56, no.11, pp.4548,4556, Nov. 2009.

[90] Y. Gritli, A. Stefani, C. Rossi, F. Filippetti, A. Chatti, "Experimental validation of doubly fed induction machine electrical faults diagnosis under time-varying conditions", *Journal of Electric Power Systems Research*, Vol. 81, Issue 3, pp. 751-766, March 2011.

[91] Gritli, Y.; Rossi, C.; Zarri, L.; Filippetti, F.; Chatti, A.; Casadei, D.; Stefani, A., "Advanced diagnosis of broken bar fault in induction machines by using Discrete Wavelet Transform under time-varying condition," *Electric Machines & Drives Conference (IEMDC), 2011 IEEE International*, vol., no., pp.424,429, 15-18 May 2011

[92] Gritli, Y.; Rossi, C.; Zarri, L.; Filippetti, F.; Chatti, A.; Casadei, D., "Double frequency sliding and wavelet analysis for rotor fault diagnosis in induction motors under time-varying operating condition," *Diagnostics for Electric Machines, Power Electronics & Drives (SDEMPED), 2011 IEEE International Symposium on*, vol., no., pp.676,683, 5-8 Sept. 2011

[93] Kia, S.H.; Henao, H.; Capolino, G.-A., "Windings monitoring of wound rotor induction machines under fluctuating load conditions," *IECON 2011 - 37th Annual Conference on IEEE Industrial Electronics Society*, vol., no., pp.3459,3465, 7-10 Nov. 2011

[94] Cruz, S. M A, "An Active–Reactive Power Method for the Diagnosis of Rotor Faults in Three-Phase Induction Motors Operating Under Time-Varying Load Conditions," *Energy Conversion, IEEE Transactions on* , vol.27, no.1, pp.71,84, March 2012

[95] Gritli, Y.; Zarri, L.; Rossi, C.; Filippetti, F.; Capolino, G.-A.; Casadei, D., "Advanced Diagnosis of Electrical Faults in Wound-Rotor Induction Machines," *Industrial Electronics, IEEE Transactions on* , vol.60, no.9, pp.4012,4024, Sept. 2013

[96] www.wwindea.org/webimages/WorldWindEnergyReport2011.pdf

[97] Nandi, S.; Bharadwaj, R.M.; Toliyat, H.A.; Parlos, A.G., "Study of three phase induction motors with incipient rotor cage faults under different supply conditions," *Industry Applications Conference, 1999. Thirty-Fourth IAS Annual Meeting. Conference Record of the 1999 IEEE*, vol.3, no., pp.1922,1928 vol.3, 1999

[98] Fiser, R.; Ferkolj, S., "Application of a finite element method to predict damaged induction motor performance," *Magnetics, IEEE Transactions on*, vol.37, no.5, pp.3635,3639, Sep 2001

[99] Finley, W.R.; Hodowanec, M.M.; Holter, W.G., "An analytical approach to solving motor vibration problems," *Industry Applications, IEEE Transactions on*, vol.36, no.5, pp.1467,1480, Sep/Oct 2000

[100] P. Vas, "Parameter Estimation, Condition Monitoring, and Diagnosis of Electrical Machines", Oxford, U.K.: Clarendon, 1993.

[101] Red Eléctrica de España, "El sitema eléctrico español, avance del informe 2012", http://www.ree.es/sistema_electrico/informeSEE-avance2012.asp, Febrero 2013.

[102] World Wind Energy Association, "2012, Small Wind World Report", 2012

[103] Tavner, P.J., "Review of condition monitoring of rotating electrical machines," *Electric Power Applications, IET*, vol.2, no.4, pp.215,247, July 2008

[104] Tavner, P. J.; Hasson, J. P., "Predicting the design life of high integrity rotating electrical machines," *Electrical Machines and Drives, 1999. Ninth International Conference on (Conf. Publ. No. 468)*, vol., no., pp.286,290, 1999

[105] O'Donnell P.: 'IEEE reliability working group, report of large motor reliability survey of industrial and commercial installations. Part I, II and III', *IEEE Trans. Ind. Appl*., 1985,21, pp. 853–872

[106] Albrecht, P. F.; Appiarius, J. C.; McCoy, R. M.; Owen, E.L.; Sharma, D. K., "Assessment of the Reliability of Motors in Utility Applications - Updated," *Energy Conversion, IEEE Transactions on*, vol.EC-1, no.1, pp.39,46, March 1986

[107] Thorsen, O.V.; Dalva, M., "Failure identification and analysis for high-voltage induction motors in the petrochemical industry," *Industry Applications, IEEE Transactions on*, vol.35, no.4, pp.810,818, Jul/Aug 1999

[108] M. Riera, "Estudio de la influencia de los armónicos de devanado en el funcionamiento de las máquinas asíncronas utilizando la teoría de los fasores espaciales". Tesis doctoral, Universidad Politécnica de Valencia, Febrero 1987.

[109] Filippetti, F.; Franceschini, G.; Tassoni, C.; Vas, P., "AI techniques in induction machines diagnosis including the speed ripple effect," *Industry Applications Conference, 1996. Thirty-First IAS Annual Meeting, IAS '96., Conference Record of the 1996 IEEE*, vol.1, no., pp.655,662 vol.1, 6-10 Oct 1996

[110] Penman, J.; Sedding, H.G.; Lloyd, B.A.; Fink, W. T., "Detection and location of interturn short circuits in the stator windings of operating motors," *Energy Conversion, IEEE Transactions on*, vol.9, no.4, pp.652,658, Dec 1994
[111] Rusek. J, "Categorization of induction machines in current signature analysis", Electrical Engineering 84 (2002) pp. 265-273
[112] BTM Consults. "International Wind Energy Department—World Market Update 2004, Forecast 2005–2009". A. Rasmussens, Ringkøbing, Denmark, 2005.
[113] Heideman, M.; Johnson, D.H.; Burrus, C.S., "Gauss and the history of the fast fourier transform," *ASSP Magazine, IEEE*, vol.1, no.4, pp.14,21, October 1984
[114] Burt, P.J.; Adelson, E.H., "The Laplacian Pyramid as a Compact Image Code," *Communications, IEEE Transactions on*, vol.31, no.4, pp.532,540, Apr 1983
[115] Cooley, J.W. and Tukey, J.W., "An algorithm for the machine calculation of complex Fourier series", *Math. Comput*. Vol.19, no. 2, pp.297-301, April 1965
[116] Widrow. B and Holf, M.E., "Adaptative Switching Circuits". *In IRE WESCON Conv. Records*, pp 96-104, IRE, New York, NY.
[117] Haykin, S.; Van Veen, B.; "Signals and Systems" John Wiley & Sons, Inc, New York, 1999
[118] Philips, C.L.; Parr J.M.; "Signals, Systems and transforms", Prentice Hall, New Jersey, 1995
[119] Proakis, J.G; Manolakis, D.G.; "Digital Signal Processing: Principles, Algorithms and Applications", Macmillas, New York, 1992.
[120] Lyons, R.G.; "Understanding digital signal processing", Prentice Hall, New Jersey, 2001.
[121] Nyquist, H., "Certain Topics in Telegraph Transmission Theory," *American Institute of Electrical Engineers, Transactions of the*, vol.47, no.2, pp.617,644, April 1928.
[122] C.E. Shannon, "Communication in the presence of noise", *Proc. Institute of Radio Engineers*, vol. 37, no. 1, pp. 10-21, Jan 1949.
[123] Jerri, A.J., "The Shannon sampling theorem—Its various extensions and applications: A tutorial review," *Proceedings of the IEEE*, vol.65, no.11, pp.1565,1596, Nov. 1977
[124] Ordaz-Moreno, A.; de Jesus Romero-Troncoso, R.; Vite-Frias, J.A.; Rivera-Gillen, J.R.; Garcia-Perez, A., "Automatic Online Diagnosis Algorithm for Broken-Bar Detection on Induction Motors Based on Discrete Wavelet Transform for FPGA Implementation," *Industrial Electronics, IEEE Transactions on*, vol.55, no.5, pp.2193,2202, May 2008.
[125] W.G. Zanardelli, E.G. Strangas, H.K. Khalil, J.M. Miller, "Wavelet-based methods for the prognosis of mechanical and electrical failures in electric motors," *Mech. Syst. Signal Process*. 19 (2005) 411–426.

[126] J. A. Antonino-Daviu, M. Riera-Guasp, M. Pineda-Sánchez, J. Pons-Llinares, R. Puche-Panadero, J. Cruz, J. Pérez, "Feature extraction for the prognosis of electromechanical faults in electrical machines through the DWT" , *Int. J. Comput. Intell. Syst*.2 (No.2) (June2009) 158–167.

[127] Eren, L.; Devaney, M.J., "Bearing damage detection via wavelet packet decomposition of the stator current," *Instrumentation and Measurement, IEEE Transactions on*, vol.53, no.2, pp.431,436, April 2004

[128] Zanardelli, W.G.; Strangas, E.G.; Aviyente, S., "Identification of Intermittent Electrical and Mechanical Faults in Permanent-Magnet AC Drives Based on Time–Frequency Analysis," *Industry Applications, IEEE Transactions on*, vol.43, no.4, pp.971,980, July-aug. 2007

[129] Rajagopalan, S.; Aller, J.M.; Restrepo, J.A.; Habetler, T.G.; Harley, R.G., "Analytic-Wavelet-Ridge-Based Detection of Dynamic Eccentricity in Brushless Direct Current (BLDC) Motors Functioning Under Dynamic Operating Conditions," *Industrial Electronics, IEEE Transactions on*, vol.54, no.3, pp.1410,1419, June 2007.

[130] Puche-Panadero, R.; Pons-Llinares, J.; Roger-Folch, J.; Pineda-Sanchez, M., "Diagnosis of eccentricity based on the Hilbert transform of the startup transient current," *Diagnostics for Electric Machines, Power Electronics and Drives, 2009. SDEMPED 2009. IEEE International Symposium on*, vol., no., pp.1,6, Aug. 31 20096-Sept. 3 2009.

[131] Antonino-Daviu, J.A.; Riera-Guasp, M.; Pineda-Sanchez, M.; Perez, R.B., "A Critical Comparison Between DWT and Hilbert–Huang-Based Methods for the Diagnosis of Rotor Bar Failures in Induction Machines," *Industry Applications, IEEE Transactions on*, vol.45, no.5, pp.1794,1803, Sept.-oct. 2009.

[132] V.K. Rai, A.R. Mohanty, "Bearing fault diagnosis using FFT of intrinsic mode functions in Hilbert–Huang transform," *Mech. Syst. Signal Process*. 21(6 August) (2007) 2607–2615.

[133] Climente-Alarcon, V.; Antonino-Daviu, J.A.; Riera-Guasp, M.; Puche, R.; Escobar-Moreira, L.; Wiener, N.; Jover-Rodriguez, P.; Arkkio, A., "Diagnosis of stator short-circuits through Wigner-Ville transient-based analysis," *Industrial Electronics, 2009. IECON '09. 35th Annual Conference of IEEE*, vol., no., pp.1097,1102, 3-5 Nov. 2009.

[134] L. Cohen, *Time-Frequency Analysis*. A.V. Oppenheim, Ed. Prentice Hall Signal Processing Series, New Jersey, 1995.

[135] Plancherel, Michel; Mittag-Leffler (1910), "Contribution à l'étude de la représentation d'une fonction arbitraire par les intégrales définies", *Rendiconti del Circolo Matematico di Palermo* 30 (1): 289–335

[136] Maragos, P.; Kaiser, J.F.; Quatieri, T.F., "Energy separation in signal modulations with application to speech analysis," *Signal Processing, IEEE Transactions on*, vol.41, no.10, pp.3024,3051, Oct 1993

[137] http://engineering.rowan.edu/~polikar/WAVELETS/WTtutorial.html ; the Wavelet Tutorial by Robi Polikar.
[138] C. S. Burrus, R. A. Gopinath, and H. Guo, *Introduction to Wavelets and Wavelet Transforms. A Primer*. Englewood Cliffs, NJ: Prentice-Hall, 1998.
[139] M.E. Frerking, "Digital Signal Processing in Communication Systems", Springer, 1994
[140] Cizek, V., "Discrete Hilbert transform," *Audio and Electroacoustics, IEEE Transactions on*, vol.18, no.4, pp.340,343, Dec 1970.
[141] Boashash, B., "Estimating and interpreting the instantaneous frequency of a signal. I. Fundamentals," *Proceedings of the IEEE*, vol.80, no.4, pp.520,538, Apr 1992.
[142] Boashash, B., "Estimating and interpreting the instantaneous frequency of a signal. II. Algorithms and applications," *Proceedings of the IEEE*, vol.80, no.4, pp.540,568, Apr 1992.
[143] Hlawatsch, F.; Boudreaux-bartels, G.F., "Linear and quadratic time-frequency signal representations," *Signal Processing Magazine, IEEE*, vol.9, no.2, pp.21,67, April 1992.
[144] Maragos, P.; Kaiser, J.F.; Quatieri, T.F., "On amplitude and frequency demodulation using energy operators," *Signal Processing, IEEE Transactions on*, vol.41, no.4, pp.1532,1550, Apr 1993.
[145] Maragos, P.; Kaiser, J.F.; Quatieri, T.F., "Energy separation in signal modulations with application to speech analysis," *Signal Processing, IEEE Transactions on*, vol.41, no.10, pp.3024,3051, Oct 1993.
[146] J. Ville, "Theorie et Application de la Notion de Signal Analytic," *Cables et Transmissions*, vol. 2A, pp. 61-74, 1948.
[147] Teager, H., "Some observations on oral air flow during phonation," *Acoustics, Speech and Signal Processing, IEEE Transactions on*, vol.28, no.5, pp.599,601, Oct 1980.
[148] J. Wolberg, "Data Analysis Using the Method of Least Squares: Extracting the Most Information from Experiments" Springer, 2005
[149] Dowdy, S. and Wearden, S. "Statistics for Research", Wiley, 1983

ANNEX I: TESTED MACHINES

This Annex details the features of the different commercial induction motors used in this thesis to validate the proposed methodology.

1 UNIVERSAL MACHINE

The universal machine set as wound rotor induction machine was used in the rotor and stator asymmetry tests working as generator. The features of the universal machine are as follows:

TABLE 44. FEATURES OF THE UNIVERSAL MACHINE

Rated Power	1.5 kW
Rated Frequency	50 Hz
Stator	
Rated Voltage	300 V (star)
Rated Current	5.5 A (star)
Resistance	4.4 Ω/phase
Num. Slots	24
Rotor	
Rated Currents	8 A (delta)
Resistance	10.15 Ω/phase
Num. Slots	36
Rated Speed	
Motor	2.800 r.p.m.
Generator	3.200 r.p.m.

Fig. 198 Universal Machine

2 WOUND ROTOR INDUCTION MACHINE 15 CV

The 15 CV wound rotor induction machine was used in the tests of rotor and stator asymmetry working as generator and motor.

The features of the 15 CV wound rotor induction machine are the followings:

TABLE 45. FEATURES OF THE 15 CV WOUND ROTOR INDUCTION MACHINE

Rated Power	11 kW
Rated Frequency	50 Hz
Pair of Poles	2
Stator	
Rated Voltage	220/380 V
Rated Current	40/23 A
Resistance	0.333 Ω/phase
Num. Slots	36
Rotor	
Rated Currents	26 A
Resistance	0.335 Ω/phase
Num. Slots	24
Rated Speed	
Motor	1.480 r.p.m.

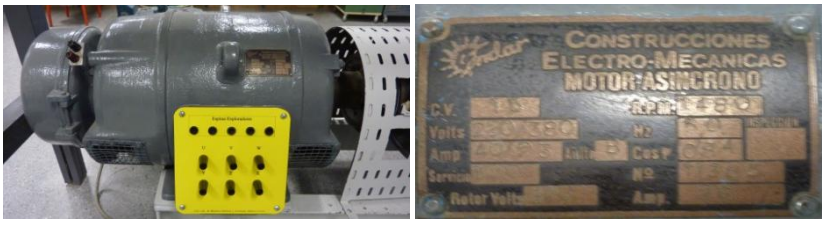

Fig. 199 15 CV Wound rotor induction machine and its nameplate.

3 SQUIRREL CAGE ROTOR INDUCTION MACHINE

The squirrel cage rotor induction machine was used in the tests of mixed eccentricity operating in motor and generator conditions. The squirrel cage rotor induction machine was also used for the validation of the methodology when the machines were fed from a VSD.

The features of the squirrel cage rotor induction machine are the followings:

TABLE 46. FEATURES OF THE SQUIRREL CAGE ROTOR INDUCTION MACHINE

Rated Power	1.1 kW
Rated Frequency	50 Hz
Pair of Poles	2
Stator	
Rated Voltage	230/400 V
Rated Current	4.4/2.55 A
Num. Slots	36
Rotor	
Num. Bars	28
Rated Speed	
Motor	1.415 r.p.m.

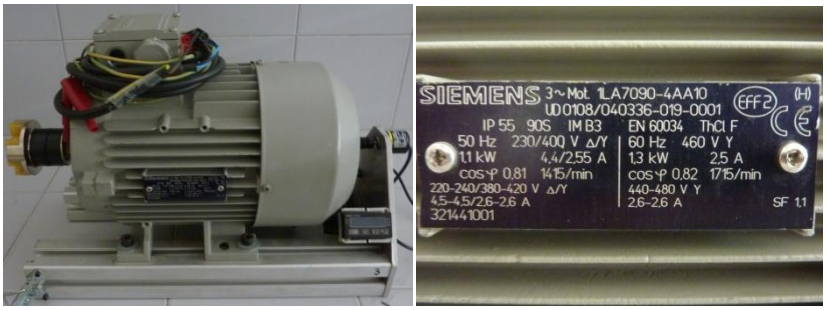

Fig. 200 Squirrel cage rotor induction machine and its nameplate.

4 600 W WOUND ROTOR INDUCTION MACHINE

The 600 W wound rotor induction machine was used in the tests of mixed eccentricity mixed working as motor and generator.

The features of the wound rotor induction machine are the followings:

TABLE 47. FEATURES OF THE WOUND ROTOR INDUCTION MACHINE

Rated Power	0.6 kW
Rated Frequency	50 Hz
Pair of Poles	2
Stator	
Rated Voltage	220/380 V
Rated Current	2.5/1.4 A
Num. Slots	36
Rotor	
Rated Voltage	220 V (star)
Num. Slots	27
Rated Speed	
Motor	1.450 r.p.m.

Fig. 201 600 W wound rotor induction machine and its nameplate.

ANNEX II: AUXILIARY EQUIPMENT AND SWITCHGEAR

The acquisition of the current signals of the tested induction machines in this thesis were captured by a digital oscilloscope Yokogawa DL-750.

The digital oscilloscope Yokogawa DL-750 combines the functions of oscilloscope and recorder due to the 30 GB hard drive built into it.

One of the main features of digital oscilloscope Yokogawa DL-750 is its modularity. This feature allows the oscilloscope to capture up to 16 analogue inputs of different nature such as signals of temperature, speed, current, voltage, etc.

The maximum sampling frequency and resolution of the device is function of the acquisition card used.

The features of the acquisition card used in this thesis allow the selection of a sampling frequency up to 10 MS/s with a resolution of 16 bits.

Finally, the oscilloscope can be connected to LAN networks facilitating the exchange of information with a PC where the captured signals can be analyzed.

Fig. 202 Digital Oscilloscope Yokohama DL-750

The acquisition of the necessary current signals, besides requiring a signal recorder, also requires the use of auxiliary switchgear.

The acquisition of the captured currents by the signal recorder required the use of a clamp Chauvin Arnoux MN 60.

Fig. 203 Clamp Chauvin Arnoux MN 60

The acquisition of speed in tests was carried out by an encoder Omron E6A2, powered with 24 V with a resolution of 200 pulses per revolution.

Fig. 204 Encoder Omron E6A2

The processing of the acquired current signals by the signal recorder is carried out on a personal computer with a processor Intel Core i7-2670QM 2.2 GHz, 8 GB DDR3 RAM.

The PLC used to control the VSD and the motorized rheostat is the micro-PLC Siemens LOGO 230RC

Fig. 205 Micro-PLC LOGO 230RC

TABLE 48. FEATURES OF THE MICRO PLC LOGO 230RC

	Logo! 230RC
Power supply	
Input voltage: rated voltage	115/120/230/240 V a.c.
Frequency	47 to 63 Hz
Digital inputs	6
Digital outputs	4
Permanent current (per output)	Max 8 A
Switching frequency	
Resistor/Lamp load	2 Hz
Inductive load	0.5 Hz

The trade name of the variable speed drive for the supply of the different machines used in this thesis is OMRON-SYSDRIVE-3G3MV.

Fig. 206 Variable speed drive OMRON - SYSDRIVE - 3G3MV

TABLE 49. FEATURES OF THE VARIABLE SPEED DRIVE OMRON-SYSDRIVE-3G3MV

Model 3G3MV-VVVVV		A4040
Power (kW)		4
Output	*Rated Power (kVA)*	6.5
	Rated Current (A)	8.6
	Rated Voltage (V)	380 a 460 V ac three phase. (function of the input voltage)
	Max Output Frequency (Hz)	400 Hz (according to parameters)
Control	*Control method*	Sinusoidal PWM (control V/f or vectorial)
	Frequency range	0.1 a 400 Hz
	Output Frequency Resolution	0.01 Hz
	Acceleration/Deceleration time	0.01 a 6 s (acceleration and deceleration time are chosen in different parameters)